

AD/A-002 833

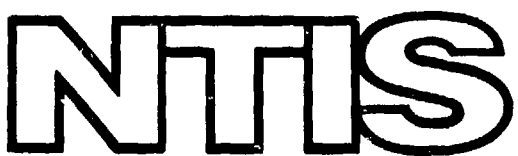
AN ANALYSIS OF LINEAR AND NON-LINEAR
COHERENT DETECTION IN ATMOSPHERIC
NOISE AT VERY LOW FREQUENCY

John T. Gamble

Rome Air Development Center
Griffiss Air Force Base, New York

November 1974

DISTRIBUTED BY:



National Technical Information Service
U. S. DEPARTMENT OF COMMERCE

UNCLASSIFIED

SECURITY CLASSIFICATION OF THIS PAGE (When Data Entered)

REPORT DOCUMENTATION PAGE		READ INSTRUCTIONS BEFORE COMPLETING FORM										
1. REPORT NUMBER RADC-TR-74-289	2. GOVT ACCESSION NO.	3. RECIPIENT'S CATALOG NUMBER <i>AD/A-002 833</i>										
4. TITLE (and Subtitle) AN ANALYSIS OF LINEAR AND NON-LINEAR COHERENT DETECTION IN ATMOSPHERIC NOISE AT VERY LOW FREQUENCY		5. TYPE OF REPORT & PERIOD COVERED In-House Report										
7. AUTHOR(s) John T. Gamble		6. PERFORMING ORG. REPORT NUMBER RADC-TR-74-289										
9. PERFORMING ORGANIZATION NAME AND ADDRESS Rome Air Development Center (DCCL) Griffiss Air Force Base, New York 13441		8. CONTRACT OR GRANT NUMBER(s) N/A										
11. CONTROLLING OFFICE NAME AND ADDRESS Rome Air Development Center (DCCL) Griffiss Air Force Base, New York 13441		10. PROGRAM ELEMENT, PROJECT, TASK AREA & WORK UNIT NUMBERS Program Element 11316F Job Order No. 616A0001										
14. MONITORING AGENCY NAME & ADDRESS (if different from Controlling Office) Same		12. REPORT DATE November 1974										
		13. NUMBER OF PAGES <i>366</i>										
16. DISTRIBUTION STATEMENT (of this Report) Approved for public release; distribution unlimited.		15. SECURITY CLAS. (of this report) UNCLASSIFIED										
17. DISTRIBUTION STATEMENT (of the abstract entered in Block 20, if different from Report) Same		15a. DECLASSIFICATION/DOWNGRADING SCHEDULE N/A										
18. SUPPLEMENTARY NOTES Presented as a Ph.D. Dissertation to Syracuse University, Syracuse, New York												
19. KEY WORDS (Continue on reverse side if necessary and identify by block number) <table style="width: 100%; border-collapse: collapse;"> <tr> <td style="width: 50%;">Atmospheric Noise</td> <td style="width: 50%;">Impulsive Noise</td> </tr> <tr> <td>Error Rates</td> <td>Low Frequency Communications</td> </tr> <tr> <td>Coherent Demodulator</td> <td>Non-Linear Receiver Analysis</td> </tr> <tr> <td>Frequency-Shift Keying</td> <td>Phase Shift Keying</td> </tr> <tr> <td>Minimum Shift Keying</td> <td>Very Low Frequency Communications</td> </tr> </table>			Atmospheric Noise	Impulsive Noise	Error Rates	Low Frequency Communications	Coherent Demodulator	Non-Linear Receiver Analysis	Frequency-Shift Keying	Phase Shift Keying	Minimum Shift Keying	Very Low Frequency Communications
Atmospheric Noise	Impulsive Noise											
Error Rates	Low Frequency Communications											
Coherent Demodulator	Non-Linear Receiver Analysis											
Frequency-Shift Keying	Phase Shift Keying											
Minimum Shift Keying	Very Low Frequency Communications											
20. ABSTRACT (Continue on reverse side if necessary and identify by block number) This report is concerned with the performance analysis of coherent modems in atmospheric noise. Specifically, Phase Shift Keying (PSK, biphasic), Coherent Frequency Shift Keying (CFSK), and Minimum Shift Keying (MSK) modems are described and analyzed for error rate performance in the non-Gaussian, impulsive atmospheric noise typical of a very low frequency (VLF) radio communication channel. The analyses include both linear and non-linear (band-pass, hard-limiting) pre-detection signal processing. In each case,												

DD FORM 1 JAN 73 1473 EDITION OF 1 NOV 65 IS OBSOLETE

UNCLASSIFIED

SECURITY CLASSIFICATION OF THIS PAGE (When Data Entered)

Reproduced by
 NATIONAL TECHNICAL
 INFORMATION SERVICE
 U.S. Department of Commerce
 Springfield VA 22151

UNCLASSIFIED

SECURITY CLASSIFICATION OF THIS PAGE(When Data Entered)

20. Abstract (Cont'd)

experimentally derived error rate performance data is presented which shows close agreement with the computational results of the analyses.

The first part of the analysis is a survey of atmospheric noise representations. This includes descriptions of the power-Rayleigh first order statistical model used in the linear and pseudo-linear (large bandwidth ratio, hard-limiting receiver) analyses and the filtered Poisson impulse process used in the analyses of small bandwidth ratio, hard-limiting receivers. Following a complete description of the modulation and demodulation processes for the three systems, a numerical procedure is developed for evaluating linear-system error probabilities. Next, the Pulse Statistical Analysis (PSA) technique (employing a filtered Poisson impulse process with monotonically related, power-Rayleigh distributed pulse amplitudes) is developed and shown to be quantitatively valid for hard-limiting receivers where the bandwidth ratio (ratio of limiter bandwidth to detection bandwidth) is less than 8. Finally, the Impulsive Noise Subtraction (INS) technique is developed in which enhancement of signal-to-noise ratios by hard-limiting is calculated and the residual (post-limiting) noise statistics are obtained by "best-fit" numerical convolution techniques. Employment of these residual signal and noise statistics in linear performance analyses is shown to yield quantitatively accurate error rate performance data for a bandwidth ratio (BWR) in the range $12 \leq BWR \leq 37.55$.

1a

UNCLASSIFIED

SECURITY CLASSIFICATION OF THIS PAGE(When Data Entered)

AN ANALYSIS OF LINEAR AND NON-LINEAR COHERENT DETECTION IN
ATMOSPHERIC NOISE AT VERY LOW FREQUENCY

John T. Gamble

Approved for public release;
distribution unlimited.

FOREWORD

The motivation for this effort, begun in 1970, was the inadequacy of the available descriptions of coherent receiver performance in very low frequency (VLF) and low frequency (LF) atmospheric noise. Extensive on-air testing of coherent VLF/LF communication systems clearly showed that their real-world performance was far different from that calculated for and measured in white Gaussian noise. Moreover, modulator-demodulator (modem) systems designed to be optimum in Gaussian noise are not necessarily optimum in atmospheric noise. Hence, a quantitatively accurate characterization of coherent detection in VLF/LF atmospheric noise would provide the capability of accurately assessing system performance and a basis for developing optimum real-world modem and receiver systems.

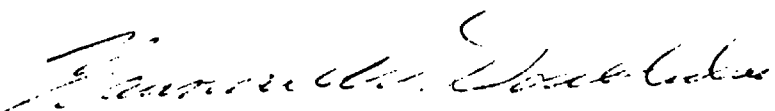
The author is greatly indebted to Dr. Donald Weiner of Syracuse University for his encouragement and conscientious, constructive counsel throughout this effort, and is especially appreciative of his suggestions and guidance in developing usable simplifying assumptions and approximations which helped make the analyses tractable.

Also of great value were the constructive criticisms of the evolving study provided by Alfred D. Paoni, David A. Kocyba, and Stanley J. Kraszewski; and the computer data handling assistance provided by Captain William A. Acree, Wayne Bonser, and Eugene Jakubowski.

This report has been reviewed by the Office of Information (OI), RADC, and approved for release to the National Technical Information Service (NTIS). At NTIS it will be available to the general public, including foreign nations.

This report has been reviewed and is approved for publication.

APPROVED:



LAURENCE W. DOUBLEDAY
Chief, Communications Transmission Branch
Communications and Navigation Division

APPROVED:



FRED I. DIAMOND

Technical Director
Communications and Navigation Division

FOR THE COMMANDER:



CARLO P. CROCETTI

Chief, Plans Office

ABSTRACT

This report is concerned with the performance analysis of coherent modems in atmospheric noise. Specifically, Phase Shift Keying (PSK, biphase), Coherent Frequency Shift Keying (CFSK), and Minimum Shift Keying (MSK) modems are described and analyzed for error rate performance in the non-Gaussian, impulsive, atmospheric noise typical of a very low frequency (VLF) radio communication channel. The analyses include both linear and non-linear (band-pass, hard-limiting) pre-detection signal processing. In each case experimentally derived error rate performance data is presented which shows close agreement with the computational results of the analyses.

The first part of the analysis is a survey of atmospheric noise representations. This includes descriptions of the power-Rayleigh first order statistical model used in the linear and pseudo-linear (large bandwidth ratio, hard-limiting receiver) analyses and the filtered Poisson impulse process used in the analyses of small bandwidth ratio, hard-limiting receivers. Following a complete description of the modulation and demodulation processes for the three systems, a numerical procedure is developed for evaluating linear-system error probabilities. Next, the Pulse Statistical Analysis (PSA) technique (employing a filtered Poisson impulse process with monotonically related, power-Rayleigh distributed pulse amplitudes) is developed and shown to be quantitatively valid for hard-limiting receivers where the bandwidth ratio (ratio of limiter bandwidth to detection bandwidth) is less than 8.

Finally, the Impulsive Noise Subtraction (INS) technique is developed in which enhancement of signal-to-noise ratios by hard-limiting is calculated and the residual (post-limiting) noise statistics are obtained by "best-fit" numerical convolution techniques. Employment of these residual signal and noise statistics in linear performance analyses is shown to yield quantitatively accurate error rate performance data for a bandwidth ratio (BWR) in the range

$12 \leq \text{BWR} \leq 37.55.$

TABLE OF CONTENTS

TABLE OF CONTENTS	v
LIST OF ILLUSTRATIONS	xiii
LIST OF TABLES	xvii
LIST OF ABBREVIATIONS	xviii
Chapter 1 INTRODUCTION	1
Sec 1.0 General	1
1.1 Object of the Investigation	3
1.2 The Report	3
1.3 Significance of the Analyses	5
1.4 Background	6
1.4.1 Analysis by Beach and George	9
1.4.2 Modem Performance in VLF Atmospheric Noise by Omura and Shaft	10
1.4.3 QPSK Performance Estimates by Linfield and Beach and Hartley	13
1.4.4 Analysis of PSK Performance by Sisco	14
1.4.5 PSK and DPSK Performance in Impulsive Noise by Bello and Esposito	15
1.4.6 Matched Filter Performance in Non-Gaussian Noise by Lindenlaub and Chen	16
1.4.7 Experimental Data by Mallinckrodt	17
1.4.8 Summary	18
1.5 Organization	18

Chapter 2	ATMOSPHERIC NOISE - DESCRIPTION AND MODELS	23
Sec 2.0	Introduction	23
2.1	Atmospheric Noise Representations	23
2.2	Noise Models	25
2.2.1	Empirical Description of the Atmospheric Noise APD by Crichlow, <u>et al</u>	26
2.2.2	Log-Normal APD Description by Peckmann	31
2.2.3	Noise Model of Beach and George	34
2.2.4	Poisson and Poisson-Poisson Noise Model of Furutsu and Ishida	36
2.2.5	Amplitude Distributions of VLF Noise by Janis Galejs	36
2.2.6	Modeling of Atmospheric Noise by Giordano	40
2.2.7	Multiplicative Noise Model by Hall	41
2.2.8	Noise Model Summary	42
2.3	Noise Model for Coherent Modem Analysis	43
2.3.1	Linear and Pseudo-Linear (Large BWR, Hard-Limiting) Receiver	44
2.3.2	Hard-Limiting, Small BWR Receiver	49
Chapter 3	COHERENT MODULATION - DEMODULATION (MODEM SYSTEMS FOR VERY LOW FREQUENCY (VLF) AND LOW FREQUENCY (LF) RADIO COMMUNICATION	62
Sec 3.1	General	62
3.2	Coherent Phase Shift Keying (PSK) Modem	66

3.3	Coherent Frequency Shift Keying (CFSK, M = 1) Modem	73
3.3.1	CFSK Post-Detection Signal-to-Noise Ratio	79
3.3.2	Relationship of CFSK Post-Detection Noise to PSK Post-Detection Noise	83
3.3.2.1	Equivalent Noise Bandwidths of PSK and CFSK Detectors	83
3.3.2.2	Numerical Estimation of the Statistics of CFSK Post-Detection Noise	86
3.3.2.2.1	Partition of the PSK Detector Noise Functional into Statistically Independent Voltages	86
3.3.2.2.2	Synthesis of the CFSK Detector Noise Functional	92
3.4	Minimum Shift Keying (MSK) Modem	96
3.4.1	MSK Modulation	96
3.4.2	MSK Detection	100
Chapter 4	PERFORMANCE OF LINEAR COHERENT VLF/LF RECEIVERS IN ATMOSPHERIC NOISE	107
Sec 4.0	Introduction	107
4.1	Development of Numerical Procedures for Evaluating Error Probabilities	108
4.1.1	Performance of the Linear PSK Receiver in Atmospheric Noise	109
4.1.2	Performance of the Linear CFSK, M = 1 Receiver in Atmospheric Noise	118

4.1.3	Performance of the Linear MSK Receiver in Atmospheric Noise	119
4.2	Validation of the Theoretical Analysis	119
4.2.1	Convergence and Comparison in Gaussian Noise	119
4.2.2	Atmospheric Noise Performance	120
4.2.2.1	Linear PSK Detection	123
4.2.2.2	Linear CFSK, $M = 1$ Detection	123
4.2.2.3	Linear MSK Detection	126
4.2.2.4	Summary	126
4.3	Optimum Linear System	128
Chapter 5	COHERENT DETECTION IN ATMOSPHERIC NOISE WITH PRE-DETECTION HARD-LIMITING PULSE STATISTICAL ANALYSIS (PSA)	132
Sec 5.1	General	132
5.2	Pulse Statistical Analysis	133
5.2.1	Coherent Detection with Hard-Limiting - One Pulse per Detection Element	133
5.2.1.1	PSK Detection	133
5.2.1.2	CFSK Detection	146
5.2.1.3	MSK Detection	171
5.2.2	Coherent Detection with Hard-Limiting and Multiple Noise Pulses per Detection Element	173
5.2.2.1	The Noise Envelope Voltage for Multiple Noise Pulses	173

5.2.2.2	Real Axis Projection of the Sum of N Independent Vectors of Equal Magnitude	174
5.2.2.3	Multiple Noise Pulses in the PSK Functional	181
5.2.2.4	Multiple Noise Pulses in the CFSK Functional	198
5.2.2.5	Multiple Noise Pulses in the MSK Functional	203
5.2.3	Evaluation of Probability of Decision Error	204
5.2.3.1	Determination of the Average Number of Impulsive Noise Pulses per Decision Element	206
5.2.3.2	Voltage Level Crossing Rate of the Envelope of Gaussian Noise	206
5.2.3.3	Relationship Between Rayleigh and Power- Rayleigh Crossing Rates	208
5.3	Evaluation of Experimental Systems	212
5.3.1	Character Error Rates	212
5.3.2	Experimental System	215
5.3.3	Effect of "Clustering" Pulse Distribution	225
5.4	Bandwidth Ratio Constraint	229
5.4.1	"Critical Pulsewidth" Versus Bandwidth Ratio (BWR)	231
5.4.2	Experimental Validity of PSA for BWR's Greater than 4	234
Chapter 6	IMPULSIVE NOISE SUBTRACTION	237
Sec 6.1	Background	237
6.2	Noise Power Reduction	239
6.2.1	Impulsive Noise Subtraction	239

6.2.2	"Small Signal" Noise Power Reduction by Cahn	241
6.2.3	"Small Signal" PSK Noise Reduction	244
6.2.4	Discussion of Noise Power Reduction Estimates	244
6.3	The Atmospheric Noise Voltage as a Sum of Statistically Independent Components	245
6.3.1	General	245
6.3.2	Determination of the Probability Densities of the Total and Impulsive Noise Voltages	247
6.3.3	Qualitative Estimate of the Residual Noise Component	254
6.3.4	"Best Fit" Synthesis	256
6.3.5	Numerical Convolution Process	257
6.3.6	Estimation of Residual Noise Statistics	260
6.4	Application of Impulsive Noise Subtraction to System Analysis	265
6.4.1	Example 1. (Hartley's Experimental Results)	267
6.4.2	Example 2. (Linfield and Beach's Experimental Results)	268
6.4.3	Example 3. (Small Bandwidth Ratio Experimental Results)	270
Chapter 7	CONCLUSIONS AND RECOMMENDATIONS	275
Sec 7.1	Overview	275
7.2	Results and Conclusions	275
7.2.1	Linear Systems Analyses	275

7.2.1.1	Coherent PSK Detector Functional	276
7.2.1.2	Coherent FSK ($M = 1$) Detector	276
7.2.1.3	MSK Detector	276
7.2.1.4	Experimental Validation of the Linear Performance Calculations	277
7.2.1.5	Comparison of Linear Systems	277
7.2.2	Non-Linear (Hard-Limiting Receiver) System Analyses	278
7.2.2.1	Analyses of Small Bandwidth Ratio (BWR) Systems by Pulse Statistical Analysis (PSA)	278
7.2.2.1.1	PSA Development	279
7.2.2.1.2	Quantitative Convergence of Error Rates Computed by Poisson and "Clustering" Statistical Distribution	279
7.2.2.1.3	Experimental Validation of PSA for CFSK and CSK (MSK Detection) Systems	280
7.2.2.1.4	Performance Differential Between CFSK and CSK (MSK Detection) Performance	280
7.2.2.1.5	BWR Limitation of PSA	281
7.2.2.2	INS Development	281
7.2.2.2.1	Enhancement of Small Signal-to-Noise Ratios in Atmospheric Noise by Hard-Limiting	281
7.2.2.2.2	Residual Noise Component	282
7.2.2.2.3	Experimental Validation of the INS Technique	282

7.2.2.2.4	BWR Limitation of INS	282
7.2.2.3	General Conclusions Concerning Non-Linear System Performance	282
7.2.2.4	General Limitations of PSA and INS	283
7.3	Recommendations for Extensions and Additions to the Investigations	283
APPENDIX A	DERIVATIONS OF SELECTED INTEGRALS	285
APPENDIX B	STATISTICAL PROPERTIES OF THE RATIO OF AMPLITUDES OF INDEPENDENT IMPULSIVE ATMOSPHERIC NOISE PULSES	297
APPENDIX C	SMALL SIGNAL ANALYSIS OF HARD-LIMITING NOISE REDUCTION IN THE PSK RECEIVER	303
APPENDIX D	TABLES OF DECISION ERROR RATES FOR LINEAR COHERENT PHASE SHIFT KEYING (PSK) DETECTION	317
BIBLIOGRAPHY		340

LIST OF ILLUSTRATIONS

Figure

1	Amplitude Probability Distributions of the Envelope of Atmospheric Noise	27
2	Bandpass Filter	57
3	Coherent Phase Shift Keying (Biphase PSK) Detector	66
4	Coherent Frequency Shift Keying (CFSK, M = 1) Detector	74
5	Probability Densities for Atmospheric Noise	89
6	MSK Modulation/Demodulation Waveforms	97
7	MSK Detector	101
8	Linear Coherent Phase Shift Keying (PSK) Detector Performance in Atmospheric Noise, $V_d = 3.75$ dB	124
9	Linear Coherent Frequency Shift Keying (CFSK, M = 1), Detector Performance in Atmospheric Noise, $V_d = 3.75$ dB	125
10	Linear Minimum Shift Keying (MSK) Detector Performance in Atmospheric Noise, $V_d = 5$ dB	127

11	Linear Coherent Phase Shift Keying (PSK)	129
	Detector Performance in Atmospheric Noise	
12	Linear Coherent Phase Shift Keying (PSK)	130
	Detector Performance in Atmospheric Noise	
13	Hard-Limiting PSK Receiver	134
14	Hard-Limiting CFSK Receiver	147
15	Arguments of $\cos^{-1} [\cdot]$ in the CFSK Detector Functional	168
16	Complementary Probability Distributions for $\sum_{i=1}^N \cos \theta_i$	180
17	Level Crossing Rate of Atmospheric Noise Envelopes	210
18	Receiver Subsystem	216
19	Normalized Bandwidth Factor for Noise Envelope Crossing Rate as a Function of Noise/Normal-Law Bandwidth Ratio	221
20	Pulse Statistical Analysis - Hard-Limiting Receiver Performance in Atmospheric Noise ($6 \text{ dB} \leq V_d \leq 7.9 \text{ dB}$ in 600 Hz)	225
21	Pulse Statistical Analysis - Hard-Limiting Receiver Performance in Atmospheric Noise ($8 \text{ dB} \leq V_d \leq 9.9 \text{ dB}$ in 600 Hz)	227
22	Pulse Statistical Analysis - Hard-Limiting Receiver Performance in Atmospheric Noise ($12 \text{ dB} \leq V_d \leq 13.9 \text{ dB}$ in 600 Hz)	228

23	Pulse Statistical Analysis - Hard-Limiting Receiver Performance in Atmospheric Noise. Error Rates Computed According to Poisson and Clustering Distributions ($8 \text{ dB} \leq V_d \leq 9.9 \text{ dB}$ in 600 Hz, $K = 1$)	230
24	Pulse Statistical Analysis - Hard-Limiting CFSK Receiver Performance in Atmospheric Noise for a Bandwidth Ratio of 12	235
25	Impulsive Noise Power Reduction	242
26	Atmospheric Noise APD Curve Showing Impulsive Component APD	246
27	Noise Probability Densities, Atmospheric Noise Voltage, Z , and Its Impulsive Component, i_n	250
28	Probability Densities for Impulsive, i_n , and Residual, r_n , Noise Voltages	262
29	Probability Densities for Atmospheric, Z , and Synthesized, Z' , Noise Voltages	263
30	V_d Ratio of the Residual Noise Component Resulting from Impulsive Noise Subtraction Vs. Input Noise V_d Ratio	264
31	CFSK Hard Limiting Receiver Performance in Atmospheric Noise Computed by Impulsive Noise Subtraction (INS)	269

32	CFSK Hard-Limiting Receiver Performance in Atmospheric Noise Computed by Impulsive Noise Subtraction (INS)	271
33	CFSK and CSK System Performance as Measured and as Computed by Pulse Statistical Analysis (PSA) and Impulsive Noise Subtraction (INS)	274

LIST OF TABLES

Table

I	V _d Ratios of Additive Independent Noise Voltages and Estimated Noise Bandwidth Ratios (BWR)	91
II	Probability of Detection Error for Coherent PSK in White Gaussian Noise (Rayleigh Envelope)	121
III	Residual Noise Output of Bandpass Hard Limiter	265

LIST OF ABBREVIATIONS

APD	Amplitude Probability Distribution	11
ASK	Amplitude Shift Keying	2
BWR	Bandwidth Ratio (Limiter Bandwidth/ Detection Bandwidth)	5
CER	Character Error Rate	122
CFSK	Coherent Frequency Shift Keying	3
CSK	Compatible Shift Keying	212
DPSK	Differential PSK	7
dB	Decibel	1
FSK	Frequency Shift Keying	2
Hz	Hertz	2
kHz	Kilohertz	1
INS	Impulsive Noise Subtraction	5
LF	Low Frequency	1
MHz	Megahertz	1
MSK	Minimum Shift Keying	3
PSA	Pulse Statistical Analysis	5
PSK	Phase Shift Keying	3
S/N	Signal-to-Noise Power Ratio	243
RIC	Receiver Impulse Characteristic	15
VLF	Very Low Frequency	1
V_d	Ratio of RMS to Average Noise Envelope Voltages	11

Chapter 1
INTRODUCTION

1.0 General

Practical radio communication was first implemented at frequencies below 1 MHz. However, because of the substantial atmospheric noise environment and physically massive, but electrically small, transmitting antennas required for this range, subsequent technology has emphasized higher frequency systems. Nevertheless, very low and low frequency (VLF/LF) communication systems in the 10-100 kHz band are still the most reliable means of very long range surface to surface communications. Some of the attractive characteristics of radio transmission in the VLF/LF band are: (1) Very low propagating signal attenuation rates - on the order of 2-5 dB per Megameter [54]; (2) Minimal signal fading where the maximum fluctuations are on the order of a few decibels and the rates are on the order of decibels/hour; (3) Very high signal phase stability which makes coherent modulation/demodulation a practical approach. On the other hand, the previously mentioned drawbacks are quite significant. The massive transmitting antenna structures use vertical elements of over 200 meters and horizontal current distribution elements (overhead "top-hats" and ground planes) which occupy areas of hundreds of acres per station. Even so, the antennas are electrically small and efficiencies above 10 percent are achieved usually at the cost of antenna bandwidths which are on the

order of 10 - 100 Hz. Because of these minimal VLF/LF radiation system bandwidths, only binary teletype signalling is practically employed. Moreover, the narrow system bandwidths lead to the use of phase-continuous, constant-envelope, angle-modulation for the teletype data transmission. (in particular, Frequency Shift Keying (FSK) rather than on-off or Amplitude Shift Keying (ASK) is typically used on the more modern systems.) The other limiting constraint is the noise environment. Here the average atmospheric noise power is approximately proportional to the inverse square of frequency [26] down to 20 kHz and it becomes increasingly impulsive at the lower frequencies. This high-level impulsive ambient noise is the usual limiting factor on VLF/LF communication system range. It is especially significant that, in spite of many years' experience in VLF/LF radio communications, there has been relatively little performance analysis of VLF/LF communications systems in the ambient atmospheric noise. This is especially true in regard to modern coherent modem systems. The reasons for this deficiency are: (1) the aforementioned emphasis on higher frequencies for radio communication; (2) the practical difficulty of mathematically representing the atmospheric noise process, which is non-Gaussian and non-stationary over any extended period; and (3) the non-linear receiver techniques used to optimize signal demodulation which complicate the analysis.

1.1 Object of the Investigation

The purpose of this study is to develop a practical means of analyzing the performance of advanced VLF/LF coherent receivers in atmospheric noise. The analysis includes both linear and non-linear pre-detection signal processing. The quantitative end product of these analyses is bit (or decision) error rate as a function of received signal to noise ratio. However, in arriving at a viable analysis which produces meaningful error rate data, there are some important considerations. First, the analytical procedure must account for the non-Gaussian nature of atmospheric noise and yet be consistent with performance analyses of these systems in Gaussian noise. It must include the effects of receiver band pass filtering. It must accurately depict the receiver non-linearities. Finally, and most significantly, the computed results should be consistent with the available, even if limited, measured performance data.

1.2 The Report

This report presents the basis and results of a comprehensive error-rate performance analysis of three coherent VLF/LF modulator/demodulator (Modem) systems in atmospheric noise. The coherent modem systems considered include: (1) Coherent Phase Shift Keying - 2 phase (PSK); (2) Minimum Shift Keying (MSK); and (3) Coherent Frequency Shift Keying (CFSK). All three of these systems employ angle modulation and maintain a constant signal envelope. However, only the latter two, MSK and CFSK, are characterized by the phase-continuous waveform necessary for compatibility with the high-Q transmitting systems. The PSK analysis is included because it is relatively simpler and provides

a basis for the analysis of the more practical MSK and CFSK systems. (A detailed description of all of these systems is provided later.) The study includes both linear and non-linear pre-detection signal processing in the receivers. Here, the term "linear" implies that signal mixing results only in frequency translation of signal plus noise, band-pass filters are passive and thus linear, and amplifiers are operating in a linear range. The non-linear receiver considered employs a band-pass hard limiter preceding the coherent detector(s). (This type of noise suppression has been shown experimentally [35] to be superior to more moderate clipping or "hole-punching" [or blanking] in low frequency atmospheric noise. Moreover, other operational experience at VLF/LF has indicated that the hard-limiting of signal plus atmospheric noise tends to minimize the effects of the atmospheric noise.)

Overall, this report consists of three major areas: (1) the basis of the analysis; (2) the development of mathematical expressions for the computation of error rates; and (3) presentation of computed error rates and their comparison with experimentally derived data. As an introduction to the performance analysis a survey of the various atmospheric noise representations is presented along with a careful description of the noise process actually used in the subsequent analysis. Likewise, there is a complete description of the signal modulation and demodulation processes for the three modems to be analyzed. The analysis, per se., is divided into two parts: (1) linear receiver detection, and (2) hard-limiting receiver detection.

In turn, the analysis of the non-linear hard-limiting receiver is divided into two general cases: (1) the case where the ratio of the limiter bandwidth to the detection bandwidth (BWR) is small (i.e., $BWR \leq 8$) for which the method of Pulse Statistical Analysis (PSA) is applicable, and (2) the case where BWR is large and the technique of Impulse Noise Subtraction (INS) is applicable. In each of these two parts, the available measured performance data is compared with the computed performance of the PSK, CFSK, and MSK detection systems.

1.3 Significance of the Analyses

As a consequence of the lag in developing comprehensive useful analyses of VLF/LF communication system performance, the design of optimum modem and receiver techniques has similarly lagged. Thus, to overcome the deleterious effects of atmospheric noise, VLF/LF system designers have often gone to the expedient of very high transmitter powers to compensate for inefficient modem techniques and receivers whose performance is drastically degraded by impulsive noise. Such systems may have some success but are inefficient. More recently, useful analyses for linear detection of non-coherent FSK and coherent PSK have been developed [39], [45], [48], [37], [14]. On the other hand, practical coherent VLF/LF modems have had only minimal analytic consideration in the literature. Only the work of Beach¹ [3] and Omura and Shaft² [42] deal with CFSK performance and these results are

¹The computed results were judged to be useful for qualitative comparisons of receiver techniques, but were quantitatively divergent from measured data. ([3], p: 196)

²Similarly, the computations are conceded to achieve "only modest agreement between theoretical and experimental results". ([42], p: 667)

quantitatively inaccurate for the more optimum non-linear receiver systems. Moreover, there has been no analytical consideration of the performance of the MSK system in atmospheric noise. The analysis in this dissertation of MSK modem performance in atmospheric noise is especially significant in that it shows MSK to be substantially more efficient than the CFSK system. Furthermore, it provides a good quantitative description of coherent system performance as improved by hard-limiting atmospheric noise reduction. The analyses presented here of these advanced, but practical, VLF/LF coherent modem systems provide a quantitative basis for the design and operation of VLF/LF communication systems.

1.4 Background

In order to put the present analysis in perspective, it is appropriate to review the more significant available experimental and analytical data on the performance of the PSK, CFSK, and MSK modems. These earlier contributions can be conveniently divided as follows:

- (1) Modem performance in Gaussian noise with linear signal processing;
- (2) Modem performance in atmospheric noise with linear signal processing; and
- (3) Modem performance in atmospheric noise with non-linear signal processing (especially noise clipping).

The performance of coherent PSK modems in Gaussian noise has been mathematically described throughout the literature [50], [24]. Because the Gaussian noise process is mathematically tractable for linear systems, theoretical analyses coincide fairly accurately with experimental measurements. The reason for this success is due

fact that, in a linear receiver system, the input signal plus Gaussian noise process results in a Gaussian random variable at the detector output. Similarly, the linear CFSK receiver produces a detector output which is a Gaussian random variable when the receiver input is a signal plus Gaussian noise process. Such analyses have been described by numerous authors [50], [29], [33]. Analyses of linear MSK detection are not so widely available - perhaps because of the more recent development of this technique. Nevertheless, Linfield and Beach [33] have provided an adequate analysis of the linear MSK receiver.

Proceeding to a consideration of analyses of linear receivers in atmospheric noise, we find the literature to be far from replete.

In fact, the only analytical techniques are addressed to PSK, differential phase shift keying (DPSK), and non-coherent FSK systems. Conversely, the only significant experimental results in VLF/LF atmospheric noise are for the CFSK and non-coherent FSK systems.

An analytical treatment of non-coherent FSK [14], [22] is an illustration for atmospheric noise of the technique proposed by Tydmore [39] for Gaussian noise. This analysis uses the reasonable assumption that a binary detection error will occur half the time the noise envelope exceeds the signal envelope. Thus, the bit error rate becomes one-half the probability that the noise envelope exceeds a voltage level equivalent to the signal voltage. (Omura and Shaft [42] produced similar numerical results by calculating the error rate of a non-coherent log-normal, rather than Rayleigh, fading channel in Gaussian noise. However, their method is not justified on a

theoretical basis.) Unfortunately, Montgomery's technique cannot be applied directly to the analysis of coherent detection in atmospheric noise. Here the method described generally by Spaulding [48] and more specifically by Shepelavey [45], does provide a means of determining the error rate performance of coherent PSK systems in atmospheric noise. This technique has been adapted in this study to the analysis of linear CFSK and MSK systems and a detailed description is included in Chapter 4. A subsequent study of Spaulding [49] considers the DPSK system in atmospheric noise. Overall then, the literature contains techniques for the analysis of linear non-coherent FSK, coherent PSK, and DPSK receivers but does not provide any analytic treatment of linear CFSK and MSK receivers in atmospheric noise. Because of the sub-optimum nature of non-coherent FSK (with respect to CFSK and especially MSK) and the unsuitability of PSK and DPSK for VLF transmission, this constitutes a significant gap in the analysis of linear VLF/LF modem techniques.

In the realm of experimental results, the only experimental performance results for linear coherent VLF/LF systems are the measured PSK data of Linfield and Plush [32] and the CFSK data of Entzminger, etal [14]. On the other hand, experimental performance data for non-coherent FSK is presented in various sources [14], [33], [53]. As before, the more optimum coherent systems are not described. Thus, it must be conceded that there is a dearth in both experimental and analytical performance data of linear coherent VLF/LF modem performance.

Although the analytical and experimental descriptions of linear CFSK and MSK modem performance in VLF/LF atmospheric noise leave much to be desired, the available treatments of non-linear CFSK and MSK modem performance in atmospheric noise are even less satisfactory. The analyses by Beach and George [3] and Omura and Shaft [42] of CFSK performance are quantitatively divergent from measured experimental results. Similarly, the CFSK performance estimates by Linfield and Beach [33] and Hartley [22] do intersect their experimental results, but only at one point (See Chapter 6). Other analytical treatments of non-linear modem performance in impulsive noise have been provided by Sisco [46] and Bello and Esposito for PSK [5] and DPSK [6] and by Lindenlaub and Chen for PSK [30]. Experimental performance data for hard-limiting reception and detection of CFSK in atmospheric noise is also presented by Linfield and Beach [33] and Hartley [22]. Other significant experimental data includes that of Mallinckrodt [35] for DPSK reception using noise-clipping and noise-blanking receivers in low frequency atmospheric noise. A brief discussion of these results is provided in the following paragraphs.

1.4.1 Analysis by Beach and George [3]

This study of modem performance in impulsive atmospheric noise addressed coherent PSK and FSK reception and non-coherent FSK reception. It further considered the effect of peak clipping at various levels, logarithmic limiting (suggested by Hall [20] to provide optimum efficiency in the face of his proposed noise model as discussed in Chapter 2), and "hole-punching", or noise-blanking. The error rate analyses are based on a pulse statistical noise model whereby the

detector functionals (time integrals of the signal plus noise processes) are expressed in terms of a truncated Edgeworth series. The resultant computed error rates for CFSK with limiting and noise blanking are substantially lower than have been achieved experimentally. Moreover, for the peak-limiting receiver, as the limiter voltage threshold increases (tending toward linear receiver operation), the error rate characteristics tend toward the same shape as that produced by Gaussian noise. This is the reverse of the experimentally observed effect where the error rate curve steepens in slope (toward that produced by Gaussian noise) as the limiter threshold is lowered (toward a hard-limiting effect) [33]. This quantitative and qualitative divergence of the analysis from known system performance is acknowledged in the study. Unfortunately, no means of rectifying the difficulties associated with this relatively sophisticated analytical model have evolved.

1.4.2 Modem Performance in VLF Atmospheric Noise by Umura and Shaft [42]

This study of modem performance in atmospheric noise addresses both linear and non-linear (clipping) reception of coherent FSK and PSK and non-coherent FSK signals. It further categorizes the linear systems as either "long integration time" (narrow detection bandwidth), where the bit rate is small enough to permit signal integration over many noise pulses, or "short integration time", where the bit rate is comparable to the reciprocal of the mean duration of noise pulses. To accommodate these different conditions, separate analyses are presented. However, all are based on the Log-Normal Noise Model which is described in Chapter 2. The paper first addresses the "long integration time" linear case and, employing the central limit theorem

in assessing the additive effect of multiple noise pulses per bit, treats the noise as being nearly Gaussian. A similar result is also obtained by employing the procedure of Crichlow, et al [11] (or utilizing Figure 26 of CCIR-322 [26]) for converting the amplitude probability distribution (APD) of wideband impulsive noise to the near-Gaussian APD consistent with a narrow detection bandwidth. The "short integration time" linear analysis employs two approaches: (1) a log-normal fading noise model for non-coherent FSK, and (2) direct integration of the detector functional for PSK using the assumed log normal noise envelope distribution (direct integration of a PSK detector functional is also employed in this dissertation in the linear system analysis of Chapter 4). Finally, the paper considers the effect of signal and noise clipping in atmospheric noise. The approach here is to apply a noise reduction factor and a corresponding signal suppression factor for the clipping process to the signal and noise terms of the expressions used for computing Gaussian-noise error probabilities.

The linear "long integration time" analysis, based upon central limit theory or Crichlow's noise bandwidth conversion principle, is only approximate for even a very narrowband communication system. For example, let the V_d ratio be defined as $V_d = \sqrt{e^2/\bar{e}^2}$ where \bar{e}^2 is the mean square envelope voltage and e is the average envelope voltage of the noise process. CCIR 322 [26] shows the average V_d ratio of summer noise at 20 kHz to be greater than 10 dB in a 200 Hz bandwidth. The effect of integrating the noise is to make it more Gaussian in character. Gaussian noise has a V_d ratio of 1.049 dB.

From Figure 26 of CCIR 322, a bit integration time of over 5 seconds is required to achieve a V_d ratio of 1.5 dB in the detection bandwidth. This corresponds to the inordinately slow teletype channel rate of .286 words per minute.

Figure 11 of this study report shows the error rate response of a coherent PSK modem in both Gaussian noise ($V_d = 1.049$ dB) and in atmospheric noise ($V_d = 1.5$ dB). These curves illustrate the relative precision of the approximation. The log normal fading noise model used for the analysis of linear, "short integration time" non-coherent FSK is shown to provide results comparable to those produced by Montgomery's method [14], [22] and in good agreement with measured experimental data. However, as the authors state, this procedure is not justifiable on a theoretical basis. The other "short integration time" analysis - that of the linear coherent PSK system - produces results practically the same as those derived for linear PSK in this study (See Chapter 4). However, their choices of V_d equal to 5 and 10 dB do not provide the best basis for comparison with the published measured data which has a V_d ratio of 3.75 dB as referenced to the detection bandwidth of 33.33 Hz [32]. Figure 8 of this report provides a comparison for $V_d = 3.75$ dB. Finally, the analysis of coherent FSK performance in a clipping receiver leads to system performance computations which are conceded to have only modest agreement with experimental data. The best agreement occurs using published experimental data obtained by Hartley and computed performance for a clipping receiver where the clipping level was expediently chosen to be 12 dB above the signal. (The authors point out that Hartley's

clipping level was "not stated".) However, Hartley specifically described the receiver as employing "a hard amplitude limiter in the output stage which produces a square-wave type output". Thus, the 12 dB clipping level employed in the computational model is clearly inappropriate for comparison with Hartley's experimental data. Hence, the implied close agreement of experimental and theoretical results is not demonstrated.

In conclusion, the most quantitatively useful contribution of the article is the analysis of linear coherent PSK detection. The analysis of narrowband linear systems which employs the Gaussian noise approximation is reasonably accurate, but such systems are unlikely to be used for practical VLF communication. Unfortunately, the analysis of coherent modems with receiver limiting (which is, by far, the most significant and practical for optimized VLF communication systems) is of very minimal accuracy.

1.4.3 CFSK Performance Estimates by Linfield and Beach [33] and Hartley [22]

The essence of the coherent FSK performance estimates by Linfield and Beach [33] and by Hartley [22] is the observation that receiver noise limiting (especially hard limiting) increases receiver system detection efficiency in atmospheric noise and causes the error rate characteristic to become steeper. These estimates employ a noise reduction factor which translates the error rate response characteristic to account for the improvement in efficiency and represents the error rate characteristic by that obtained in white Gaussian noise. Although the experimental data yields an error rate response which is steeper

than that obtained in a linear system, the slope is not as steep as that obtained with white Gaussian noise. It follows that a noise reduction factor can be determined either empirically or by analytical estimates such that the Gaussian response agrees with the experimental results at one point. However, the difference in response slopes makes this estimation method relatively inaccurate over any significant range of error probabilities. It should be noted, however, that the measured experimental data included in the articles does provide an invaluable basis for validating some of the computational results developed later in this report.

1.4.4 Analysis of PSK Performance by Sisco [45]

This study investigated the effect of limiting on the performance of a coherent PSK detector in MF (450 kHz) atmospheric noise. First, an estimate of linear modem performance is proposed wherein the noise voltage is assumed to be 3 dB below the noise envelope voltage, but similarly distributed. Using this 3 dB noise power reduction, Montgomery's method [39] is then applied to determine the appropriate error probability. This procedure, in effect, estimates the performance of the coherent linear PSK detector to be 3 dB more efficient than a corresponding differentially coherent PSK detector whose error rate (as estimated by Montgomery's method) is $1/2$ the probability that the noise envelope is greater than the signal. This technique, at best, is grossly approximate since the noise voltage and noise envelope voltage have drastically different probability densities. In the case of receiver limiting, a performance estimate is obtained as follows:

(1) The "clipped-noise" APD is numerically integrated to determine the noise power reduction; and (2) the linear-receiver bit-error rate characteristic, as described earlier, is adjusted by this noise reduction estimate. The quantitative results of this procedure differ greatly from the measured experimental data. As might be expected, this translation of an already questionable linear performance characteristic to account for the non-linear receiver response yields an equally questionable result for the non-linear system.

1.4.5 PSK and DPSK Performance in Impulsive Noise by Bello and Esposito [5], [6]

These studies present a theoretical investigation of coherent and differentially coherent PSK detection by linear and hard-limiting receivers in impulsive noise. The analysis is based on: (1) the derivation of the Receiver Impulse Characteristic (RIC) defined by

$$R_k(\Gamma, \delta) = \frac{1}{(2\pi)^k} \int_0^{2\pi} \dots \int_0^{2\pi} P_k(E|\Gamma, \delta, \psi) d\psi$$

where $R_k(\Gamma, \delta)$ is the Kth order RIC, Γ is a K-dimensional noise pulse amplitude vector, δ is a K-dimensional pulse occurrence time vector, ψ is a K-dimensional noise phase vector, and $P_k(E|\Gamma, \delta, \psi)$ is the conditional error probability given that K noise impulses occur per bit (with the parameters Γ, δ, ψ); and (2) the application of the various order RIC's in an overall error probability expression given by:

$$P_e = \sum_{k=1}^{\infty} P_k \int_{\Gamma} \int_{\delta} R_k(\Gamma, \delta) W_k(\Gamma, \delta) d\Gamma d\delta \quad (1)$$

where P_k is the probability that exactly K noise pulses occur, and w_k is the joint density function of the parameters Γ, δ .

Because of the formidable nature of the above expressions for $K > 1$, this procedure was applied for $K = 1$ only to linear and hard limiting receivers. Here the numerical results imply limiter improvement of detection efficiencies in log-normally distributed noise by factors greater than 40 dB. This is much greater than has been achieved in practice at VLF and implies that the first order solution of (1) is insufficient for VLF; unfortunately, the higher order statistics for VLF atmospheric noise are not available. It should be pointed out, however, that the pulse statistical analysis (PSA) developed later in Chapter 5 of this report might be obtained by suitable extension and modification of the RIC approach.

1.4.6 Matched Filter Performance in Non-Gaussian Noise by Lindenlaub and Chen [30]

This was an investigation of the performance of a matched filter (synchronous coherent) PSK detector in Gaussian noise plus impulsive noise. The investigation was both mathematical and experimental. Because the direct sum of white Gaussian noise and impulse noise as used in the study has some resemblance to the VLF atmospheric noise process, it provides some insight as to the expected performance of coherent detectors in an atmospheric noise environment. The general conclusion of the study, that the signal-to-noise ratio required for a given bit error rate in the impulsive noise is much greater than that required for Gaussian noise, is consistent with observed error rate

performance in atmospheric noise. A corollary conclusion of this paper is that a limiter preceding the matched filter detector drastically reduces the degradation produced by the impulsive noise, but does not significantly affect that caused by the additive Gaussian noise. The efficacy of this procedure has also been observed in atmospheric noise. However, because no combination of Gaussian and impulsive noise processes has been demonstrated thus far to be equivalent to atmospheric noise, the analytical portions of this study are not directly applicable to the real-world atmospheric noise environment.

1.4.7 Experimental Data by Mallinckrodt [5]

In addition to the previously mentioned measured performance data of Linfield and Plush (Linear PSK) [32], Linfield and Beach (Coherent FSK in a limiting receiver) [33], Hartley (Linear Non-Coherent FSK, Coherent FSK in a limiting receiver) [22], Entzinger et al (Linear Non-Coherent FSK, Linear Coherent FSK) [14], a significant experimental contribution has been made by Mallinckrodt [35]. This effort measured the effect of receiver limiting and noise blanking on differential PSK detection efficiency at low frequency. This carefully controlled measurement program established that both limiting and noise-blanking greatly reduce the deleterious effects of impulsive atmospheric noise. More significantly, however, it quantitatively demonstrated the superiority of noise limiting over noise blanking for performance enhancement. Moreover, it showed that hard limiting invariably equalled or surpassed any other noise clipping or limiting strategy in improving system performance. The combination of this experimental finding and the wide operational prevalence of hard

limiting receivers (based on practical experience) has led to restricting the study in this report to linear and hard-limiting receiver systems.

1.4.8 Summary

Overall, it has been shown that the literature contains adequate analyses of the coherent PSK, CFSK, and MSK detectors in Gaussian noise. In atmospheric noise, the only quantitatively accurate analysis is for linear PSK detection. Although the PSK system is impractical for VLF communication (because of its incompatibility with the narrow-band transmitting systems), this analysis of PSK can be adapted to treat the more practical CFSK and MSK systems. In the realm of non-linear reception of signals in atmospheric noise, there has been no quantitatively satisfactory analysis of coherent modems. Even the work of Beach and George [3], which is the most careful analytical treatment of non-linear detection in VLF atmospheric noise, does not achieve close agreement with experimental results. Other analytical treatments, which employ modified Gaussian-noise performance descriptions, are even less descriptive of system performance in the non-Gaussian atmospheric noise environment.

1.5 Organization

This study addresses five essential topics in developing the overall analysis. Therefore, the remainder of the report is appropriately divided into six additional chapters. Five are analytical or descriptive and one consolidates the findings and conclusions. These

subsequent chapters are: (2) Atmospheric Noise - Description and Models; (3) Coherent PSK, CFSK, and MSK Modem Systems; (4) Analysis of Linear Coherent Modem Performance; (5) Pulse Statistical Analysis (PSA) - Predetection Hard-Limiting with a Small Bandwidth Ratio (BWR); (6) Impulsive Noise Subtraction - Predetection Hard-Limiting with a Large Bandwidth Ratio (BWR); and (7) Discussion of Results and Conclusions. The content of each of these chapters is briefly described below.

Chapter 2, which discusses the VLF noise environment, presents a general discussion of VLF atmospheric noise characteristics, a survey of atmospheric noise models, and a detailed description of the atmospheric noise parameters used in the subsequent analyses of this study. Because the purpose of this study is the quantitative description of modem performance and not the development or theoretical validation of noise models, primary reliance has been placed on empirical noise descriptions. Thus, the atmospheric noise representation emphasized in this chapter largely coincides with that empirically developed by Crichlow, et al [10], [11] and tabulated in CCIR 322 [26]. However, for the analysis of the hard-limiting, small BWR receiver, this representation is adapted to account for the amplitudes of individual noise pulses of a Poisson process.

Chapter 3 contains a functional and mathematical description of the Phase Shift Keying (PSK), Coherent Frequency Shift Keying (CFSK), and Minimum Shift Keying (MSK) modem systems. The functional descriptions are based upon simplified block diagrams and the mathematical descriptions include a definition of the signal structure and a

development of the detector functionals (outputs of the coherent or matched filter, detectors) for each of the systems. Finally, and possibly most significant, a quantitative relationship between detection and CFSK and MSK detection is developed. This result is essential to the subsequent analyses of linear CFSK and MSK in Chapter 4 and non-linear (predetection hard-limiting in a bandwidth wider than the detection bandwidth) CFSK and MSK in Chapter 5.

Chapter 4 presents an analysis of the coherent detection process in atmospheric noise where the receiving systems are linear (that is, where the predetection signal processing is linear). This analysis is based on the direct numerical evaluation of the PSK detector function and the application of the aforementioned results of Chapter 3 to obtain a description of CFSK and MSK detector performance. Here, measured experimental PSK data by Linfield and Plush [32] and CFSK and MSK data by Entzminger, et al [14] is presented with the corresponding computed performance to demonstrate the accuracy of these linear analyses.

Chapter 5 considers the analysis of modem performance where predetection hard-limiting is employed. This approach employs pulse statistical analysis (PSA) to calculate the "capture" effect of atmospheric noise pulses having random phase angles on the predetection limiter. The noise pulses in this analysis are assumed to be independently produced (thus implying a Poisson distribution for the number of pulses in a bit interval) and to have monotonically distributed amplitude (according to the appropriate amplitude probability distribution, APD) during each bit or detector-decision interval. Computational results of this procedure are presented which show a good correspondence to

experimental CFSK and MSK data for a bandwidth ratio (ratio of limiter bandwidth to detection bandwidth) of 3.7. Moreover, these computational results show a 5-6 dB difference in efficiency between CFSK and MSK detection which corresponds closely to the experimental results. This performance differential is not obtained by linear demodulation (see Chapters 3, 4); or predicted by Gaussian noise or modified Gaussian noise [42] analyses. The final part of this chapter is a theoretical and experimental demonstration that the PSA technique is not applicable to the analysis of hard-limiting systems where the bandwidth ratio (BWR) is substantially greater than 8.

As a consequence of the BWR limitation of the PSA technique presented in Chapter 5, the case where the BWR is large is considered separately in Chapter 6. Here, an approach, designated Impulsive Noise Subtraction (INS), is used to obtain computed detection performance of large BWR coherent systems. This approach employs the hypothesis that hard-limiting, in effect, selectively subtracts an impulsive noise component from the overall atmospheric noise. Three independent analyses are shown to predict similar signal-to-noise ratio enhancement factors in atmospheric noise and a "best fit" synthesis procedure is used to estimate the "residual noise" component which remains after the postulated impulsive noise subtraction. This "residual noise" plus signal is then analyzed by means of the noise bandwidth conversion procedures of CCIR 322 [26] and the linear system analytical results of Chapter 4. In two large BWR cases, where measured data is given in the literature, CFSK system performance computed by INS is in remarkably

close agreement. Conversely, however, a third example where the BWR = 3.7 demonstrates that the INS procedure is inappropriate for such small BWR's.

The overall findings of Chapters 4, 5 and 6 are consolidated and discussed in Chapter 7. Here, some general conclusions are drawn from the computational results. Foremost of these is that MSK detection is clearly superior to CFSK detection in atmospheric noise. Secondly, the computational results quantitatively verify the substantial improvement in detection efficiency produced by predetection limiting. Finally, the quantitative results clearly show the relative advantage of hard-limiting in the widest practical predetection bandwidth (here, the practical limitation is the need to have sufficient receiver selectivity to exclude other VLF signals and man-made interference).

Chapter 2

ATMOSPHERIC NOISE - DESCRIPTION AND MODELS

2.0 Introduction

Atmospheric noise at very low frequency (VLF) and low frequency (LF), specifically in the range 10-100 kHz, is the principal constraint on efficient signal detection at these frequencies. Because of the excellent radio propagation which characterizes this frequency range, the atmospheric noise produced by lightning discharges - even at great ranges - is received at amplitudes usually much greater than receiver-system generated noise. Thus, the ambient atmospheric noise is the predominant natural noise component in the input of a typical VLF/LF receiver. This atmospheric noise is highly impulsive and non-stationary over any extended time interval (greater than 10-15 minutes). Its impulsiveness is further characterized by high dynamic range on the order of 60 dB or more. On the other hand, the low amplitude "background component" of the atmospheric noise tends to be nearly Gaussian (Rayleigh envelope) in nature. Unfortunately, the VLF atmospheric noise process has no readily apparent closed-form mathematical description. This has resulted in the variety of proposed descriptive models which are found in the literature.

2.1 Atmospheric Noise Representations

Virtually all representations of the atmospheric noise process are based upon compiled first order noise amplitude statistics such as found

in CCIR 322 [26]. Commonly the complement of the first order cumulative probability distribution of the noise envelope voltage is plotted. This representation, known as the Amplitude Probability Distribution (APD), gives the probability that the noise envelope voltage exceeds a given reference voltage as a function of the reference voltage.

At this point, it is appropriate to clearly specify how the noise envelope voltage is actually observed. The noise envelope voltage is measured at the output of a linear receiver whose bandwidth, dynamic range, and gain are adjusted to provide the maximum output signal power without clipping the large amplitude atmospheric noise pulses. The resultant bandpass noise signal then drives a non-coherent envelope detector whose output is proportional to the noise envelope process as band limited by the receiver predetection filtering. Periodic samples of the detector output voltage, which constitute observations of the noise envelope process in the receiver bandwidth, are then compiled over a prescribed time interval and the resultant statistical distribution of the sample envelope voltages defines the noise APD. In addition to the compiled APD's, an impulsiveness form factor, V_d , defined to be the ratio of the RMS noise envelope voltage to average noise envelope voltage, is widely used to describe the noise impulsiveness. It should be noted that the statistical moments involved in the definition of V_d are ensemble rather than time averages. The two averages are not equivalent since the atmospheric noise envelope process is non stationary and, therefore, not ergodic.

2.2. Noise Models

In order to proceed to analyses of communication system performance in the atmospheric noise environment, it is necessary to have useable mathematical models of the noise. These usually involve mathematical descriptions which are more sophisticated than the noise envelope APD, but which are consistent with the noise APD. Atmospheric noise models vary from the entirely empirical assignment of a convenient mathematical expression to the noise APD to theoretically developed (based on the physical nature of the noise process) models. In this latter case, as previously noted, measured noise statistics provide both a basis for the formulation of the model and a check of its accuracy.

Some general observations of these types of atmospheric noise models are appropriate at this point. The purely empirical description of the APD developed by Crichlow, et al [10], disregarding noise pulse amplitude, width and spacing distributions, cannot provide a basis for analyzing system performance where noise impulses are the primary contributor to modem error rates. This is especially true for non-linear communication receivers where noise pulse widths are significant fractions of a bit (or detector decision element) in duration. In the case of non-linear reception (small BWR, hard-limiting), a useable noise model must account for noise pulse statistics. Also, it is necessary to recognize that the shape of a typical noise pulse as observed at the input to a detector (or predetection bandpass limiter) is dependent on the impulse response of the receiver predetection filters. This characteristic has led to the development of "filtered impulse" noise models (based on a time sequence of amplitude distributed impulses at the receiver input) such

as developed by Beach and George [3], Furutsu and Ishida [16], Galejs [17], Giordano and Haber [18], and Nakai [40]. (Likewise, a type of "filtered impulse" model is employed in Chapter 5 of this study.) A brief description and discussion of the more significant of the available models is presented in the following sections.

2.2.1 Empirical Description of the Atmospheric Noise APD by Crichlow, et al [10] and CCIR 322 [26]

This model describes the APD of atmospheric noise by two straight lines and an interconnecting circular arc on Rayleigh graph paper. The Rayleigh paper is constructed with the abscissa linear in terms of the variable $-20 \log_{10} (-\ln_e P(E))$, where $P(E)$ is the probability that the noise envelope exceeds the threshold voltage, E . The ordinate is linear in terms of $20 \log_{10} (E/E_0)$ where E_0 is the root mean square (RMS) value of E . Figure 1 shows typical APD curves plotted on Rayleigh paper. The lower straight line portion which has a slope of $-1/2$ has the equation given by

$$20 \log_{10} (E/E_0) = K' - \frac{1}{2} \left\{ -20 \log_{10} [-\ln P(E)] \right\} \quad (2)$$

or

$$2 \log_{10} (E) - 2 \log_{10} (E_0) - K'/10 = \log_{10} [-\ln P(E)] \quad (2a)$$

or

$$\log_{10} (E^2) - \log_{10} (2E^2) = \log_{10} [-\ln P(E)]$$

where

$$\log_{10} (2E^2) = 2 \log_{10} (E_0) + K'/10, \quad (3)$$

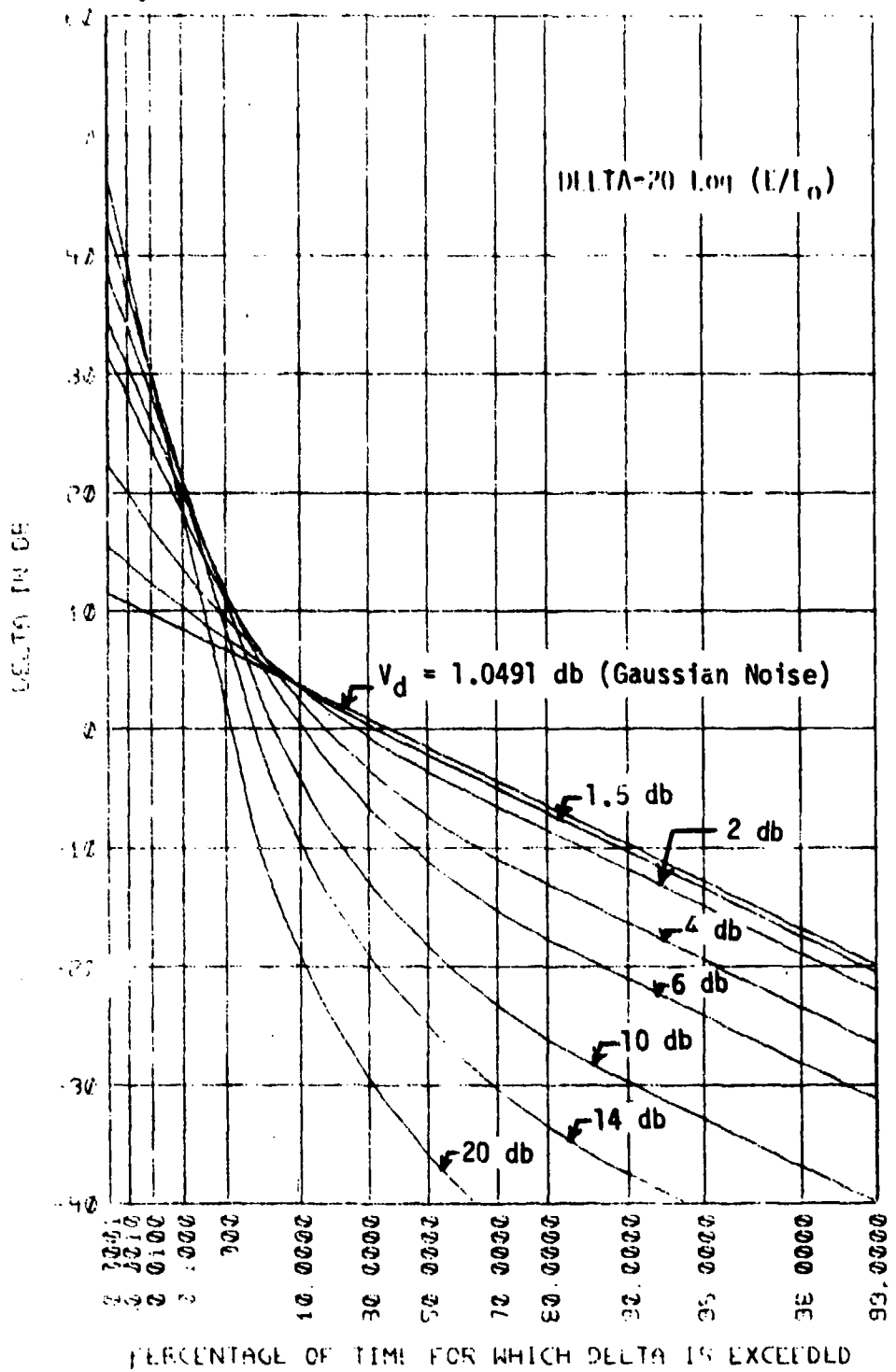


Figure 1. Amplitude Probability Distributions of Envelope of Atmospheric Noise

Thus,

$$-\ln P(E) = E^2/2\sigma^2 \quad (4)$$

and

$$P(E) = e^{-E^2/2\sigma^2} \quad (5)$$

Equation (5) gives the probability that a Rayleigh distributed random variable will exceed the value E . Since Gaussian noise has a Rayleigh envelope, Equation (5) corresponds to the APD for Gaussian noise. The steeper straight-line portion of the overall APD can similarly be shown to define an APD of the form

$$P(A) = \exp[-A^{2/x}/2\sigma^2] \quad (6)$$

where $\frac{x}{2}$ is the slope of the upper portion of the APD. Such a steep straight APD can be obtained by the transformation of the Rayleigh distributed random variable e according to the power law:

$$a = e^{\frac{x}{2}}. \quad (7)$$

Since $P(E) = P_r(e \geq E) = 1 - F_e(E)$ where $F_e(E)$ is the cumulative probability distribution of e , the probability density function of e is given by

$$\begin{aligned} f_e(E) &= \frac{d}{dE} F_e(E) = \frac{d}{dE} [1 - P(E)] = -\frac{dP(E)}{dE} \quad (8) \\ &= \frac{E}{\sigma^2} e^{-E^2/2\sigma^2}. \end{aligned}$$

By transformation of variables

$$f_a(A) = f_e(E) \left| \frac{dE}{dA} \right|. \quad (9)$$

Hence, substituting (7) and (8) in (9)

$$f_a(A) = \frac{A^{\frac{3}{2}x-1}}{X 6^2} e^{-\frac{A^{\frac{3}{2}x}}{26^2}}. \quad (10)$$

It follows that

$$P(A) = P_r(a \geq A) = \int_A^{\infty} f_a(u) du = e^{-\frac{A^{\frac{3}{2}x}}{26^2(6)}}.$$

Commonly, the steep straight line is referred to a "Power-Rayleigh" APD. It has been shown [10] that three statistical averages of the atmospheric noise envelope voltage are generally sufficient to describe the APD. These averages are: (1) The mean square envelope voltage, \bar{e}^2 ; (2) The average envelope voltage, \bar{e} ; and (3) The average logarithm of the envelope voltage, $\overline{L_n}(e)$. Moreover, it has been determined from observation of compiled statistical data that the V_d ratio ($\sqrt{\bar{e}^2/\bar{e}^2}$) in decibels is linearly related to $\overline{L_n}(e)$ in decibels. This relationship is given by ([11], p. 714)

$$\overline{L_n}(e) = 1.69 V_d \quad (11)$$

and is used to compile the typical APD curves in CCIR 322 [26] as a function of the parameter V_d . Also, Crichlow's approach provides a means for obtaining an APD curve appropriate to a receiver bandwidth other than the 200 Hz noise bandwidth used in CCIR 322 [11]. This

bandwidth conversion can be readily accomplished by means of the V_d translation chart given by Figure 26 of CCIR 322 [26].

The advantages of this noise representation are quite clear. First, only two measurements, the rms and average noise envelope voltages which define the V_d ratio, are required to specify the noise APD. Secondly, this description of the APD permits the rapid graphical construction of APD curves and a straightforward piecewise (mathematical) functional description which is well suited for numerical analysis by digital computer. Third, parameters for constructing APD's in this manner have been completely defined [10], [11] and tabulated [10], [26]. Moreover, this APD description is specifically related to the authoritative worldwide noise predictions of CCIR 322 [26]. Finally, it has been shown that this APD description provides close agreement with extensive compiled noise statistics [10]. The latter lends confidence in the quantitative adequacy of this approach.

On the other hand, this description has two deficiencies. First, its development is not based on any physical or theoretical principles. However, this would be a minor objection, at most, if the model described the actual noise process sufficiently to permit accurate system analysis. In the aforementioned case where detector performance is significantly affected by individual noise pulses, the APD alone is not sufficient to describe the noise pulse structure. Thus, the second, and more significant, deficiency of this empirical noise description is its failure to specify the noise pulse structure, or, in effect, noise statistics higher than first order. This latter

difficulty with the Crichlow formulation has necessitated a more sophisticated noise representation for the analysis of the hard-limiting small bandwidth ratio (BWR) systems in Chapter 5 of this dissertation.

Nevertheless, the Crichlow representation has been found to be useful for the analysis of the linear systems in Chapter 4 and the hard-limiting large BWR systems in Chapter 6. Moreover, the "Power-Rayleigh" APD of the impulsive noise component is used in Chapter 5 as a basis for developing the noise pulse amplitude statistical structure. Thus, as is shown in the subsequent analyses, the empirical noise description of Crichlow, et al is quite useful for the analysis of VLF/LF coherent modem performance.

2.2.2 Lognormal APD Description by Beckmann [4]

An important contribution to the description of the atmospheric noise process has been made by Beckmann [4]. This development provides a theoretical substantiation for Crichlow's empirical APD description and relates the VLF atmospheric noise APD to the known characteristics of VLF radio propagation. The noise process description is based on the response of a narrow band receiver to an input sequence of impulses whose occurrence in time is Poisson-distributed; the amplitude distribution of these impulses is based on long range VLF propagation theory. Considering the amplitude distribution, a particular noise impulse at the receiver input has an amplitude, E_p , given by

$$E_p = \frac{K\sqrt{P_0}}{d} \exp\left(-\sum_{j=1}^n \delta_j d_j\right) \quad (12)$$

where K is a propagation constant, P_0 is the peak power of a given noise pulse, δ_j is the attenuation constant for the j th discrete propagation path, d_j is the length of the j th path, and $d = \sum_j^n d_j$. This may also be written as

$$E_p = e^\alpha = \exp \left[- \sum_{j=1}^n \delta_j d_j + \frac{1}{2} \ln P_0 - \ln d + \ln K \right]. \quad (13)$$

Here, the first three terms in the argument of α are random. If the fluctuations in $\ln(P_0)$ and $\ln(d)$ are considered to be relatively smaller than the fluctuations of $\sum \delta_j d_j$, then the shape of the probability distribution of α is governed primarily by this latter term, the sum of attenuations. Thus, if a typical propagation path can be described by a large number, n , of independent propagation path sections (which is reasonable because of the multiple earth-ionosphere wavehops over a long range path), the central limit theorem implies that $\sum \delta_j d_j$ tends toward a Gaussian probability distribution. It follows that α is also Gaussian with a probability density function of the form

$$f_\alpha(A) = \frac{1}{\sqrt{2\pi}\sigma} e^{-\frac{(A-\mu)^2}{2\sigma^2}} \quad (14)$$

where

$$\mu = E\{\alpha\}.$$

Using (13), the density function for e_p , is given by

$$f_{e_p}(E_p) = f_\alpha(A) \left| \frac{dA}{dE_p} \right| = \frac{1}{\sqrt{2\pi}^6 E_p} e^{-\frac{(\ln E_p - \mu)^2}{2\sigma^2}} \quad (15)$$

which is a lognormal probability density function. As pointed out by Beckmann, this probability distribution of the peak impulse amplitude of the atmospheric noise envelope coincides with that postulated by Horner and Harwood [24] (but not theoretically justified).

Subsequent development employs the typical decaying time-exponential receiver response to Poisson-distributed, non-overlapping, high-amplitude, lognormally distributed noise impulses and multiple overlapping low amplitude noise pulses. The Poisson distribution implies independent impulsive noise sources and, consequently, statistically independent times of occurrence. It is shown that the high amplitude noise impulses produce a log-normally distributed noise envelope voltage which closely approximates the "Power Rayleigh" APD which is employed by Crichlow to describe the impulsive portion of the noise. The low amplitude overlapping pulses are argued to produce a Rayleigh distributed noise envelope (characteristic of a Gaussian process). These two disjoint regions of the atmospheric noise APD (lognormal for high amplitude and Rayleigh for low amplitude) are then interconnected by a circular arc (as constructed on Rayleigh graph paper) to produce a continuous overall noise envelope APD. This final result is in close quantitative agreement with Crichlow's empirical APD description and, consequently, with the compiled noise statistics cited by Crichlow [10].

Although this noise model is clearly consistent with measured first order noise envelope statistics, it has been shown [3], [18], [20], [51] that the times of occurrence of lightning strokes are not statistically independent. This results because a single lightning discharge contains multiple strokes whose times of occurrence display a clear statistical dependence [3]. (It is shown in Chapter 3, however, that the assumption of statistically independent noise pulse arrival times is sufficient for the analysis of practical communication systems where the detection element (bit) lengths are on the order of 20 msec. or less (corresponding to teletype transmission at 75 words per minute or greater).) Also, as noted by Giordano [18], Beckmann's development does not address noise statistics beyond the first order.

Overall, the work of Beckmann provides a more profound theoretical foundation to empirical noise representations such as that of Crichlow. However, since Beckmann's results virtually coincide with Crichlow's, Beckmann's representation is of similar quantitative merit for the numerical analysis of system performance. In conclusion, Beckmann's results are quantitatively equivalent but more difficult to describe mathematically and in terms of compiled statistics than is Crichlow's representation.

2.2.3 Noise Model of Beach and George [3]

A more sophisticated approach to VLF atmospheric noise modeling is that employed by Beach and George in their analysis of VLF and receiving systems. Here Beckmann's model is modified to account for

noise bursts from various independent noise sources with each exhibiting an empirically determined pulse-per-noise-burst statistical distribution given by:

$$P(N_0) = (1-\nu)\nu^{N_0-1} \quad (16)$$

where $P(N_0)$ is the probability of N_0 noise pulses in a burst and usually $.5 < \nu < .86$ (but $0 \leq \nu \leq 1$ in any case).

As in Beckmann's work, a log-normal density function is employed to describe the statistics of the noise pulse amplitudes.

Thus, this model does account for the statistical time dependence between multiple strokes in a given lightning discharge. An illustrative APD synthesized by means of this noise process (page 170) closely approximates a typical (CCIR 322) APD curve in the higher amplitude ranges but diverges significantly in the lower amplitude ranges; although this pulse statistical model is a good approximation to measured noise statistics in the impulsive range, it is clearly not sufficient to describe even the first order noise statistics over a wide amplitude range. At this point, it is not known to what extent this deficiency in the noise model contributes to inaccuracy in communication system performance analysis based on this model. However, as noted in Chapter 1, the quantitative modem performance estimates obtained by the use of this model are clearly divergent from experimental results. In conclusion, this noise model, although it accounts for noise pulse statistical dependencies, is of questionable efficacy for communication system performance analyses.

2.2.4 Poisson and Poisson-Poisson Noise Model of Furutsu and Ishida [16]

This work examines the envelope of the output voltage of a narrow-band receiver when the input consists of independent (poisson distributed) impulses whose amplitudes are exponentially distributed. In addition, Poisson-Poisson noise, which consists of Poisson-distributed groups of Poisson-distributed individual impulses, is considered. This latter noise process model was specifically devised to account for predischarge components as well as main discharge components in HF atmospheric noise. In this frequency range, computed noise APD's showed good agreement with measured noise statistics. At VLF, it appears that noise pulse dependencies might be accommodated by the Poisson-Poisson process. However, this has yet to be demonstrated.

Although the work of Furutsu and Ishida treats noise processes which have some physical similarity to VLF atmospheric noise, the probability densities obtained are mathematically formidable (in terms of integrals). Moreover, the exponential pulse amplitude distribution is obviously not consistent with the empirically accurate power-Rayleigh [10] or log-normal [4] representations. Hence, the Poisson or Poisson-Poisson process results of Furutsu and Ishida are deemed unsuitable for the subsequent analyses in this dissertation.

2.2.5 Amplitude Distributions of VLF Noise by Janis Galejs [17]

This study of ELF and VLF atmospheric noise APD's proposes that the noise APD can be derived from the peak amplitude distributions of lightning discharges which can be approximated by the sum of two exponentials. The resultant APD's predicted by this method differ

greatly from those actually measured. The reason for this discrepancy may well be the fact that propagation effects, such as considered by Beckmann [4] and Giordano [18], are not included. Significantly, this analysis introduces the method of determining the probability density of the noise envelope voltage by means of characteristic functions. This technique is outlined below:

- (1) Let the received noise waveform produced by a single lightning discharge be given by

$$f(t) \cos [\omega_0 t + \theta(t)],$$

where $f(t)$ is the sum of two exponentials.

- (2) Assume the noise voltage, V , is obtained by detection in an integrating filter according to

$$V = \frac{1}{T} \int_0^T f(t) \cos [\omega_0 t + \theta(t)] \cos \omega_0 t dt. \quad (17)$$

- (3) If the phase process $\theta(t)$ is nearly constant during the interval $(0, T)$ and double frequency components are disregarded, (17) becomes

$$V \approx a \cos \theta \quad (18)$$

where

$$a = \frac{1}{T} \int_0^T f(t) dt, \quad (18a)$$

$f(t)$ is the sum of two exponentials, and θ is uniformly distributed on $(-\pi, \pi)$ and statistically independent of a .

(4) The joint probability density function of a and θ is given by

$$f_{a,\theta}(A, \theta) = \frac{1}{2\pi} f_a(A). \quad (19)$$

(5) Consequently, the characteristic function of the observed noise voltage is given by

$$\begin{aligned} F_V(j\zeta) &= E\left\{e^{-j\zeta V}\right\} \\ &= E\left\{e^{-j\zeta A \cos \theta}\right\} \\ &= \int_0^\infty dA \int_{-\pi}^{\pi} d\theta f_{a,\theta}(A, \theta) e^{-j\zeta A \cos \theta} \\ &= \int_0^\infty J_0(\zeta A) f_a(A) dA. \end{aligned} \quad (20)$$

This is also known as the Hankel Transform of the probability density of a , the noise envelope voltage.

(6) Next it is assumed that noise voltages produced by n independent lightning voltages are then added by superposition in the linear noise receiver. If these voltages are assumed to have identical statistics and to be mutually statistically independent, the composite voltage, V_n , observed at the noise detector, has a characteristic

function given by

$$F_{V_n}(j\zeta) = F_\nu(j\zeta)^n. \quad (21)$$

(7) Now it is assumed that the composite observed noise voltage, V_n , can be expressed as

$$V_n = a_n \cos \phi, \quad (22)$$

where a_n is the envelope voltage of the composite noise components and ϕ is statistically independent of a_n and uniformly distributed on $(-\pi, \pi)$. The characteristic function of V_n is then given by

$$F_{V_n}(j\zeta) = \int_0^\infty J_0(\zeta A) f_{a_n}(A) dA, \quad (23)$$

where $f_{a_n}(A)$ is the probability density of the composite noise envelope voltage.

(8) Applying the inverse Hankel Transform (A6) to (23) the cumulative noise envelope voltage density is found to be

$$f_{a_n}(A) = \int_0^\infty d\zeta A \zeta J_0(\zeta A) F_{V_n}(j\zeta) \quad (24)$$

$$= \int_0^\infty d\zeta A \zeta J_0(\zeta A) F_\nu(j\zeta)^n. \quad (25)$$

This final result is then integrated to compute the APD by

$$P(E) = Pr(e \geq E) = \int_E^\infty f_{a_n}(A) dA. \quad (26)$$

(It should be noted that Giordano [18] also employed this procedure in his later, more comprehensive noise model development.)

2.2.6 Modeling of Atmospheric Noise by Giordano [18]

This VLF atmospheric noise modeling study is a comprehensive synthesis of Poisson-related noise pulse statistics, narrowband receiver response, VLF radio propagation effect, and geographical noise source distributions. Here, the aforementioned Hankel transform technique (see 2.2.5 Galejs [17]) is applied to the development of noise APD's. The resultant synthesized APD's are shown to agree with measured data where the best agreement occurs at the highest noise amplitude levels. In addition to the theoretical synthesis of APD's in this work, an effort is made to account for statistical dependence between the occurrence times of time adjacent noise pulses. In this phase of the synthesis, the noise process is approximately characterized by known noise pulse level crossing statistics and noise pulse spacing statistics. Unfortunately, the mathematical representation(s) of this latter process are formidable, and not really suitable for the analysis of non-linear small BWR coherent communications systems.

Overall, this work does show that the geographical distribution of noise sources, radio propagation effects, and radio receiver impulse response can be combined to approximately account for measured VLF/LF noise statistics. On the other hand, the results are not readily applicable to the analysis of small BWR non-linear systems and the first order results, useful for the analysis of linear and large BWR non-linear systems, are less precise than the simpler representations of Crichlow [10] and Beckmann [4].

2.2.7 Multiplicative Noise Model by Hall [20]

This noise model consists of a narrowband zero mean Gaussian process $n(t)$, amplitude modulated by an independent stationary process, $a(t)$, such that the result,

$$y(t) = a(t)n(t), \quad (27)$$

is an accurate description of received atmospheric noise. Hall asserts that a good fit can be obtained if the power spectrum of the baseband process, $a(t)$, does not significantly overlap the spectrum of the bandpass Gaussian process, $n(t)$. This "generalized 't' model" yields a closed-form APD representation, $P(E)$, given by

$$P(E) = \frac{\gamma^{\theta-1}}{(E^2 + \gamma^2)^{(\theta-1)/2}}. \quad (28)$$

where $2 < \theta < 4$ for VLF noise and γ is chosen in accordance with θ and an "appropriate" value of the average noise envelope voltage.

This APD representation provides fairly good agreement with measured noise data of medium amplitude, but poorer agreement at the amplitude extremes. One obvious drawback in the use of this model for practical system analyses is the indefinite nature of the parameters θ and γ . Although a fairly good APD fit to measured data can be obtained by a proper choice of θ and γ , there is no specific basis (i.e., bandwidth, frequency, or other) for an apriori selection of these parameters. A final observation as provided by Hall is that $\overline{e^2} = \infty$ for $2 < \theta \leq 3$. This illustrates that (28)

cannot correspond to physical atmospheric noise. Because of this discrepancy, a modification to (28) is introduced which does provide for finite average noise power. This modified noise model results in greater mathematical complexity and the introduction of the additional implicitly defined mathematical parameters ξ and β as shown in the "modified" APD expression for $\theta = 3$

$$P(E) = \frac{\gamma^2}{E^2 + \gamma^2} e^{-\frac{E^2}{\theta^2 \sigma^2 \gamma^2}} \quad (29)$$

In addition to the derivation of the closed form APD expressions (28) and (29), Hall also derives expressions for average envelope crossing rates and pulse spacing distributions. These latter results also involve the model parameters θ and γ .

Overall, Hall's noise model development has the clear advantage of closed form mathematical representations. On the other hand, there are significant problems with its physical validity, the selection and use of implicitly defined algebraic parameters, and, consequently, the model's ultimate accuracy.

2.2.8 Noise Model Summary

The contributions of the preceding VLF atmospheric noise modeling efforts can be summarized as follows: (1) The first order statistics of atmospheric noise are specified by the noise APD for the envelope and a uniform probability density for the statistically independent phase; (2) First order statistics can be calculated from the narrowband receiver response to inputs of various impulsive noise processes;

(3) Measured noise-pulse-spacing statistics show that times of noise pulse occurrence are not statistically independent because of the time dependence of multiple strokes in a single lightning discharge. This latter situation makes the employment of a Poisson-distributed (reflecting statistically independent pulse occurrence times) impulsive noise process generally inaccurate. Nevertheless, it is shown in the next section and in Chapter 5 that the Poisson-distributed assumption is sufficiently accurate for the analysis of practical, standard-rate (70-100 words/minute) VLF radio-teletype systems.

2.3 Noise Model for Coherent Modem Analysis

In the noise models various mathematical structures have been proposed, and modified as necessary, to approximate the compiled noise APD data, account for receiver response, and to account for measured pulse time statistics such as level crossing rate and occurrence-time distributions. When considering the various models for a specific problem, it is desirable to choose the simplest representation which is sufficient to describe the system. In the subsequent performance analyses, it is shown that the noise envelope voltage, which is described by the APD, and the statistically independent noise phase suffice for the treatment of linear systems. This is also true in the case of hard-limiting large BWR systems where individual noise pulses have minimal effect on detection error probabilities. On the other hand, the predominant cause of detection errors in the hard-limiting small BWR systems is the post-

detection noise produced by distinct noise impulses. In this latter case it is necessary for the noise model to account for noise pulse statistics. Because of these two distinct situations and the desirability of using the simplest adequate noise description for system analysis, two distinct noise representations are used in this dissertation.

2.3.1 Linear and Pseudo-Linear (Large BWR Hard-Limiting) Receiver

In the case of linear systems, the detection process involves the multiplication of the received signal by a local coherent reference, time integration of this product over a decision interval, and a comparison of the resultant detector functional with an appropriate decision threshold. Mathematically, this detector functional, R_d , is given by

$$R_d = \frac{1}{T} \int_0^T s(t) c(t) dt \quad (30)$$

where T is the decision interval, $s(t)$ is the incoming signal, and $c(t)$ is the local coherent reference signal.

In general, the incoming signal consists of the desired signal, proportional to the coherent reference signal, and additive noise. Thus,

$$s(t) = Dc(t) + n(t) \quad (31)$$

or, in terms of the carrier frequency, w_0 ,

$$S(t) = DC(t) \cos w_0 t + e(t) \cos [w_0 t + \theta(t)] \quad (32)$$

where $e(t)$ and $\theta(t)$ are the narrowband envelope and phase of the noise process, $n(t)$.

Substituting (32) into (30),

$$\begin{aligned} R_d = & \frac{1}{2T} \int_0^T DC^2(t) [1 + \cos 2w_0 t] dt \\ & + \frac{1}{2T} \int_0^T C(t)e(t) [\cos(2w_0 t + \theta(t)) \\ & \quad + \cos \theta(t)] dt. \end{aligned} \quad (33)$$

Disregarding high frequency terms, this yields the baseband functional, R_b , where

$$R_b = \frac{1}{2T} \int_0^T DC^2(t) dt + \frac{1}{2T} \int_0^T C(t)e(t) \cos \theta(t) dt. \quad (34)$$

If the phase process is assumed to be nearly constant throughout the decision interval (that is, $\theta(t) = \theta, 0 \leq t \leq T$) and independent of $e(t)$, then the noise component of the functional is given by

$$\frac{\cos \theta}{2T} \int_0^T C(t) e(t) dt. \quad (35)$$

Defining the effective noise envelope voltage to be

$$E = \frac{1}{T} \int_0^T C(t) e(t) dt, \quad (36)$$

the noise component of R_b can be expressed as $\frac{E_{cos\theta}}{2}$

In the special case of PSK modulation, a constant amplitude and phase coherent reference signal is used so that $C(t) = C$. It follows that (36) becomes

$$E_p = \frac{C}{T} \int_0^T e(t) dt. \quad (37)$$

(It should be noted that this voltage constitutes an observation of the noise envelope process in a detection bandwidth $1/T$ as described in 2.1. Hence, it is this envelope voltage whose statistics are described by the APD curves of Figure 1.)

This may also be written in the form of the convolution integral

$$E_p = \int_0^T \hat{C}(T-t) e(t) dt, \quad (38)$$

where

$$\hat{C}(t) = \begin{cases} \frac{C}{T}, & 0 \leq t \leq T \\ 0, & \text{elsewhere.} \end{cases} \quad (38a)$$

Thus, it is apparent that E_p may be considered as the response of a linear filter at $t=T$ to the input $e(t)$ where the impulse response of the filter is given by $C(t)$. The transfer function of this filter is given by

$$\begin{aligned}
 H_o(j\omega) &= \int_{-\infty}^{\infty} \hat{C}(t) e^{-j\omega t} dt \\
 &= \frac{C}{T} \int_0^T e^{-j\omega t} dt \\
 &= \frac{C}{T} \left[\frac{i - e^{-j\omega T}}{j\omega} \right]. \tag{39}
 \end{aligned}$$

Thus, the magnitude squared of the transfer function, $|H_o(j\omega)|^2$, is

$$\begin{aligned}
 |H_o(j\omega)|^2 &= [H_o(j\omega) \times H_o(-j\omega)] \\
 &= \frac{C^2}{T^2} \frac{[1 - e^{-j\omega T}][1 - e^{j\omega T}]}{\omega^2} \\
 &= C^2 \frac{\sin^2 \frac{\omega T}{2}}{\left(\frac{\omega T}{2}\right)^2}. \tag{40}
 \end{aligned}$$

It follows that equivalent noise bandwidth, B_n , is given by

$$B_n \triangleq \frac{\frac{1}{2\pi} \int_{-\infty}^{\infty} |H_o(jw)|^2 dw}{|H_o(0)|^2}$$

Applying Parseval's theorem,

$$\begin{aligned} B_n &= \frac{\int_{-\infty}^{\infty} \hat{C}(t)^2 dt}{|H_o(0)|^2} \\ &= \frac{\int_0^T \left(\frac{C}{T}\right)^2 dt}{C^2} \\ &= \frac{1}{T} \end{aligned} \quad (41)$$

Thus, the noise component of the PSK detector functional can be represented by an envelope voltage, E_p , at a statistically independent phase angle θ where θ is uniformly distributed on the interval $(-\pi, \pi)$. The envelope voltage is derived by the linear filtering of the input noise envelope process, $e(t)$, in a noise bandwidth which is the inverse of the binary element length, T . The method of Crimmon [11], or Figure 26 of CCIR 322 [26], enables the APD of the noise in one receiver bandwidth to be converted to the proper APD for another bandwidth. Therefore, measured or tabulated noise process APD's can be converted from a reference receiver bandwidth to the detection bandwidth, B_n , so as to yield an APD which defines the statistics of the PSK post-detection noise envelope voltage E_p . In conclusion, the measured or tabulated noise APD (when properly translated to the noise bandwidth

(cross-correlation, or matched-filter, detector) and the independent phase (assuming nearly constant noise phase over the detection interval), are sufficient to define the post detection noise component of the coherent (matched filter) detector functional. Because of this result, and the desirability of the simplest sufficient noise representation, Crichlow's empirical APD description is employed in the linear analyses of Chapter 4 and the modified linear analyses of Chapter 6 where the residual noise after predetection wideband hard-limiting is closely approximated by atmospheric noise of lower power and impulsiveness. It should be emphasized here that this selection is only on the basis of simplicity and does not preclude other noise models which accurately describe the noise APD. Thus, other, more mathematically complex, noise representations could also be used. Nevertheless, it is believed the Crichlow noise description is the most practical for linear and pseudo-linear (large BWR, hard-limiting receiver, Chapter 6) system analysis where first order noise statistics suffice.

2.3.2 Hard-Limiting, Small BWR Receiver

The second required noise model is one which accounts for the statistics of distinct atmospheric noise pulses. Here again, it is desirable to employ the simplest sufficient mathematical noise description. In terms of mathematical tractability, a Poisson-distributed (independent times of occurrence) sequence of noise pulses is the simplest time-statistical structure. However, as shown by Beach and George [3], multiple noise pulses in a given lightning discharge have

statistically dependent times of occurrence. Although a Poisson-distribution is thus generally inaccurate, its simplicity is so attractive that it must be reconsidered - even if only as an approximation.

First, consider the case of independent noise pulses. It has been shown [13] that a sequence of pulses whose occurrence times are statistically independent constitutes a Poisson process. Here, the probability that K noise pulses occur in T seconds is given by

$$Pr(K \in T) = \frac{(\alpha T)^K}{K!} e^{-\alpha T}, K=0,1,2,\dots \quad (42)$$

where α is the average occurrence rate and \in signifies "exists in".

Now, considering the random variable t to be the time between pulses, it is seen that the event that t exceeds T coincides with the event that zero pulses occur in T seconds. Hence,

$$Pr(t > T) = Pr(K=0 \in T) = e^{-\alpha T}, T \geq 0. \quad (43)$$

From this, the probability density function, $f_t(T)$ is found to be

$$f_t(T) = -\frac{d}{dT} Pr(t > T) = \alpha e^{-\alpha T}, T \geq 0. \quad (44)$$

As noted by Beach and George [3] and Giordano [18], measured pulse interval statistics exhibit this behavior only at the lowest amplitudes. At the higher amplitude levels there appears to be a tendency toward clustering. This clustering effect is attributed to the statistical

dependence of pulse occurrence times of multiple-stroke lightning discharges. Beach and George [3] have determined that the probability density function of the time interval between successive strokes of such multiple-stroke discharges can be approximated by

$$P_t(T) = h^2 T e^{-hT}, \quad T \geq 0, \quad (45)$$

where $h > 0$.

This expression indicates a maximum pulse density in the vicinity of $T = 1/h$ and clearly exemplifies the clustering tendency as opposed to the Poisson distribution (44) of independent pulses.

The characteristic function, $G_t(j\zeta)$, of the clustered pulse interval, t , is given by

$$G_t(j\zeta) = \int_0^\infty P_t(T) e^{-j\zeta T} dT = \frac{h^2}{(h + j\zeta)^2}. \quad (46)$$

Replacing $j\zeta$ by S

$$G_t(S) = \frac{h^2}{(h + S)^2}. \quad (47)$$

In turn, the characteristic function of the sum of K such statistically independent intervals, is given by

$$G_{t_K}(s) = G_t(s)^K = \frac{h^{2K}}{(h+s)^{2K}} \quad (48)$$

$$= \mathcal{L}[P_{t_K}(T)] \quad (49)$$

where $\mathcal{L}[\cdot]$ denotes the one-sided Laplace transform, and $P_{t_K}(T)$ is the probability density function of t_K .

Now, the probability that $t_k \leq T$ is given by the probability distribution

$$G_{t_K}(T) = \int_0^T P_{t_K}(u) du. \quad (50)$$

Its Laplace transform is

$$\begin{aligned} \mathcal{L}[G_{t_K}(T)] &= \mathcal{L}\left[\int_0^T P_{t_K}(u) du\right] \\ &= \frac{1}{s} \mathcal{L}[P_{t_K}(T)] \\ &= \frac{1}{s} G_{t_K}(s) = \frac{h^{2K}}{s(h+s)^{2K}}. \end{aligned} \quad (51)$$

However, the event that $t_k \leq T$ is also the event that K or more pulses occur in the interval $(0, T)$. Hence,

$$\mathcal{L}[P_r(n \geq K \mid T)] = \frac{h^{2K}}{s(h+s)^{2K}}. \quad (52)$$

The probability that exactly K pulses occur in the interval $(0, T)$ is given by

$$P_r(K \in T) = P_r(n = K \in T) = P_r(n \geq K \in T) - P_r(n \geq K+1 \in T). \quad (53)$$

Hence,

$$\begin{aligned} \mathcal{L}[P_r(K \in T)] &= \mathcal{L}[P_r(n \geq K \in T) - P_r(n \geq K+1 \in T)] \\ &= \mathcal{L}[P_r(n \geq K \in T)] \\ &\quad - \mathcal{L}[P_r(n \geq K+1 \in T)] \\ &= \frac{h^{2K}}{s(h+s)^{2K}} - \frac{h^{2(K+1)}}{s(h+s)^{2(K+1)}} \\ &= \frac{h^{2K}(2h+s)}{(h+s)^{2(K+1)}}. \end{aligned} \quad (54)$$

(54) can be rewritten as

$$\mathcal{L}[P_r(K \in T)] = \frac{h^{2K+1}}{(h+s)^{2(K+1)}} + \frac{h^{2K}}{(h+s)^{2(K+1)}}. \quad (55)$$

Thus, performing the inverse transformation,

$$Pr(K \in T) = e^{-hT} \left[\frac{(hT)^{2K+1}}{(2K+1)!} + \frac{(hT)^{2K}}{(2K)!} \right]. \quad (56)$$

The average number of pulses in the interval $(0, T)$ is given by

$$\overline{K(T)} = \sum_{K=0}^{\infty} K Pr(K \in T). \quad (57)$$

Taking Laplace transforms of both sides of (57) results in

$$\begin{aligned} \mathcal{L}[\overline{K(T)}] &= \mathcal{L}\left[\sum_{K=0}^{\infty} K Pr(K \in T)\right] \\ &= \sum_{K=0}^{\infty} K \mathcal{L}[Pr(K \in T)] \\ &= \frac{2h+s}{(h+s)^2} \sum_{K=0}^{\infty} K \left[\frac{h^2}{(h+s)^2} \right]^K. \end{aligned} \quad (58)$$

Since $h > 0$ and s can be chosen such that $\operatorname{Re}[s] > 0$

$$\left| \frac{h^2}{(h+s)^2} \right| < 1 \quad (59)$$

and

$$\sum_{K=0}^{\infty} K \left[\frac{h^2}{(h+s)^2} \right]^K = \frac{\frac{h^2}{(h+s)^2}}{\left[1 - \frac{h^2}{(h+s)^2} \right]^2} = \frac{h^2(h+s)^2}{s^2(2h+s)^2}.$$

Substitution of this result into (58) yields

$$\begin{aligned}\mathcal{L}[\bar{K}(T)] &= \frac{h^2}{s^2(2h+s)} \\ &= \frac{h}{2s^2} - \frac{1}{4s} + \frac{1}{4(2h+s)}. \quad (60)\end{aligned}$$

Finally, taking the inverse transform results in

$$\bar{K}(T) = \frac{hT}{2} - \frac{1}{4} + \frac{1}{4} e^{-2hT}. \quad (61)$$

This latter result shows that the pulse occurrence rate is not constant for the multiple clustered pulses of a given lightning discharge. On the other hand, the pulse occurrence rate is constant for the former case of statistically independent occurrence times. Moreover, the statistical distributions of pulses in the interval $(0, T)$ given by (42) and (56) are clearly dissimilar. Because of these dissimilarities, one might expect that modern error rate computations which depend on the probability, $\Pr(K \in T)$, would likewise produce greatly dissimilar results for the two pulse statistical distributions. The "real-world" situation likely involves both independent individual pulses and clustered pulses. Thus, the most representative statistical distribution can be expected to yield quantitative results lying somewhere between the two extreme cases of all independent pulses and all clustered pulses.

Fortunately, these two bounding pulse statistical distributions are shown in Chapter 5 (see Figure 23) to yield virtually equivalent

error rate characteristics for both CFSK and MSK detection. Moreover, the error rates calculated in accordance with (42) (for all pulses occurring at statistically independent times) are seen to correspond slightly more closely to the measured data than those computed by (56). In view of the virtual equivalence of the computed results and the greater mathematical simplicity of the Poisson distribution (as well as slightly better correspondence to measured performance), the Poisson assumption was used for the computation of error rates in this dissertation.

To complete the specification of the noise model for the hard-limiting, small BWR system, it is necessary to describe the amplitude distribution of the noise pulses in a detection interval. As previously discussed, the steep Power-Rayleigh (or Log-Normal) portion of the noise APD describes the envelope of the impulsive portion of the noise. The following discussion shows that the noise envelope voltage, as observed at the output of a narrowband receiver, is directly proportional to the input noise pulse amplitudes. Hence, the noise pulse amplitudes must also have a Power-Rayleigh (or Log-Normal) statistical distribution.

To begin the discussion, consider the effect of linear bandpass filtering (typical of a narrowband receiver) on received atmospheric noise impulses. To minimize complexity, the bandpass filter which is analyzed is an RLC filter of the form shown in Figure 2.

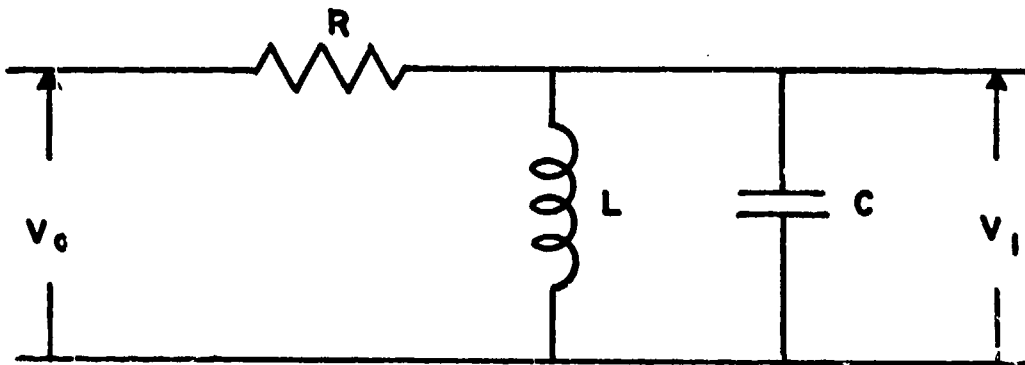


Figure 2. Bandpass Filter

This filter has a transfer function, $H_1(j\omega)$, given by

$$\begin{aligned}
 H_1(j\omega) &= \frac{V_i}{V_o} = \frac{j\omega L}{R - \omega^2 RLC + j\omega L} \\
 &= \frac{-j2b_1\omega}{\omega^2 - \omega_0^2 - j2b_1\omega} \quad (62)
 \end{aligned}$$

where $\omega_0^2 = \frac{1}{LC}$, $b_1 = \frac{1}{2RC}$ and ω is the angular frequency in radians/sec., the 3 dB (or half-power) bandwidth is $2b_1$ radians/sec., and the equivalent noise bandwidth is $b_1/2$ Hz or πb_1 radians/sec.

The impulsive input to the filter (receiver) is an antenna voltage which is produced by the radiation from lightning discharges. A typical stroke of a lightning discharge consists of a very large electrostatic-discharge current conducted over an ionized path between clouds or between a cloud and ground. Because of the magnitude of the conduction current and the rapid rise and decay times, substantial electromagnetic

energy is radiated. An expression for the vertically polarized electric field (principal component of the Poynting vector) radiated by a typical lightning stroke has been developed by Watt [54] and is given by

$$E_z(t) = -\frac{2M_I'(t)}{10^7 d} \quad (63)$$

where $M_I'(t)$ is the time derivative of the instantaneous current-height moment in ampere meters/second, d is the distance from the source in meters, and d is much greater than the discharge height.

Because the rise and decay of the stroke current are extremely rapid (on the order of microseconds), the current-height moment can be closely approximated by an impulse function. With this approximation, a lightning stroke at time t_0 produces an electric field at d meters given by

$$E_z(t) = \frac{-2M_I}{10^7 d} \frac{d}{dt} \delta(t-t_0)$$

where $\delta(\cdot)$ is the unit impulse function and

$$M_I = \int_{-\infty}^{\infty} M_I(t) dt. \quad (64)$$

In turn, the antenna voltage is proportional to this electric field so that the receiver input is of the form

$$e_o(t) = P_r \frac{d}{dt} \delta(t-t_0). \quad (65)$$

This input has the Fourier transform, $E_o(j\omega)$, given by

$$E_o(j\omega) = \int_{-\infty}^{\infty} e_o(t) e^{-j\omega t} dt \\ = j\omega P_1 e^{-j\omega t_0}. \quad (66)$$

The output of the filter, $e_1(t)$, is then given by

$$e_1(t) = \frac{1}{2\pi} \int_{-\infty}^{\infty} H_1(j\omega) E_o(j\omega) e^{j\omega t} d\omega \\ = \frac{1}{2\pi} \int_{-\infty}^{\infty} \frac{2P_1 b_1 \omega^2 e^{j\omega(t-t_0)}}{\omega^2 - \omega_0^2 - j2b_1 \omega} d\omega. \quad (67)$$

Assuming $b_1^2 \ll \omega_0^2$, as is usually the case,

$$e_1(t) \approx \frac{Pb_1}{\pi} \int_{-\infty}^{\infty} \frac{\omega^2 e^{j\omega(t-t_0)} d\omega}{(\omega - \omega_0 - jb_1)(\omega + \omega_0 - jb_1)} \\ = \frac{Pb_1}{\omega_0} \cdot \frac{1}{2\pi} \int_{-\infty}^{\infty} \left[\frac{(\omega_0 + jb_1)^2 e^{j\omega(t-t_0)}}{(\omega - \omega_0 - jb_1)} \right. \\ \left. - \frac{(\omega_0 - jb_1)^2 e^{j\omega(t-t_0)}}{(\omega + \omega_0 - jb_1)} \right] d\omega$$

$$e_1(t) = \frac{-2P_1 b_1 e^{-b_1(t-t_0)}}{\omega_0} \left[(\omega_0^2 - b_1^2) \sin \omega_0(t-t_0) \right. \\ \left. + 2\omega_0 b_1 \cos \omega_0(t-t_0) \right], \quad (68)$$

$$t \geq t_0.$$

Now, assuming $\omega_0 \gg b$, it follows that

$$e_r(t) \approx -2b, P, \omega_0 e^{-b, (t-t_0)} \sin \omega_0 (t-t_0). \quad (69)$$

This can also be written as

$$e_r(t) = e(t) \cos [\omega_0 t + \theta(t)] \quad (32)$$

where

$$\begin{aligned} e(t) &= 2b, P, \omega_0 e^{-b, (t-t_0)} u(t-t_0) \\ &\triangleq P e^{-b, (t-t_0)} u(t-t_0), \end{aligned} \quad (70)$$

$u(\cdot)$ is the unit step function, P is the received pulse amplitude, and

$$\theta(t) = \frac{\pi}{2} - \omega_0 t. \quad (71)$$

Substitution of (70) into (36) yields the observed envelope voltage, $E(t_0)$, as a function of the time of pulse occurrence:

$$E(t_0) = \frac{P}{T} \int_0^T e^{-b, (t-t_0)} C(t) u(t-t_0) dt. \quad (72)$$

Assume that the occurrence time, t_0 , is uniformly distributed with a probability density, $f_{t_0}(t_0)$, of $1/T$ over the observation interval $(0, T)$. Hence, E , the expected (or effective) value of the observed noise envelope, given P , is obtained by

$$\begin{aligned}
 E &= \langle E(t_0) \rangle_{t_0} = \int_{t_0}^T E(T_0) f_{t_0}(T_0) dT_0 \\
 &= \frac{P}{T^2} \int_{t_0}^T dT_0 \int_{T_0}^T e^{-b_1(t-T_0)} C(t) dt. \quad (72a)
 \end{aligned}$$

This result shows that the noise envelope voltage, E , resulting from a single noise impulse is directly proportional to the received impulse amplitude, P . Therefore, the probability densities of E and P have the same functional form. In conclusion, then, the received pulse amplitudes, P , must also have a power Rayleigh (or log-normal) APD, just as the observed noise envelope voltage, E .

Chapter 3
COHERENT MODULATION - DEMODULATION (MODEM) SYSTEMS
FOR VERY LOW FREQUENCY (VLF) AND LOW FREQUENCY
(LF) RADIO COMMUNICATION

3.1 General

Radio communication at VLF/LF, because of bandwidth constraints, is restricted to binary teletype at rates on the order of 100 words/min (75 bits/second) or less. Also, VLF/LF communication channels are usually limited in range by ambient, highly impulsive, atmospheric noise rather than receiving system internal noise [54]. Here the high level of this noise environment and ultimate transmitter power and cost limitations make the increased efficiency of coherent modulation and detection desirable. Fortunately, VLF/LF propagation is characterized by minimal signal fading and very high propagating signal-phase stability. Thus, coherent modulation and detection is a practical scheme for VLF/LF radio communication. Because of the attractiveness of coherent synchronous operation, coherent modems are rapidly supplanting the older non-coherent, and often non-synchronous, modems in VLF/LF communication systems.

Although the foregoing considerations indicate the suitability of synchronous coherent VLF/LF communication, the number of possible modulation techniques is greatly limited by two practical system constraints. First, because of the narrow bandwidth (high-Q) of

efficient transmitting antenna systems, transmitted signal waveforms must be continuous so as to minimize transient effects produced by modulation transitions (teletype keying). Second, because practical transmitting antenna systems are peak-power (insulator voltage) limited, constant amplitude signals are necessary to maximize the power radiated from the antennas. These restrictions dictate the use of: (1) Angle modulation to maintain constant signal amplitude, and (2) Frequency shift keying (FSK) rather than phase shift keying (PSK) to maintain signal waveform continuity. Here, a synchronous coherent FSK signal, $s(t)$, can be mathematically specified by

$$s(t) = S \cos(\omega_0 + i_k \frac{M\pi}{T})t, (K-1)T \leq t \leq KT, \quad (73)$$

$$K = 1, 2, 3 \dots,$$

where S is the signal amplitude, ω_0 is the nominal carrier (or center) frequency in radians/sec., $i_k = \pm 1$ according to the state of the k^{th} binary data element, M is the FSK modulation index, and T is the length of a binary signal element.

It is apparent that each of the possible shift frequency components retains a constant RF phase angle and is suitable for coherent detection. However, this formulation does not assure waveform continuity at frequency shifts. Addressing this problem, consider the signal voltage at the end of the K^{th} element, , given by

$$\begin{aligned} s(KT) &= S \cos(\omega_0 + i_k \frac{M\pi}{T})KT \\ &= S \cos(\omega_0 KT + i_k MK\pi). \end{aligned} \quad (74)$$

Postulating a frequency shift at $t = KT$ so that $i_{K+1} = -i_K$, it follows that

$$\begin{aligned} S(KT^+) &= S \cos(\omega_0 + i_{K+1} \frac{M\pi}{T}) KT \\ &= S \cos(\omega_0 KT + i_{K+1} MK\pi) \\ &= S \cos(\omega_0 KT - i_K MK\pi). \end{aligned} \quad (75)$$

Continuity requires that

$$S(KT^-) = S(KT^+) \quad (76)$$

or

$$\cos(\omega_0 KT + i_K MK\pi) = \cos(\omega_0 KT - i_K MK\pi)$$

or

$$\sin \omega_0 KT \sin MK\pi = 0. \quad (77)$$

Since K is an integer, then M must also be an integer. Thus, a coherently detectable FSK signal whose shift frequency components each have long-term phase coherence must have an integer modulation index. Consequently, the minimum non-zero modulation index, M , is one. The generation and coherent detection of this FSK (CFSK, $M = 1$) signal is discussed in Section 3.3.

Now consider an alternative to the above condition of true long-term signal coherence. If the K th signal element ($s(t), (K-1)T \leq t \leq KT$) is permitted to be either phase coherent or shifted in phase by π radians, then (75) becomes

$$S(KT^+) = \pm S \cos(\omega_0 KT - i_K MK\pi). \quad (78)$$

Hence, the waveform continuity condition becomes

$$\cos(\omega_0 KT - i_k MK\pi) = \pm \cos(\omega_0 KT + i_k MK\pi). \quad (79)$$

Assuming phase coherence for K even and antiphase coherence for K odd, (79) yields

$$\begin{cases} \sin \omega_0 KT \sin i_k MK\pi = 0, & K \text{ even} \\ \cos \omega_0 KT \cos i_k MK\pi = 0, & K \text{ odd}. \end{cases} \quad (80)$$

It is readily apparent that (80) is satisfied for

$$M = N + \frac{1}{2}, \quad N = 0, \pm 1, \pm 2, \dots \quad (81)$$

Thus, a modulation index of an integer plus 1/2 yields a continuous FSK waveform whose shift frequency components are phase coherent (Modulo π radians). The case where $M = 1/2$ is especially significant in that the optimum MSK modem employs an FSK, $M = 1/2$ waveform. This system is discussed in Section 3.4.

Although the requirement for waveform continuity precludes the use of coherent phase shift keying (PSK) for practical, high-powered, VLF/LF signal transmission, a consideration of PSK is invaluable for the later analysis of the practical CFSK, MSK, and CSK systems. (The CSK modem, described in Chapter 5, employs MSK detection and differential post-detection logic to demodulate the data.) The biphase (phase reversal) PSK technique is somewhat simpler to describe and analyze than the

coherent FSK systems. Moreover, the mathematical description of the PSK post-detection noise voltage magnitude (or envelope) [10] closely describes the actual APD statistical measurement process. Thus, the discussion and analysis of the PSK system, presented in Section 3.2, provides insight to and a standard of comparison for the FSK modems.

3.2 Coherent Phase Shift Keying (PSK) Modem

The coherent PSK modem provides a useful performance standard for assessing the performance of coherent binary modems. Although its discontinuous signal waveform is incompatible with high-powered VLF/LF transmitting systems, it provides mathematically optimum detection efficiency in a non-fading white Gaussian noise environment [50]. Thus, the PSK system is an appropriate choice for a theoretical consideration of coherent modems.

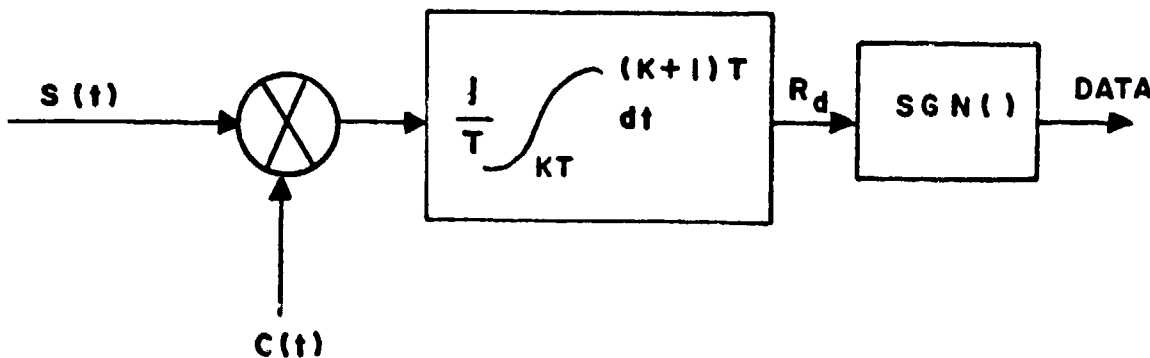


Figure 3. Coherent Phase Shift Keying
(Biphase PSK) Detector

Figure 3 is a functional block diagram of a coherent PSK detector.

Here, the input signal plus noise, $s(t)$, is given by

$$s(t) = S \cos(\omega_0 t + h_k \pi) + n(t), \quad (82)$$
$$KT \leq t \leq (K+1)T, \quad k=0, 1, \dots,$$

where S is the signal amplitude, ω_0 is the angular carrier frequency, $h_k = 0, 1$ according to the binary state of the k th data element, $n(t)$ is the additive noise process, and T is the length of a data element.

The coherent reference signal, $c(t)$, is given by

$$c(t) = S_1 \cos \omega_0 t. \quad (83)$$

The output of the integrator, R_d , (also designated the PSK detector functional) is given by

$$R_d = \frac{1}{T} \int_{KT}^{(K+1)T} c(t) s(t) dt$$
$$= \frac{1}{T} \int_{KT}^{(K+1)T} [S_1 \cos \omega_0 t] \times [S \cos(\omega_0 t + h_k \pi) + n(t)] dt \quad (84)$$

To facilitate further development, it is convenient to express $n(t)$ as

$$n(t) = e(t) \cos[\omega_0 t + \theta(t)], \quad (85)$$

where $e(t)$ and $\theta(t)$ are the noise envelope and phase processes, respectively.

Also, noting that the carrier frequency, ω_c , is typically much greater than the signal and noise process bandwidths at the detector input, it is apparent that the double frequency components in the integrand of (84) contribute negligibly to the value of the functional R_d . Thus, it is reasonable to neglect these high frequency components and consider the baseband component, R_b , of the functional. Substituting (85) into (84) and neglecting high frequency components,

$$R_b = \frac{SS_1}{2} \cos(h_k \pi) + \frac{S_1}{2T} \int_{kT}^{(k+1)T} e(t) \cos \theta(t) dt \quad (86)$$

Since the VLF atmospheric noise process has been observed to be approximately stationary for up to 10-15 minutes, the time base of the integral in (86) may be translated to $k = 0$ (for small k) to yield

$$R_b = \frac{SS_1}{2} \cos(h_k \pi) + \frac{S_1}{2T} \int_0^T e(t) \cos \theta(t) dt. \quad (87)$$

The binary decision is based on the algebraic sign of the detector functional R_b . Thus, the probability of a decision error, P_{ep} , is given by

$$P_{ep} = \Pr(R_b \geq 0 | h_k = 1) \Pr(h_k = 1) + \Pr(R_b < 0 | h_k = 0) \Pr(h_k = 0). \quad (88)$$

If the channel is symmetric, then

$$\Pr(R_b \geq 0 | h_k = 1) = \Pr(R_b < 0 | h_k = 0),$$

and (88) simplifies to

$$\begin{aligned} P_{ep} &= \Pr(R_b \geq 0 | h_k = 1) \\ &= \Pr\left[-\frac{SS_1}{2} + \frac{S_1}{2T} \int_0^T e(t) \cos \theta(t) dt > 0\right] \\ &= \Pr\left[\frac{1}{T} \int_0^T e(t) \cos \theta(t) dt > S\right]. \end{aligned} \quad (88a)$$

Further, if the phase process $\theta(t)$ is assumed to vary slowly with time so as to be nearly constant throughout the interval $(0, T)$, then the replacement of $\theta(t)$ by the random variable θ yields

$$P_{ep} = \Pr\left[\frac{\cos \theta}{T} \int_0^T e(t) dt > S\right]. \quad (90)$$

This expression is employed in Chapter 4 to derive quantitative PSK error rate performance in atmospheric noise. However, for the comparative analyses of CFSK and MSK detection in this chapter, it is necessary to determine the mean and variance of the PSK detector functional. Let the noise process, $n(t)$, be expressed in terms of its quadrature components by

$$n(t) = n_c(t)\cos \omega_0 t - n_s(t)\sin \omega_0 t. \quad (91)$$

Here, the quadrature components of the process, $n_c(t)$ and $n_s(t)$, are assumed to be zero mean and uncorrelated so that

$$E\{n_c(t)\} = E\{n_s(t)\} = E\{n_c(t)n_s(t)\} = 0. \quad (92)$$

Moreover, each is assumed to be approximately white and of equal spectral intensity $N_0/2$ watts/Hz. Thus,

$$\begin{aligned} R_{xx}(t_1, t_2) &\triangleq E\{n_c(t_1)n_c(t_2)\} = R_{yy}(t_1, t_2) \\ &\triangleq E\{n_s(t_1)n_s(t_2)\} = \frac{N_0}{2}\delta(t_1, t_2). \end{aligned} \quad (93)$$

Because the noise spectrum is assumed to be even around the carrier frequency, it also follows that

$$R_{xy}(t_1, t_2) \triangleq E\{n_c(t_1)n_s(t_2)\} = -R_{yx}(t_1, t_2) \\ \triangleq -E\{n_s(t_1)n_c(t_2)\} = 0. \quad (93a)$$

Substituting (91) into (84) and neglecting the double frequency components, the baseband detector functional, R_b , is

$$R_b = \frac{SS_1}{2} \cos(h_k \pi) \\ + \frac{S_1}{2T} \int_{KT}^{(K+1)T} n_c(t) dt. \quad (94)$$

The mean value is given by

$$\bar{R}_b = E\{R_b\} = \frac{SS_1}{2} \cos(h_k \pi) \\ + \frac{S_1}{2T} \int_{KT}^{(K+1)T} E\{n_c(t)\} dt \\ = \frac{SS_1}{2} \cos(h_k \pi). \quad (95)$$

The variance is given by

$$\begin{aligned}
 \text{Var}(R_b) &= \overline{(R_b - \bar{R}_b)^2} \\
 &= \frac{S_1^2}{4T^2} \int_{KT}^{(K+1)T} dt_1 \int_{KT}^{(K+1)T} dt_2 E\{n_c(t_1)n_c(t_2)\} \\
 &= \frac{S_1^2}{4T^2} \int_{KT}^{(K+1)T} dt_1 \int_{KT}^{(K+1)T} dt_2 \left[\frac{N_0}{2} \delta(t_1 - t_2) \right] \\
 &= \frac{S_1^2 N_0}{8T} \tag{96}
 \end{aligned}$$

In the special case where the noise process is Gaussian, the detector functional, R_b , is a Gaussian random variable. Here, the probability of error, P_e , is given by (88a)

$$\begin{aligned}
 P_{ep} &= P_r(R_b \geq 0 | h_k = 1) \\
 &= \frac{1}{\sqrt{2\pi} \sqrt{\text{Var}(R_b)}} \int_0^\infty \exp \left[\left(U - \bar{R}_{b|h_k=1} \right)^2 / 2 \text{Var}(R_b) \right] dU \\
 &= \frac{1}{\sqrt{2\pi}} \sqrt{\frac{8T}{S_1^2 N_0}} \int_0^\infty \exp \left[\left(U + \frac{SS_1}{2} \right)^2 / 4T / S_1^2 N_0 \right] dU
 \end{aligned}$$

Making the substitution

$$V = \frac{U + SS_1/2}{S_1} \sqrt{\frac{4T}{N_0}},$$

$$P_{ep} = \frac{1}{\sqrt{\pi}} \int_{\sqrt{\frac{S^2 T}{N_0}}}^\infty e^{-V^2} dV \tag{97}$$

$$P_{\text{ep}} = \frac{1}{2} \left[1 - \text{Erf} \left(\sqrt{\frac{S^2/2}{N_0/2T}} \right) \right]. \quad (98)$$

Since S is the received signal amplitude, $S^2/2$ is the received signal power. Also from (41), $1/T$ is the detector noise bandwidth so that $N_0/2T$ is the received noise power in the detection bandwidth. Hence, the argument of $\text{Erf}(\cdot)$ in (98) is simply the received signal-to-noise voltage ratio as referenced to the detection bandwidth. In Chapter 4, the direct numerical evaluation of (90) for Gaussian noise is shown to coincide with this latter well known theoretical result.

3.3 Coherent Frequency Shift Keying (CFSK, $M = 1$) Modem

(1) The only coherent modem now used for VLF/LF communication is the coherent frequency shift keying (CFSK, $M = 1$) system. This technique, as shown in Section 3.1, employs two shift frequency signal components which are characterized by long term phase coherence. The modulation index, M , is chosen to be an integer to insure continuity is maintained in the signal waveform at all times during frequency shift modulation. Mathematically, the transmitted CFSK, $M = 1$, waveform is described by (73) where $M = 1$.

The addition of the additive noise process $n(t)$ to this transmitted signal then yields the following mathematical expression, $s(t)$, for the received CFSK, $M = 1$, waveform

$$s(t) = S \cos \left(\omega_0 + i_k \frac{\pi}{T} t \right) + n(t), \quad (99)$$

$$KT \leq t \leq (K+1)T, \quad K=0, 1, \dots,$$

where S is the received signal amplitude, ω_0 is the nominal carrier (center) frequency, and

$$i_k = 1 - 2 h_k \quad (99a)$$

(where $h_k = 0, 1$ according to the binary state of the k th data element).

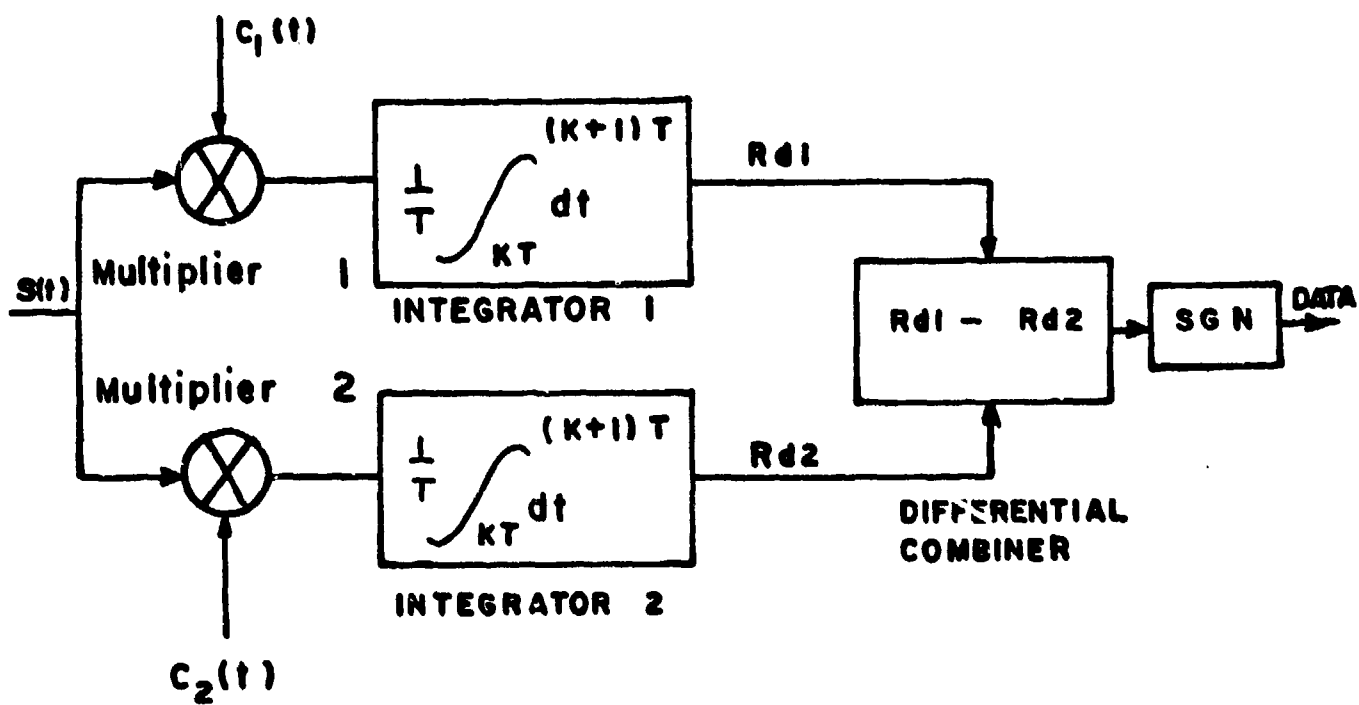


Figure 4. Coherent Frequency Shift Keying
(CFSK, $M = 1$) Detector

Figure 4 is a functional block diagram of a CFSK detector. Here, the input signal plus noise, as defined by (99), is coherently detected in two parallel correlators. The coherent reference signals, $c_1(t)$ and $c_2(t)$, are given by

$$c_1(t) = S_1 \cos(\omega_0 - \frac{\pi}{T})t, \quad (100)$$

and

$$c_2(t) = S_2 \cos(\omega_0 + \frac{\pi}{T})t. \quad (101)$$

The outputs of the two correlators are (utilizing (91))

$$\begin{aligned} R_{d1} &= \frac{1}{T} \int_{kT}^{(k+1)T} S(t) c_1(t) dt \\ &= \frac{1}{T} \int_{kT}^{(k+1)T} [S \cos(\omega_0 + i_k \frac{\pi}{T})t + \\ &\quad + n_c(t) \cos \omega_0 t - n_s(t) \sin \omega_0 t] \times \\ &\quad \times [S_1 \cos(\omega_0 - \frac{\pi}{T})t] dt, \end{aligned} \quad (102)$$

and

$$\begin{aligned} R_{d2} &= \frac{1}{T} \int_{kT}^{(k+1)T} [S \cos(\omega_0 + i_k \frac{\pi}{T})t + \\ &\quad + n_c(t) \cos \omega_0 t - n_s(t) \sin \omega_0 t] \times \\ &\quad \times [S_2 \cos(\omega_0 + \frac{\pi}{T})t] dt. \end{aligned} \quad (103)$$

Neglecting double frequency components in the integrand,

$$R_{d1} \approx \frac{SS_1}{2T} \int_{kT}^{(k+1)T} \cos(i_k + 1) \frac{\pi t}{T} dt + \\ + \frac{S_1}{2T} \int_{kT}^{(k+1)T} [n_c(t) \cos \frac{\pi t}{T} - n_s(t) \sin \frac{\pi t}{T}] dt, \quad (104)$$

and

$$R_{d2} \approx \frac{SS_1}{2T} \int_{kT}^{(k+1)T} \cos(i_k - 1) \frac{\pi t}{T} dt + \\ + \frac{S_1}{2T} \int_{kT}^{(k+1)T} [n_c(t) \cos \frac{\pi t}{T} + n_s(t) \sin \frac{\pi t}{T}] dt. \quad (105)$$

Since $E\{n_c(t)\} = E\{n_s(t)\} = 0$, it immediately follows that

$$\overline{R_{d1}} = \frac{SS_1}{2T} \int_{kT}^{(k+1)T} \cos(i_k + 1) \frac{\pi t}{T} dt \quad (106)$$

and

$$\overline{R_{d2}} = \frac{SS_1}{2T} \int_{KT}^{(K+1)T} \cos(i_k - 1) \frac{\pi t}{T} dt. \quad (107)$$

Under the hypothesis $h_k = 0, i_k = 1$ (from (99a)), (106) and (107) yield the conditional detector functionals:

$$\overline{R_{d1|0}} = 0 \quad (108)$$

$$\overline{R_{d2|0}} = \frac{SS_1}{2}. \quad (109)$$

Alternatively, the hypothesis $h_k = 1$ leads to

$$\overline{R_{d1|1}} = \frac{SS_1}{2} \quad (110)$$

$$R_{d2|1} = 0. \quad (111)$$

These latter results illustrate that the two shift frequency signals are orthogonal on the interval $(KT, (K+1)T)$ for integer k's.

Proceeding to a consideration of the noise components of the two detector functionals, it is convenient to define

$$N_1 \triangleq R_{d1} - \overline{R_{d1}} = \frac{S_1}{2T} \int_{KT}^{(K+1)T} [n_c(t) \cos \frac{\pi t}{T} - n_s(t) \sin \frac{\pi t}{T}] dt \quad (112)$$

and

$$N_2 \triangleq R_{d2} - \overline{R_{d2}} = \frac{S_1}{2T} \int_{KT}^{(K+1)T} [n_c(t) \cos \frac{\pi t}{T} + n_s(t) \sin \frac{\pi t}{T}] dt \quad (113)$$

The decision rule for the detector is based on the algebraic sign of $(R_{d1} - R_{d2})$. Under the hypothesis $h_k = 0$, a decision error occurs when $(R_{d1|0} - R_{d2|0}) > 0$ and under $h_k = 1$ an error occurs when $(R_{d1|1} - R_{d2|1}) < 0$. Thus, the probability of decision error, P_{ec} , is given by

$$P_{ec} = P_r[(R_{d1|0} - R_{d2|0}) > 0] P_r[h_k = 0] + P_r[(R_{d1|1} - R_{d2|1}) < 0] P_r[h_k = 1]. \quad (114)$$

If the channel is symmetric, then

$$P_r[(R_{d1|0} - R_{d2|0}) > 0] = P_r[(R_{d1|1} - R_{d2|1}) < 0] \quad (115)$$

and (114) simplifies to

$$\begin{aligned} P_{ec} &= \Pr [(R_{d1|1} - R_{d2|1}) < 0] \\ &= \Pr \left[\frac{SS_1}{2} + N_1 - N_2 < 0 \right] \\ &= \Pr \left[\frac{SS_1}{2} < N_2 - N_1 \right]. \end{aligned} \quad (116)$$

3.3.1 CFSK Post-Detection Signal-to-Noise Ratio

Examining the noise component of (116), the total post-detection noise power is given by

$$\overline{(N_2 - N_1)^2} = E \left\{ N_2^2 - 2N_1N_2 + N_1^2 \right\}. \quad (117)$$

Utilizing (112), it is found that

$$\begin{aligned}
 E\left\{N_1^2\right\} &= \frac{S_1^2}{4T^2} \int_{kT}^{(k+1)T} dt_1 \int_{kT}^{(k+1)T} dt_2 \times \\
 &\quad \times E\left\{n_c(t_1) \cos \frac{\pi t_1}{T} - n_s(t_1) \sin \frac{\pi t_1}{T}\right\} \times \\
 &\quad \times \left[n_c(t_2) \cos \frac{\pi t_2}{T} - n_s(t_2) \sin \frac{\pi t_2}{T}\right] \\
 &= \frac{S_1^2}{4T^2} \int_{kT}^{(k+1)T} dt_1 \int_{kT}^{(k+1)T} dt_2 \times \\
 &\quad \times \left[E\left\{n_c(t_1) n_c(t_2) \cos \frac{\pi t_1}{T} \cos \frac{\pi t_2}{T}\right\}\right. \\
 &\quad + E\left\{n_s(t_1) n_s(t_2) \sin \frac{\pi t_1}{T} \sin \frac{\pi t_2}{T}\right\} \\
 &\quad - E\left\{n_c(t_1) n_s(t_2) \cos \frac{\pi t_1}{T} \sin \frac{\pi t_2}{T}\right\} \\
 &\quad \left. - E\left\{n_s(t_1) n_c(t_2) \sin \frac{\pi t_1}{T} \cos \frac{\pi t_2}{T}\right\}\right] \\
 &= \frac{S_1^2}{4T^2} \int_{kT}^{(k+1)T} dt_1 \int_{kT}^{(k+1)T} dt_2 \times \\
 &\quad \times \left[\frac{N_o}{2} \delta(t_1 - t_2) \cos \frac{\pi t_1}{T} \cos \frac{\pi t_2}{T}\right. \\
 &\quad \left. + \frac{N_o}{2} \delta(t_1 - t_2) \sin \frac{\pi t_1}{T} \sin \frac{\pi t_2}{T}\right] \\
 &= \frac{S_1^2}{4T^2} \int_{kT}^{(k+1)T} \frac{N_o}{2} dt_1 = \frac{S_1^2 N_o}{8T} . \quad (118)
 \end{aligned}$$

Similarly, utilizing (113),

$$E\{N_2^2\} = \frac{S_1^2 N_0}{8T}. \quad (119)$$

Finally,

$$\begin{aligned}
 E\{N_1 N_2\} &= \frac{S_1^2}{4T^2} \int_{KT}^{(K+1)T} dt_1 \int_{KT}^{(K+1)T} dt_2 \times \\
 &\quad \times E\left\{ \left[n_c(t_1) \cos \frac{\pi t_1}{T} - n_s(t_1) \sin \frac{\pi t_1}{T} \right] \times \right. \\
 &\quad \times \left. \left[n_c(t_2) \cos \frac{\pi t_2}{T} + n_s(t_2) \sin \frac{\pi t_2}{T} \right] \right\} \\
 &= \frac{S_1^2}{4T^2} \int_{KT}^{(K+1)T} dt_1 \int_{KT}^{(K+1)T} dt_2 \times \\
 &\quad \times \left[E\left\{ n_c(t_1) n_c(t_2) \right\} \cos \frac{\pi t_1}{T} \cos \frac{\pi t_2}{T} \right. \\
 &\quad \left. - E\left\{ n_s(t_1) n_s(t_2) \right\} \sin \frac{\pi t_1}{T} \sin \frac{\pi t_2}{T} \right. \\
 &\quad \left. + E\left\{ n_c(t_1) n_s(t_2) \right\} \cos \frac{\pi t_1}{T} \sin \frac{\pi t_2}{T} \right. \\
 &\quad \left. - E\left\{ n_s(t_1) n_c(t_2) \right\} \sin \frac{\pi t_1}{T} \cos \frac{\pi t_2}{T} \right] \\
 &= \frac{S_1^2}{4T^2} \int_{KT}^{(K+1)T} dt_1 \int_{KT}^{(K+1)T} dt_2 \times \\
 &\quad \times \left[\frac{N_0}{2} \delta(t_1 - t_2) \cos \frac{\pi}{T}(t_1 + t_2) \right] \\
 &= \frac{S_1^2}{4T^2} \int_{KT}^{(K+1)T} dt_1 \frac{N_0}{2} \cos \frac{2\pi t_1}{T} = 0. \quad (120)
 \end{aligned}$$

Substituting (118), (119), and (120) into (117), the total post-detection noise power is

$$\overline{(N_2 - N_1)^2} = \overline{N_2^2} + \overline{N_1^2} = \frac{S_1^2 N_0}{4T}. \quad (121)$$

It should be noted that the CFSK post-detection noise power is exactly twice that of the PSK detector given by (96). On the other hand, the magnitude of the mean values (signal component) of the final CFSK and PSK detector functionals are equal and given by (95, PSK) and (106, 107, CFSK) as

$$|R_b| = \left| \overline{(R_{d1} - R_{d2})} \right| = \frac{SS_1}{2}. \quad (122)$$

Hence, for equal input signal powers and equal noise intensity, the post-detection signal-to-noise ratio of the CFSK system is exactly one-half (or -3 dB) that of the PSK system.

In the special case where the input noise is Gaussian, the resultant noise components produced in the linear detector functionals are Gaussian random variables. Thus, the condition of a 3 dB higher signal-to-noise ratio in the PSK detector suffices to show that the CFSK system requires exactly twice the signal power as does the PSK system for a given error probability (at the same data rate and in the same Gaussian noise environment). On the other hand, this 3 dB difference in post-detection signal-to-noise ratios does not necessarily imply an exact 3 dB difference in detection efficiencies for non-Gaussian

noise. The following discussion develops a general relationship between the PSK and CFSK post-detection noise voltage probability densities and the consequent error rate characteristics. This result is of primary interest for non-Gaussian noise, but it is also valid for Gaussian noise.

3.3.2 Relationship of CFSK Post-Detection Noise to PSK

Post-Detection Noise

3.3.2.1 Equivalent Noise Bandwidths of the PSK and CFSK Detectors

In the PSK detector, the observed noise envelope voltage is given by (36) where $c(t) \triangleq C$. From this (41) gives the equivalent noise bandwidth, B_n , of the PSK detector (or matched filter) as

$$B_n = 1/T \quad (41)$$

where T is the bit length.

In the case of the CFSK detector, the observed noise envelope voltage is given by (36) where $c(t) \triangleq C \sin \frac{\pi t}{T}$, $0 \leq t \leq T$. This defines the CFSK post-detection noise envelope voltage, E_c , as

$$E_c = \frac{1}{T} \int_0^T C \sin \frac{\pi t}{T} e(t) dt \quad (123)$$

This can also be expressed in the form of the convolution integral

$$E_c = \int_0^T \hat{C}(T-t) e(t) dt \quad (123a)$$

where

$$\hat{C}(t) = \begin{cases} \frac{C}{T} \sin \frac{\pi t}{T}, & 0 \leq t \leq T \\ 0, & \text{elsewhere.} \end{cases} \quad (123b)$$

From this it is apparent that E_c may also be considered to be the response of a linear filter at $t = T$ to the input $e(t)$ where the impulse response of the filter is given by $C(t)$. The transfer function of this filter is given by

$$H_c(j\omega) = \int_{-\infty}^{\infty} \hat{C}(t) e^{-j\omega t} dt$$

$$= \frac{C}{T} \int_0^T \sin \frac{\pi t}{T} e^{-j\omega t} dt. \quad (124)$$

The equivalent noise bandwidth of this filter is then given by

$$B_{nc} \triangleq \frac{\frac{1}{2\pi} \int_{-\infty}^{\infty} |H_c(j\omega)|^2 d\omega}{|H_c(0)|^2}. \quad (125)$$

Applying Parseval's Theorem, this becomes

$$\begin{aligned}
 B_{nc} &= \frac{\int_{-\infty}^{\infty} \hat{C}(t)^2 dt}{|H_c(0)|^2} \\
 &= \frac{\int_0^T \frac{C^2}{T^2} \sin^2\left(\frac{\pi t}{T}\right) dt}{\left|\frac{C}{T} \int_0^T \sin \frac{\pi t}{T} dt\right|^2} \\
 &= \frac{C^2/2T}{(2C/\pi)^2} = \frac{\pi^2}{8T}. \tag{126}
 \end{aligned}$$

Hence, the ratio of the CFSK and PSK detector equivalent noise bandwidth is

$$B_{nc}/B_n = \pi^2/8 = 1.2337. \tag{127}$$

This result implies that the V_d ratio of the CFSK post-detection noise corresponds to an observation bandwidth $\pi^2/8$ that of the PSK detector.

In the case of non-Gaussian noise, the V_d ratio of the VFSK post-detection noise can be found by employing this noise bandwidth conversion and the V_d ratio for PSK post-detection in Figure 26 of CCIR 322 [26]. The quantitative effect of this bandwidth conversion is that the V_d ratio (or impulsiveness) of the CFSK post-detection noise is slightly greater than that of PSK noise. In Gaussian noise,

on the other hand, the bandwidth conversion does not affect the Gaussian character of the post-detection noise components. Thus the noise bandwidth conversion principle is independent of the earlier observation that the PSK detector is exactly 3 dB more efficient than the CFSK detector in white Gaussian noise. However, at this point, it is valuable to seek some substantiation for the bandwidth conversion principle in approximately white, non-Gaussian, atmospheric noise. To this end, the following approximate analysis is presented.

3.3.2.2 Numerical Estimation of the Statistics of CFSK Post-Detection Noise

3.3.2.2.1 Partition of the PSK Detector Noise Functional into Statistically Independent Voltages

First, consider the possible subdividing of the PSK detector noise functional. The PSK post-detection noise voltage, N_p , is given by the second term of (94)

$$N_p = \frac{S_i}{2T} \int_{KT}^{(K+1)T} n_c(t) dt . \quad (128)$$

Assuming the noise process $n_c(t)$ is approximately stationary over several bit intervals, K can be specified as zero without affecting the statistics of N_p . This results in

$$N_p = \frac{S_i}{2T} \int_0^T n_c(t) dt . \quad (129)$$

This expression can be rewritten as

$$N_p = \sum_{K=1}^M \frac{1}{M} N_{pk} \quad (130)$$

where

$$N_{pk} = \frac{S_1}{2(T/M)} \int_{(k-1)T/M}^{kT/M} n_c(t) dt. \quad (130a)$$

Again, approximate stationarity implies that the N_{pk} 's have identical probability densities. Moreover, it should be noted that the N_{pk} 's constitute noise voltages as obtained by detection in the noise bandwidth M/T , which is M times as great as the overall detection bandwidth, $1/T$. Therefore, it can be concluded that the variance (or effective noise power) of each N_{pk} is M times as great as that of N_p .

Also,

$$\overline{N_{pk} N_{pl}} = \frac{S_1^2 M^2}{4T^2} \int_{(k-1)T/M}^{kT/M} dt_1 \int_{(l-1)T/M}^{LT/M} dt_2 E\{n_c(t_1) n_c(t_2)\}. \quad (131)$$

In the case where the noise is approximately white and of spectral intensity $N_0/2$, application of (93) yields

$$\overline{N_{pk} N_{pl}} = \frac{S_1^2 M^2 N_0}{8T^2} \int_{(k-1)T/M}^{kT/M} dt_1 \int_{(l-1)T/M}^{LT/M} dt_2 \delta(t_1 - t_2)$$

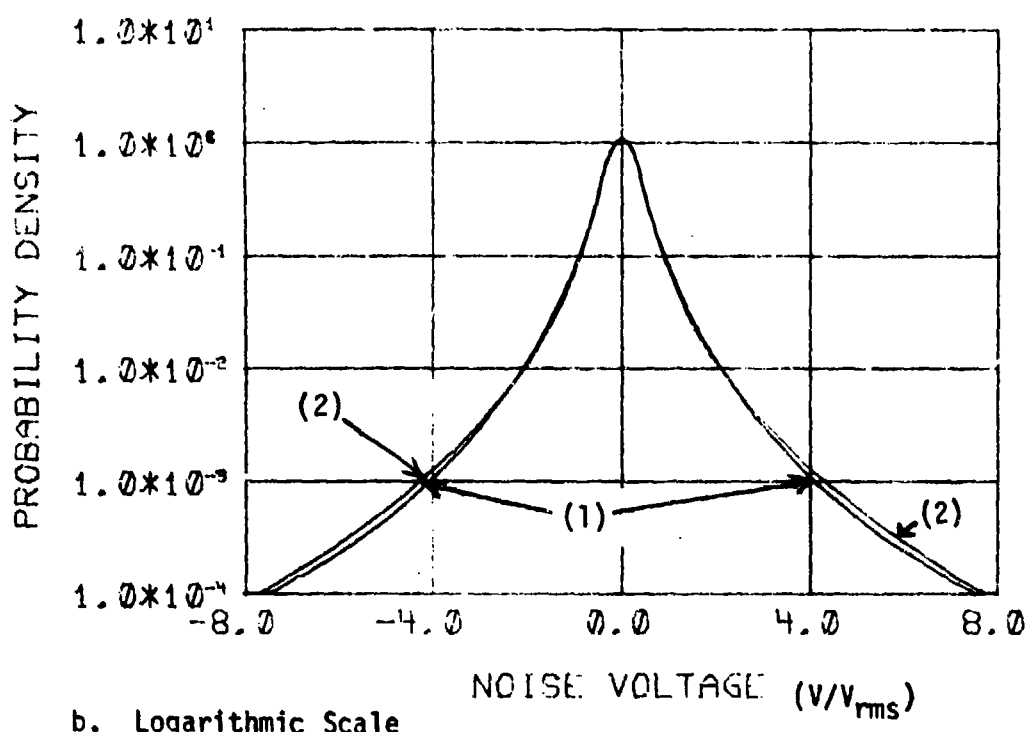
$$\frac{N_{pk}}{N_{PL}} = \begin{cases} \frac{S_1^2 \cdot \gamma^2 N_0}{8 I^2}, & K=L \\ 0, & K \neq L \end{cases} \quad (132)$$

Hence, the voltages N_{pk} are uncorrelated. Now it is postulated that the N_{pk} 's are statistically independent for an appropriate (but as yet undetermined) M so that the probability density of N_p equals the Mth order convolution of the probability densities of (N_{pk}/M) . (The scale factor M^{-1} is necessary to obtain equal variances). Mathematically, this can be written as

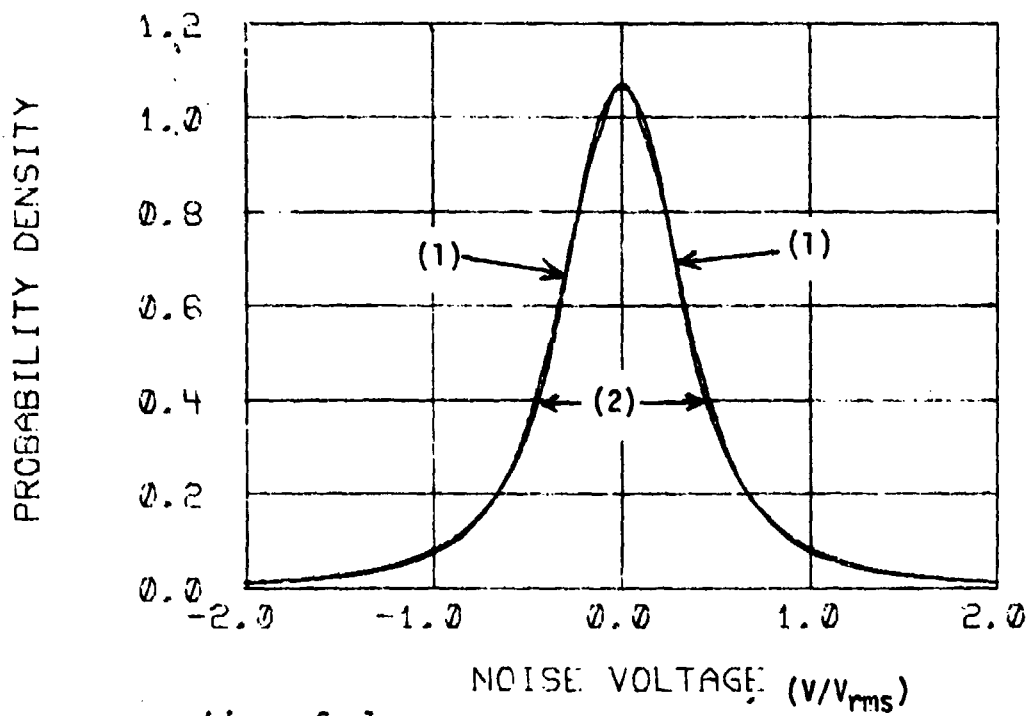
$$f_{N_p}(z) = f_{N_{p1}/M}(z) * \dots * f_{N_{pM}/M}(z). \quad (133)$$

(In the special case of white Gaussian noise, (133) holds for all values of M because uncorrelated Gaussian samples are also statistically independent.)

In order to determine the existence and proper value of M for (133) to hold for the non-Gaussian atmospheric noise case, Mth order convolutions of the probability densities of (N_{pk}/M) were evaluated by a numerical integration procedure similar to that described in detail in Chapter 6. Here the probability density of the samples, (N_{pk}/M) , was defined by a V_d ratio corresponding to the M/T detection bandwidth as obtained from Figure 26 of CCIR 322 [26]. Figure 5 shows the probability density of the atmospheric noise voltage, N_p , for $V_d = 3.75$ and the synthesized noise probability density obtained by the fifth-order convolution of sample noise voltage, N_{pk} , probability densities. In



b. Logarithmic Scale



a. Linear Scale

Figure 5. Probability Densities for Atmospheric Noise: (1) $V_d(V_1) =$

$$3.75 \text{ db}, (2) V_d(V_2) = 3.64 \text{ db} \text{ where } V_2 = \sum_{k=1}^5 U_k, U_k \text{'s}$$

 Statistically Independent, and $V_d(U_k) = 6.7 \text{ db.}$

this case, the sample noise voltage V_d ratio is 6.7 dB and the V_d ratio of the sum of the five statistically independent sample voltages is computed to be 3.64 dB. The close agreement of the V_d ratios and the two probability densities is apparent.

In addition to the illustrative example, other sample noise probability densities were numerically convolved to obtain synthesized approximations of noise voltage densities at V_d 's of 2.5 and 5 dB. The V_d ratios obtained by these convolution syntheses are summarized in Table I. Column (1) contains V_d ratios assumed for the total atmospheric noise voltage, N_p . Columns (2) and (6) list the corresponding V_d ratios of sample voltages as obtained from Figure 26 of CCIR 322 [26] for noise bandwidth multiplications by 3 and 5 respectively. Finally, Columns (3) and (7) show the V_d ratios for the uniformly weighted sums of three and five statistically independent sample voltages, respectively. It can be seen that the V_d ratio for the sample voltage sums is less sensitive to the number of samples, M , as the resultant V_d ratios tend toward the Gaussian noise V_d ratio of 1.049 dB. In the limiting case where the sample voltages are Gaussian, the sum of these voltages is also Gaussian and, consequently, the resultant V_d ratio is independent of M . Moreover, the results tabulated in Columns (3) and (7) indicate that (133) holds for some M where $3 \leq M \leq 5$ and the V_d ratio of the PSK post-detection noise voltage, N_p , lies between 2.5 and 5 dB.

TABLE I

V_d RATIOS OF ADDITIVE INDEPENDENT ATMOSPHERIC NOISE
VOLTAGES AND ESTIMATED NOISE BANDWIDTH RATIOS (BWR)*

		3 Voltage Samples				5 Voltage Samples					
Total Noise	V_d	Sample	Uniform Weighting	Sinusoidal Weighting	Estimated	Sample	Uniform Weighting	Sinusoidal Weighting	Estimated		BWR
		(1)	(2)	(3)	(4)	(5)	(6)	(7)	(8)		(9)
2.5	3.75	2.47	2.79	1.2	4.5	2.48	2.77		2.77	1.2	
3.75	6.0	3.93	4.38	1.25	6.7	3.64	4.11		4.11	1.25	
5.0	8.0	5.15	5.74	1.25	10.0	5.50	6.20		6.20	1.25	

* From Figure 26, CCIR 322 [26]

3.3.2.2.2 Synthesis of the CFSK Detector Noise Functional

Based on this latter indication of the existence of an M satisfying (133) and the close correspondence of original and synthesized noise voltage probability densities (as illustrated by Figure 5), it is concluded that the PSK detector voltage produced by atmospheric noise, N_p , is closely approximated by the sum of a proper number of statistically independent, identically distributed, sample voltages.

Having established that the PSK detector functional, N_p , can be accurately partitioned into M independent sample voltages, it is now appropriate to consider the noise component of the CFSK detector functional. If the expression for the CFSK error probability (116) is rewritten with N_1 and N_2 replaced by (112) and (113), the following expression results:

$$\begin{aligned}
 P_{ec} &= Pr \left\{ \frac{SS_i}{2} < \frac{S_i}{2T} \int_{KT}^{(K+1)T} [n_c(t) \cos \frac{\pi t}{T} \right. \\
 &\quad \left. + n_s(t) \sin \frac{\pi t}{T}] dt \right. \\
 &\quad \left. - \frac{S_i}{2T} \int_{KT}^{(K+1)T} [n_c(t) \cos \frac{\pi t}{T} \right. \\
 &\quad \left. - n_s(t) \sin \frac{\pi t}{T}] dt \right\} \\
 &= Pr \left\{ \frac{SS_i}{2} < \frac{S_i}{T} \int_{KT}^{(K+1)T} n_s(t) \sin \frac{\pi t}{T} dt \right\}. \quad (134)
 \end{aligned}$$

Here, the noise component, N_c , of the CFSK detector functional is given by the right side of the inequality indicated in the argument of $P_r\{\cdot\}$. Hence,

$$N_c \triangleq \frac{S_1}{T} \int_{KT}^{(K+1)T} n_s(t) \sin \frac{\pi t}{T} dt. \quad (135)$$

Again assuming the noise process $n_s(t)$ is approximately stationary over several bit intervals, K can be specified as zero without affecting the statistics of N_p . This results in

$$N_c = \frac{S_1}{T} \int_0^T n_s(t) \sin \frac{\pi t}{T} dt. \quad (136)$$

This expression indicates that the CFSK post-detection noise voltage, N_c , consists of the time integration of a quadrature component of the atmospheric noise process as multiplied by the sinusoidal weighting function: $(S_1/T) \sin \frac{\pi t}{T}$. On the other hand, the PSK post-detection noise voltage, N_p , consists of the time integration of a quadrature component of the atmospheric noise process as multiplied by the constant weighting function: $S_1/2T$. Because of this difference, there is no clear relationship between the statistics of the CFSK post-detection noise and corresponding PSK post-detection noise. However, it is possible to approximate the sinusoidal weighting function in the integrand of (136) by rectangular steps of equal width. This yields

$$N_c \approx \sum_{k=1}^M \frac{1}{M} \alpha_k N_{PK} \quad (137)$$

where

$$\sum_{K=1}^M \int_{(K-1)T/M}^{KT/M} a_k^n dt = \int_0^T \sin^n\left(\frac{\pi t}{T}\right) dt, \quad (138)$$

and N_{pk} is given by (130a). (It should be noted that $a_k = a_{M-k+1}$, $k = 1, \dots, (M-1)/2$, for odd M's. Thus, the $(M+1)/2$ relationships of (138) define the step amplitudes so as to equate the moments of the sine branch and its stepwise approximation to the maximum extent possible for a given value of M.)

Now the previously demonstrated principle that the N_{pk} 's are approximately statistically independent for the proper choice of M ($3 \leq M \leq 5$, for $2.5 \text{ dB} \leq V_d \leq 5 \text{ dB}$) can be employed for the stepwise-approximated CFSK noise functional. In this case, a probability density can be obtained for the CFSK noise voltage, as approximated by (137), by the Mth order convolution of the probability densities of $(a_k N_{pk}/M)$. Mathematically, this can be written as

$$f_{N_c}(z) = f_{a_1 N_{p1}/M}(z) * \dots * f_{a_M N_{pM}/M}(z), \quad (139)$$

where the a_k 's are the aforementioned sinusoidal weighting factors.

To obtain approximate CFSK noise voltage statistics comparable to those already computed for the PSK detector, (139) was evaluated numerically for noise samples identical to those used for the preceding PSK syntheses. The V_d ratios of these sums of sinusoidally-weighted, statistically independent noise sample voltages are presented in Columns (4) and (8) of Table I. It is apparent that the V_d ratios for these synthesized CFSK (sinusoidally weighted) voltages are invariably greater than for the corresponding PSK (uniformly weighted samples) noise voltages. At this point, reference to Figure 26 of CCIR 322 [26] readily establishes a remarkably consistent relationship between the corresponding terms of Columns (3) and (4), and (7) and (8). Although the construction of Figure 26, CCIR 322 [26] permits only minimal resolution, it is sufficient to show that the CFSK noise (Columns (4), (8)) correspond to a bandwidth 1.2 - 1.25 times as great as the PSK noise (Columns (3), (7)). This result clearly confirms the earlier theoretical result (127) which indicated that the CFSK post-detection noise would be characterized by a detection bandwidth $1.234 (= \pi^2/8)$ times as great as the PSK noise. This characteristic of the CFSK noise, coupled with its already proved 3 dB greater power, means that the CFSK error probability is equal to the PSK error rate at a 3 dB lower signal-to-noise ratio where the V_d ratio of the noise corresponds to the bandwidth $\pi^2/8T$ rather than the $1/T$ of a PSK detector. The experimental results of Chapter 4 lend further credence to this conclusion,

3.4 Minimum Shift Keying (MSK) Modem

Minimum Shift Keying is a modulation technique for transmitting binary data which involves minimum frequency shifting and produces a continuous signal waveform at all times. As noted earlier, the actual signal is an FSK, $M = 1/2$ waveform whose upper and lower shift frequency components are phase coherent-modulo π radians. Although the signal appears as FSK, the MSK detection process employs coherent phase detection at the center frequency rather than correlation at the upper and lower shift frequencies. The subsequent discussion and analysis demonstrates that this linear MSK performance coincides in Gaussian noise with that of PSK and is somewhat better in atmospheric noise. Consequently, MSK detection is at least 3 dB more efficient than the previously described CFSK, $M = 1$ detection.

3.4.1 MSK Modulation

First, consider the MSK modulation process. The waveforms depicted in Figure 6 illustrate the waveforms involved. The MSK modulation process begins with the time division demultiplexing of the input data (Figure 6a) into two subchannel binary sequences (Figures 6b, 6c) where the subchannel elements are $2T$ long. The X subchannel sequence is used to biphase modulate an amplitude modulated waveform $A_x(t)$, (see Figure 6d) given by

$$A_x(t) = S \left| \sin \frac{\pi t}{2T} \right| \sin \omega t. \quad (144a)$$

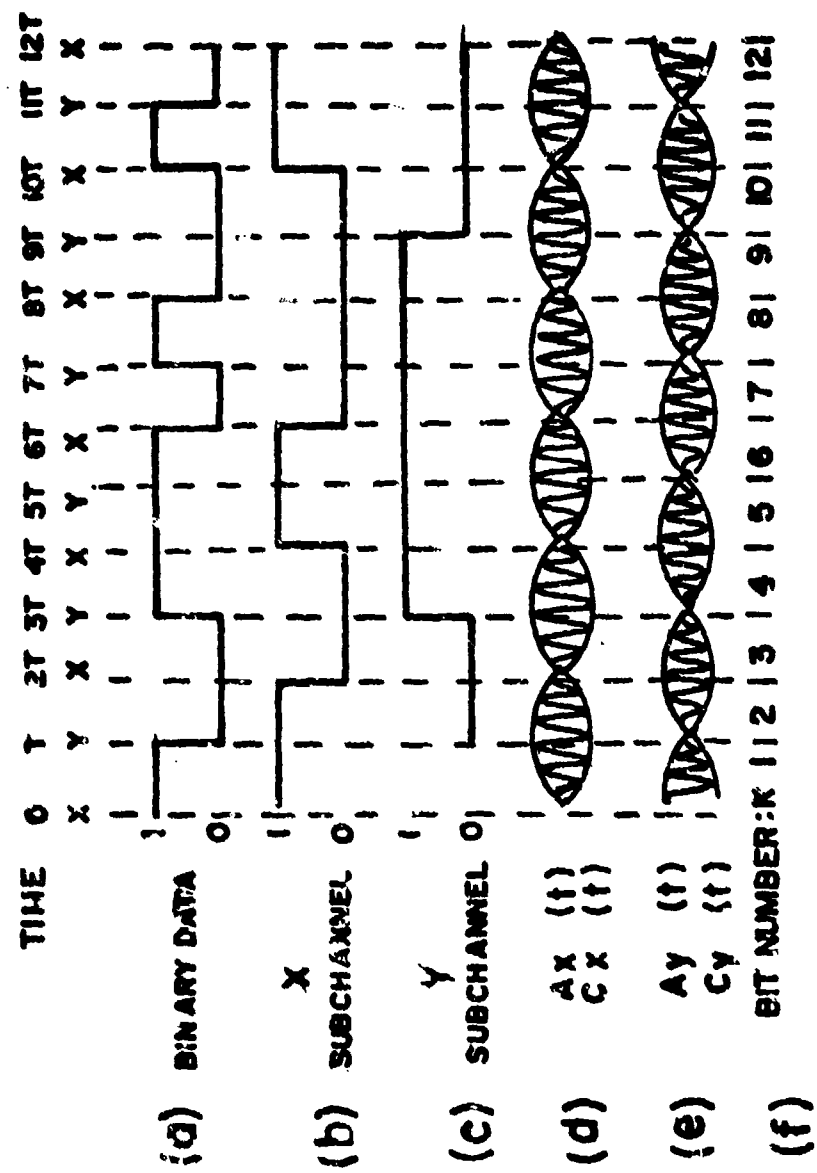


Figure 6. MSK Modulation/Demodulation Waveforms

The Y subchannel sequence similarly modulates $A_y(t)$ (see Figure 6e), given by

$$A_y(t) = S \left| \cos \frac{\pi t}{2T} \right| \cos \omega t. \quad (144b)$$

(Note that $A_x(t)$ has zero amplitude at the times when the X subchannel sequence may change state. The same condition exists for $A_y(t)$ and the Y subchannel sequence.)

This phase modulation yields

$$S_x(t) = i_k A_x(t), \quad (K-1)T \leq t \leq (K+1)T, \quad (145a)$$

$K \text{ odd},$

and

$$S_y(t) = i_k A_y(t), \quad (K-1)T \leq t \leq (K+1)T, \quad (145b)$$

$K \text{ even},$

where $i_k = 1 - 2h_k$ and $h_k = 0, 1$ according to the k th data element.

Substituting (144a) and (144b) in (145a) and (145b) and accounting for the absolute value signs leads to

$$S_x(t)_K = i_k S \sin \frac{\pi}{2T} [t - (K-1)T] \sin \omega t, \quad (146a)$$

$(K-1)T \leq t \leq (K+1)T, \quad K \text{ odd},$

and

$$S_y(t)_k = i_k S \cos \frac{\pi}{2T} [t - kT] \cos \omega_0 t, \quad (146b)$$
$$(k-1)T \leq t \leq (k+1)T, \quad k \text{ even.}$$

Now, for k odd, the k th MSK signal element, $S(t)_k$,
 $(k-1)T \leq t \leq kT$, consists of the sum of $S_x(t)$ and $S_y(t)$ (but with $k-1$ replacing k in (146b)). Here, $S(t)_k$ is given by

$$S(t)_k = i_k S \sin \frac{\pi}{2T} [t - (k-1)T] \sin \omega_0 t$$
$$+ i_{k-1} S \cos \frac{\pi}{2T} [t - (k-1)T] \cos \omega_0 t$$
$$= i_{k-1} S \cos \left[\omega_0 - i_k i_{k-1} \frac{\pi}{2T} \right] t \pm \frac{(k-1)}{2} \pi$$
$$= (-1)^{\frac{k-1}{2}} i_{k-1} S \cos \left[\omega_0 - i_k i_{k-1} \frac{\pi}{2T} \right] t, \quad (147)$$
$$(k-1)T \leq t \leq kT, \quad k \text{ odd.}$$

From this, it is apparent that the instantaneous frequency of the MSK signal is governed by the state of time adjacent data elements. The implication of (147) is that an odd element MSK modulator output signal is at the lower shift frequency during the k th interval when the k th data bit is the same state as its immediate predecessor.

On the other hand, if the k th bit is of the state opposite to its predecessor, then the output is at the upper shift frequency. For the next signal element, ($kT \leq t \leq (k+1)T$), is also added to $S_y(t)$ but with $k+1$ replacing k in (146b). This results in

$$\begin{aligned}
 S(t)_{k+1} &= i_k S \sin \frac{\pi}{2T} [t - (k-1)T] \sin \omega_0 t \\
 &\quad + i_{k+1} S \cos \frac{\pi}{2T} [t - (k+1)T] \cos \omega_0 t \\
 &= -i_k S \sin \frac{\pi}{2T} [t - (k+1)T] \sin \omega_0 t \\
 &\quad + i_{k+1} S \cos \frac{\pi}{2T} [t - (k+1)T] \cos \omega_0 t \\
 &= (-1)^{\frac{k+1}{2}} i_{k+1} S \cos [\omega_0 + i_k i_{k+1} \frac{\pi}{2T}] t, \quad (148) \\
 &\quad KT \leq t \leq (k+1)T, \quad k \text{ odd}.
 \end{aligned}$$

This result shows that an even MSK element is at the upper shift frequency if the even data bit and its immediate predecessor are of the same state. If the even bit and its predecessor are of opposite state, then the MSK signal is at the lower shift frequency. It is obvious, then, that there is no direct relationship between the binary state of the input data and the MSK signal output frequency. Because of this characteristic, the MSK signal cannot be readily demodulated by conventional non-coherent FSK detectors.

3.4.2 MSK Detection

Detection of the MSK signal involves the time-sequential phase detection of the subchannel signal elements, $S_x(t)$ and $S_y(t)$ as defined

by (146a) and (146b). Figure 7 is a simplified block diagram of a MSK detector.

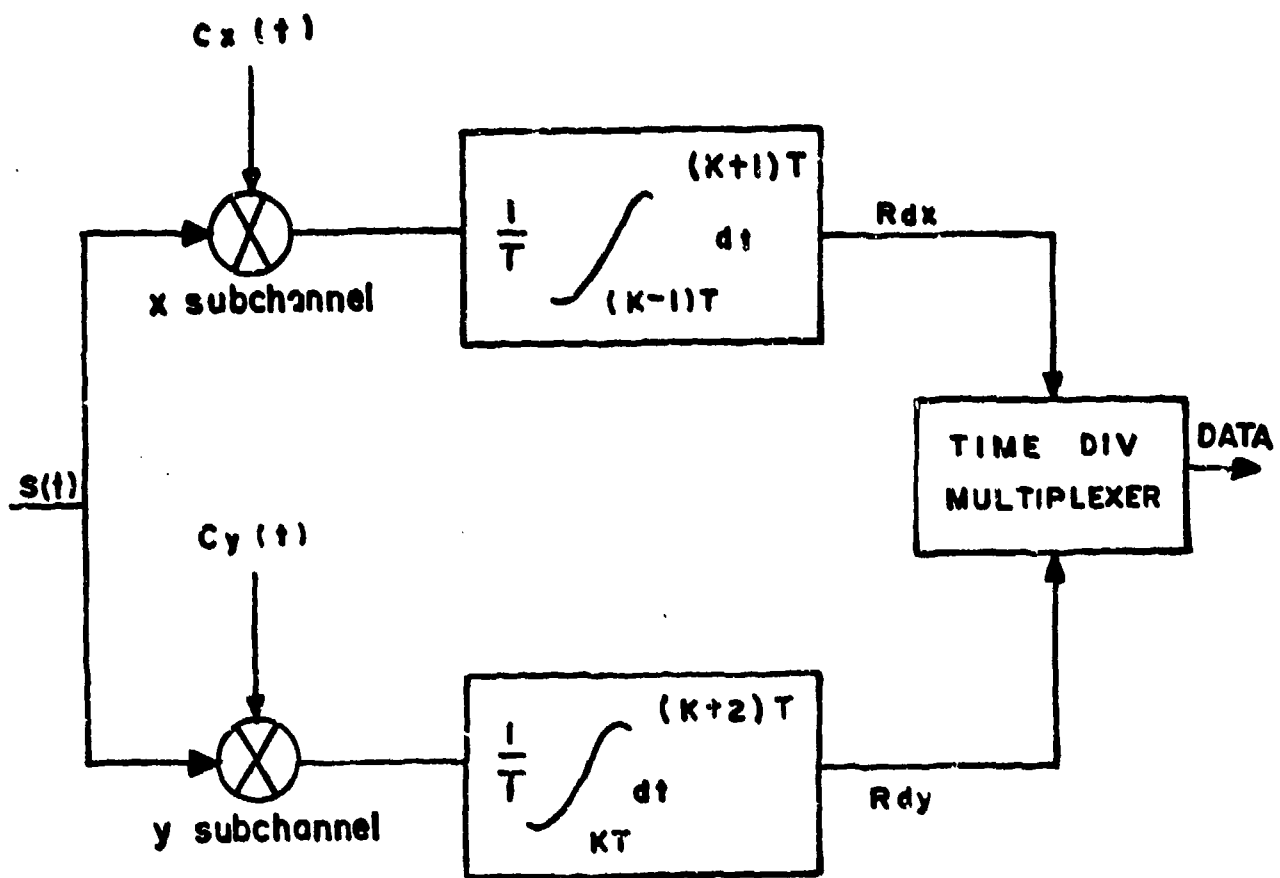


Figure 7. MSK Detector

The input signal plus noise, utilizing the narrowband noise representation (91) and the MSK signal representation (147) and (148), is given by

$$S(t) = S(t)_k + n_c(t) \cos \omega t - n_s(t) \sin \omega t, (K-1)T \leq t \leq KT \quad (149)$$

where

$$S(t)_k = \begin{cases} (-1)^{\frac{k-1}{2}} i_{k-1} S \cos[\omega_0 - i_k i_{k-1} \frac{\pi}{2T}]t, & k \text{ odd} \\ (-1)^{\frac{k}{2}} i_k S \cos[\omega_0 + i_k i_{k+1} \frac{\pi}{2T}]t, & k \text{ even}, \end{cases} \quad (149a)$$

$$i_k = 1 - 2h_k,$$

and $h_k = 0, 1$ according to the binary state of the k th data element.

The X subchannel coherent reference signal, $c_x(t)$, is given by (Figure 6d)

$$\begin{aligned} c_x(t) &= S_1 \left| \sin \frac{\pi t}{2T} \right| \sin \omega_0 t \\ &= S_1 \sin \frac{\pi}{2T} [t - (k-1)T] \sin \omega_0 t \\ &= (-1)^{\frac{k-1}{2}} S_1 \sin \frac{\pi t}{2T} \sin \omega_0 t, \\ &\quad (K-1)T \leq t \leq (K+1)T, K \text{ odd}. \end{aligned} \quad (150)$$

The Y subchannel coherent reference signal, $c_y(t)$, is given by (Figure 5e)

$$\begin{aligned} c_y(t) &= S_1 \left| \cos \frac{\pi t}{2T} \right| \cos \omega_0 t \\ &= S_1 \cos \frac{\pi}{2T} [t - kT] \cos \omega_0 t \\ &= (-1)^{\frac{k}{2}} S_1 \cos \frac{\pi t}{2T} \cos \omega_0 t, \\ &\quad (K-1)T \leq t \leq (K+1)T, K \text{ even}. \end{aligned} \quad (151)$$

Because the subchannel signal components are of the same form and equal power, detector performance should be the same for both subchannels. Therefore, the following analysis of X subchannel detection also suffices for Y subchannel detection. With reference to (149), (150), X subchannel signal elements correspond to K odd and, as shown by Figure 6b, the kth subchannel signal element is defined over the time interval $[(k-1)T, (k+1)T]$. Postulating that the kth data bit has $h_k = 1$ so that $i_k = -1$, the input signal becomes

$$S(t) = S(t)_K + n_c(t) \cos \omega_0 t - n_s(t) \sin \omega_0 t, \\ (K-1)T \leq t \leq (K+1)T,$$

where

$$S(t)_K = \begin{cases} (-1)^{\frac{K-1}{2}} i_{K-1} S \cos [\omega_0 + i_{K-1} \frac{\pi}{2T}] t, & (K-1)T \leq t \leq KT \\ (-1)^{\frac{K+1}{2}} i_{K+1} S \cos [\omega_0 - i_{K+1} \frac{\pi}{2T}] t, & KT \leq t \leq (K+1)T \end{cases} \quad (152)$$

Expanding $S(t)_K$ results in

$$S(t)_K = \begin{cases} (-1)^{\frac{K-1}{2}} i_{K-1} S \left\{ \cos \left(\frac{i_{K-1} \pi t}{2T} \right) \cos \omega_0 t - \sin \left(\frac{i_{K-1} \pi t}{2T} \right) \sin \omega_0 t \right\}, & (K-1)T \leq t \leq KT \\ (-1)^{\frac{K+1}{2}} i_{K+1} S \left\{ \cos \left(\frac{i_{K+1} \pi t}{2T} \right) \cos \omega_0 t + \sin \left(\frac{i_{K+1} \pi t}{2T} \right) \sin \omega_0 t \right\}, & KT \leq t \leq (K+1)T \end{cases}$$

$$s(t)_k = \begin{cases} (-1)^{\frac{k-1}{2}} S \left\{ i_{k-1} \cos \frac{\pi t}{2T} \cos \omega_0 t - \sin \frac{\pi t}{2T} \sin \omega_0 t \right\}, & (k-1)T \leq t \leq kT \\ (-1)^{\frac{k+1}{2}} S \left\{ i_{k+1} \cos \frac{\pi t}{2T} \cos \omega_0 t + \sin \frac{\pi t}{2T} \sin \omega_0 t \right\}, & kT \leq t \leq (k+1)T. \end{cases} \quad (153)$$

The output of the X subchannel detector is the functional R_{dx} , given by

$$R_{dx} = \frac{1}{T} \int_{(k-1)T}^{(k+1)T} c_x(t) s(t) dt. \quad (154)$$

Employing (150), (152), (153) in (154) and again disregarding high frequency components in the integrand (because the signal and noise process bandwidths are assumed to be much smaller than the frequency ω_0),

$$\begin{aligned} R_{dx} &= \frac{S_1}{2T} \int_{(k-1)T}^{(k+1)T} \left[-\frac{S}{2} - (-1)^{\frac{k-1}{2}} n_s(t) \sin \frac{\pi t}{2T} \right] dt \\ &= -\frac{SS_1}{2} - \frac{S_1}{2T} \int_{(k-1)T}^{(k+1)T} (-1)^{\frac{k-1}{2}} n_s(t) \sin \frac{\pi t}{2T} dt \end{aligned} \quad (155)$$

In this case, a decision error occurs when $R_{dx} > 0$. Hence the probability of MSK detection error, P_{e_m} , is given by

$$P_{em} = Pr(R_{dx} > 0) = Pr(-R_{dx} < 0)$$

$$= Pr \left[\frac{SS_1}{2} + \frac{S_1}{2T} \int_{(K-1)T}^{(K+1)T} (-1)^{\frac{k-1}{2}} n_s(t) \sin \frac{\pi t}{2T} dt < 0 \right]$$

$$= Pr \left\{ \frac{SS_1}{2} < - \frac{S_1}{2T} \int_{2KT}^{2(K+1)T} (-1)^{\frac{k-1}{2}} n_s[t-(K+1)T] \times \sin \frac{\pi}{2T}[t-(K+1)T] dt \right\}$$

$$= Pr \left\{ \frac{SS_1}{2} < \frac{S_1}{2T} \int_{2KT}^{2(K+1)T} n_s[t-(K+1)T] \sin \frac{\pi t}{2T} dt \right\}. \quad (156)$$

Since $n_s(t)$ is assumed to be approximately stationary over several bit intervals, the argument of $n_s[\cdot]$ in (156) may be translated to t without affecting the statistics of the argument of $Pr[\cdot]$ in (156). This translation results in

$$P_{em} = Pr \left[\frac{SS_1}{2} < \frac{S_1}{2T} \int_{2KT}^{2(K+1)T} n_s(t) \sin \frac{\pi t}{2T} dt \right]. \quad (157)$$

Recall the previously derived expression for CFSK error probability:

$$P_{ec} = Pr \left[\frac{SS_1}{2} < \frac{S_1}{T} \int_{KT}^{(K+1)T} n_s(t) \sin \frac{\pi t}{T} dt \right]. \quad (134)$$

It is apparent that if the CFSK binary signal elements are doubled in length (so that T is replaced by $2T$ in (134), then the CFSK error probability (at the transmission rate $1/2T$ bits/sec.) equals the MSK error probability (at the rate $1/T$ bits/sec.). In other words, the signal components of the MSK and CFSK detector functionals are equal, but the noise component of the MSK functional is identical to CFSK noise as detected in $1/2$ the corresponding (for the same data rate) detection bandwidth. Hence, the MSK post-detection signal-to-noise ratio is twice as great (+3 dB) as the CFSK signal-to-noise ratio. Moreover, the narrower MSK detector bandwidth causes the MSK post-detection noise to be less impulsive for non-Gaussian input noise.

Finally, it is appropriate to compare this result with the PSK system. Because the MSK post-detection signal-to-noise ratio is 3 dB greater than with the CFSK system, the MSK and PSK systems have the same post-detection signal-to-noise ratios. However, the PSK post-detection noise has a V_d ratio which corresponds to the equivalent noise bandwidth ($1/T$) while the MSK noise V_d ratio corresponds to the bandwidth ($\pi^2/16T$). Hence, the MSK post-detection noise is less impulsive for atmospheric input noise because of the narrower effective observation bandwidth. In the special case where the input noise process is Gaussian, both the PSK and MSK post-detection noise components are Gaussian random variables. Thus, the equivalence of post-detection signal-to-noise ratios insures that MSK and PSK error rate performance is identical (and 3 dB better than CFSK, $M = 1$) for Gaussian noise.

Chapter 4
PERFORMANCE OF LINEAR COHERENT VLF/LF
RECEIVERS IN ATMOSPHERIC NOISE

4.0 Introduction

The preceding PSK, CFSK, and MSK modem descriptions and analyses have developed general mathematical expressions (90), (142), (143), (158) for detection error probabilities (bit error rates). In terms of relative performance, it was shown that the CFSK post-detection signal-to-noise ratio is 3 dB less than the PSK and the CFSK noise V_d ratio corresponds to a bandwidth $\pi^2/8$ times as great as the $1/T$ PSK detection bandwidth. Also, the MSK detector produces the same post-detection signal-to-noise ratio as PSK but the MSK noise component is statistically the same as PSK noise observed in $\pi^2/16$ times the corresponding PSK detection bandwidth. In the special case where the input noise process is Gaussian, the post-detection noise components are Gaussian random variables whose statistics can be described by well-known, closed-form mathematical functions. Thus, the detection error probabilities for these systems can be expressed in closed-form (98). On the other hand, the statistics of received atmospheric noise are not accurately described by single, mathematically-tractable, closed-form expressions (see Chapter 2). Instead, atmospheric noise statistics are most accurately described numerically or by piecewise-algebraic expressions (see 2.1). Here, numerical methods must necessarily be employed in the evaluation of the error probability

expressions (90), (134) and (157). This chapter is thus concerned with the development of a numerical procedure for evaluating these error probability expressions and the presentation of comparable experimental performance data.

4.1 Development of Numerical Procedures for Evaluating Error Probabilities

The numerical procedure for evaluating detection error probabilities is related to the work of Spaulding [48] and similar to the numerical integration procedure developed by Shepelavey [45]. However, the integration technique developed here is adaptable to any arbitrarily defined noise APD (such as those of typical atmospheric noise) and is especially suitable for digital computer computation. The actual computational procedure is described in detail for evaluation of PSK error probabilities (90).

Because of the relationships developed in 3.3.2 and 3.4 between CFSK, MSK, and PSK detector performance, the PSK results can be readily adapted to describe CFSK and MSK performance. Hence, similar detailed computational developments for CFSK detection (142, 143) and MSK detection (158) would be largely redundant and are thus omitted. Finally, error rate performance of each of the systems, as computed by the numerical procedures of this chapter, is compared with the published PSK performance data of Linfield and Plush [32] and the CFSK and MSK data of Entzinger, *et al* [14]. The good agreement between computed and measured performance in each case clearly substantiates the validity of the linear PSK, CFSK, and MSK performance analyses.

4.1.1 Performance of the Linear PSK Receiver in Atmospheric Noise

The biphase coherent PSK modem is first considered. In this case, all receiver functions preceding the coherent phase detector are essentially linear so that only linear bandwidth conversion [11] is necessary to define an appropriate noise amplitude probability distribution. From 3.2 the probability of PSK detection error, P_{ep} , is given by

$$P_{ep} = Pr \left(\frac{\cos \theta}{T} \int_0^T e(t) dt > S \right) \quad (90)$$

where θ is uniformly distributed on $(-\pi, \pi)$ and $e(t)$ is the narrowband noise envelope process.

Now, employing the relationship (37) with $C = 1$, the integral of (90) can be replaced with the observed (in a $1/T$ Hz bandwidth) noise voltage, E_p , to yield

$$P_{ep} = Pr (E_p \cos \theta > S) \quad (159)$$

where E_p is a random variable statistically independent of the noise phase, θ .

Division of both sides of the inequality by the RMS value of the noise envelope voltage then yields

$$P_{ep} = Pr (E_p \cos \theta > \hat{S}) \quad (160)$$

where E is the ratio of the noise envelope voltage to the RMS noise envelope voltage (so that $\overline{E^2} = 1$) and \hat{S} is the ratio of the RMS signal envelope voltage (or signal amplitude) to the RMS noise envelope voltage. (It is apparent from the foregoing definition that \hat{S} is also the square root of the signal to noise power ratio.)

Proceeding, (160) may be rewritten as

$$P_{ep} = Pr\left(1 \geq \cos \theta \geq \frac{\hat{S}}{E}\right). \quad (161)$$

Here the outer inequality implies $E \geq \hat{S}$. (161) then becomes

$$P_{ep} = Pr\left[\cos^{-1}\left(\frac{\hat{S}}{E}\right) \geq |\theta|, E \geq \hat{S}\right] \quad (162)$$

where $\cos^{-1}(\cdot)$ is the principal value of $\cos^{-1}(\cdot)$ since both \hat{S} and E are non-negative and $\hat{S}/E > 0$.

Equivalently

$$P_{ep} = Pr\left[-\cos^{-1}\left(\frac{\hat{S}}{E}\right) \leq \theta \leq \cos^{-1}\left(\frac{\hat{S}}{E}\right), E \geq \hat{S}\right] \quad (162a)$$

or

$$P_{ep} = \int_{\hat{S}}^{\infty} dE \int_{-\cos^{-1}\left(\frac{\hat{S}}{E}\right)}^{\cos^{-1}\left(\frac{\hat{S}}{E}\right)} f_{\theta|E}(E, \theta) d\theta, \quad (162b)$$

where $f_{e,\theta}(E, \theta)$ is the joint probability density function of the normalized noise envelope voltage and phase.

Since E and θ are statistically independent and θ is uniformly distributed on $(-\pi, \pi)$, this reduces to

$$P_{ep} = \frac{1}{2\pi} \int_{\hat{s}}^{\infty} f_e(E) dE \int_{-\cos^{-1}(\frac{\hat{s}}{E})}^{\cos^{-1}(\frac{\hat{s}}{E})} d\theta$$

$$= \frac{1}{2\pi} \int_{\hat{s}}^{\infty} -\frac{d}{dE}[P(E)] dE \int_{-\cos^{-1}(\frac{\hat{s}}{E})}^{\cos^{-1}(\frac{\hat{s}}{E})} d\theta \quad (163)$$

where $P(E) = P(e > E)$ is the noise amplitude probability distribution as described by the curves of Figure 1. It follows that

$$P_{ep} = \frac{1}{2\pi} \int_{\hat{s}}^{\infty} -d[P(E)] \times 2 \cos^{-1}(\frac{\hat{s}}{E})$$

$$= \frac{1}{\pi} \int_{\infty}^{\hat{s}} \cos^{-1}(\frac{\hat{s}}{E}) dP(E). \quad (163a)$$

Considering the values of $\cos^{-1} \left(\frac{\hat{S}}{E} \right)$ for $S \leq E \leq \infty$, note that

$$\cos^{-1} \left(\frac{\hat{S}}{E} \right) = 0 \leq \cos^{-1} \left(\frac{\hat{S}}{E} \right) \leq \lim_{E \rightarrow \infty} \cos^{-1} \left(\frac{\hat{S}}{E} \right) = \frac{\pi}{2}. \quad (164)$$

Partitioning the range of values of $\cos^{-1} \left(\frac{\hat{S}}{E} \right)$ into n equal angles of size $\pi/2n$, the expression for P_E (163a) can similarly be partitioned into n integrals. The upper and lower limits of integration for the i th integral, E_i^U and E_i^L , respectively, must satisfy

$$\cos^{-1} \left(\frac{\hat{S}}{E_i^U} \right) = (i-1) \frac{\pi}{2n} \quad (165a)$$

and

$$\cos^{-1} \left(\frac{\hat{S}}{E_i^L} \right) = i \frac{\pi}{2n} . \quad (165b)$$

These equations yield

$$E_i^U = \frac{\hat{S}}{\cos \frac{(i-1)\pi}{2n}} \quad (166a)$$

and

$$E_i^L = \frac{\hat{S}}{\cos \frac{i\pi}{2n}} . \quad (166b)$$

Thus, the indicated n-fold partition of (163a) yields

$$\begin{aligned}
 P_{ep} &= \frac{1}{\pi} \int_{-\infty}^{\hat{S}} \cos^{-1}\left(\frac{\hat{S}}{E}\right) dP(E) \\
 &= \frac{1}{\pi} \sum_{i=1}^n \int_{E_i^-}^{E_i^+} \cos^{-1}\left(\frac{\hat{S}}{E}\right) dP(E) \\
 &= \frac{1}{\pi} \sum_{i=1}^n I_i
 \end{aligned}$$

where

$$I_i \triangleq \int_{\frac{\hat{S}}{\cos \frac{i\pi}{2n}}}^{\frac{\hat{S}}{\cos \frac{(i-1)\pi}{2n}}} \cos^{-1}\left(\frac{\hat{S}}{E}\right) dP(E). \quad (167)$$

Examining the i th integral of (167), and in particular, $\cos^{-1}\left(\frac{\hat{S}}{E}\right)$, it is noted that

$$\left. \frac{i\pi}{2n} = \cos^{-1}\left(\frac{\hat{S}}{E}\right) \right|_{E = \frac{\hat{S}}{\cos \frac{i\pi}{2n}}} \geq \left. \cos^{-1}\left(\frac{\hat{S}}{E}\right) \right|_{E \geq \frac{\hat{S}}{\cos \frac{i\pi}{2n}}} \quad (168a)$$

and

$$\frac{(i-1)\pi}{2n} = \cos^{-1}\left(\frac{\hat{S}}{E}\right) \leq \cos^{-1}\left(\frac{\hat{S}}{E}\right) \quad (168b)$$
$$E = \frac{\hat{S}}{\cos\frac{(i-1)\pi}{2n}} \quad E \leq \frac{\hat{S}}{\cos\frac{(i-1)\pi}{2n}}$$

These results lead to

$$\frac{i\pi}{2n} \geq \cos^{-1}\left(\frac{\hat{S}}{E}\right) \geq \frac{(i-1)\pi}{2n} \quad (169)$$
$$\frac{\hat{S}}{\cos\frac{(i-1)\pi}{2n}} \leq E \leq \frac{\hat{S}}{\cos\frac{i\pi}{2n}}$$

Substitution of these bounds in the integrand of (167) yields

$$\int_{\frac{\hat{S}}{\cos\frac{i\pi}{2n}}}^{\frac{\hat{S}}{\cos\frac{(i-1)\pi}{2n}}} \frac{i\pi}{2n} dP(E) \geq \int_{\frac{\hat{S}}{\cos\frac{i\pi}{2n}}}^{\frac{\hat{S}}{\cos\frac{(i-1)\pi}{2n}}} \cos^{-1}\left(\frac{\hat{S}}{E}\right) dP(E) \quad (170)$$
$$\geq \int_{\frac{\hat{S}}{\cos\frac{i\pi}{2n}}}^{\frac{\hat{S}}{\cos\frac{(i-1)\pi}{2n}}} \frac{(i-1)\pi}{2n} dP(E)$$

or

$$\begin{aligned}
 & \frac{i\pi}{2n} \left\{ P\left[\frac{\hat{s}}{\cos \frac{(i-1)\pi}{2n}}\right] - P\left[\frac{\hat{s}}{\cos \frac{i\pi}{2n}}\right] \right\} \triangleq I_i^u \\
 & \geq I_i = \int_{\frac{\hat{s}}{\cos \frac{(i-1)\pi}{2n}}}^{\frac{\hat{s}}{\cos \frac{i\pi}{2n}}} \cos^{-1}\left(\frac{\hat{s}}{E}\right) dP(E) \quad (171) \\
 & \geq \frac{(i-1)\pi}{2n} \left\{ P\left[\frac{\hat{s}}{\cos \frac{(i-1)\pi}{2n}}\right] - P\left[\frac{\hat{s}}{\cos \frac{i\pi}{2n}}\right] \right\} \triangleq I_i^l
 \end{aligned}$$

Now, performing n -fold summations and division by π on the outer terms of (171), it follows that

$$\begin{aligned}
 P_e^u & \triangleq \frac{1}{\pi} \sum_{i=1}^n I_i^u = \frac{1}{\pi} \cdot \frac{\pi}{2n} \left\{ \sum_{i=1}^n i P\left[\frac{\hat{s}}{\cos \frac{(i-1)\pi}{2n}}\right] \right. \\
 & \quad \left. - \sum_{i=1}^n i P\left[\frac{\hat{s}}{\cos \frac{i\pi}{2n}}\right] \right\} \\
 & = \frac{1}{2n} \left\{ \sum_{i=0}^{n-1} i P\left[\frac{\hat{s}}{\cos \frac{i\pi}{2n}}\right] + \sum_{i=0}^{n-1} P\left[\frac{\hat{s}}{\cos \frac{i\pi}{2n}}\right] \right. \\
 & \quad \left. - \sum_{i=1}^n i P\left[\frac{\hat{s}}{\cos \frac{i\pi}{2n}}\right] \right\} \\
 & = \frac{1}{2n} \left\{ \sum_{i=0}^{n-1} P\left[\frac{\hat{s}}{\cos \frac{i\pi}{2n}}\right] - n P[\infty] \right\} \\
 & = \frac{1}{2n} \sum_{i=0}^{n-1} P\left[\frac{\hat{s}}{\cos \frac{i\pi}{2n}}\right] \quad (172)
 \end{aligned}$$

and

$$\begin{aligned} P_e^L &\triangleq \frac{1}{\pi} \sum_{i=1}^n I_i^L = \frac{1}{\pi} \frac{\pi}{2n} \left\{ \sum_{i=1}^n (i-1) P \left[\frac{\hat{S}}{\cos \frac{(i-1)\pi}{2n}} \right] \right. \\ &\quad \left. - \sum_{i=1}^n (i-1) P \left[\frac{\hat{S}}{\cos \frac{i\pi}{2n}} \right] \right\} \\ &= \frac{1}{2n} \left\{ \sum_{i=0}^{n-1} i P \left[\frac{\hat{S}}{\cos \frac{i\pi}{2n}} \right] \right. \\ &\quad \left. - \sum_{i=1}^n i P \left[\frac{\hat{S}}{\cos \frac{i\pi}{2n}} \right] \right\} \\ &\quad + \sum_{i=1}^n P \left[\frac{\hat{S}}{\cos \frac{i\pi}{2n}} \right] \} \\ &= \frac{1}{2n} \left\{ \sum_{i=1}^n P \left[\frac{\hat{S}}{\cos \frac{i\pi}{2n}} \right] - n P[\infty] \right\} \\ &= \frac{1}{2n} \sum_{i=1}^n P \left[\frac{\hat{S}}{\cos \frac{i\pi}{2n}} \right]. \end{aligned} \tag{173}$$

Since

$$\begin{aligned} I_i^U &\geq I_i \geq I_i^L, \\ \frac{1}{\pi} \sum_{i=1}^n I_i^U &= P_e^U \geq \frac{1}{\pi} \sum_{i=1}^n I_i = P_{ep} \\ &\geq \frac{1}{\pi} \sum_{i=1}^n I_i^L = P_e^L. \end{aligned} \quad (174)$$

Substituting (172) and (173) into (174) results in

$$\frac{1}{2n} \sum_{i=0}^{n-1} P\left[\frac{\hat{S}}{\cos \frac{i\pi}{2n}}\right] \geq P_{ep} \geq \frac{1}{2n} \sum_{i=1}^n P\left[\frac{\hat{S}}{\cos \frac{i\pi}{2n}}\right]. \quad (175)$$

Since $P[\infty] = 0$ (where $i = n$), the upper and lower error probability bounds in (175) differ only by the first term of the upper bound, $P[\hat{S}]/2n$, (where $i = 0$). It is obvious that this term can be made arbitrarily small by the selection of n sufficiently large. Thus,

$$\lim_{n \rightarrow \infty} P_e^U = \lim_{n \rightarrow \infty} P_e^L. \quad (176)$$

However, it might be expected that the arithmetic average of these bounds converges to an accurate estimate of P_{ep} much more rapidly than either of the bounds. Thus, the detection error probability, P_{ep} , is defined by this average to be

$$\begin{aligned} P_{ep} &= \frac{1}{2} [P_e^U + P_e^L] \\ &= \frac{1}{4n} P[\hat{S}] + \frac{1}{2n} \sum_{i=1}^{n-1} P\left[\frac{\hat{S}}{\cos \frac{i\pi}{2n}}\right]. \end{aligned} \quad (176a)$$

Here, the function $P[\cdot]$ is the normalized noise APD (as depicted in Figure 1) whose V_d ratio is adjusted to the detection bandwidth ($1/T$). The variable \hat{S} is the square root of the signal-to-noise power ratio as referenced to the detection bandwidth ($1/T$).

4.1.2 Performance of the Linear CFSK, $M = 1$ Receiver in Atmospheric Noise

The bit error rate performance of the linear CFSK detector is readily obtained by combining the results of 3.3.2 and the preceding PSK analysis. CFSK detection is 3 dB less efficient than PSK detection where the non-Gaussian post-detection noise corresponds to an observation bandwidth $\pi^2/8$ times as great. The probability of CFSK detection error, P_{ec} , is the same as that for PSK (176), except that the signal-to-noise voltage ratio, \hat{S} , must be reduced to $\hat{S}/\sqrt{2}$ (-3 dB) and the V_d ratio increased according to the bandwidth ratio $\pi^2/8$. Thus, the CFSK bit error rate (or detection error probability), P_{ec} , is given by

$$P_{ec} = \frac{1}{4n} P\left[\hat{S}/\sqrt{2}\right] + \frac{1}{2n} \sum_{l=1}^{n-1} P\left[\hat{S}/\sqrt{2} \cos \frac{l\pi}{2n}\right] \quad (177)$$

where $P[\cdot]$ is the normalized noise APD whose V_d is referenced to the observation bandwidth ($\pi^2/8$) and \hat{S} is the square root of the signal-to-noise power ratio referenced to the detection bandwidth ($1/T$).

4.1.3 Performance of the Linear MSK Receiver in Atmospheric Noise

Similarly, the bit error rate performance of the linear MSK detector is readily obtained by combining the results of Chapter 3.4 and the preceding PSK analysis. From 3.4, MSK detection produces the same post-detection signal to noise power ratio as PSK (for equal input signal-to-noise ratios and data rates), but the MSK post-detection noise component is statistically equivalent to PSK noise observed in $\pi^2/16$ the detection bandwidth. Thus, the expression for the probability of MSK detection error, P_{em} , is identical to that for PSK (176) except that the APD, $P[\cdot]$ must be characterized by a V_d ratio adjusted to the observation bandwidth $\pi^2/16T$ for input data elements of T seconds. Hence, the MSK bit error rate (or detection error probability) can be expressed by

$$P_{em} = \frac{1}{4n} P[\hat{S}] + \frac{1}{2n} \sum_{i=1}^{n-1} P\left[\hat{S}/\cos \frac{i\pi}{2n}\right] \quad (178)$$

where $P[\cdot]$ is the normalized APD as referenced to $\pi^2/16T$, T being the duration of an input data element, and \hat{S} is the square root of the signal-to-noise power ratio referenced to the bandwidth ($1/T$).

4.2 Validation of the Theoretical Analysis

4.2.1 Convergence and Comparison in Gaussian Noise

To examine the efficacy of this estimate in typical atmospheric noise ($V_d = 9 \text{ dB}$), P_e^U and P_e^L , and P_e were computed by (172), (173), and (176) respectively, for various values of n. In this case, it was

found that the arithmetic average, P_{ep} , with $n = 20$, yielded the same numerical accuracy as was obtained by convergence of P_e^U and P_e^L at $n = 5000$. Similarly, Table II, which lists error probabilities for Gaussian noise as computed by (176) and as computed by series evaluation ([1], Equation 7.1.26) of the theoretical expression (98), clearly shows the efficacy of the numerical procedure (176) for $n = 20$. Obviously, greater values of n could be used to obtain greater accuracy, but $n = 20$ provides accuracy equal to or better than most experimental data. Thus, a quantitatively adequate criterion for the convergence of the PSK error probability has been determined. Moreover, it has been shown that PSK error probability in Gaussian noise as calculated according to this procedure virtually coincides with that obtained by the classical procedure.

4.2.2 Atmospheric Noise Performance

The remaining, and clearly most pertinent, problem is the validation of the procedure for performance in non-Gaussian atmospheric noise.

Table II. Probability of Detection Error for Coherent PSK
in White Gaussian Noise (Rayleigh Envelope)

Signal\Noise (dB)	Theoretical Error Rate*	Numerical Estimate**
-10	.32736	.32736
-8	.28671	.28672
-6	.23923	.23923
-4	.18611	.18612
-2	.13064	.13065
0	.07865	.07865
2	.03751	.03751
4	.012501	.012501
6	.0023884	.0023882
8	.0001909	.0001909
10	3.8756x10 ⁻⁶	3.8718x10 ⁻⁶

* $P_{ep} = 1/2 [1 - \text{erf}(\sqrt{S/N})]$, Computed by (7.1.26, [1])

** $P_{ep} = 1/80 \exp[-S/N] + 1/40 \sum_{i=1}^{19} \exp\left[-(S/N)\left(\cos \frac{i\pi}{40}\right)^{-2}\right]$,

Equation (i76) with n = 20, P(E) = EXP [-E²].

Because the present analysis constitutes an original theoretical development for the non-Gaussian noise environment, experimental performance data is the only appropriate standard of comparison. Fortunately, measured performance data in atmospheric noise is available for linear coherent PSK [32], CFSK, M = 1 [14], and MSK [14] detection. The PSK experimental data, presented by Linfield and Plush [32], is in the form of measured bit error rates (probability of detection error) at various signal-to-noise ratios. On the other hand, the CFSK, M = 1 and MSK data, presented by Entzminger, et al

[14], is in the form of measured teletype character error rates.

Here, the comparable theoretical character error rate, CER, must be derived from the theoretical bit error rate, P_e .

The synchronous CFSK and MSK teletype systems employ 7.0 Baudot code where each binary element is equal in length and only five of the seven elements in a block actually define an alphanumeric character. (The other two binary elements are start-stop bits intended to establish long-term system synchronization.) Any one or more decision errors in the sequence of five data elements will cause the character to be decoded and printed incorrectly, thus producing a character error. On the other hand, isolated errors in either the stop or start elements do not produce character errors if long-term system synchronism is maintained. Thus, assuming synchronism, the probability of a correct binary decision q , is given by

$$q = 1 - P_e \quad (179)$$

where P_e is the bit error probability.

Assuming that bit errors in a Baudot character are mutually independent, the probability that all five are decoded correctly, P_c , is given by

$$P_c = q^5 = (1 - P_e)^5. \quad (180)$$

This is the probability that a character will be decoded correctly. Hence, the probability that a character will be decoded incorrectly, the character error rate (CER), is given by

$$CER = 1 - P_c = 1 - (1 - P_e)^5. \quad (181)$$

4.2.2.1 Linear PSK Detection

The first experimental data to be considered is that of Linfield and Plush [32]. This PSK detector performance was measured in additive atmospheric noise at 16.6 kHz (VLF) at a data rate of 33.3 bits/second (constituting a detection bandwidth, $1/T$, of 33.3 Hz for coherent detection). The noise had a measured V_d ratio of approximately 10 dB in a 376 Hz bandwidth. By Figure 26 of CCIR 322 [26], this converts to a V_d ratio of 3.75 dB in the 33.3 Hz detection bandwidth of the experimental system. Figure 8 shows this data with the theoretical PSK error rate as computed by (176) with $n = 20$. The close agreement of the theoretical and measured bit error rates is apparent.

4.2.2.2 Linear CFSK, M = 1 Detection

Experimental atmospheric noise performance data for CFSK, $M = 1$ detection has been presented by Entzminger, et al [14]. Here, the system was operated at a signalling rate of 50 bauds (50 bits/second) in atmospheric noise at 27.5 kHz. The noise had a V_d ratio of 7 dB measured in a 218 Hz bandwidth. This converts (by CCIR 322 [26]) to a V_d ratio of 3.75 dB in the 50 Hz detection bandwidth and 4.15 dB in the 50 ($\pi^2/8$) Hz observation bandwidth. Figure 9 shows this measured CFSK data with the theoretical CFSK CER as computed by (177) with $n = 20$ and (181). Here, the correspondence between the computed and measured CER's is somewhat poorer than for the PSK system (Figure 8), but still within about 3 dB. However, the fact that the measured performance is better than calculated for ideal linear detection implies that some non-linear noise cancellation might have existed

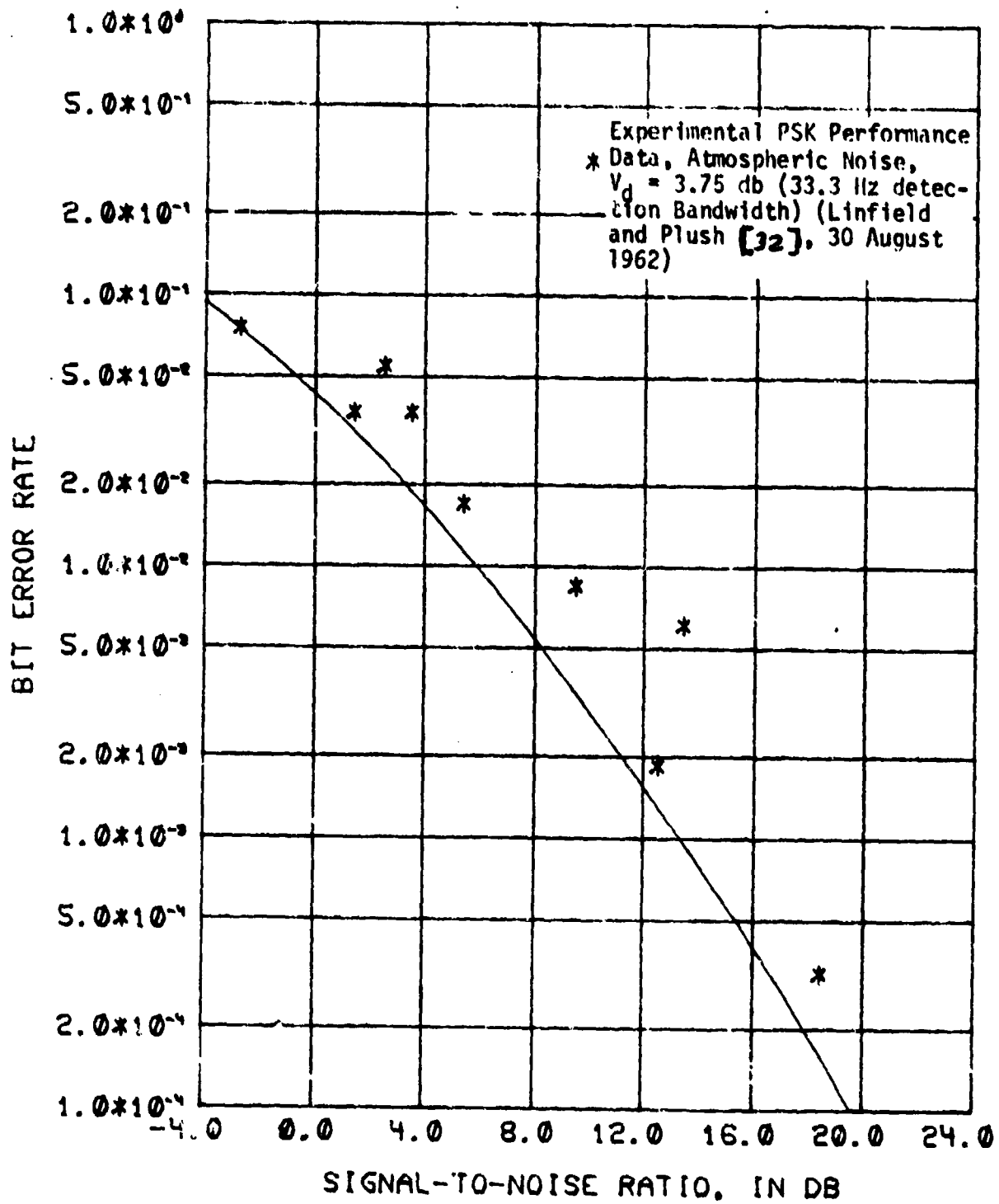


Figure 8. Linear Coherent Phase Shift Keying (PSK) Detector Performance in Atmospheric Noise, $V_d = 3.75 \text{ db}$.

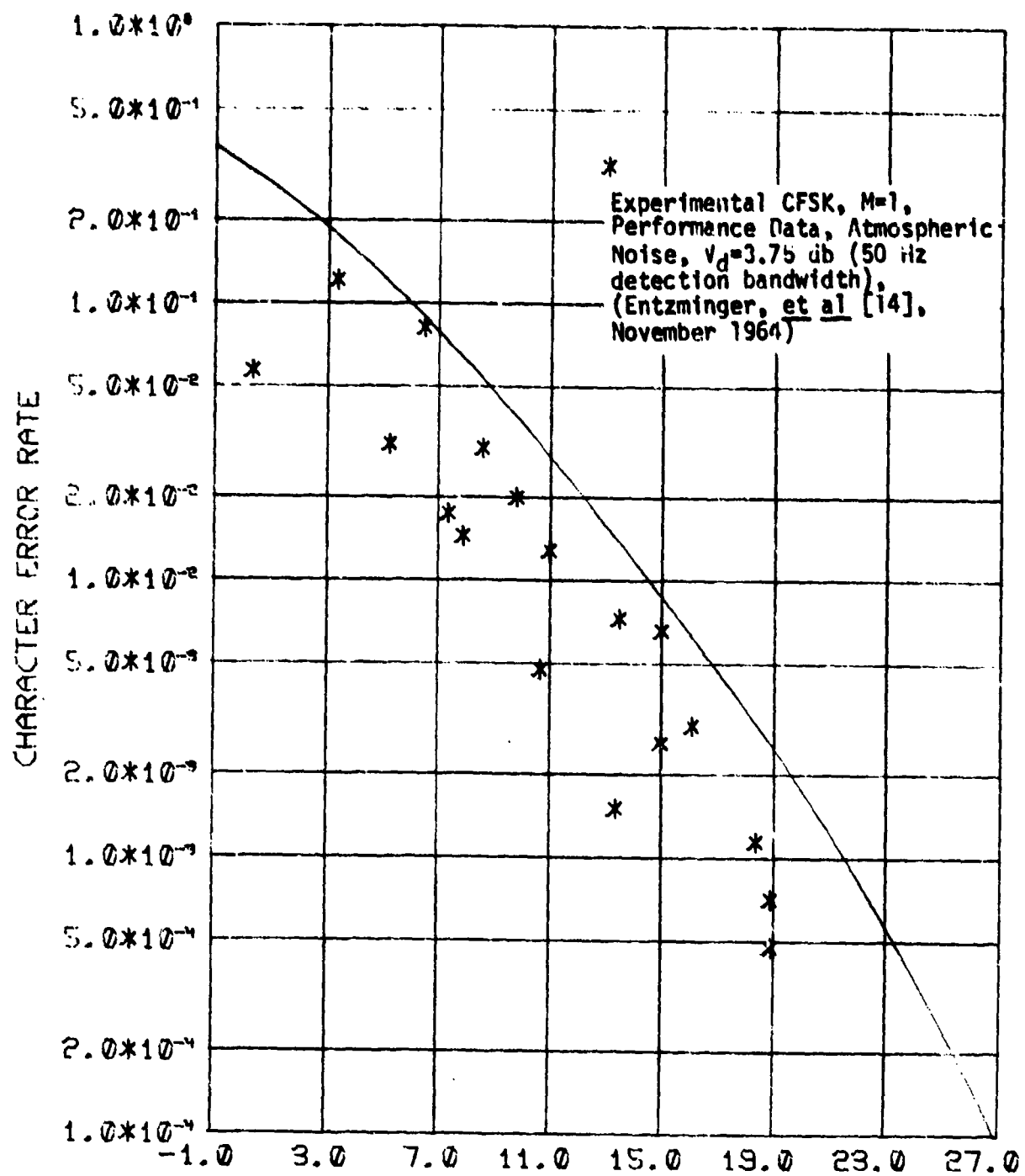


Figure 9. Linear Coherent Frequency Shift Keying (CFSK, M=1)
Detector Performance in Atmospheric Noise, $V_d = 3.75$ db.

in the experimental system. The dramatic effect of even slight non-linearities such as peak clipping is shown by other experimental results. For instance, Linfield and Beach [33] found that noise clipping 19 dB above the signal envelope produced at least 4 dB improvement in CFSK error performance in simulated atmospheric noise. Thus, even minimal impulsive noise clipping in the experimental receiving system could well account for this performance differential between measured and ideal linear detection.

4.2.2.3 Linear MSK Detection

In addition to CFSK data, experimental atmospheric noise performance data for MSK detection has been presented by Entzminger, et al [14]. This MSK system was operated at a signalling rate of 40 bauds (40 bits/second) in atmospheric noise at 27.5 kHz. The noise had a V_d ratio of 10 dB in 243 Hz bandwidth which converts to a V_d ratio of 4.15 dB in the 24.7 Hz ($\pi^2/16T$) MSK noise functional bandwidth. Figure 10 shows this measured MSK data with the theoretical MSK CER as computed by (178) with $n = 20$ and (181). Again, the agreement of measured and computed CER's is quite close.

4.2.2.4 Summary

The foregoing discussions have shown that the expressions for error probability (176), (177), (178) derived in this chapter, yield results which coincide with theoretical Gaussian noise analyses. In addition, close agreement exists between theoretical and measured performance in non-Gaussian atmospheric noise. Thus, the quantitative validity of the linear detection analyses of this chapter has been substantiated.

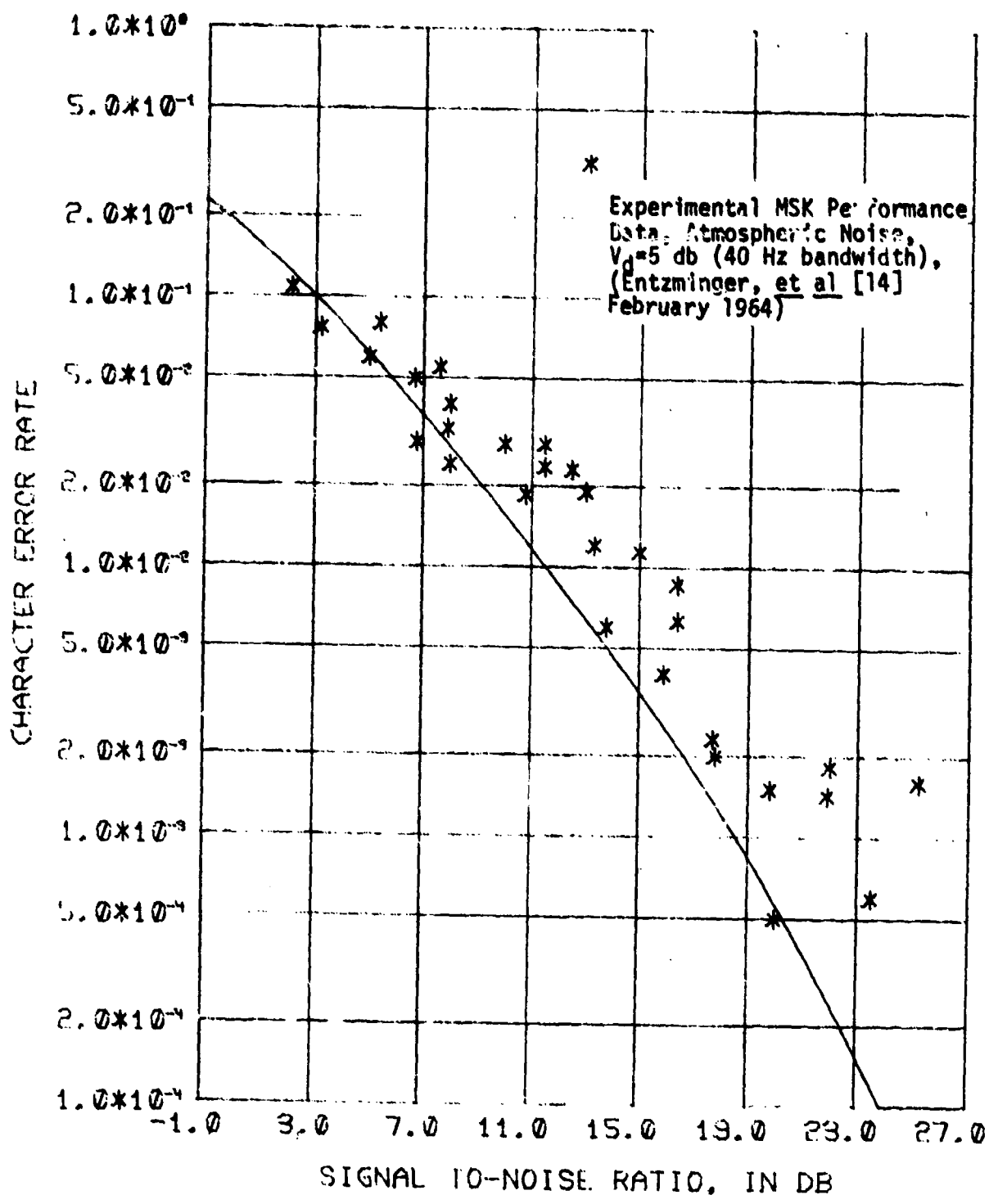


Figure 10. Linear Minimum Shift Keying (MSK) Detector Performance in Atmospheric Noise, $V_d = 5$ db.

4.3 Optimum Linear Coherent System

In addition to the experimental and corresponding theoretical results of Figures 8, 9 and 10, error rates for linear PSK detection in atmospheric noise of varying impulsiveness (V_d ratios) are plotted in Figures 11 and 12. (A more complete tabulation of PSK error rates is contained in Appendix D.)

The error rate characteristics of Figures 11 and 12 tend to flatten out with increasing impulsiveness, or V_d ratio. Thus, significantly more signal power is required to achieve a given low error probability as the V_d ratio increases. A corollary observation is that the error rate performance characteristic is steeper for Gaussian noise than for any non-Gaussian atmospheric noise. It is apparent that Gaussian noise error rate performance is the limiting case of atmospheric noise performance as the noise impulsiveness decreases. Thus, it is apparent that detection efficiency can be substantially improved by a reduction in the ambient noise impulsiveness. As noted in Chapter 1, atmospheric noise impulsiveness varies with the bandwidth of observation. Thus, an increase in binary element length, T , reduces the PSK and CFSK detection bandwidth, $1/T$, and consequently, the post detection noise impulsiveness. For this reason, the MSK post-detection noise component (equivalent to noise observed in bandwidth $(\pi^2/16T)$) is clearly less impulsive than the corresponding noise components of the PSK and CFSK detectors. Moreover, the MSK detector post-detection signal-to-noise ratio is equal to the PSK

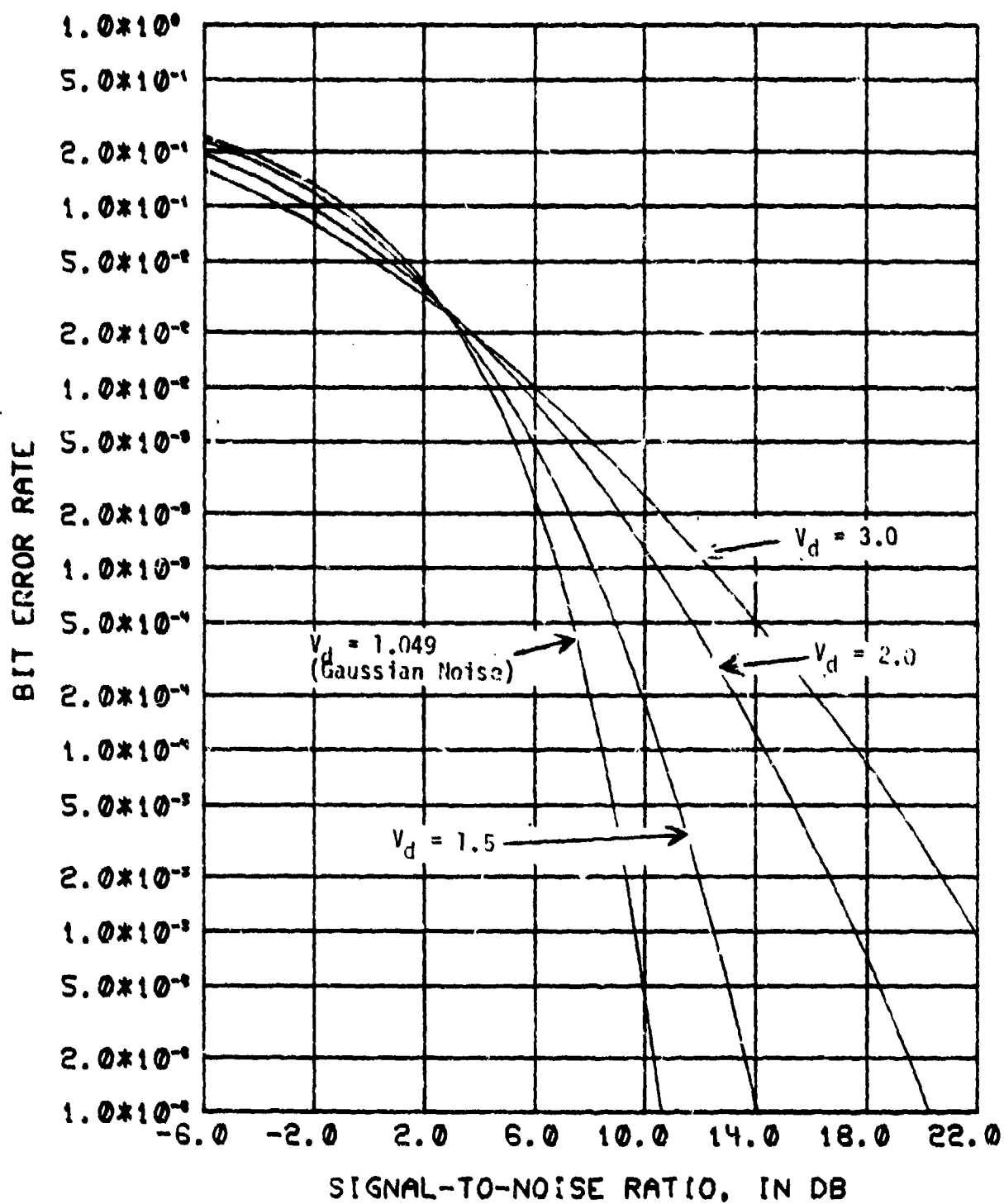


Figure 11. Linear Coherent Phase Shift Keying (PSK) Detector Performance in Atmospheric Noise

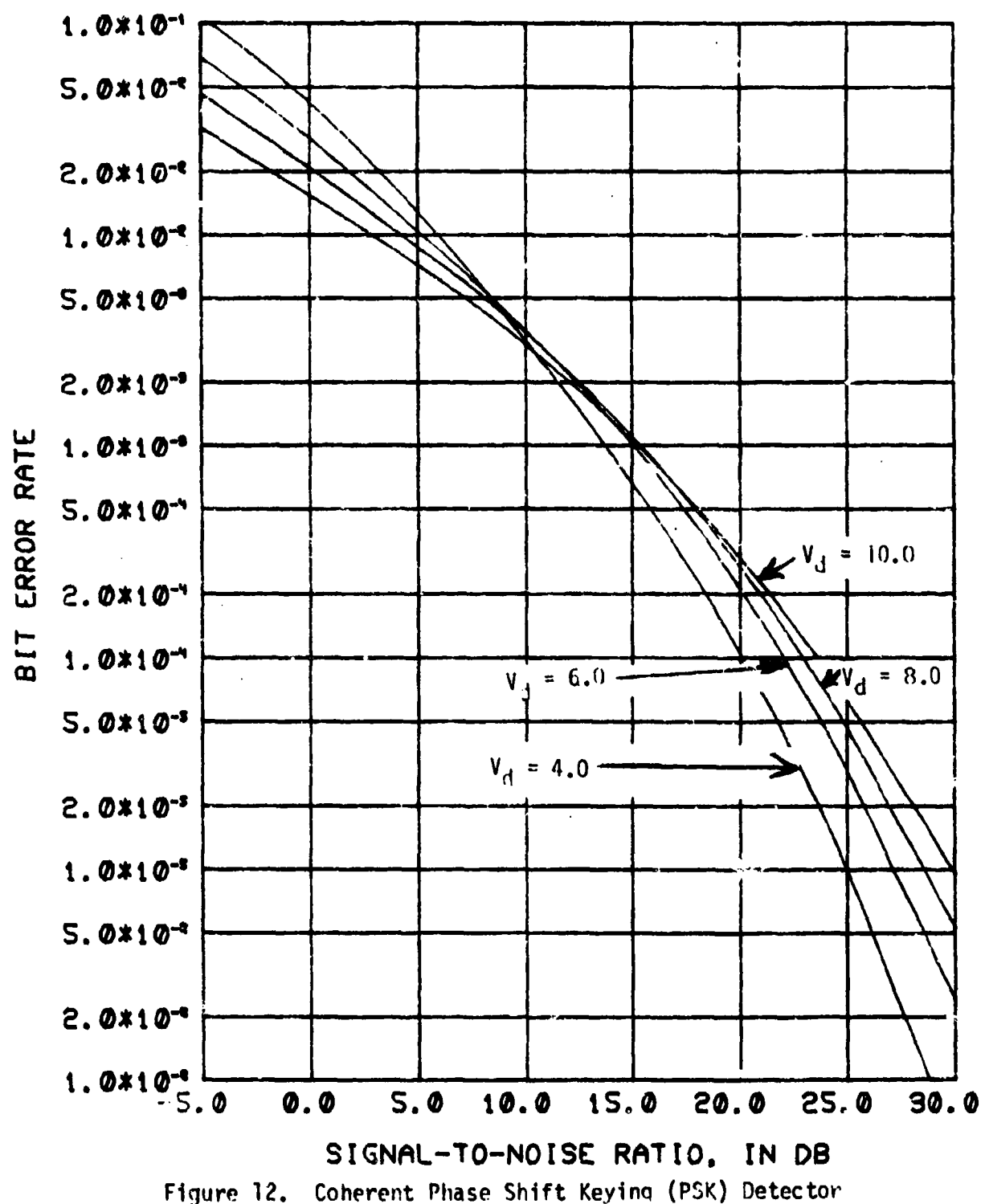


Figure 12. Coherent Phase Shift Keying (PSK) Detector Performance in Atmospheric Noise

detector and is 3 dB higher than the CFSK detector. Hence, the MSK system is clearly more efficient than either PSK and CFSK.

This, in addition to the continuous waveform (see 3.1) and the minimum bandwidth of the MSK signal spectrum [14], makes the MSK modem the optimum choice for practical coherent binary communication (with linear detection) in atmospheric noise.

Chapter 5

COHERENT DETECTION IN ATMOSPHERIC NOISE WITH PRE-DETECTION

HARD-LIMITING - PULSE STATISTICAL ANALYSIS (PSA)

5.1 General

The remaining system performance analyses and results in this study are concerned with receiving systems which employ pre-detection hard-limiting. Hence, the hard-limiting process is the extreme case of the non-linear noise-clipping process whose efficacy in impulsive noise has been investigated experimentally and described by Hartley [22], Linfield and Beach [33], and Mallinckrodt [35]. Because these experimental results showed that hard-limiting equalled or exceeded any noise-blanking (hole-punching) process or less-stringent clipping strategy, performance of the hard-limiting receiver constitutes an upper bound for practical non-linear receiver performance. Moreover, practical circuit realization of the hard-limiting process is relatively easier to obtain than that of other non-linear responses. Thus, a reliable hard-limiter is likely to be the most efficient non-linear pre-detection processor - both functionally and economically. For this reason, the subsequent analyses of this chapter and Chapter 6 are confined to the hard-limiting receiver system.

The present chapter analyzes the performance of PSK, CFSK and MSK detectors preceded by bandpass hard-limiters on the basis of atmospheric

noise pulse statistics. This technique, Pulse Statistical Analysis (PSA), is used to derive bit error probability expressions for the three coherent systems. In turn, character error rates for CFSK and CSK (MSK detection and differential post detection decoding) modems are compared with some measured performance data. Finally, it is shown that the PSA technique is suitable only for systems where the ratio of the hard-limiter bandwidth to detection bandwidth (BWR) is on the order of eight or less.

5.2 Pulse Statistical Analysis (PSA)

The PSA development is presented in three phases. First, detection error probability expressions are derived for the three modems where only one noise pulse is assumed to occur in a given element. Next, the noise model is extended to the case where multiple noise pulses occur in a single detection element. The error probability expressions are accordingly modified for the multiple noise pulse distributions. Finally, pulse occurrence statistics are applied to obtain average error rate probabilities.

5.2.1 Coherent Detection with Hard-Limiting - One Noise Pulse per Detection Element

5.2.1.1 PSK Detection

The hard-limiting PSK detector is similar to the linear PSK detector of 3.2, but it also includes a pre-detection bandpass hard-limiter. Figure i3 is a simplified block diagram of the hard-limiting PSK receiver.

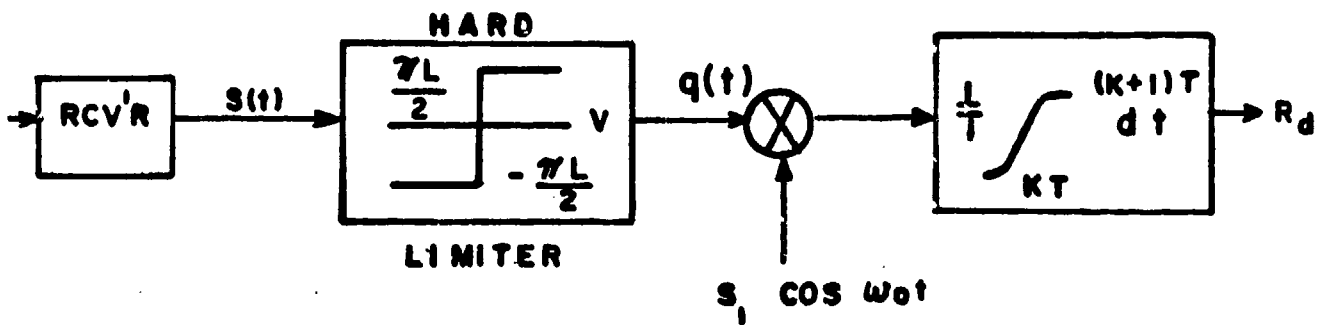


Figure 13. Hard-Limiting PSK Receiver

In this system, the detector output is the functional R_d , given by

$$R_d = \frac{S_i}{T} \int_{KT}^{(K+1)T} q(t) \cos \omega_0 t dt,$$

where $q(t)$ is the output of the limiter. Assume an input to the limiter given by

$$S(t) = S \cos(\omega_0 t + h_k \pi) + e(t) \cos(\omega_0 t + \theta(t)) \quad (182)$$

where S is the signal amplitude, $e(t)$ is the noise envelope process, $h_k = 0, 1$ according to the binary state of the k th bit. The output of the limiter, $q(t)$, has a rectangular waveform whose amplitude is denoted as $\frac{\pi L}{2}$ for convenience. Here, the important simplifying assumption is made that individual noise pulse amplitudes are much greater than the signal amplitude, but the signal amplitude is much greater than the

noise envelope otherwise. In this case, the larger amplitude component, noise pulse or continuous signal, suppresses the smaller component [9] and consequently "captures" the limiter. Hence the zero crossings of $q(t)$ are determined by the larger component of $s(t)$. When $S \geq e(t)$ (no noise impulse present), the zero crossings are identical to those of $\cos \omega_0 t$ and when $S < e(t)$ (during a noise impulse), the zero crossings are identical to those of $\cos [\omega_0 t + \theta(t)]$. Postulating $h_k = 1$, the output of the limiter can be written as

$$q(t) = \begin{cases} -\frac{\pi L}{2} SGN\{\cos \omega_0 t\}, & S \geq e(t) \\ \frac{\pi L}{2} SGN\{\cos [\omega_0 t + \theta(t)]\}, & S < e(t). \end{cases} \quad (183)$$

Now, postulating a noise pulse centered at t_c such that during the k th interval $e(t) > S$ for $t_1 \leq t \leq t_2$, the noise component produced by the integrator, N_p , is given by

$$N_p = \frac{1}{T} \int_{t_1}^{t_2} \frac{\pi L S_i}{2} SGN\{\cos[\omega_0 t + \theta(t)]\} \cos \omega_0 t dt. \quad (184)$$

Assuming the noise phase to be approximately constant over the interval (t_1, t_2) and introducing a shift in the time origin, N_p becomes

$$N_p \approx \frac{\pi L S_i}{2 T} \int_{t_1 + \frac{\theta}{\omega_0}}^{t_2 + \frac{\theta}{\omega_0}} SGN\{\cos \omega_0 t\} \cos [\omega_0 t - \theta] dt, \quad (185)$$

The function $SGN\{\cos \omega_0 t\}$ may be rewritten in a Fourier cosine series as

$$SGN\{\cos \omega_0 t\} = \frac{4}{\pi} \sum_{K \text{ odd}}^{\infty} \frac{1}{k} \cos k\omega_0 t. \quad (186)$$

Substitution of this into (185) yields

$$\begin{aligned} N_p &= \frac{2LS_1}{T} \sum_{K \text{ odd}}^{\infty} \frac{1}{k} \int_{t_1 + \frac{\theta}{\omega_0}}^{t_2 + \frac{\theta}{\omega_0}} \cos k\omega_0 t \cos [\omega_0 t - \theta] dt \\ &= \frac{LS_1}{T} \left\{ \int_{t_1 + \frac{\theta}{\omega_0}}^{t_2 + \frac{\theta}{\omega_0}} [\cos \theta + \cos(2\omega_0 t - \theta)] dt \right. \\ &\quad \left. + \sum_{K=3,5,\dots}^{\infty} \frac{1}{k} \int_{t_1 + \frac{\theta}{\omega_0}}^{t_2 + \frac{\theta}{\omega_0}} \cos k\omega_0 t \cos (\omega_0 t - \theta) dt \right\}. \end{aligned} \quad (187)$$

Since the signal and noise process bandwidths are much smaller than the center frequency, ω_0 , the contributions of the high frequency components of the integrand are negligible. Hence, the noise component is closely approximated by the first term of (187) resulting in

$$N_p \approx \frac{LS_1}{T} (t_2 - t_1) \cos \theta, \quad 0 \leq t_1 < t_2 \leq T. \quad (188)$$

The signal component, S_p , on the other hand, is given by

$$S_p = \frac{1}{T} \int_0^{t_1} -\frac{\pi L S_i}{2} \text{SGN}\{\cos \omega_n t\} \cos \omega_n t dt \\ + \frac{1}{T} \int_{t_2}^T -\frac{\pi L S_i}{2} \text{SGN}\{\cos \omega_n t\} \cos \omega_n t dt. \quad (189)$$

Again, employing (186) and disregarding high frequency components in each integrand yields

$$S_p \approx -\frac{L S_i}{T} [T - (t_2 - t_1)]. \quad (190)$$

These results show that the magnitude of the post detection noise component is directly proportional to the "noise capture" interval, $(t_2 - t_1)$, and the signal component is proportional to the bit length minus the capture interval.

Under the hypothesis that $h_k = 1$, a decision error occurs whenever $R_d > 0$. Utilizing (188) and (190), this event can also be expressed as

$$R_d = S_p + N_p = \frac{L S_i}{T} [-T + (t_2 - t_1) + (t_2 - t_1) \cos \theta] \\ > 0. \quad (191)$$

In the k th bit, the capture interval, $(t_2 - t_1)$, is physically constrained to be no greater than the bit length, T . When $(t_2 - t_1) > T$, $(t_2 - t_1)$ must be replaced by T in (191). Thus, the event $R_d > 0$ is equivalent to

$$\cos \theta > 0 \quad \text{for } (t_2 - t_1) > T$$

and

(192)

$$1 \geq \cos \theta > \frac{T - (t_2 - t_1)}{(t_2 - t_1)} \quad \text{for } (t_2 - t_1) \leq T.$$

This result leads to an expression for the overall decision error probability, P_{ep} , given by

$$\begin{aligned} P_{ep} = \Pr(R_d > 0) &= \Pr \left\{ 1 \geq \cos \theta > \frac{T - (t_2 - t_1)}{(t_2 - t_1)}, \right. \\ &\quad \left. (t_2 - t_1) \leq T \right\} + \quad (193) \\ &\quad + \Pr \left\{ \cos \theta > 0, (t_2 - t_1) > T \right\}. \end{aligned}$$

Since $(t_2 - t_1)$ is a function only of the noise envelope, it is statistically independent of the noise phase, θ . In addition, the event in the first term on the right side of (193) can be equivalently described in terms of inverse functions. (It should be noted that an error can occur only if $(t_2 - t_1) > T/2$, which also coincides with the bound $\cos \theta = 1$ in (193).) These changes result in

$$\begin{aligned} P_{ep} &= \Pr \left\{ |\theta| < \cos^{-1} \left[\frac{T - (t_2 - t_1)}{(t_2 - t_1)} \right], \right. \\ &\quad \left. T/2 \leq (t_2 - t_1) \leq T \right\} \quad (193a) \\ &\quad + \Pr \left\{ \cos \theta > 0 \right\} \times \Pr \left\{ (t_2 - t_1) > T \right\}. \end{aligned}$$

Finally, if θ is uniformly distributed on $(-\pi, \pi)$, this becomes

$$P_{ep} = P_r \left\{ |\theta| < \cos^{-1} \left[\frac{T - (t_2 - t_1)}{T/2} \right], \frac{T}{2} \leq (t_2 - t_1) \leq T \right\} + \frac{1}{2} P_r \left\{ (t_2 - t_1) > T \right\} \quad (194)$$

or

$$P_{ep} = P_r \left\{ |\theta| < \cos^{-1} \left[\frac{T - V_1}{V_1} \right], \frac{T}{2} \leq V_1 \leq T \right\} + \frac{1}{2} P_r \left\{ V_1 > T \right\} \quad (194a)$$

where

$$V_1 \triangleq t_2 - t_1. \quad (194b)$$

At this point, it is appropriate to consider the "capture interval", V_1 , more closely. This time interval is obviously defined by its width and time of occurrence. The noise pulse width, Δ , is defined to be the interval that the envelope of the received noise pulse exceeds the desired signal amplitude, or, alternatively, the time required for the envelope of a received noise pulse to decay to the signal amplitude. Thus, the predetection noise pulse width, Δ , is found by solving the inequality

$$e(t) \geq S, \quad t_0 \leq t \leq t_0 + \Delta \quad (195)$$

where $e(t)$ is the envelope of the receiver response to a noise impulse at $t = t_0$ and S is the received signal amplitude.

If the single-tuned RLC filter of Figure 2 is utilized as a simplified approximation of typical receiver predetection filtering, the received noise envelope is given by (70). By employing (70) with t replaced by $t_0 + \Delta$ to obtain equality in (195), there results

$$S = Pe^{-b_1(t_0 + \Delta - t_0)} \\ = Pe^{-b_1\Delta}, \quad (196)$$

where P is the received noise pulse amplitude and $2b_1$ is the 3 dB bandwidth of the predetection filter in radians/second.

This leads to

$$\Delta = \frac{1}{b_1} \ln(P/S). \quad (197)$$

It is convenient to express the random variable P in terms of E , the conditional expected envelope voltage given P , as observed in the detection bandwidth. Evaluating (72a) with $c(t) = 1$, for PSK, the following expression for the conditional noise envelope voltage, E , is obtained.

$$E = \frac{P}{T^2} \int_0^T dT_0 \int_{T_0}^T e^{-b_1(t-T_0)} dt \\ = \frac{P}{b_1 T} \left[1 - \frac{1}{b_1 T} (1 - e^{-b_1 T}) \right]. \quad (198)$$

Hence,

$$\Delta = \frac{1}{b_1} L_n \left\{ \frac{b_1 T E}{S} \left[1 - \frac{1}{b_1 T} (1 - e^{-b_1 T}) \right]^{-1} \right\}$$
$$= \frac{1}{b_1} L_n \left[\frac{b_1 T E}{S} \right] - \frac{1}{b_1} L_n \left[1 - \frac{1}{b_1 T} (1 - e^{-b_1 T}) \right]. \quad (199)$$

It should be noted that in practical communication receivers, the predetection filter bandwidth (b_1/π Hz) is equal to or greater than the detection bandwidth ($1/T$ Hz). In this case,

$$b_1 T \geq \pi. \quad (199a)$$

Hence

$$\frac{1}{b_1} L_n \left[1 - \frac{1}{b_1 T} (1 - e^{-b_1 T}) \right] \approx 0, \quad (199b)$$

and

$$\Delta \approx \frac{1}{b_1} L_n \left[\frac{b_1 T E}{S} \right]. \quad (199c)$$

The other essential descriptor of the capture interval is its time of occurrence. Here, the simplifying assumption is made that a binary decision error is only caused by a noise pulse occurring entirely within the bit interval. Although this obviously excludes the effect of noise pulses which overlap into adjacent bit intervals, this assumption does lead to mathematically tractable error probability expressions.

More importantly, however, the resulting computational results give good agreement with experimental data. Based on this assumption, the following definitions are obtained:

$$t_1 \triangleq t_c - \frac{\Delta}{2}, \quad (200a)$$

and

$$t_2 \triangleq t_c + \frac{\Delta}{2}, \quad (200b)$$

where

$$\frac{\Delta}{2} \leq t_c \leq T - \frac{\Delta}{2},$$

and t_c is assumed to be uniformly distributed on $(\frac{\Delta}{2}, T - \frac{\Delta}{2})$.

Substitution of (200a) and (200b) into (194b) yields

$$V_1 = t_2 - t_1 = \Delta. \quad (201)$$

Application of (199) yields

$$V_1 = -\frac{1}{b_1} L_n \left[\frac{b_1 T E}{S} \right] - \frac{1}{b_1} L_n \left[1 - \frac{1}{b_1 T} (1 - e^{-b_1 T}) \right]. \quad (202)$$

and, for $b_1 T \gg 1$, as is usually the case,

$$V_1 \approx \frac{1}{b_1} L_n \left[\frac{b_1 T E}{S} \right]. \quad (203)$$

Substitution of (201) into (194a) results in

$$P_{ep} = P_r \left\{ |\theta| < \cos^{-1} \left[\frac{T-\Delta}{\Delta} \right], T/2 \leq \Delta \leq T \right\} + \frac{1}{2} P_r \left\{ \Delta > T \right\} \quad (204)$$

$$= \int_{E_1}^{E_2} dE \int_0^{\cos^{-1} \left[\frac{T-\Delta}{\Delta} \right]} 2 f_{e_{\text{tot}}}(\theta, E) d\theta \quad (205)$$

$$+ \frac{1}{2} \int_{E_2}^{\infty} f_e(E) dE,$$

where

$$\Delta \Big|_{E=E_1} = T/2,$$

or

$$E_1 = \frac{S}{b,T} e^{b,T/2}, \quad (205a)$$

and

$$\Delta \Big|_{E=E_2} = T,$$

or

$$E_2 = \frac{S}{b,T} e^{b,T}. \quad (205b)$$

Now, assuming the noise phase to be uniformly distributed on $(-\pi, \pi)$ and statistically independent of the envelope voltage, E , (205) becomes

$$P_{ep} = \frac{1}{\pi} \int_{E_1}^{E_2} \cos^{-1} \left[\frac{T - \Delta}{\Delta} \right] f_e(E) dE + \frac{1}{2} \int_{E_1}^{\infty} f_e(E) dE \quad (206)$$

where E_1 , E_2 , and Δ are given by (205a), (205b), and (199c) respectively.

At this point, it should be noted that the first term of (206) is of exactly the same form as (163). Thus, the numerical procedure developed in 4.1.1 is used to evaluate (206). In this case, the n -fold partition of the first integral of (206) yields

$$\cos^{-1} \left[\frac{b_i T - L_n(b_i T E_i^U / S)}{L_n(b_i T E_i^U / S)} \right] = (i-1) \frac{\pi}{2n} \quad (207a)$$

and

$$\cos^{-1} \left[\frac{b_i T - L_n(b_i T E_i^L / S)}{L_n(b_i T E_i^L / S)} \right] = i \frac{\pi}{2n} \quad (207b)$$

where E_i^U and E_i^L are the upper and lower bounds on the i th partition integral, respectively.

These results, in turn, yield

$$E_i^U = \frac{S}{b_1 T} \exp \left[\frac{b_1 T}{1 + \cos \frac{(i-1)\pi}{2n}} \right] \quad (208a)$$

and

$$E_i^L = \frac{S}{b_1 T} \exp \left[\frac{b_1 T}{1 + \cos \frac{i\pi}{2n}} \right]. \quad (208b)$$

Next, substitution of (208b) for (166b) in the arguments of (175) yields

$$\begin{aligned} & \frac{1}{2n} \sum_{i=0}^{n-1} P \left\{ \frac{S}{b_1 T} \exp \left[\frac{b_1 T}{1 + \cos \frac{i\pi}{2n}} \right] \right\} \\ & \geq \frac{1}{\pi} \int_{E_1}^{E_2} \cos^{-1} \left[\frac{b_1 T - \ln(b_1 T E/S)}{\ln(b_1 T E/S)} \right] f_e(E) dE \quad (209) \\ & \geq \frac{1}{2n} \sum_{i=1}^n P \left\{ \frac{S}{b_1 T} \exp \left[\frac{b_1 T}{1 + \cos \frac{i\pi}{2n}} \right] \right\}. \end{aligned}$$

Finally, approximating the first term of (206) by the average of its indicated upper and lower bounds (209), and noting that $E_2 = \frac{S}{b,T} e^{b,T}$, (206) becomes

$$P_{ep} \approx \frac{1}{2} P \left\{ \frac{S}{b,T} e^{b,T} \right\} + \frac{1}{4n} \left[P \left\{ \frac{S_1}{b,T} e^{\frac{b,T}{2}} \right\} + P \left\{ \frac{S}{b,T} e^{b,T} \right\} \right] \quad (210)$$

$$+ \frac{1}{2n} \sum_{i=1}^{n-1} P \left\{ \frac{S}{b,T} \exp \left[\frac{b,T}{1 + \cos \frac{i\pi}{2n}} \right] \right\}$$

5.2.1.2 CFSK Detection

The hard-limiting CFSK detector consists of the CFSK detector as depicted in Figure 4, but preceded by a bandpass hard-limiter. Rearranging and combining the linear multiplication integration and differential combination functions of Figure 4 and adding the predetection receiver and limiter, result in an equivalent block diagram of the hard-limiting CFSK receiver. This is depicted in Figure 14.

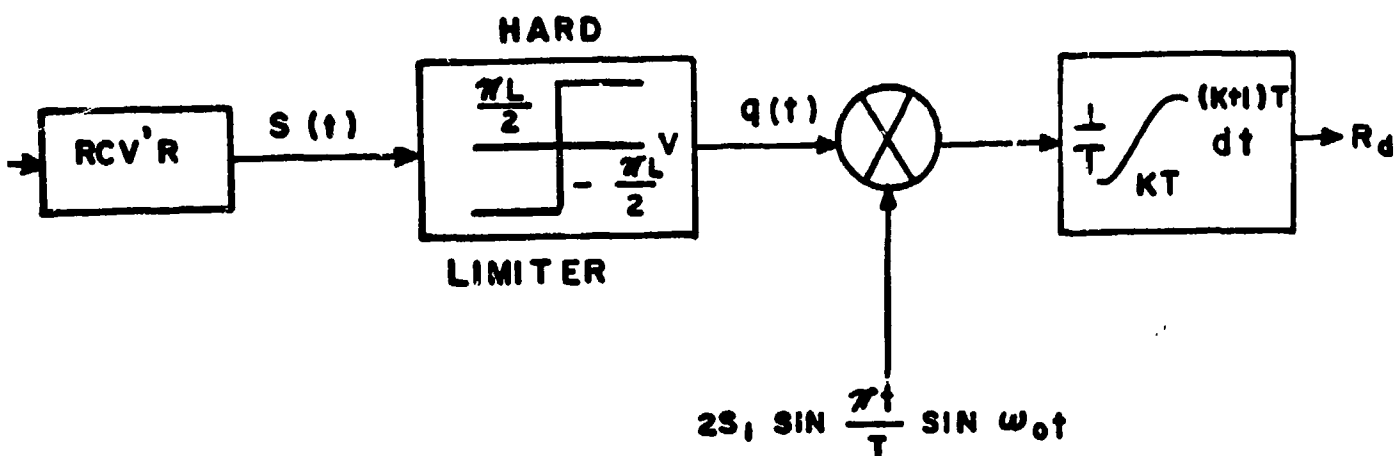


Figure 14. Hard-Limiting CFSK Receiver

Here, the detector functional, R_d , is given by

$$R_d = \frac{2S_1}{T} \int_{KT}^{(K+1)T} q(t) \sin \frac{\pi t}{T} \sin \omega_0 t dt, \quad (211)$$

where $q(t)$ is the output of the limiter. If the input to the limiter is given by

$$S(t) = S \cos(\omega_0 + \frac{\pi}{T})t + e(t) \cos[\omega_0 t + \alpha(t)], \quad (211a)$$

where S is the signal amplitude, $e(t)$ is the noise envelope process, and the upper shift frequency, $\omega_0 + \frac{\pi}{T}$, is chosen arbitrarily, then the output of the limiter has a rectangular waveform. For convenience, the

amplitude is denoted as $\frac{\pi L}{2}$. The zero crossings of $q(t)$ are assumed to be identical to the larger component of $s(t)$. When $s \geq e(t)$, the zero crossings are identical to those of $\cos(\omega_0 + \frac{\pi}{T})t$ and when $s < e(t)$, the zero crossings are identical to those of $\cos[\omega_0 t + \theta(t)]$. Thus, the output of the limiter can be written as

$$q(t) = \begin{cases} \frac{\pi L}{2} SGN\{\cos(\omega_0 + \frac{\pi}{T})t\}, & s \geq e(t) \\ \frac{\pi L}{2} SGN\{\cos[\omega_0 t + \theta(t)]\}, & s < e(t). \end{cases} \quad (212)$$

For a single noise pulse centered at $t = t_c$ such that during the k th interval $e(t) > s$ for $t_1 \leq t \leq t_2$, the noise component produced by the integrator, N_c , is given by

$$N_c \approx -\frac{1}{T} \int_{t_1}^{t_2} \pi L s, SGN\{\cos[\omega_0 t + \theta(t)]\} \times \sin \frac{\pi t}{T} \sin \omega_0 t dt, \quad (213)$$

where t_1 and t_2 are given by (200a) and (200b), respectively.

Assuming the noise phase to be approximately constant over the interval (t_1, t_2) and introducing a shift in the time origin, N_c becomes

$$N_c \approx \frac{\pi L s}{T} \int_{t_1 + \frac{\theta}{\omega_0}}^{t_2 + \frac{\theta}{\omega_0}} SGN\{\cos \omega_0 t\} \sin\left(\frac{\pi t}{T} - \frac{\pi \theta}{\omega_0 T}\right) \times \sin(\omega_0 t - \theta) dt. \quad (214)$$

Substituting (186) in (214) results in

$$N_c \approx \frac{4LS_1}{T} \sum_{K \text{ odd}}^{\infty} \frac{1}{K} \int_{t_1 + \frac{\theta}{\omega_0}}^{t_2 + \frac{\theta}{\omega_0}} \cos K\omega_0 t \sin \frac{\pi}{T}(t - \frac{\theta}{\omega_0}) \times \\ \times \sin(\omega_0 t - \theta) dt \quad (215)$$

$$= \frac{2LS_1}{T} \left\{ \int_{t_1 + \frac{\theta}{\omega_0}}^{t_2 + \frac{\theta}{\omega_0}} [-\sin \theta + \sin(2\omega_0 t - \theta)] \times \right. \\ \times \sin \frac{\pi}{T}(t - \frac{\theta}{\omega_0}) dt \\ \left. + \sum_{K=3,5,\dots}^{\infty} \frac{2}{K} \int_{t_1 + \frac{\theta}{\omega_0}}^{t_2 + \frac{\theta}{\omega_0}} \cos K\omega_0 t \sin \frac{\pi}{T}(t - \frac{\theta}{\omega_0}) \times \right. \\ \left. \times \sin(\omega_0 t - \theta) dt \right\}. \quad (216)$$

Since the filtered noise process bandwidth is much smaller than the center frequency, ω_0 , the contribution of the high frequency components of the integrand is negligible. Hence, the first term of (216) predominates, yielding

$$N_c \approx -\frac{2LS_1}{T} \sin \theta \int_{t_1 + \frac{\theta}{\omega_0}}^{t_2 + \frac{\theta}{\omega_0}} \sin \frac{\pi}{T}(t - \frac{\theta}{\omega_0}) dt \\ = \frac{2LS_1}{T} \sin \theta \left[\cos \frac{\pi t_2}{T} - \cos \frac{\pi t_1}{T} \right]. \quad (217)$$

Again, it should be noted that the maximum value of N_c occurs when the capture interval equals the bit length. For this case, $t_1 = 0$, $t_2 = T$ and $N_c = (-4LS/\pi)\sin\theta$. The linear transformation $\phi = \theta + \frac{\pi}{2}$ results in

$$N_c = \begin{cases} \frac{2LS}{\pi} \cos\phi \left[\cos \frac{\pi t_2}{T} - \cos \frac{\pi t_1}{T} \right], & t_2 - t_1 \leq T \\ -\frac{4LS}{\pi} \cos\phi, & t_2 - t_1 > T. \end{cases} \quad (218)$$

The complementary signal component of the detector functional, S_c , is given by

$$\begin{aligned} S_c = & \frac{1}{T} \int_0^T \pi LS, \operatorname{SGN} \left\{ \cos \left(\omega_0 + \frac{\pi}{T} \right) t \right\} \times \\ & \times \sin \frac{\pi t}{T} \sin \omega_0 t dt \\ & + \frac{1}{T} \int_{t_2}^T \pi LS, \operatorname{SGN} \left\{ \cos \left(\omega_0 + \frac{\pi}{T} \right) t \right\} \times \\ & \times \sin \frac{\pi t}{T} \sin \omega_0 t dt. \end{aligned} \quad (219)$$

Substituting (186) in (219) results in

$$\begin{aligned}
 \ddot{S}_c &= \frac{4LS_1}{T} \sum_{K \text{ odd}}^{\infty} \frac{1}{K} \int_0^{t_1} \cos K(w_0 + \frac{\pi}{T})t \sin \frac{\pi t}{T} \times \\
 &\quad \times \sin \omega_0 t dt \\
 &\quad + \frac{4LS_1}{T} \sum_{K \text{ odd}}^{\infty} \frac{1}{K} \int_{t_2}^T \cos K(w_0 + \frac{\pi}{T})t \sin \frac{\pi t}{T} \times \\
 &\quad \times \sin \omega_0 t dt \\
 &= \frac{4LS_1}{T} \left\{ -\frac{1}{4} \int_0^{t_1} \left[1 - \cos \frac{2\pi t}{T} \right] \left[1 - \cos 2\omega_0 t \right] dt \right. \\
 &\quad - \frac{1}{4} \int_{t_2}^T \left[1 - \cos \frac{2\pi t}{T} \right] \left[1 - \cos 2\omega_0 t \right] dt \\
 &\quad \left. + \frac{1}{4} \int_0^{t_1} \sin \frac{2\pi t}{T} \sin 2\omega_0 t dt \right. \\
 &\quad \left. + \frac{1}{4} \int_{t_2}^T \sin \frac{2\pi t}{T} \sin 2\omega_0 t dt \right\} \quad (220) \\
 &\quad + \sum_{K=3,5,\dots}^{\infty} \frac{1}{K} \int_0^{t_1} \cos K(w_0 + \frac{\pi}{T})t \sin \frac{\pi t}{T} \times \\
 &\quad \times \sin \omega_0 t dt \\
 &\quad + \sum_{K=3,5,\dots}^{\infty} \frac{1}{K} \int_{t_2}^T \cos K(w_0 + \frac{\pi}{T})t \sin \frac{\pi t}{T} \times \\
 &\quad \times \sin \omega_0 t dt
 \end{aligned}$$

Also, since the signal bandwidth is much smaller than the center frequency, ω_c , the contributions of the high frequency components of the integrand are negligible. Hence, only the first two terms of (230) contribute significantly to S_c , and

$$S_c \approx \begin{cases} -\frac{LS_1}{T} [T - (t_2 - t_1) \\ - \frac{I}{2\pi r} (\sin \frac{2\pi r t_2}{T} - \sin \frac{2\pi r t_1}{T})], & t_2 - t_1 \leq T \\ 0, & t_2 - t_1 > T \end{cases} \quad (221)$$

Therefore, the total functional, R_d , given that the upper shift frequency signal is transmitted, is the sum of N_c (218) and S_c (221):

$$R_d = \begin{cases} -\frac{LS_1}{T} [T - (t_2 - t_1) - \frac{I}{2\pi r} (\sin \frac{2\pi r t_2}{T} - \sin \frac{2\pi r t_1}{T}) \\ - \frac{2T}{\pi r} \cos \phi (\cos \frac{\pi r t_2}{T} - \cos \frac{\pi r t_1}{T})], & t_2 - t_1 \leq T \\ -\frac{4LS_1}{\pi r} \cos \phi, & t_2 - t_1 > T \end{cases} \quad (221a)$$

or

$$R_d = \begin{cases} -\frac{Ls_1}{T} [T - V_i - T/2\pi(V_2 - V_3) \\ \quad - \frac{2T}{\pi}(V_4 - V_5) \cos \phi], V_i \leq T \\ -\frac{4Ls_1}{\pi} \cos \phi, V_i > T, \end{cases} \quad (222)$$

where

$$V_i = t_2 - t_1, \quad (201)$$

$$V_2 = \sin \frac{2\pi t_2}{T}, \quad (222a)$$

$$V_3 = \sin \frac{2\pi t_1}{T}, \quad (222b)$$

$$V_4 = \cos \frac{\pi t_2}{T}, \quad (222c)$$

$$V_5 = \cos \frac{\pi t_1}{T}. \quad (222d)$$

Here, a decision error occurs when $R_d > 0$. However, the problem of noise pulse position is now significant. In this case, the detector functional is a transcendental function of pulse position and pulse width (or, effectively, noise envelope voltage, E) as opposed to the simpler PSK functional which is a linear function of pulse width only.

An exact CFSK error probability expression must include statistical averaging with respect to both t_c (pulse position) and E (pulse width). However, the transcendental character of the detector functional promises to make an exact computation very formidable. This is further compounded by the unavailability of a closed-form expression for the envelope voltage probability density. Therefore, it is desirable to seek a simplified, but viable, alternative to an exact solution of the CFSK error probability.

To this end, a truncated Taylor Series expansion is developed as an approximation of the CFSK error probability.

The average probability of error, P_{ec} , is given by

$$P_{ec} = \langle P_{ec|t_c} \rangle_{t_c} \quad (223)$$

$$= \int f_{t_c}(T_c) P_{ec|t_c} dT_c, \quad (223a)$$

where, from (220a) and (220b),

$$f_{t_c}(T_c) = \frac{1}{T - \Delta}, \quad \frac{\Delta}{2} \leq T_c \leq T - \frac{\Delta}{2}, \quad (224)$$

and the conditional error probability (given t_c) $P_{ec|t_c}$ is given by

$$P_{ec|t_c} = Pr(R_d > 0) = Pr\left\{\frac{2T}{\pi}(V_4 - V_5) \cos \phi > T - V_1 - \frac{T}{2\pi}(V_2 - V_3), V_1 \leq T\right\} \quad (225)$$

$$+ Pr\left\{-\frac{4LS_1}{\pi} \cos \phi, V_1 > T\right\}.$$

Since $-\cos \phi$ and $\cos \phi$ have identical probability densities for ϕ uniformly distributed on $(-\frac{\pi}{2}, \frac{3\pi}{2})$, $|V_4 - V_5| \cos \phi$ can replace $(V_4 - V_5) \cos \phi$ in (225). This results in

$$P_{ec|t_c} = Pr\left\{\frac{2T}{\pi}|V_4 - V_5| \cos \phi > T - V_1 - \frac{T}{2\pi}(V_2 - V_3), V_1 \leq T\right\}$$

$$+ Pr\left\{-\frac{4LS_1}{\pi} \cos \phi > 0, V_1 > T\right\}$$

$$= Pr\left\{1 \geq \cos \phi > \frac{T - V_1 - (T/2\pi)(V_2 - V_3)}{(2T/\pi)|V_4 - V_5|}, V_1 \leq T\right\} \quad (226)$$

$$+ Pr\left\{-\frac{4LS_1}{\pi} \cos \phi > 0, V_1 > T\right\}$$

Noting that θ is statistically independent of t_c and E , (226) can be rewritten as

$$P_{ec|t_c} = P_r \left\{ |\phi| \leq \cos^{-1} \left[\frac{T - V_1 - (T/2\pi)(V_2 - V_3)}{(2T/\pi)|V_4 - V_5|} \right], \right. \\ \left. V_0 \leq V_1 \leq T \right\} \quad (227)$$

$$+ \frac{1}{2} P_r \left\{ V_1 > T \right\},$$

where

$$\left. \frac{T - V_1 - (T/2\pi)(V_2 - V_3)}{(2T/\pi)|V_4 - V_5|} \right]_{V_1 = V_0} = 1. \quad (227a)$$

This can also be rewritten as

$$P_{ec|t_c} = \frac{1}{\pi} \int_{E_1}^{E_2} f_e(E) dE \int_0^{\cos^{-1} \left[\frac{T - V_1 - (T/2\pi)(V_2 - V_3)}{(2T/\pi)|V_4 - V_5|} \right]} d\phi \\ + \frac{1}{2} \int_{E_2}^{\infty} f_e(E) dE, \quad (228)$$

where

$$V_1 \Big|_{E=E_1} = V_0 \quad (228a)$$

V_0 is given by (227a) and

$$V_1 \Big|_{E=E_2} = T. \quad (228b)$$

Proceeding,

$$\begin{aligned} P_{ec|t_c} &= \int_{E_1}^{E_2} \frac{1}{\pi} \cos^{-1} \left[\frac{T - V_1 - (T/2\pi)(V_2 - V_3)}{(2T/\pi)|V_4 - V_5|} \right] \times \\ &\quad \times f_e(E) dE \\ &+ \frac{1}{2} \int_{E_2}^{\infty} f_e(E) dE \end{aligned} \quad (229)$$

$$= \int_{E_1}^{\infty} g(V_1, V_2, V_3, V_4, V_5) f_e(E) dE, \quad (230)$$

where

$$\begin{aligned} \mathcal{B}(V_1, V_2, V_3, V_4, V_5) &\triangleq \mathcal{B}(\underline{V}) \\ &= \frac{1}{\pi} \cos^{-1} \left[\frac{I - V_1 - (T/2\pi)(V_2 - V_3)}{(2T/\pi)|V_4 - V_5|} \right] \times \\ &\quad \times [U(V_1 - V_0) - U(V_1 - T)] \\ &\quad + \frac{1}{2} U(V_1 - T), \end{aligned} \quad (231)$$

$U[\cdot]$ is the unit step function, and V_0 is given by (227a). (It should be noted that $\mathcal{B}(\underline{V})$ is a continuous function of E for $V_1 \geq V_0$.) Also, (227a) implies that

$$\mathcal{B}(\underline{V}) \Big|_{V_1 = V_0} = 0. \quad (231a)$$

The unit step function $U(V_k - Y)$, can also be expressed in integral form ([1], 4.3.142) as

$$\begin{aligned} U(V_k - Y) &= \frac{1}{2} + \frac{1}{\pi} \int_0^\infty \sin \pi z (V_k - Y) \frac{dz}{z} \\ &= \frac{1}{\pi} \int_0^\infty [\sin \pi z + \sin \pi z (V_k - Y) \frac{dz}{z}] \end{aligned} \quad (232)$$

Substitution of (232) in (231) results in

$$\begin{aligned}
 P(V) &= \frac{1}{\pi^2} \int_0^\infty \cos^{-1} \left[\frac{T - V_1 - (T/2\pi)(V_2 - V_3)}{(2T/\pi)|V_4 - V_5|} \right] \times \\
 &\quad \times \left[\sin \pi(V_1 - V_0)z - \sin \pi(V_1 - T)z \right] \frac{dz}{z} \quad (233) \\
 &\quad + \frac{1}{\pi T} \int_0^\infty \frac{1}{2} \left[\sin \pi(V_1 - T)z + \sin \pi z \right] \frac{dz}{z}.
 \end{aligned}$$

At this point, it is convenient to define \hat{V}_i , $i = 1, \dots, 5$, as the value of the random variable V_i as averaged with respect to t_c .

Mathematically:

$$\hat{V}_i \triangleq \langle V_i \rangle_{t_c}, \quad i = 1, \dots, 5. \quad (234)$$

Since $|V_4 - V_5| > 0$ for $0 < V_1 \leq T$ and $V_0 > 0$, the integrand of the first term on the right side of (233) is an analytic function of all the V_i 's for $0 < V_0 \leq V_1 \leq T$. Therefore, the first integrand of (233) can be expressed in a multivariate Taylor series in terms of V_i 's. Likewise, the second integrand of (233) is an analytic function of V_1 for any finite V_1 . Specifically, then, it is possible to express the integrands as power series in $(V_1 - \hat{V}_1)$.

Thus, the function $\rho(\underline{v})$ can be represented as

$$\begin{aligned} \rho(\underline{v}) &= \frac{1}{\pi} \int_0^\infty dz \left\{ I_E(\hat{v}) \right. \\ &\quad + \sum_{i=1}^5 (V_i - \hat{V}_i) \left[\frac{\partial I_E}{\partial V_i} \right]_{\underline{v}=\hat{v}} \\ &\quad + \frac{1}{2!} \sum_{i=1}^5 \sum_{j=1}^5 (V_i - \hat{V}_i)(V_j - \hat{V}_j) \left[\frac{\partial^2 I_E}{\partial V_i \partial V_j} \right]_{\underline{v}=\hat{v}} \\ &\quad \left. + \text{Higher order terms} \right\}, \end{aligned} \quad (235)$$

where

$$\begin{aligned} I_E &= \frac{1}{\pi z} \cos^{-1} \left[\frac{T - V_1 - (T/2\pi)(V_2 - V_3)}{(2T/\pi)|V_4 - V_5|} \right] \times \\ &\quad \times \left[\sin \pi(V_1 - V_0)z - \sin \pi(V_1 - T)z \right] \quad (236) \\ &\quad + \frac{1}{2z} \left[\sin \pi(V_1 - T)z + \sin \pi z \right]. \end{aligned}$$

Because of the unavailability of a closed-form expression for the probability density of E , computation of high order statistical moments of V_i 's is very difficult to obtain. Therefore, it is worthwhile to see if the exact, but formidable, evaluation of (235) can be simplified. Specifically, it is proposed that the integrand of (235),

I_g , be approximated by the constant plus linear terms of the indicated Taylor series representations. In 5.3, it is shown that this truncated series approximation does provide close quantitative agreement with measured experimental results. These approximations yield

$$P(V) \approx \frac{1}{\pi} \int_0^\infty dz \left\{ I_g(\hat{V}) + \sum_{i=1}^5 (V_i - \hat{V}_i) \left[\frac{\partial I_g}{\partial V_i} \right]_{V=\hat{V}} \right\}, \quad (237)$$

where I_g is given by (236).

Substituting (237) into (230) and (230), in turn, into (223) yields

$$P_{ec} = \left\langle \int_{E_1}^\infty f_e(E) dE \times \frac{1}{\pi} \int_0^\infty dz \left\{ I_g(\hat{V}) + \sum_{i=1}^5 (V_i - \hat{V}_i) \left[\frac{\partial I_g}{\partial V_i} \right]_{V=\hat{V}} \right\} \right\rangle_{t_c} \quad (238)$$

$$= \int_{E_1}^\infty f_e(E) dE \times \frac{1}{\pi} \int_0^\infty dz \left\{ I_g(\hat{V}) + \sum_{i=1}^5 \left\langle (V_i - \hat{V}_i) \right\rangle_{t_c} \left[\frac{\partial I_g}{\partial V_i} \right]_{V=\hat{V}} \right\}, \quad (239)$$

where E_1 is given by (228a).

However, from (234)

$$\langle(v_i - \hat{v}_i)\rangle_{t_c} = \langle v_i - \langle v_i \rangle_{t_c} \rangle_{t_c} = 0. \quad (240)$$

Also note that $\left[\frac{\partial I_E}{\partial v_i} \right]_{V=\hat{V}}$ is a finite constant for $0 \leq v_i \leq T$.
Hence, (239) reduces to

$$\begin{aligned} P_{ec} &= \int_{E_1}^{\infty} f_e(E) dE \times \frac{1}{\pi} \int_0^{\infty} dz \{ I_E(\hat{v}) \} \\ &= \int_{E_1}^{\infty} f_e(E) dE \times \frac{1}{\pi} \int_0^{\infty} \frac{dz}{z} \times \\ &\quad \times \left\{ \frac{1}{\pi} \cos^{-1} \left[\frac{T - \hat{v}_i - (T/2\pi)(\hat{v}_2 - \hat{v}_3)}{(2T/\pi)|\hat{v}_4 - \hat{v}_5|} \right] \times \right. \\ &\quad \times [\sin \pi(\hat{v}_i - \hat{v}_0) z - \sin \pi(\hat{v}_i - T) z] \\ &\quad \left. + \frac{1}{2} [\sin \pi(\hat{v}_i - T) z - \sin \pi z] \right\} \\ &= \int_{E_1}^{\infty} f_e(E) dE \left\{ \frac{1}{\pi} \cos^{-1} \left[\frac{T - \hat{v}_i - (T/2\pi)(\hat{v}_2 - \hat{v}_3)}{(2T/\pi)|\hat{v}_4 - \hat{v}_5|} \right] \times \right. \\ &\quad \times [U(\hat{v}_i - \hat{v}_0) - U(\hat{v}_i - T)] + \\ &\quad \left. + \frac{1}{2} U(\hat{v}_i - T) \right\} \end{aligned}$$

$$P_{ec} = \frac{1}{\pi} \int_{E_1}^{E_2} \cos^{-1} \left[\frac{T - \hat{V}_1 - (T/2\pi)(\hat{V}_2 - \hat{V}_3)}{(2T/\pi)|\hat{V}_4 - \hat{V}_5|} \right] \times f_e(E) dE$$

$$+ \frac{1}{2} \int_{E_2}^{\infty} f_e(E) dE, \quad (241)$$

where

$$\left. \frac{T - \hat{V}_1 - (T/2\pi)(\hat{V}_2 - \hat{V}_3)}{(2T/\pi)|\hat{V}_4 - \hat{V}_5|} \right|_{\hat{V}_1 = \hat{V}_o} = 1, \quad (241a)$$

$$\left. \hat{V}_1 \right|_{E = E_1} = \hat{V}_o, \quad (241b)$$

$$\left. \hat{V}_1 \right|_{E = E_2} = T, \quad (241c)$$

and $\underline{V} = \hat{V}$.

In order to complete this portion of the analysis, it is necessary to evaluate the V_i 's.

V_1 is given by (201) as

$$V_1 = \Delta. \quad (201)$$

Hence, employing (234),

$$\hat{V}_1 = \langle V_1 \rangle_{t_c} = \Delta. \quad (242)$$

Also, from (234), (222a), and (222b),

$$\hat{V}_2 - \hat{V}_3 = \left\langle \sin \frac{2\pi t_2}{T} - \sin \frac{2\pi t_1}{T} \right\rangle_{t_c}. \quad (242a)$$

Substituting (200a) and 200b) and applying (224) yields

$$\begin{aligned}\hat{V}_2 - \hat{V}_3 &= \frac{1}{(T-\Delta)} \int_{\frac{\Delta}{2}}^{T-\frac{\Delta}{2}} \left[\sin \frac{2\pi}{T} \left(T_c + \frac{\Delta}{2} \right) \right. \\ &\quad \left. - \sin \frac{2\pi}{T} \left(T_c - \frac{\Delta}{2} \right) \right] dT_c \\ &= \frac{2}{(T-\Delta)} \sin \frac{\pi\Delta}{T} \int_{\frac{\Delta}{2}}^{T-\frac{\Delta}{2}} \cos \frac{2\pi T_c}{T} dT_c \\ &= \frac{T}{\pi(T-\Delta)} \sin \frac{\pi\Delta}{T} \left[\sin \frac{2\pi T_c}{T} \right]_{\frac{\Delta}{2}}^{T-\frac{\Delta}{2}} \\ &= -\frac{2T}{\pi(T-\Delta)} \left(\sin \frac{\pi\Delta}{T} \right)^2.\end{aligned} \quad (242b)$$

From (234), (222c), and (222d),

$$\hat{V}_4 - \hat{V}_5 = \left\langle \cos \frac{\pi t_2}{T} - \cos \frac{\pi t_1}{T} \right\rangle_{t_c}. \quad (242c)$$

Again, substituting (200a) and (200b) and applying (224) yields

$$\begin{aligned} \hat{V}_4 - \hat{V}_5 &= \frac{1}{(T-\Delta)} \int_{\frac{\Delta}{2}}^{T-\frac{\Delta}{2}} \left[\cos \frac{\pi}{T} (T_c + \frac{\Delta}{2}) \right. \\ &\quad \left. - \cos \frac{\pi}{T} (T_c - \frac{\Delta}{2}) \right] dT_c \end{aligned}$$

$$= -\frac{2}{(T-\Delta)} \sin \frac{\pi \Delta}{2T} \int_{\frac{\Delta}{2}}^{T-\frac{\Delta}{2}} \sin \frac{\pi T_c}{T} dT_c$$

$$= \frac{2T}{\pi(T-\Delta)} \sin \frac{\pi \Delta}{2T} \left[\cos \frac{\pi T_c}{T} \right]_{\frac{\Delta}{2}}^{T-\frac{\Delta}{2}}$$

$$= -\frac{4T}{\pi(T-\Delta)} \sin \frac{\pi \Delta}{2T} \cos \frac{\pi \Delta}{2T}$$

$$= -\frac{2T}{\pi(T-\Delta)} \sin \frac{\pi \Delta}{T}. \quad (242d)$$

$$|\widehat{V}_4 - \widehat{V}_5| = \frac{2T}{\pi(T-\Delta)} \sin \frac{\pi\Delta}{T}. \quad (242e)$$

Substituting (242), (242b) and (242c) in (241) yields

$$\begin{aligned} P_{ec} = & \frac{1}{\pi} \int_{E_1}^{E_2} \cos^{-1} \left[\frac{T-\Delta + (T/\pi)^2 (\sin \frac{\pi\Delta}{T})/(T-\Delta)}{(4T^2/\pi)[\sin \frac{\pi\Delta}{T}/\pi(T-\Delta)]} \right] \times \\ & \times f_e(E) dE \\ & + \frac{1}{2} \int_{E_2}^{\infty} f_e(E) dE. \end{aligned} \quad (243)$$

At this point, it is apparent that the argument of $\cos^{-1} [\cdot]$ in (243) is not a combination of linear terms as it is in the PSK case (206). However, in order to employ the numerical integration technique previously developed for the PSK functional, it is necessary to find Δ 's for arbitrary arguments of $\cos^{-1} [\cdot]$. Unfortunately, the exact argument of $\cos^{-1} [\cdot]$ in (243) is a transcendental function of Δ and thus, the first integral of (243) is not directly suitable for numerical evaluation. Therefore, it is desirable to express the argument of $\cos^{-1} [\cdot]$ as a combination of linear terms to facilitate the numerical evaluation of (243). Because the second term of the numerator is zero at $\Delta = 0$, and $\Delta = T$ and much less than the linear terms for $0 \leq \Delta \leq T$, it may be neglected to yield

$$T-\Delta + (T/\pi)^2 \left(\sin \frac{\pi\Delta}{T}\right)^2 / (T-\Delta) \approx T-\Delta. \quad (243a)$$

(It should be noted that both the left and right sides of this expression are zero at $\Delta = T$.)

Also, the denominator of the argument of $\cos^{-1} [\cdot]$ may be approximated as

$$(4T/\pi) \frac{\sin(\frac{\pi\Delta}{T})}{\pi(T-\Delta)} \approx \frac{4}{\pi} \Delta. \quad (243b)$$

(Here it should be noted that both sides of (243b) agree exactly for $\Delta = 0, T$, the limiting values.)

Incorporating these approximations in the argument of $\cos^{-1} [\cdot]$ in (243) results in the overall approximation

$$\frac{T-\Delta + (T/\pi)^2 \left(\sin \frac{\pi\Delta}{T}\right)^2 / (T-\Delta)}{(2T/\pi)^2 \sin \frac{\pi\Delta}{T} / (T-\Delta)} \approx \frac{T-\Delta}{(4/\pi)\Delta}. \quad (243c)$$

Figure 15 shows both sides of this relationship (243c) as a function of Δ/T . It should be noted that the exact and approximate curves nearly coincide at a value of 1 where $\Delta/T \approx .45$. This intercept corresponds to the minimum fractional pulse width which can cause a decision error. Also, the curves coincide at 0 when $\Delta/T = 1$. Therefore, substituting (243c) in (243) results in

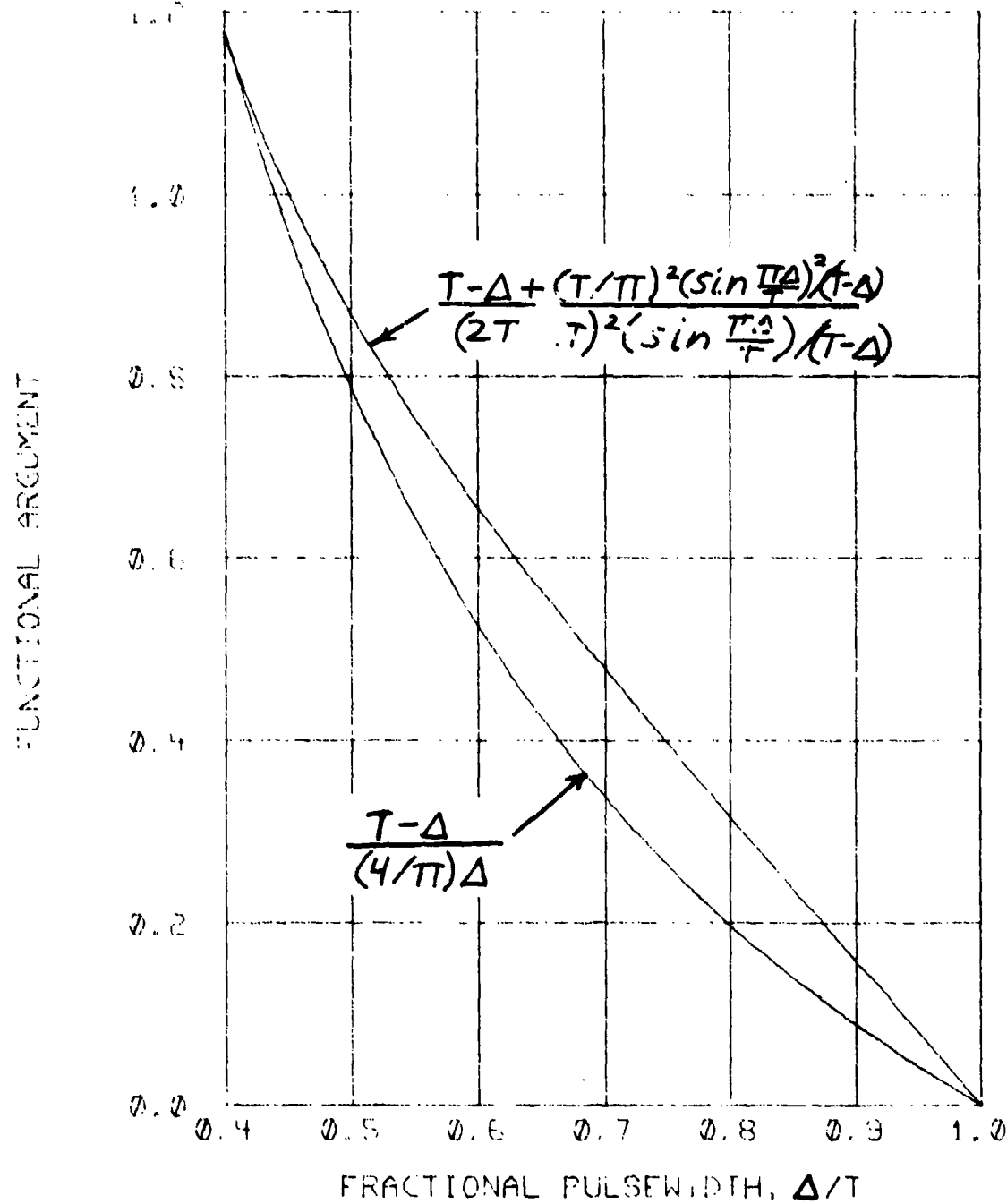


Figure 15. Arguments of $\cos^{-1}(\cdot)$ in the CFSK Detector Functional:

(1) $\frac{T-\Delta + (T/\pi)^2 (\sin \frac{\pi\Delta}{T})^2 / (T-\Delta)}{(2T/\pi)^2 (\sin \frac{\pi\Delta}{T}) / (T-\Delta)}$, from (243); and as

approximated by (2) $\frac{T-\Delta}{(4/\pi)\Delta}$, from (243c).

$$P_{ec} \approx \frac{1}{\pi} \int_{E_1}^{E_2} \cos^{-1} \left[\frac{T - \Delta}{(4/\pi)\Delta} \right] f_e(E) dE + \frac{1}{2} \int_{E_2}^{\infty} f_e(E) dE, \quad (243d)$$

where E_1 and E_2 are defined by (241a), (241b), and (241c). (Note that E_2 corresponds to $\Delta = T$.)

Also

$$P_{ec} = \frac{1}{\pi} \int_{E_1}^{E_2} \cos^{-1} \left[\frac{b, T - L_n(b, TE/S)}{(4/\pi)L_n(b, TE/S)} \right] \times \\ \times f_e(E) dE + \frac{1}{2} \int_{E_2}^{\infty} f_e(E) dE. \quad (243e)$$

Here the minimum capture interval, \hat{V}_0 , must satisfy

$$\left. B(\underline{v}) \right|_{\hat{V}_1 = \hat{V}_0} = 0 \quad (244)$$

or

$$\frac{T - \hat{V}_0}{(4/\pi)\hat{V}_0} = 1$$

or

$$\hat{V}_0 = T/[1 + (4/\pi)], \quad (244a)$$

so that, substituting \hat{V}_0 for Δ in (199c),

$$E_i = \frac{S}{b_i T} e^{b_i T / (1 + 4/\pi)} \quad (244b)$$

It is apparent that the final CFSK error probability expression (243d) is quite similar to the preceding PSK result (206), differing only in the lower limit and the coefficient of the denominator of $\cos^{-1} [\cdot]$ in the first integral. Thus, the PSK numerical evaluation procedure can be applied directly, except that here the n-fold partition of the first integral requires that

$$\cos^{-1} \left[\frac{b_i T - L_n(b_i T E_i^U / S)}{(4/\pi) L_n(b_i T E_i^U / S)} \right] = (i-1) \frac{\pi}{2n} \quad (245a)$$

and

$$\cos^{-1} \left[\frac{b_i T - L_n(b_i T E_i^L / S)}{(4/\pi) L_n(b_i T E_i^L / S)} \right] = i \frac{\pi}{2n} \quad (245b)$$

where E_i^U and E_i^L are the upper and lower bounds on the i th partition integral, respectively.

From (245a) and (245b) E_i^U and E_i^L are found to be

$$E_i^U = \frac{S}{b_i T} \exp \left[\frac{b_i T}{1 + (4/\pi) \cos \frac{i\pi}{2n}} \right] \quad (246a)$$

and

$$E_i^L = \frac{S}{b,T} \exp \left[\frac{b,T}{1 + (4/\pi) \cos \frac{i\pi}{2n}} \right]. \quad (246b)$$

Substituting (246b) for (208b) in (210) results in

$$\begin{aligned} P_{ec} \approx & \frac{1}{2} P \left\{ \frac{S}{b,T} e^{b,T} \right\} + \\ & + \frac{1}{4n} \left[P \left\{ \frac{S}{b,T} e^{b,T/(1+4/\pi)} \right\} \right. \\ & \left. + P \left\{ \frac{S}{b,T} e^{b,T} \right\} \right] + \\ & + \frac{1}{2n} \sum_{i=1}^{n-1} P \left\{ \frac{S}{b,T} \exp \left[\frac{b,T}{1 + (4/\pi) \cos \frac{i\pi}{2n}} \right] \right\}. \end{aligned} \quad (247)$$

5.2.1.3 MSK Detection

At this point, hard-limiting MSK receiver error-rate performance can be obtained directly by applying the results of the MSK system analysis of 3.4 to the hard-limiting CFSK performance estimates. First, it should be noted that a predetection bandpass hard-limiter affects a received MSK signal-plus-noise exactly the same way as it does the CFSK signal-plus-noise. This conclusion is based on the fact that the MSK signal has an FSK waveform which differs from the CFSK waveform only in the magnitude of its frequency deviation from center frequency (or modulation index). Therefore, the instantaneous phase (or frequency)

of the fundamental component of the limiter output coincides with that of the larger input component - desired signal or noise. Subsequent to the limiter, the MSK and CFSK detectors are functionally identical to those described in 3.4 and 3.3, respectively. Hence, the error rate of the hard-limiting MSK system is functionally related to that of the hard-limiting CFSK system in the same manner as for the post-limiter detectors described in 3.3 and 3.4.

Specifically, it was determined in 3.4 that the error probability of the MSK detector (157) is of the same functional form as that of the CFSK detector (142). In particular, the MSK expression (157) can be obtained by replacing T by 2T in the CFSK expression (142). Therefore, this substitution in the hard-limiting CFSK error rate expression (247) results in an expression for the MSK single-noise-pulse error probability, P_{em} :

$$\begin{aligned}
 P_{em} = & \frac{1}{2} P \left\{ \frac{S}{2b,T} e^{2b,T} \right\} + \\
 & + \frac{1}{4n} \left[P \left\{ \frac{S}{2b,T} e^{2b,T/(1+4/\pi)} \right\} \right. \\
 & \quad \left. + P \left\{ \frac{S}{2b,T} e^{2b,T} \right\} \right] + \\
 & + \frac{1}{2n} \sum_{i=1}^{n-1} P \left\{ \frac{S}{2b,T} \exp \left[\frac{2b,T}{1+(4/\pi) \cos \frac{i\pi}{2n}} \right] \right\} \tag{248}
 \end{aligned}$$

These resultant hard-limiting receiver error probabilities for one noise pulse per bit are computed on the basis of first-order truncated Taylor series approximations. As noted earlier, a more ideal treatment would be to compute the error probabilities as an exact function of noise pulse occurrence time and then average with respect to occurrence time. However, the fact that the detector functionals involve transcendental functions of the occurrence time and noise pulse amplitude makes this latter approach impractically formidable.

Although no experimental VLF data is available for validating the approximate PSK analysis, the subsequent multiple noise pulse analyses of CFSK and MSK performance are clearly validated by measured data.

5.2.2 Coherent Detection with Hard-Limiting and Multiple Noise Pulses per Detection Element

5.2.2.1 The Noise Envelope Voltage for Multiple Noise Pulses

The preceding discussions have addressed the case where only one noise pulse, if any, occurs during a detection period (bit length). In order to consider the case of multiple noise pulses, it is first necessary to refine the definition of the noise envelope voltage, E . Because of the impulsive nature of the atmospheric noise, certain simplifying assumptions are employed. These are: (1) noise pulses exceeding the signal level are considered to be non-overlapping; (2) the phase angles of the noise pulses are statistically independent;

and (3) pulse amplitudes within a given detection element have a monotonic amplitude relationship wherein any two pulses most nearly equal in amplitude have amplitudes in the ratio $r \leq 1$. Thus, from (70) the multiple-pulse noise envelope process would be of the form:

$$e(t) = \sum_{i=0}^{N-1} p_r^i e^{-b_i(t-\tau_i)} u(t-\tau_i). \quad (249)$$

5.2.2.2 Real Axis Projection of the Sum of N Independent Vectors of Equal Magnitude

Before proceeding to a consideration of detector functional performance in the face of multiple independent noise pulses, it is necessary to consider the effective contribution (real axis projection) of the vector sum of multiple vectors having equal amplitudes but uniformly distributed phase angles. Briefly, the problem is to assess

$$E_{\partial N} \triangleq \operatorname{Re} \left\{ \sum_{i=1}^N E e^{j\theta_i} \right\}, \quad (250)$$

and, in particular, to derive a useful probabilistic expression for z_N where

$$\bar{z}_N = \sum_{i=1}^N \cos \theta_i \quad (251)$$

and the θ_i 's are statistically independent and each uniformly distributed on $(-\pi, \pi)$.

Obviously,

$$\beta_1 = \cos \theta, \quad -\pi \leq \theta \leq \pi,$$

and

$$P_{\beta_1}(z) \triangleq P_r(\beta_1 \geq z) = P_r(\cos \theta \geq z),$$

or

$$\begin{aligned} P_{\beta_1}(z) &= P_r(|\theta| \leq \cos^{-1}(z)), \\ &= \int_{-\cos^{-1}(z)}^{\cos^{-1}(z)} f_{\theta}(\theta) d\theta. \end{aligned} \tag{252}$$

However,

$$f_{\theta}(\theta) = \frac{1}{2\pi},$$

and thus,

$$P_{\beta_1}(z) = \frac{1}{2\pi} \int_{-\cos^{-1}(z)}^{\cos^{-1}(z)} d\theta = \frac{1}{\pi} \cos^{-1}(z). \tag{253}$$

Now, using the method described by Bennett [7], a general procedure is developed for evaluating $P_{j_N}(z)$ for $N > 1$. Considering the probability density function, $f_{j_N}(z)$, where

$$j_N = \sum_{i=1}^N \cos \theta_i, \quad (253a)$$

it is obvious that

$$f_{j_N}(z) = 0, |z| > N. \quad (253b)$$

Thus, since

$$\int_{-N}^N f_{j_N}(z) dz = 1, \quad (253c)$$

and $f_{j_N}(z)$ is piecewise continuous, $f_{j_N}(z)$ can be represented by a Fourier exponential series:

$$f_{j_N}(z) = \begin{cases} \sum_{m=-\infty}^{\infty} C_m e^{\frac{j m \pi z}{N}}, & -N \leq z \leq N \\ 0, & \text{elsewhere.} \end{cases} \quad (254)$$

Here, the coefficients C_m are given by

$$C_m = \frac{1}{2N} \int_{-N}^N f_{j_N}(z) e^{-j \frac{m \pi z}{N}} dz$$

$$C_m = \frac{1}{2N} \int_{-\infty}^{\infty} f_{\beta_N}(z) e^{-j \frac{m\pi z}{N}} dz$$

$$= \frac{1}{2N} \int_{-N}^{N} f_{\beta_N}(z) e^{-j \frac{m\pi z}{N}} dz. \quad (255)$$

However,

$$\int_{-\infty}^{\infty} f_{\beta_N}(z) e^{-j \frac{m\pi z}{N}} dz = F_{\beta_N}(j\frac{m\pi}{N}) \quad (255a)$$

is the characteristic function of the random variable, z_N .

Since

$$\beta_N = \sum_{i=1}^N \beta_i, \quad (255b)$$

where

$$\beta_i = \cos \theta_i,$$

and the θ_i 's are statistically independent,

$$F_{\beta_N}(j\frac{m\pi}{N}) = \prod_{i=1}^N F_{\beta_i}(j\frac{m\pi}{N}). \quad (256)$$

Evaluating the characteristic function for z_i ,

$$\begin{aligned} F_{3i}(j\zeta) &= E\left\{e^{-j\zeta z_i}\right\} \\ &= \frac{1}{2\pi} \int_{-\pi}^{\pi} e^{-j\zeta \cos \theta_i} d\theta_i \\ &= J_0(\zeta). \end{aligned} \tag{257}$$

Hence,

$$F_{3N}(j\zeta) = \prod_{i=1}^N F_{3i}(j\zeta) = J_0^N(\zeta), \tag{258}$$

and

$$\begin{aligned} C_m &= \frac{1}{2N} F_{3N}(j\zeta) \Big|_{\zeta = \frac{m\pi}{N}} \\ &= \frac{1}{2N} J_0^N\left(\frac{m\pi}{N}\right). \end{aligned} \tag{259}$$

The probability density function is then given by

$$\begin{aligned}
 f_{Z_N}(z) &= \frac{1}{2N} \sum_{m=-\infty}^{\infty} J_0^N\left(\frac{m\pi}{N}\right) e^{j\frac{m\pi z}{N}} \\
 &= \frac{1}{2N} \left\{ 1 + \sum_{m=1}^{\infty} J_0^N\left(\frac{m\pi}{N}\right) \times \right. \\
 &\quad \times \left. \left[e^{j\frac{m\pi z}{N}} + e^{-j\frac{m\pi z}{N}} \right] \right\} \\
 &= \frac{1}{2N} \left\{ 1 + 2 \sum_{m=1}^{\infty} J_0^N\left(\frac{m\pi}{N}\right) \cos\left(\frac{m\pi z}{N}\right) \right\} \quad (260)
 \end{aligned}$$

for $-N \leq z \leq N$ and is zero otherwise. Note that $f_{Z_N}(z)$ is an even function of z .

Also,

$$\begin{aligned}
 P_{Z_N}(z) &= \int_z^N f_{Z_N}(u) du \\
 &= \frac{1}{2N} \int_z^N \left\{ 1 + 2 \sum_{m=1}^{\infty} J_0^N\left(\frac{m\pi}{N}\right) \times \right. \\
 &\quad \times \left. \cos\left(\frac{m\pi u}{N}\right) \right\} du \\
 &= \frac{1}{2N} \left\{ N - z + \frac{2N}{\pi} \sum_{m=1}^{\infty} m J_0^N\left(\frac{m\pi}{N}\right) \times \right. \\
 &\quad \times \left. \sin\left(\frac{m\pi z}{N}\right) \right\} \quad (261)
 \end{aligned}$$

for $-N \leq z \leq N$ and zero otherwise.

Figure 16 illustrates the form of $P_{Z_N}(z)$ for representative values of N .

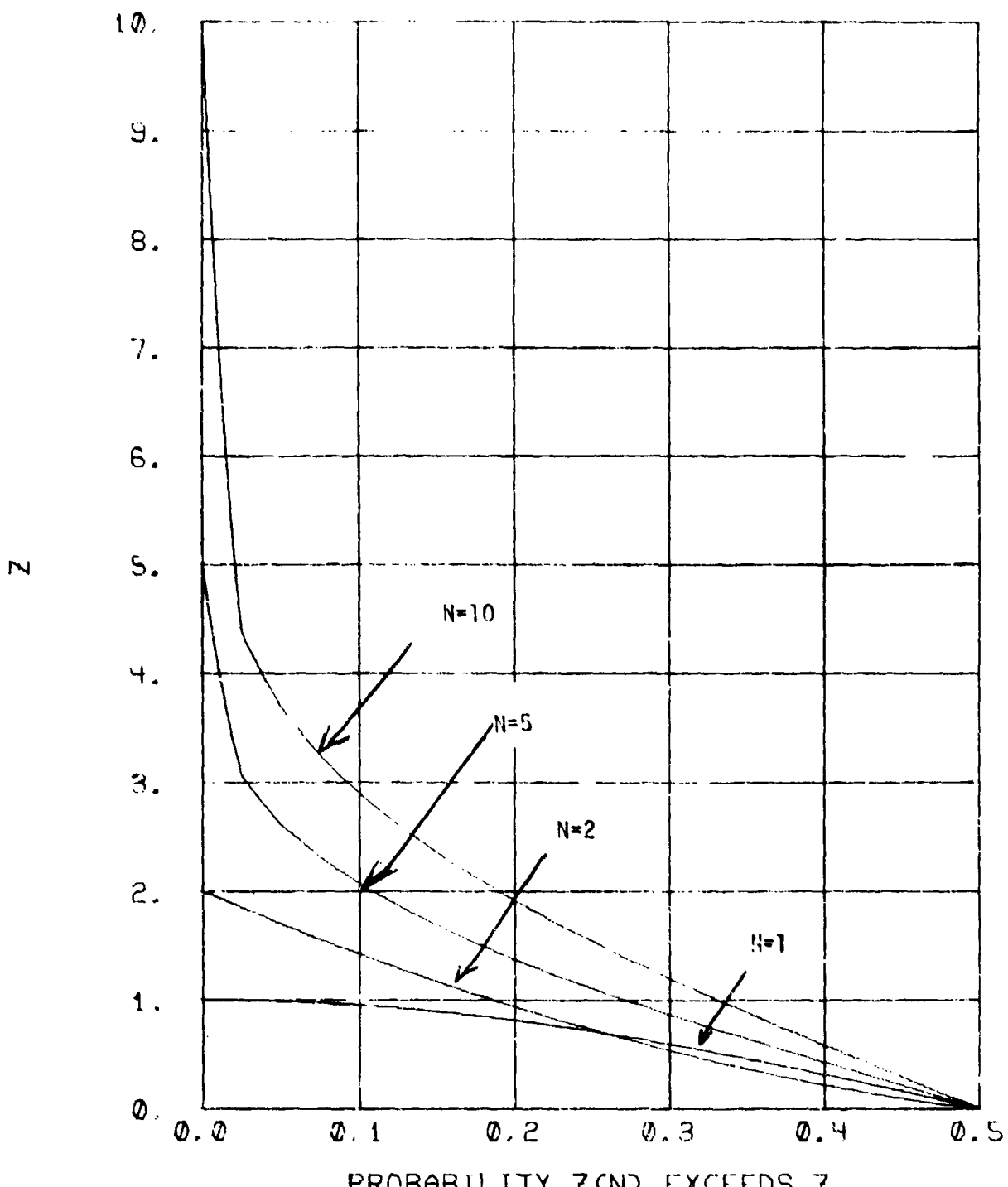


Figure 16. Complementary Probability Distributions for
 $\sum_{i=1}^N \cos \theta_i$; ($\Pr \sum \cos \theta_i \geq Z$)

5.2.2.3 Multiple Noise Pulses in the PSK Functional

Now, extending the analysis to a consideration of multiple noise pulses occurring during one detection element, the simplifying assumptions of non overlapping pulses (above the signal level), statistically independent phase angles, and a constant ratio, $r \leq 1$, monotonically relating the amplitudes of any two pulses most nearly equal in amplitude are used. This latter condition implies, that for a sequence of N noise pulses in $(0, T)$ having the maximum amplitude P , the total noise input consists of the set of pulses:

$$\left\{ P r^i e^{-b(t-t_i)}, i = 0, 1, \dots, N-1 \right\}.$$

The sequence of N noise pulses whose envelopes exceed the signal amplitude, S , produces a net limiter capture interval which is the sum of the capture intervals of the individual pulses. The duration of the i th capture interval, produced by the i th pulse, is given by (197) as

$$\Delta_i = \frac{1}{b}, L_n\left(\frac{P_i}{S}\right) = \frac{1}{b}, L_n\left(\frac{P r^i}{S}\right). \quad (262)$$

In turn, the average contribution of this capture interval to the total post detection noise, N_{p1} , is given by (188) with Δ_i replacing $(t_2 - t_1)$,

$$N_{Pi} = \frac{LS_1}{T} \Delta_i \cos \theta_i, \quad i=0, 1, \dots, N-1. \quad (263)$$

Hence, the total post detection noise component, N_{PIN} is given by

$$N_{PIN} = \sum_{i=0}^{N-1} N_{Pi} = \frac{LS_1}{T} \sum_{i=0}^{N-1} \Delta_i \cos \theta_i. \quad (264)$$

On the other hand, substitution of the total capture interval, for $(t_2 - t_1)$ in (190) yields the post-detection signal component

$$S_{PIN} = \begin{cases} -\frac{LS_1}{T} \left[T - \sum_{i=0}^{N-1} \Delta_i \right], & \sum \Delta_i \leq T \\ 0, & \sum \Delta_i > T \end{cases}. \quad (265)$$

Consequently, under the same hypothesis as 5.2.1.1, the PSK detector functional, $R_{d/N}$, conditioned on N noise pulses, is given by

$$R_{d/N} = S_{PIN} + N_{PIN}$$

$$= \begin{cases} \left[-\frac{LS_1}{T} \left(T - \sum_{i=0}^{N-1} \Delta_i \right) \right. \\ \left. + \frac{LS_1}{T} \sum_{i=0}^{N-1} \Delta_i \cos \theta_i \right], & \sum \Delta_i \leq T \\ \frac{LS_1}{T} \sum_{i=0}^{N-1} \Delta_i \cos \theta_i, & \sum \Delta_i > T \end{cases}. \quad (266)$$

It should be noted that R_d/N , as given by (266), is a function of the random variables P (or, equivalently, E), r , θ_i ($i = 0, 1, \dots, N-1$), and N . Hence, the present analysis, which is based on the random variable R_d/N , does consider its random constituents. For given values of the random variable r and N , a decision error occurs whenever $R_d/N > 0$. Thus, the probability of error, conditioned on r and N , is given by

$$\begin{aligned} P_{\text{ep}}|N, r &= \Pr[R_d/N > 0] \\ &= \Pr\left[-\frac{LS_1}{T}\left(T - \sum_{i=0}^{N-1} \Delta_i\right) + \frac{LS_1}{T} \sum_{i=0}^{N-1} \Delta_i \cos \theta_i > 0, \right. \\ &\quad \left. \sum \Delta_i \leq T\right] \\ &\quad + \Pr\left[\frac{LS_1}{T} \sum_{i=0}^{N-1} \Delta_i \cos \theta_i > 0, \sum \Delta_i > T\right] \end{aligned}$$

or

$$\begin{aligned} P_{\text{ep}}|N, r &= \Pr\left[\sum_{i=0}^{N-1} \Delta_i \cos \theta_i > T - \sum_{i=0}^{N-1} \Delta_i, \sum \Delta_i \leq T\right] \\ &\quad + \Pr\left[\sum_{i=0}^{N-1} \Delta_i \cos \theta_i > 0 \mid \sum \Delta_i > T\right] \times \\ &\quad \times \Pr\left[\sum \Delta_i > T\right]. \quad (266a) \end{aligned}$$

In 5.2.2.2, the probability density of the sum of equally weighted sinusoids whose phase angles are statistically independent and uniformly distributed on $(-\pi, \pi)$ is derived. In particular, it is shown (260) that this probability density is an even function. Moreover, Bennett [7], in his more general treatment of the subject, shows that the density function for arbitrarily weighted sinusoids, whose phase angles are also uniformly distributed on $(-\pi, \pi)$ and statistically independent, is an even function ([7], (25)). Hence, the probability density of the random variable $Y (\triangleq \sum \Delta_i \cos \theta_i > 0)$ is an even function of Y . Consequently,

$$\Pr[Y = \sum \Delta_i \cos \theta_i > 0] = \frac{1}{2}. \quad (267)$$

Using this result and (262) in (266a) leads to

$$\begin{aligned} P_{\text{per}, N, r} &= \Pr \left[\frac{1}{b}, \sum_{i=0}^{N-1} L_n \left(\frac{\Pr^i}{S} \right) \cos \theta_i > T - \frac{1}{b}, \sum_{i=0}^{N-1} L_n \left(\frac{\Pr^i}{S} \right), \sum \Delta_i \leq T \right] \\ &\quad + \frac{1}{2} \Pr \left[\frac{1}{b}, \sum_{i=0}^{N-1} L_n \left(\frac{\Pr^i}{S} \right) > T \right]. \end{aligned} \quad (270)$$

In order to express this result in terms of the observed (post-detection) noise envelope, E , it is convenient to first determine the contribution of the i th observed noise pulse voltage, E_i , to the overall envelope voltage. From (198) when $b, T \gg 1$

$$E_i \approx \frac{P_i}{b, T} = \frac{Pr^i}{b, T}, \quad i = 0, 1, \dots, N-1. \quad (271)$$

Since the noise process for a bit interval, T , consists of the set of N pulses whose amplitudes are $\{Pr^i, i=0, 1, \dots, N-1\}$, the observed noise voltage for the interval is given by

$$E = \sum_{i=0}^{N-1} E_i = \frac{P}{b, T} \sum_{i=0}^{N-1} r^i. \quad (272)$$

Thus,

$$P \approx \frac{b, T E}{\sum r^i}. \quad (273)$$

Substituting this result in (270) yields

$$\begin{aligned}
 P_{\text{epin}} &= \Pr \left[\frac{1}{b, T} \sum_{i=0}^{N-1} L_n \left(\frac{b, T E r^i}{S \sum_{j=0}^{N-1} r^j} \right) \cos \theta_i > \right. \\
 &\quad \left. T - \frac{1}{b, T} \sum_{i=0}^{N-1} L_n \left(\frac{b, T E r^i}{S \sum_{j=0}^{N-1} r^j} \right), \sum \Delta_i \leq T \right] \\
 &\quad + \frac{1}{2} \Pr \left[\frac{1}{b, T} \sum_{i=0}^{N-1} L_n \left(\frac{b, T E r^i}{S \sum_{j=0}^{N-1} r^j} \right) > T \right] \\
 &= \Pr \left[\frac{1}{b, T} L_n \left(\frac{b, T E}{S \sum_{j=0}^{N-1} r^j} \right) \sum_{i=0}^{N-1} \cos \theta_i > \right. \\
 &\quad \left. 1 - \frac{1}{b, T} L_n r \sum_{i=0}^{N-1} i (1 + \cos \theta_i) \right. \\
 &\quad \left. - \frac{N}{b, T} L_n \left(\frac{b, T E}{S \sum_{j=0}^{N-1} r^j} \right), \sum \Delta_i \leq T \right] \\
 &\quad + \frac{1}{2} \Pr \left[\frac{N}{b, T} L_n \left(\frac{b, T E}{S \sum_{j=0}^{N-1} r^j} \right) + \frac{N(N-1)}{2 b, T} L_n r > T \right].
 \end{aligned} \tag{274}$$

At this point, it is necessary to consider the term $\sum_{i=0}^{N-1} i \cos \theta_i$ more closely. Clearly, this term and $\sum_{i=0}^{N-1} \cos \theta_i \triangleq \mathfrak{Z}_N$ are not statistically independent. Therefore, it is proposed to approximate $\sum_{i=0}^{N-1} i \cos \theta_i$ by its expected value, conditioned on \mathfrak{z}_N . First, consider

$$\begin{aligned}\mathfrak{z}_N &= E\left\{\mathfrak{z}_N | \mathfrak{z}_N\right\} = E\left\{\sum_{i=0}^{N-1} i \cos \theta_i | \mathfrak{z}_N\right\} \\ &= \sum_{i=0}^{N-1} E\left\{\cos \theta_i | \mathfrak{z}_N\right\} \\ &= N E\left\{\cos \theta_i | \mathfrak{z}_N\right\}. \quad (274a)\end{aligned}$$

Hence,

$$E\left\{\cos \theta_i | \mathfrak{z}_N\right\} = \frac{1}{N} \mathfrak{z}_N. \quad (274b)$$

Therefore,

$$\begin{aligned}\sum_{i=0}^{N-1} i \cos \theta_i &\approx E\left\{\sum_{i=0}^{N-1} i \cos \theta_i | \mathfrak{z}_N\right\} = \sum_{i=0}^{N-1} i E\left\{\cos \theta_i | \mathfrak{z}_N\right\} \\ &= \frac{N-1}{2} \mathfrak{z}_N. \quad (274c)\end{aligned}$$

With this approximation (274) becomes

$$\begin{aligned}
 P_{EP|N,r} = & \Pr \left\{ \frac{1}{b,T} \left[L_n \frac{b,TE}{U,S} + \frac{N-1}{2} U_2 \right]_{z_N} > \right. \\
 & \quad \left. 1 - \frac{N(N-1)U_2}{2b,T} \right. \\
 & \quad \left. - \frac{N}{b,T} L_n \left(\frac{b,TE}{U,S} \right), \right. \\
 & \quad \left. \sum \Delta_i \leq T \right\} \\
 & + \frac{1}{2} \Pr \left\{ \frac{N}{b,T} L_n \left(\frac{b,TE}{U,S} \right) + \frac{N(N-1)}{2b,T} U_2 > 1 \right\},
 \end{aligned} \tag{275}$$

where

$$U_1 = \sum_{j=0}^{N-1} r^j, \tag{276a}$$

$$U_2 = L_n r, \tag{276b}$$

and z_N is given by (253a).

Also,

$$\begin{aligned} P_{ep|N,r} &= \Pr \left\{ \exists_N > \frac{b,T - \left[\frac{N(N-1)}{2} U_2 + N L_n \left(\frac{b,T E}{U,S} \right) \right]}{L_n \left(\frac{b,T E}{U,S} \right) + \frac{N-1}{2} U_2}, \right. \\ &\quad \left. \sum \Delta_i \leq T \right\} \\ &+ \frac{1}{2} \Pr \left\{ \frac{N}{b,T} L_n \left(\frac{b,T E}{U,S} \right) + \frac{N(N-1)}{2 b,T} U_2 > 1 \right\} \\ &= \int_{E_1}^{E_2} f_e(E) dE \int_{z=0}^{\infty} f_{\exists_N}(z) dz \\ &\quad z = \left[\frac{b,T - U_2 \frac{N(N-1)}{2} - N L_n \left(\frac{b,T E}{U,S} \right)}{L_n \left(\frac{b,T E}{U,S} \right) + \frac{N-1}{2} U_2} \right] \\ &+ \frac{1}{2} \int_{E_2}^{\infty} f_e(E) dE, \end{aligned}$$

or

$$P_{ePN,r} = \int_{E_1}^{\infty} f_e(E) dE g(\underline{u}), \quad (276a)$$

where

$$\begin{aligned} g(\underline{u}) &= g(u_1, u_2) \\ &= P_{zN} \left\{ \frac{b_1 T - U_2 \frac{N(N-1)}{2} - N \ln \left(\frac{b_1 T E}{u_1 s} \right)}{\ln \left(\frac{b_1 T E}{u_1 s} \right) + \frac{N-1}{2} U_2} \right\} x \\ &\times [U(E - E_1) - U(E - E_2)] \\ &+ \frac{1}{2} U(E - E_2) \end{aligned} \quad (277)$$

and $P_{zN} [\cdot]$ is given by (261), E_1 is the least value of E such that an error can occur ($\sum \Delta_i = T/2$), and E_2 is the value of E such that $\sum \Delta_i = T$, and the first term has the value 1/2.

These limits of integration are based on two distinct considerations. From (277), the argument of $P_{zN} [\cdot]$ increases as E decreases. However, the definition of z_N , (253a), constrains $z_N \leq N$ and thus, $P_{zN} [z]$ is non zero for $z < N$. This maximum value, N , of the argument of P_{zN} corresponds to the minimum value of E , E_1 .

Hence,

$$\frac{\frac{b_1 T - U_2}{2} \frac{N(N-1)}{2} - N \ln\left(\frac{b_1 T E}{U_1 S}\right)}{\ln\left(\frac{b_1 T E}{U_1 S}\right) + \frac{N-1}{2} U_2} = N,$$

or

$$E_1 = \frac{U_1 S}{b_1 T} \exp\left[\frac{b_1 T}{2N} - \frac{(N-1)}{2} U_2\right]. \quad (278)$$

Since

$$P_{3N} [\cdot] \Big|_{E=E_1} = P_{3N} [N] = 0, \quad (278a)$$

$$g(U) \Big|_{E=E_1} = 0. \quad (278b)$$

Also, $g(U)$ increases monotonically with E up to a maximum of $1/2$ (where the detector voltage results from noise alone and $\sum \Delta_i = T$).

Consequently, at $E = E_2$ (where $\sum \Delta_i = T$),

$$P_{3N} \left[\frac{\frac{b_1 T - U_2 N(N-1)}{2} - N \ln\left(\frac{b_1 T E}{U_1 S}\right)}{\ln\left(\frac{b_1 T E}{U_1 S}\right) + \frac{N-1}{2} U_2} \right] = \frac{1}{2}, \quad (279)$$

or

$$\frac{b_1 T - u_2 \frac{N(N-1)}{2} - N \ln\left(\frac{b_1 T E}{u_1 s}\right)}{\ln\left(\frac{b_1 T E}{u_1 s}\right) + \frac{N-1}{2} u_2} = 0,$$

or

$$E_2 = \frac{u_1 s}{b_1 T} \exp\left[\frac{b_1 T}{N} - \frac{(N-1)}{2} u_2\right]. \quad (280)$$

Rewriting the unit step functions of (277) in integral form (232)
results in

$$\begin{aligned} g(u) &= \frac{1}{\pi} \int_0^\infty \left\{ P_{3N} \left[b_1 T - u_2 \frac{N(N-1)}{2} \right. \right. \\ &\quad \left. \left. - N \ln\left(\frac{b_1 T E}{u_1 s}\right) \right] \right. \\ &\quad \left. \left. \frac{1}{\ln\left(\frac{b_1 T E}{u_1 s}\right) + \frac{N-1}{2} u_2} \right\} \times \right. \\ &\quad \times \left[\sin \pi(E - E_1)v - \sin \pi(E - E_2)v \right] \quad (281) \\ &\quad + \frac{1}{2} \left[\sin \pi(E - E_2)v + \sin \pi(E - E_1)v \right] \frac{dv}{v}. \end{aligned}$$

Since the integrand of the first term is an analytic function of U_1 and U_2 for $E_1 \leq E \leq E_2$, it may be expanded in a bivariate Taylor series about \hat{U}_1 and \hat{U}_2 where

$$\hat{U}_i \triangleq \langle U_i \rangle_r . \quad (282)$$

Likewise, the integrand of the second term can be expanded in a Taylor series about $E_2 = \hat{E}_2$ where

$$\hat{E}_2 = \langle E_2 \rangle_r . \quad (282a)$$

Recall that the average probability of error, conditioned on N alone, is given by

$$\begin{aligned} P_{eP|N} &= \langle P_{eP|N,r} \rangle_r \\ &= \left\langle \int_{E_1}^{\infty} g(\underline{U}) f_e(E) dE \right\rangle_r \\ &= \int_{E_1}^{\infty} f_e(E) dE \langle g(\underline{U}) \rangle_r . \end{aligned} \quad (283)$$

Thus, if the integrands of $g(\underline{U})$ in (281) are approximated by the constant plus linear terms of the indicated Taylor series expansions, (283) becomes

$$P_{EPIN} = \int_{E_1}^{\infty} f_e(E) dE \cdot \frac{1}{\pi} \int_{-\infty}^{\infty} \left\{ P_{3N} \left[\frac{b_1 T - \hat{U}_2 \frac{N(N-1)}{2} - NL_n \left(\frac{b_1 TE}{\hat{U}_2 S} \right)}{L_n \left(\frac{b_1 TE}{\hat{U}_2 S} \right) + \frac{N-1}{2} \hat{U}_2} \right] \times \right. \right. \\ \times \left[\sin \pi(E - \hat{E}_1) v - \sin \pi(E - \hat{E}_2) v \right] \\ \left. \left. + \left[\sin \pi(E - \hat{E}_2) v + \sin \pi \bar{v} \right] \right\} \frac{dv}{v}. \right. \quad (284)$$

(Note that the averaging indicated by (283) reduces the linear terms of the Taylor series to zero.)

This result can also be rewritten as

$$P_{EPIN} = \int_{\hat{E}_1}^{\hat{E}_2} P_{3N} \left[\frac{b_1 T - \hat{U}_2 \frac{N(N-1)}{2} - NL_n \left(\frac{b_1 TE}{\hat{U}_2 S} \right)}{L_n \left(\frac{b_1 TE}{\hat{U}_2 S} \right) + \frac{N-1}{2} \hat{U}_2} \right] \times \\ \times f_e(E) dE \quad (285) \\ + \frac{1}{2} \int_{\hat{E}_2}^{\infty} f_e(E) dE.$$

The statistics of the random variable r and the functions $L_n r$ and r^i are derived in Appendix B. There the mean value of $L_n r$ ($\approx U_2$) is derived and is given by

$$\hat{U}_2 \triangleq \overline{\ln r} = -X \ln 2, \quad (B12)$$

where X is the ratio of the slope of the impulsive noise component (Power Rayleigh) APD to the slope of the near-Gaussian noise component (Rayleigh) APD.

However, the moments $\overline{r^j}$ are only defined in terms of definite integrals or infinite series expansions. Hence, the averaging process is only indicated here as

$$\hat{U}_1 \triangleq \sum_{j=0}^{N-1} \frac{1}{r^j}, \quad (286)$$

but \hat{U}_1 is retained to simplify the ensuing mathematical expressions.

Substituting (B12) in (278) and (280) results in

$$\hat{E}_1 = \frac{\hat{U}_1 S}{b_1 T} \exp\left[\left(b_1 T + N(N-1)X \ln 2\right)/2N\right] \quad (287)$$

and

$$\hat{E}_2 = \frac{\hat{U}_1 S}{b_1 T} \exp\left[\left(b_1 T + .5N(N-1)X \ln 2\right)/N\right]. \quad (288)$$

Substituting (B12) and (286) in (285) yields

$$P_{ePN} = \int_{\hat{E}_1}^{\hat{E}_2} P_{3N} \left[\frac{b_1 T + .5 N(N-1) X L_n - N L_n (b_1 T E_i / \hat{U}_s)}{-.5(N-1) X L_n 2 + L_n (b_1 T E_i / \hat{U}_s)} \right] \times \\ \times f_e(E) dE \\ + \frac{1}{2} \int_{\hat{E}_2}^{\infty} f_e(E) dE. \quad (289)$$

This result is of the same form as (206) for the single noise pulse case, except that $P_{2N}[\cdot]$ replaces $\frac{1}{\pi} \cos^{-1}[\cdot]$ for $N > 1$. (Note that $P_{2N}[\cdot] \equiv \frac{1}{\pi} \cos^{-1}[\cdot]$ and that (206) is the particular case of (289) where $N = 1$.)

Again, the numerical procedure of 4.1.1 is applied to evaluate (289). The M-fold partition of the first integral defines upper and lower limits, E_i^U and E_i^L , respectively, of the ith integral which must satisfy

$$P_{3N} \left[\frac{b_1 T + .5 N(N-1) X L_n 2 - N L_n (b_1 T E_i^U / \hat{U}_s)}{-.5(N-1) X L_n 2 + L_n (b_1 T E_i^U / \hat{U}_s)} \right] = \frac{i-1}{2M}, \quad (290a)$$

and

$$P_{3N} \left[\frac{b_1 T + .5 N(N-1) X L_n 2 - N L_n (b_1 T E_i^L / \hat{U}_s)}{-.5(N-1) X L_n 2 + L_n (b_1 T E_i^L / \hat{U}_s)} \right] = \frac{i}{2M}. \quad (290b)$$

These relationships yield

$$E_i^u = \frac{\hat{u}, s}{b, T} \exp \left\{ \frac{b, T + .5(N + P_{3N}^{-1} \left[\frac{i-1}{2M} \right]) (N-1) X L_n 2}{N + P_{3N}^{-1} \left[\frac{i-1}{2M} \right]} \right\} \quad (291a)$$

and

$$E_i^L = \frac{\hat{u}, s}{b, T} \exp \left\{ \frac{b, T + .5(N + P_{3N}^{-1} \left[\frac{i}{2M} \right]) (N-1) X L_n 2}{N + P_{3N}^{-1} \left[\frac{i}{2M} \right]} \right\} \quad (291b)$$

Finally, utilizing (291b) in place of (208b) in (210),

$$P_{CP/N} = \frac{1}{2} P \left\{ \frac{\hat{u}, s}{b, T} \exp \left[(b, T + .5N(N-1) X L_n 2) / N \right] \right\}$$

$$+ \frac{1}{4M} \left(P \left\{ \frac{\hat{u}, s}{b, T} \exp \left[(b, T + .5N(N-1) X L_n 2) / N \right] \right\} \right)$$

$$+ P \left\{ \frac{\hat{u}, s}{b, T} \exp \left[(b, T + N(N-1) X L_n 2) / 2N \right] \right\} \quad (292)$$

$$+ \frac{1}{2M} \sum_{i=1}^{M-1} P \left\{ \frac{\hat{u}, s}{b, T} \exp \left[\frac{b, T + .5(N + P_{3N}^{-1} \left[\frac{i}{2M} \right]) \cdot (N-1) X L_n 2}{N + P_{3N}^{-1} \left[\frac{i}{2M} \right]} \right] \right\}$$

5.2.2.4 Multiple Noise Pulses in the CFSK Functional

In order to analyze CFSK detector performance with multiple noise pulses per bit, it is convenient to begin with one of the final results of the earlier single-pulse analysis. Specifically, the probability of a CFSK error was given by

$$P_{ec} = \frac{1}{T} \int_{E_1}^{E_2} \cos^{-1} \left[\frac{T-\Delta}{(4/\pi)\Delta} \right] f_e(E) dE + \frac{1}{2} \int_{E_2}^{\infty} f_e(E) dE, \quad (243d)$$

or

$$P_{ec} = \int_0^{\infty} P_{c11}(E) f_e(E) dE, \quad (293)$$

where $g_{c11}(E)$, the conditional error probability, given E , and one noise pulse per bit, is defined by

$$P_{c11}(E) = \begin{cases} \frac{1}{\pi} \cos^{-1} \left[\frac{T-\Delta}{(4/\pi)\Delta} \right], & E_1 \leq E \leq E_2 \\ \frac{1}{2}, & E_2 < E. \end{cases} \quad (293a)$$

However, $g_{c11}(E)$ can also be expressed as

$$P_{c11}(E) = \begin{cases} \frac{1}{\pi} \int_0^{\cos^{-1} \left[\frac{T-\Delta}{(4/\pi)\Delta} \right]} d\theta, & E_1 \leq E \leq E_2 \\ \frac{1}{2}, & E_2 < E \end{cases}$$

or

$$g_{c11}(E) = Pr\left[|\theta| < \cos^{-1}\left[\frac{T-\Delta}{(4/\pi)\Delta}\right], E_1 \leq E \leq E_2\right]$$

$$+ \frac{1}{2} Pr\left[E_2 < E\right],$$

or

$$g_{c11}(E) = Pr\left[\cos\theta > \frac{T-\Delta}{(4/\pi)\Delta}, \Delta \leq T\right]$$

$$+ Pr\left[\cos\theta > 0, \Delta > T\right],$$

or

$$g_{c11}(E) = Pr\left[(4/\pi)\Delta \cos\theta > T-\Delta, \Delta \leq T\right] \quad (294)$$

$$+ Pr\left[(4T/\pi)\cos\theta > 0, \Delta > T\right].$$

With this latter formulation of g_{c11} , an expression for the multiple noise pulse case, $g_{c/n}$, can be obtained directly by replacing Δ with $\sum \Delta_i$ and $\Delta \cos\theta$ with $\sum \Delta_i \cos\theta_i$. This yields

$$P_{c|N,r}(E) = Pr \left[\frac{4}{\pi} \sum_{i=0}^{N-1} \Delta_i \cos \theta_i > T - \sum_{i=0}^{N-1} \Delta_i, \sum \Delta_i \leq T \right] \\ + Pr \left[\left(\frac{4T}{\pi} \right) \sum_{i=0}^{N-1} \cos \theta_i > 0, \sum \Delta_i > T \right], \quad (295)$$

where $P_{c|N,r}(E)$ is the conditional probability of CFSK error, given E , r , and N . Utilizing (262) and (273), this becomes

$$P_{c|N,r}(E) = \begin{cases} Pr \left[\frac{4}{\pi b, T} L_n \left(\frac{b, TE}{S \sum_{j=0}^{N-1} r_j} \right) \sum_{i=0}^{N-1} \cos \theta_i > 1 - \frac{1}{b, T} L_n \left(\sum_{i=0}^{N-1} i \left(1 + \frac{4}{\pi} \cos \theta_i \right) \right) - \frac{N}{b, T} L_n \left(\frac{b, TE}{S \sum_{j=0}^{N-1} r_j} \right) \right], \sum \Delta_i \leq T \quad (295a) \\ \frac{1}{2}, \left[\frac{N}{b, T} L_n \left(\frac{b, TE}{S \sum_{j=0}^{N-1} r_j} \right) + \frac{N(N-1)}{2b, T} L_n \right] > T \end{cases}$$

Application of (274c) results in

$$P_{c|N,r}(E) = \begin{cases} Pr \left\{ \frac{4}{\pi b, T} \left[L_n \left(\frac{b, TE}{U, S} \right) + \frac{N-1}{2} U_2 \right] 3_N > 1 - \frac{N(N-1)}{2b, T} U_2 - \frac{N}{b, T} L_n \left(\frac{b, TE}{U, S} \right) \right\}, \sum \Delta_i \leq T \quad (296) \\ \frac{1}{2}, \left[\frac{N}{b, T} L_n \left(\frac{b, TE}{U, S} \right) + \frac{N(N-1)}{2b, T} L_n \right] > T \end{cases}$$

where U_1 and U_2 are given by (276a) and (276b), respectively, and z_N by (253a). This result can be rewritten as

$$P_{c/N, r}(E) = \begin{cases} \Pr \left\{ z_N > b, T - \frac{N(N-1)}{2} U_2 - N \ln \left(\frac{b, TE}{U, S} \right) \right. \\ \quad \left. - (4/\pi) \left[\ln \left(\frac{b, TE}{U, S} \right) + \frac{(N-1)}{2} U_2 \right] \right\}, \\ \sum \Delta_i \leq T \\ \frac{1}{2}, \quad \sum \Delta_i = \\ \left[\frac{N}{b,} \ln \left(\frac{b, TE}{U, S} \right) + \frac{N(N-1)}{2b,} \right] > T, \end{cases} \quad (297)$$

or

$$P_{c/N, r} = P_{z_N} \left\{ b, T - \frac{N(N-1)}{2} U_2 - N \ln \left(\frac{b, TE}{U, S} \right) \right. \\ \quad \left. - (4/\pi) \left[\ln \left(\frac{b, TE}{U, S} \right) + \frac{(N-1)}{2} U_2 \right] \right\} \\ \times \left[U(E - E_1) - U(E - E_2) \right] \\ + \frac{1}{2} U(E - E_2), \quad (298)$$

where E_1 is the root of $P_{zn}[\cdot] = 0$ and E_2 is the root of $P_{zn}[\cdot] = 1/2$ and corresponds to $\sum \Delta_i = T$. At this point, it is expedient to note the similarity of (298) and the corresponding PSK expression (277). The only difference between \mathcal{E} (\mathbb{U}) from (277) and $P_{c/N,r}$ from (298) is that the argument of $P_{zn}[\cdot]$ in $P_{c/N,r}$ (298) is multiplied by $\pi/4$. Because of this similarity, it is possible to simply modify the final results of the PSK analysis to account for the $\pi/4$ multiplier in the argument of $P_{zn}[\cdot]$. Therefore, the CFSK error probability, conditioned on N noise pulses, is obtained by suitably modifying (289) to yield (202)

$$P_{ec|N} = \int_{\hat{E}_1}^{\hat{E}_2} P_{3N} \left[\frac{b_1 T + .5N(N-1) \times L_n 2 - NL_n \left(\frac{b_1 T E}{\alpha_s} \right)}{(4/\pi) \left[-.5(N-1) \times L_n 2 + L_n \left(\frac{b_1 T E}{\alpha_s} \right) \right]} \right] \times$$

$$\times f_c(E) dE \quad (299)$$

$$+ \frac{1}{2} \int_{\hat{E}_2}^{\infty} f_c(E) dE ,$$

where \hat{E}_1 is given by (286) and \hat{E}_2 by (288).

On the other hand, the lower limit of the first integral, E_1 , must satisfy

$$P_{3N} \left\{ \frac{b_1 T + .5N(N-1) \times L_n 2 - NL_n \left(\frac{b_1 T \hat{E}_1}{\alpha_s} \right)}{(4/\pi) \left[-.5(N-1) \times L_n 2 + L_n \left(\frac{b_1 T \hat{E}_1}{\alpha_s} \right) \right]} \right\} = 0. \quad (300)$$

This leads to

$$\frac{b_1 T + .5 N(N-1) \times L_n 2 - N \ln \left(\frac{b_1 T \hat{E}_1}{Q_s} \right)}{(4/\pi) \left[-.5(N-1) \times L_n 2 + \ln \left(\frac{b_1 T \hat{E}_1}{Q_s} \right) \right]} = N$$

or

$$\hat{E}_1 = \frac{\hat{Q}_s}{b_1 T} \exp \left\{ \left[\pi b_1 T / (4 + \pi r) + .5 N(N-1) \times L_n 2 \right] / N \right\} \quad (301)$$

As in the PSK case of 5.2.2.3, the numerical integration procedure of 4.1.1 is applied to evaluate (299).

5.2.2.5 Multiple Noise Pulses in the MSK Functional

From the preceding analyses of MSK detection, it was determined that the MSK error probability expressions are of exactly the same form as the CFSK expressions. The only difference is that the element length, T , of the CFSK expression is replaced by $2T$ for the MSK expression, given the same data transmission rate for both systems. Therefore, the MSK error probability, P_{em}/N , for N noise pulses is readily obtained by substituting $2T$ for T in (288), (299), and (301). This substitution results in

$$P_{\text{err}/N} = \int_{\hat{E}_1}^{\hat{E}_2} P_{3N} \left\{ \frac{2b,T + .5N(N-1)XL_n 2 - NL_n \left(\frac{2b,T E}{Q,S} \right)}{(4/\pi) [-.5(N-1)XL_n 2 + L_n \left(\frac{2b,T E}{Q,S} \right)]} \times f_e(E) dE \right. \\ \left. + \frac{1}{2} \int_{\hat{E}_2}^{\infty} f_e(E) dE \right\} \quad (302)$$

where

$$\hat{E}_1 = \frac{\hat{Q},S}{2b,T} \exp \left\{ \left[2\pi b,T / (4 + \pi) + .5N(N-1)XL_n 2 \right] / N \right\} \quad (303)$$

and

$$\hat{E}_2 = \frac{\hat{Q},S}{2b,T} \exp \left\{ (2b,T + .5N(N-1)XL_n 2) / N \right\}. \quad (304)$$

The first integral of (302) can also be evaluated by the numerical procedure of 4.1.1.

5.2.3 Evaluation of the Probability of Decision Error

The preceding results have given decision error probabilities as a function of signal-to-noise ratio conditioned on the number of noise pulses, N , per decision element. The total error probability, P_e , is clearly given by

$$P_e = \sum_{N=1}^{\infty} P_{e|N} P_r(N) \quad (305)$$

where $P_{e|N}$ is the probability of decision error given N noise pulses in a decision element, and $P_r(N)$ is the probability of N pulses. As an initial estimate, the times of occurrence of the noise pulses are assumed to be statistically independent. In this case, the probability of N noise pulses occurring in a time period T will have the Poisson distribution

$$P_r(N) = \frac{(\alpha T)^N}{N!} e^{-\alpha T}, \quad (42)$$

where α is the average pulse arrival rate in pulses/second.

Also, error rates are computed on the basis of a "clustered" noise pulse distribution which is more descriptive of the multiple noise pulses emanating from a single lightning discharge. Under this condition, the probability of N pulses occurring in a time period, T , is given by

$$P_r(N) = e^{-hT} \left[\frac{(hT)^{2N+1}}{(2N+1)!} + \frac{(hT)^{2N}}{(2N)!} \right] \quad (56)$$

where the average number of pulses, \bar{N} , in T seconds is given by

$$\bar{N} = hT/2 - 1/4 + 1/4 e^{-2hT}. \quad (61)$$

The following section describes a method for estimating $\propto T$ (under the assumption of statistically independent pulse occurrence times) or \bar{N} (under the assumption of "clustered" pulse occurrence times).

5.2.3.1 Determination of the Average Number of Impulsive Noise Pulses

Per Decision Element

In Figure 1, several Amplitude Probability Distributions of the envelope of atmospheric noise are shown. As previously noted, each of these curves consists of three regions: (1) The straight-line region, corresponding to the lowest amplitude levels (greatest probability of being exceeded) whose slope is $-1/2$; (2) The medial region, consisting of a circular arc; and (3) The impulsive high-amplitude region, which is a straight line whose slope is given by $-X/2$ [10]. It should be noted that the straight line labeled $V_d = 1.05$ dB, whose slope is $-1/2$, depicts the Complementary Distribution Function ($Pr[e \geq E]$) of the envelope of Gaussian Noise, a Rayleigh distribution. Although the present analysis is predicated on the higher amplitude impulsive noise being the preponderant cause of binary decision errors, a consideration of the principally Gaussian low-amplitude component of the noise is useful. Specifically, the characteristic of interest is the voltage-level crossing rate of the noise envelope.

5.2.3.2 Voltage-Level Crossing Rate of the Envelope of Gaussian Noise

In considering the Gaussian component of the overall atmospheric noise, it is appropriate to apply a result derived by Rice [44] giving the voltage-level crossing rate of the envelope of Gaussian noise.

Although the actual atmospheric noise may not be strictly Gaussian in

any amplitude range, the effect of large numbers of overlapping independent (in time of occurrence and in phase-relative to a coherent receiver reference signal) pulses is to produce a nearly Gaussian noise process in accordance with the central limit theorem. Thus, the use of Rice's expression for the level crossing rate (with positive slope) of the noise envelope is clearly accurate for sufficiently low noise amplitude levels. This expression for the voltage level crossing rate, α , is given by (4.10)

$$\alpha = \left[\frac{b_2}{2\pi b_0} \right]^{\frac{1}{2}} \nu e^{-\nu^2/2} \quad (306)$$

where α is the rate of positive-slope crossings per second, ν is the ratio of the crossing-voltage level to the RMS voltage,

$$b_2 = (2\pi)^2 \int_0^\infty W(f) (f - f_0)^2 df, \quad (307)$$

and

$$b_0 = \int_0^\infty W(f) df, \quad (308)$$

$W(f)$ is the one-sided power spectral density of the noise, f is frequency, and f_0 is the center frequency.

It should be noted that the average number of noise pulses above a given level in T seconds is simply the product of the average crossing rate and time, αT . This parameter can be employed directly

in (42) for the Poisson distribution; also it can be substituted for N in (61) to derive the parameter hT in order to employ (56) for the "clustering" pulse distribution.

5.2.3.3 Relationship Between Rayleigh and Power-Rayleigh Crossing Rates

Now proceeding from the amplitude range where the atmospheric noise is nearly Gaussian, a necessary condition is postulated for the pulse rate statistics where the amplitude probability distribution transitions from a Rayleigh envelope to the curved region and subsequent Power-Rayleigh (straight line of $-X/2$ slope) envelope. The condition is that the pulse rate (number of noise pulses exceeding a voltage threshold per second) should be a continuous function of the threshold voltage level. In particular, the average noise pulse rate should be continuous at the point where the APD curve begins its circular-arc region above the low-amplitude Rayleigh straight line. This point, U_1 , is, of course, the point of tangency between the circular and Rayleigh portions of the APD curve.

Using (306) to find α corresponding to the U_1 voltage level, a point of reference is established for determining envelope crossing (noise pulse) rates for other, higher voltage thresholds. Since the crossing rate will be shown to decrease at higher voltage levels, this value of α will consequently be an upper bound on the average pulse rate for voltage thresholds at or about U_1 . Moreover, this result provides a useful starting point for determining a functional relationship between the impulsive noise pulse rate, α , and the voltage threshold, V .

Turning to statistical data on voltage-level crossing rates compiled in the literature [51], [24], [25], [31] for VLF/LF atmospheric noise, it has been determined that the level crossing rate, α , is of the form

$$\alpha = (AV)^{-K} \quad (309)$$

where A is a proportionality factor and $.85 \leq K \leq 3.0$. To illustrate this characteristic, Figure 17 (by Watt and Maxwell [51]) shows $K \approx 1.16$ for atmospheric noise at 22 kHz. The data of Horner and Harwood [24] indicates $1 \leq K \leq 2$ for narrowband VLF atmospheric noise at frequencies in the 10-35 kHz range (an illustrative curve gives $K \approx 1.03$). Linfield's [31] 10 kHz wideband (6 kHz) noise data shows $.85 \leq K \leq 3.0$. On the other hand, Ibukun's [25] LF (113 kHz) noise data indicates $1.75 \leq K \leq 3.0$ for tropical (Ibadan, Nigeria) atmospheric noise at higher frequencies. It should be noted that higher values of K imply a smaller rate of high-amplitude noise pulses (and, hence, lower impulsive noise power) which is typical of higher frequencies. Conversely, the lower values of K imply a greater rate of high-amplitude pulses (and, hence, higher impulsive noise power) which is more typical of VLF noise. Consistent with this observation, it is shown that error rate curves computed in this chapter for $.85 \leq K \leq 1.5$ correspond most closely to experimentally measured VLF error rate data.

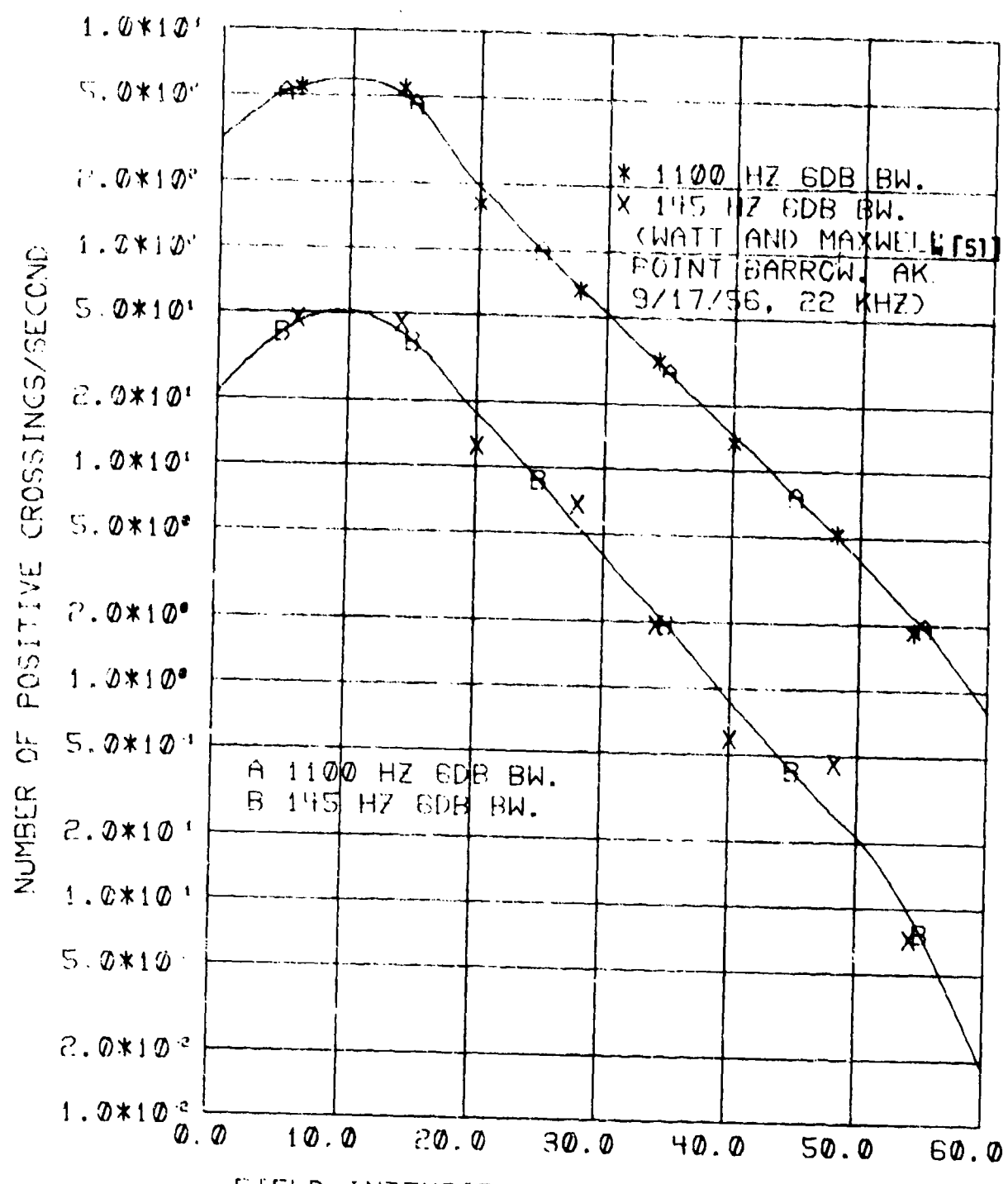


Figure 17. Level Crossing Rate of Atmospheric Noise Envelopes

Returning to the level crossing rate α_r , computed by (306) for $V = \frac{U_1}{U_r}$ (where U_1 is the voltage on the APD curve which corresponds to the intersection (tangency) of the straight-line Rayleigh curve and the circular-arc portion), it is postulated that α_r also satisfies

$$\alpha_r = (AU_1)^{-K} \quad (310)$$

Moreover,

$$\alpha(V) = (AV)^{-K} \quad (311)$$

for $V \geq U_1$.

This immediately yields

$$\alpha(V) = \alpha_r \left(\frac{V}{U_1}\right)^{-K}, \quad V \geq U_1. \quad (312)$$

Moreover, $K > 0$ insures that

$$\alpha(V) \leq \alpha_r, \quad V \geq U_1. \quad (313)$$

Although the accuracy of (312) is likely to decrease rapidly for $V < U_1$, the range $V \geq U_1$ is of the most practical interest for communication system performance where low error rates are necessary.

With these relationships, it is now possible to compute decision error rates for the three coherent systems PSK, CFSK, MSK. Specifically, the procedure is as follows: (1) the reference pulse occurrence rate, α_r , is determined by (306) for a noise envelope threshold at the intersection of the Rayleigh and curved portions of

the noise APD; (2) the pulse occurrence rate, α , for the required voltage level (signal to noise voltage ratio in the hard-limiter input bandwidth) is computed by (312); (3) αT is employed directly in (42) for independent pulses or substituted for N in (61) and the root (hT) employed in (56) for clustered pulses; and (4) either (42) or (56) is employed in (305) to obtain the desired average error probability.

5.3 Evaluation of Experimental Systems

In order to obtain a quantitative appreciation of the foregoing analysis, it is desirable to illustrate the methods used in evaluating a practical system. In this case, the use of the same system parameters permits a direct comparison of measured and computed results.

5.3.1 Character Error Rates

As in the case of the linear CFSK and MSK systems of Chapter 4, the experimental data is in terms of teletype character error rates. In the performance discussion of the linear CFSK system of Chapter 4, the relationship between decision (or bit) error rate and teletype character error rate, CER, was derived. This relationship is given by

$$CER = 1 - (1 - P_{ec})^5, \quad (179)$$

where P_{ec} is the probability of a CFSK decision error.

This expression is also applicable for the experimental CFSK (hard-limiting receiver) system described in this section. On the other hand, it is not applicable to the experimental Compatible Shift Keying (CSK) (MSK detection, but differential demodulation) receiver.

Therefore, it is appropriate to derive the correct relationship between the MSK detection error probability and the subsequent CSK demodulation character error rate.

The compatible shift keying (CSK) system is a coherent frequency shift keying modem which uses a modulation index of 1/2 rather than the unity index of the CFSK system thus far discussed. However, the basic demodulation process is identical with that of the MSK system. This process can be best explained by considering the mathematical expression for the CSK waveform. Here the CSK signal is given by

$$S(t) = KS \cos(\omega_0 + \ell \frac{\pi}{2T})t \quad (314)$$

where T is the duration of a binary element, $\ell = \pm 1$ according to the data state (thus producing the FSK modulation), and $K = \pm 1$ so as to maintain phase continuity at frequency shifts.

Rewriting,

$$\begin{aligned} S(t) &= KS \cos \omega_0 t \cos \ell \frac{\pi t}{2T} \\ &\quad - KS \sin \omega_0 t \sin \ell \frac{\pi t}{2T}. \end{aligned} \quad (315)$$

It is apparent that the first term is independent of the value of ℓ . Moreover, at $t = \pm 2nT$, $n = 0, 1, \dots$, the first term has an envelope maximum and K remains constant at these points to maintain waveform continuity.

On the other hand, the second term changes sign as λ changes so that when frequency shifts occur at $t = (1 \pm 2n)T$, $n = 0, 1, \dots$, K changes sign to maintain waveform continuity. This effectively produces a RF phase reversal in the first term at an envelope zero.

Thus, the effect of frequency shift keying is to produce sequential phase reversals in the two quadrature terms of $s(t)$. MSK detectors can be used to demodulate the phase modulation of these two quadrature components of the signal. However, the information is not contained in the phase state, per se; it is contained in the frequency state. This is readily handled, nevertheless, as the instantaneous frequency is directly defined by the phase difference of these two components. That is, expressing the first component as

$$c_1(t) = S \cos \frac{\pi t}{2T} \sin(\omega_c t + \phi_c), \quad (316)$$

and the second component as

$$s_1(t) = S \sin \frac{\pi t}{2T} \cos(\omega_c t + \phi_s), \quad (317)$$

where

$$\phi_c, \phi_s = \pm \frac{\pi}{2},$$

the upper shift frequency exists when $|\phi_c - \phi_s| = 0$ and the lower shift frequency exists when $|\phi_c - \phi_s| = \pi$. Thus, the data is recovered from quadrature MSK detectors according to the difference (modulo 2π) of the indicated phase state. This differential post-detection process

obviously produces a sequential pair of binary output errors for each isolated MSK-detector, phase-decision error. In the case of 7.0 Baudot teletype code, there are six MSK-detector phase decisions affecting the sequence of five binary data elements of each character. A correct sequence of five binary data elements requires the correct detection of a sequence of six MSK-detection elements. This probability is given by:

$$P_c = q^6 = (1 - P_e)^6 \quad (318)$$

where P_e is the probability of a MSK-decision error. Finally, the probability of a CSK character error, or CER, is given by

$$CER = 1 - P_c = 1 - (1 - P_e)^6. \quad (319)$$

5.3.2 Experimental System

Proceeding to a description of the experimental receiving system, Figure 18 is a block diagram of a VLF receiver subsystem used to measure the quantitative performance of CFSK and CSK (MSK detection with differential post-detection logic) modems in an actual atmospheric noise environment. It is apparent that the receiver subsystem depicted here corresponds to the receiver-detection systems previously discussed, except for the overall pre-detection filtering.

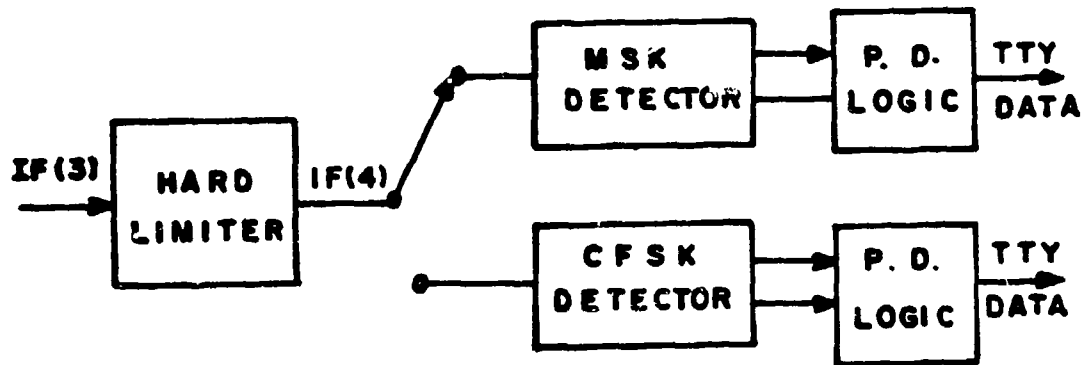
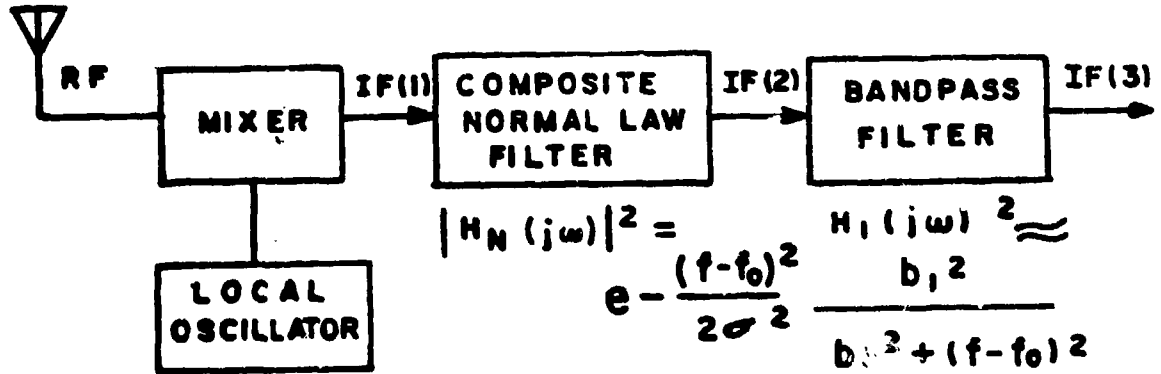


Figure 18. Receiver Subsystem

Here the actual bandpass filtering which occurs prior to mixing is combined with subsequent IF filtering to yield an approximately Gaussian, or normal-law, composite filter function. This is followed by an optional bandpass filter whose noise bandwidth is substantially less than the noise bandwidth of the preceding normal-law filter. The remainder of the receiver operates as described in the preceding discussions of the MSK and CFSK detectors (including the hard limiting).

Considering the composite bandpass filter function $|H_c(j\omega)|^2$, it is noted that

$$|H_c(j\omega)|^2 = |H_N(j\omega)|^2 \times |H_1(j\omega)|^2$$

$$= \frac{b_1^2 e^{-\frac{(f-f_0)^2}{2\sigma^2}}}{b_1^2 + (f-f_0)^2}, \quad (320)$$

where $2b_1$ is the 3 db. bandwidth of the single-tuned filter in H_1 .

Now assuming the noise at the receiver input to be approximately white, the power spectral density, $W(f)$, at the final pre-detection filter output is proportional to the composite filter function,

$|H_c(j\omega)|^2$. In order to employ (306) for the computation of envelope crossing rates, the moments b_0 and b_2 are computed by (307) and (308):

$$b_2 = (2\pi)^2 \int_0^\infty W(f) (f-f_0)^2 dF, \quad (307)$$

$$b_0 = \int_0^\infty W(f) dF, \quad (308)$$

where

$$W(f) = N_0 |H_c(j\omega)|^2,$$

$$= N_0 \frac{b_1^2 e^{-\frac{(f-f_0)^2}{2\sigma^2}}}{b_1^2 + (f-f_0)^2}, \quad (321)$$

and N_0 is the noise intensity.

Thus,

$$b_2 = (2\pi b_1)^2 N_0 \int_0^\infty \frac{(f-f_0)^2 e^{-\frac{(f-f_0)^2}{2\epsilon^2}} df}{b_1^2 + (f-f_0)^2} \quad (322)$$

and

$$b_0 = b_1^2 N_0 \int_0^\infty \frac{e^{-\frac{(f-f_0)^2}{2\epsilon^2}} df}{b_1^2 + (f-f_0)^2} \quad (323)$$

Here, the substitution $f = f-f_0$ and the conditions that $f_0 \gg 0$, $b_1 \ll f_0$ and $\epsilon \ll f_0$ permit the accurate approximations

$$b_2 \approx (2\pi b_1)^2 N_0 \int_{-\infty}^\infty \frac{f^2 e^{-\frac{f^2}{2\epsilon^2}} df}{b_1^2 + f^2}, \quad (324)$$

and

$$b_0 \approx b_1^2 N_0 \int_{-\infty}^\infty \frac{e^{-\frac{f^2}{2\epsilon^2}} df}{b_1^2 + f^2}. \quad (325)$$

Moreover, the integrands of both expressions are even functions so that

$$b_2 = 2(2\pi b_1)^2 N_0 \int_0^\infty \frac{f^2 e^{-\frac{f^2}{2\epsilon^2}} df}{b_1^2 + f^2} \quad (326)$$

and

$$b_0 = 2 b_1^2 N_0 \int_0^\infty \frac{e^{-\frac{f^2}{2\sigma^2}} df}{b_1^2 + f^2}. \quad (327)$$

It should be noted that the noise bandwidth of the normal-law filter is given by

$$\begin{aligned} B_N &= \frac{\int_0^\infty |H_n(j\omega)|^2 df}{|H_n(0)|^2} = \int_0^\infty e^{-\frac{(f-f_0)^2}{2\sigma^2}} df \\ &= 2 \int_0^\infty e^{-\frac{f^2}{2\sigma^2}} df = \sqrt{2\pi} 6 \text{ Hz}. \end{aligned} \quad (328)$$

Indefinite integrals of the form of b_0 , (327), have been solved to yield

$$b_0 = \pi b_1 N_0 e^{\frac{b_1^2}{2\sigma^2}} \left[1 - \Phi\left(\frac{b_1}{\sqrt{2}\sigma}\right) \right] \quad (A3)$$

where

$$\Phi(z) = \frac{2}{\sqrt{\pi}} \int_0^z e^{-t^2} dt. \quad (329)$$

Turning to b_2 :

$$\begin{aligned}
 b_2 &= 2(2\pi b_1)^2 N_0 \int_0^\infty \left[1 - \frac{b_1^2}{b_1^2 + f^2} \right] e^{-\frac{f^2}{2\sigma^2}} df \\
 &= (2\pi b_1)^2 \left[2N_0 \int_0^\infty e^{-\frac{f^2}{2\sigma^2}} df - b_0 \right] \\
 &= (2\pi b_1)^2 N_0 \left\{ \sqrt{2\pi} \sigma - \pi b_1 e^{\frac{b_1^2}{2\sigma^2}} \times \right. \\
 &\quad \left. \times \left[1 - \Phi\left(\frac{b_1}{\sqrt{2}\sigma}\right) \right] \right\}. \tag{329a}
 \end{aligned}$$

Thus, the filter-bandwidth-related constant term of (306), the Bandwidth Factor, is given by

$$\left[\frac{b_2}{2\pi b_0} \right]^{\frac{1}{2}} = \sqrt{2\pi} b_1 \left\{ \frac{\sqrt{\frac{2}{\pi}} \sigma e^{-\frac{b_1^2}{2\sigma^2}}}{b_1 \left[1 - \Phi\left(\frac{b_1}{\sqrt{2}\sigma}\right) \right]} - 1 \right\}^{\frac{1}{2}}. \tag{330}$$

Figure 19 shows the normalized Bandwidth Factor, $\left[\frac{b_2}{2\pi b_0} \right]^{\frac{1}{2}} / B_{nc}$,

as a function of B_{nc}/B_n , where B_{nc} is the noise bandwidth of the cascaded Normal-Law and single tuned filters and B_n is the noise bandwidth of the Normal-Law filter alone.

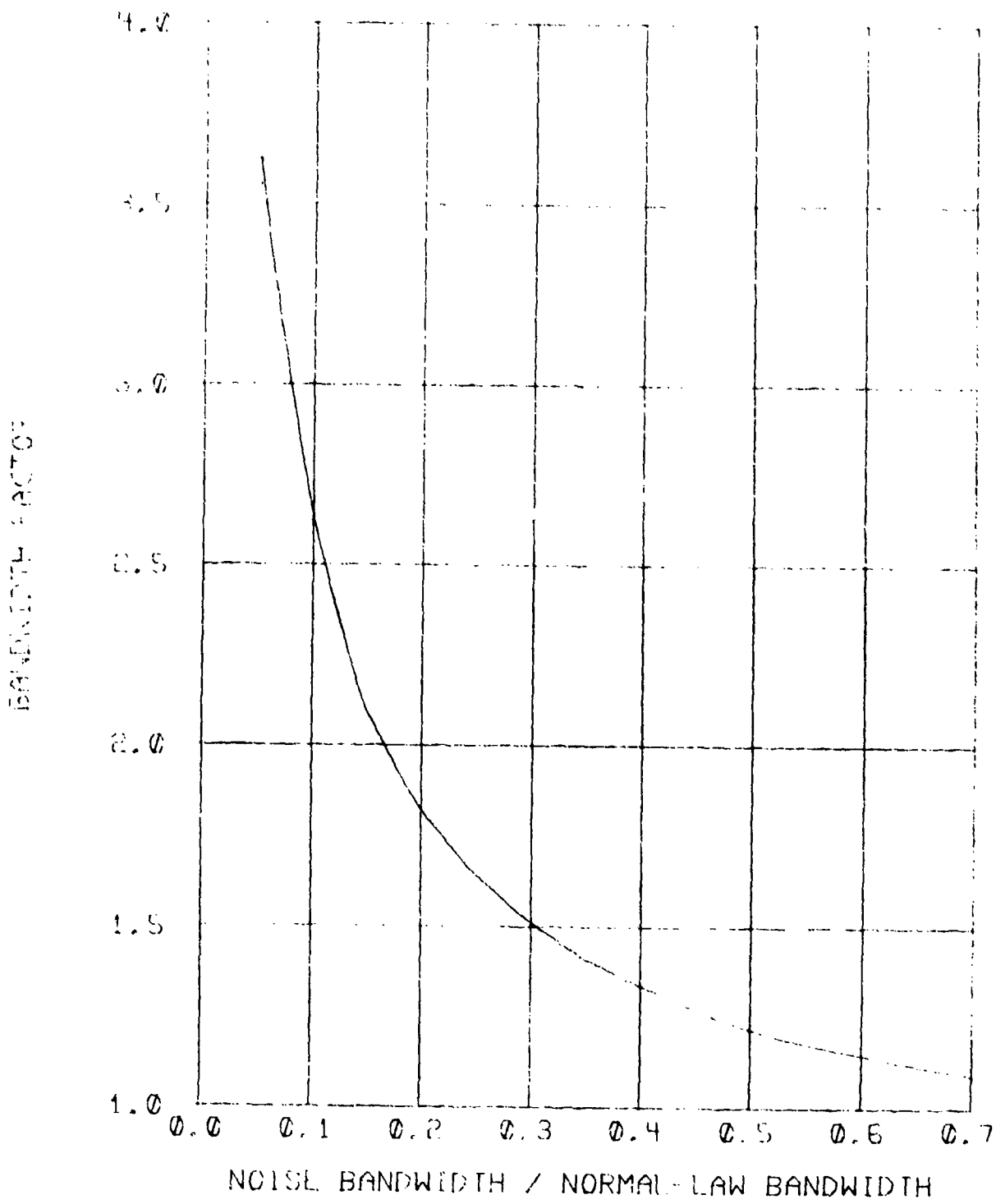


Figure 19. Normalized Bandwidth Factor for Noise Envelope Crossing Rate as a Function of Noise/Normal-Law Bandwidth Ratio.

In terms of the previously derived parameters, B_{nc} is given by

$$B_{nc} = \int_0^{\infty} |H_c(j\omega)|^2 df = b_1 / N_0 . \quad (331)$$

It is apparent that the ratio $\left[\frac{b_1}{2\pi b_0} \right]^{\frac{1}{2}}$ B_{nc} approaches unity as B_{nc}/B_n approaches unity. Moreover, at the limit $B_{nc}/B_n = 1$, where the filter function is identically Gaussian (Normal-Law), the multiplier $\left[\frac{b_1}{2\pi b_0} \right]^{\frac{1}{2}}$ equals the noise bandwidth.

In this particular system as tested, the noise bandwidth of the normal-law filter was 4.25 times as great as the 3 dB bandwidth of the series combination of the normal-law and bandpass filters.

Thus, if $2b'$ is the 3 dB bandwidth of the cascaded filters (in Hz),

$$|H_c(j2\pi b')|^2 = .5$$

or

$$\frac{b_1^2 e^{-\frac{b'^2}{2b'^2}}}{b_1^2 + b'^2} = .5 \quad (332)$$

Also,

$$\frac{\sqrt{2\pi} 6}{2b'} = 4.25$$

or

$$b' = \frac{\sqrt{2\pi} 6}{8.50},$$

or

$$\frac{b'^2}{26^2} = \frac{\pi}{(8.5)^2} = .0436. \quad (333)$$

Hence,

$$\frac{.9574 b_1^2}{b_1^2 + b'^2} = .5$$

or

$$b_1 = 1.044 b'. \quad (334)$$

Also,

$$\frac{b_1}{6} = \frac{1.044 \sqrt{2\pi}}{8.5} = .308. \quad (335)$$

Thus, evaluating α_r ,

$$\alpha_r = \sqrt{2\pi b_1} \left\{ \frac{\sqrt{\frac{2}{\pi}} e^{-.0474}}{.308 \times [1 - \Phi(.218)]} - 1 \right\} \nu e^{-\frac{\nu^2}{2}} \quad (336)$$

$$= 3.754 b_1 \nu e^{-\frac{\nu^2}{2}} = 3.9192 b' \nu e^{-\frac{\nu^2}{2}}, \quad (337)$$

where α_r is in pulses per second.

Now for bit-lengths of T seconds, the decision element length is T seconds for the CFSK system and 2T seconds for the MSK system. It thus follows that the average number of noise pulses per decision is given by the product of α_r and the decision element length. Replacing b' by its previously defined angular equivalent, b (in radians per second), and carrying out the indicated multiplications,

$$\alpha_r T_{CFSK} = .6238 b T \nu e^{-\nu^2/2}, \quad (338)$$

and

$$\alpha_r T_{MSK} = 1.2475 b T \nu e^{-\nu^2/2}, \quad (339)$$

where ν is the ratio of APD and Rayleigh curve voltages, ($\frac{U_1}{U_r}$), defined previously.

Finally, overall average error rates are computed by

$$P_e = \sum_{N=1}^{\infty} P_{e|N} Pr(N), \quad (305)$$

where $Pr(N)$ is given by (42) for independent pulse occurrence times,

$$\alpha_r T = \begin{cases} .6238 b T \nu e^{-\nu^2/2}, & CFSK \end{cases} \quad (338)$$

$$\begin{cases} .6238 b T \nu e^{-\nu^2/2}, & CFSK \\ 1.2475 b T \nu e^{-\nu^2/2}, & MSK, \end{cases} \quad (339)$$

$$\alpha(\nu) T = \alpha_r T \left(\frac{\nu}{U_1} \right)^{-K} \quad (312)$$

and $K = .85, 1.0, 1.2, 1.5$.

The resultant CER curves are presented on Figures 20, 21, and 22 with measured data points superimposed.

Examination of the computed results and the corresponding measured data presented on Figures 20, 21, and 22 leads to the conclusion that the "best fit" value of K varies inversely with the V_d ratio. For instance, in Figure 20, where $6 \leq V_d \leq 7.9$, the error rate computed for $K = 1.5$ most nearly corresponds to the measured data; on the other hand, in Figure 22, where $12 \leq V_d \leq 13.9$, the error rate computed for $K = .85$ more nearly corresponds to the measured data. This result is consistent with the earlier observation that lower values of K imply proportionately greater impulsive noise power (higher V_d ratios) in the overall atmospheric noise environment.

5.3.3 Effect of "Clustering" Pulse Distribution

The preceding quantitative estimates were based on the Poisson pulse statistical distribution. However, this is strictly accurate only if the occurrence times of the noise pulses are statistically independent. As pointed out in Chapter 2, significant noise pulse statistical data exhibits a clustering tendency; this is attributed to multiple strokes in a given lightning discharge. In this case, the probability of N pulses in T seconds is given by

$$P_r(N) = e^{-hT} \left[\frac{(hT)^{2N+1}}{(2N+1)!} + \frac{(hT)^{2N}}{(2N)!} \right], \quad (56)$$

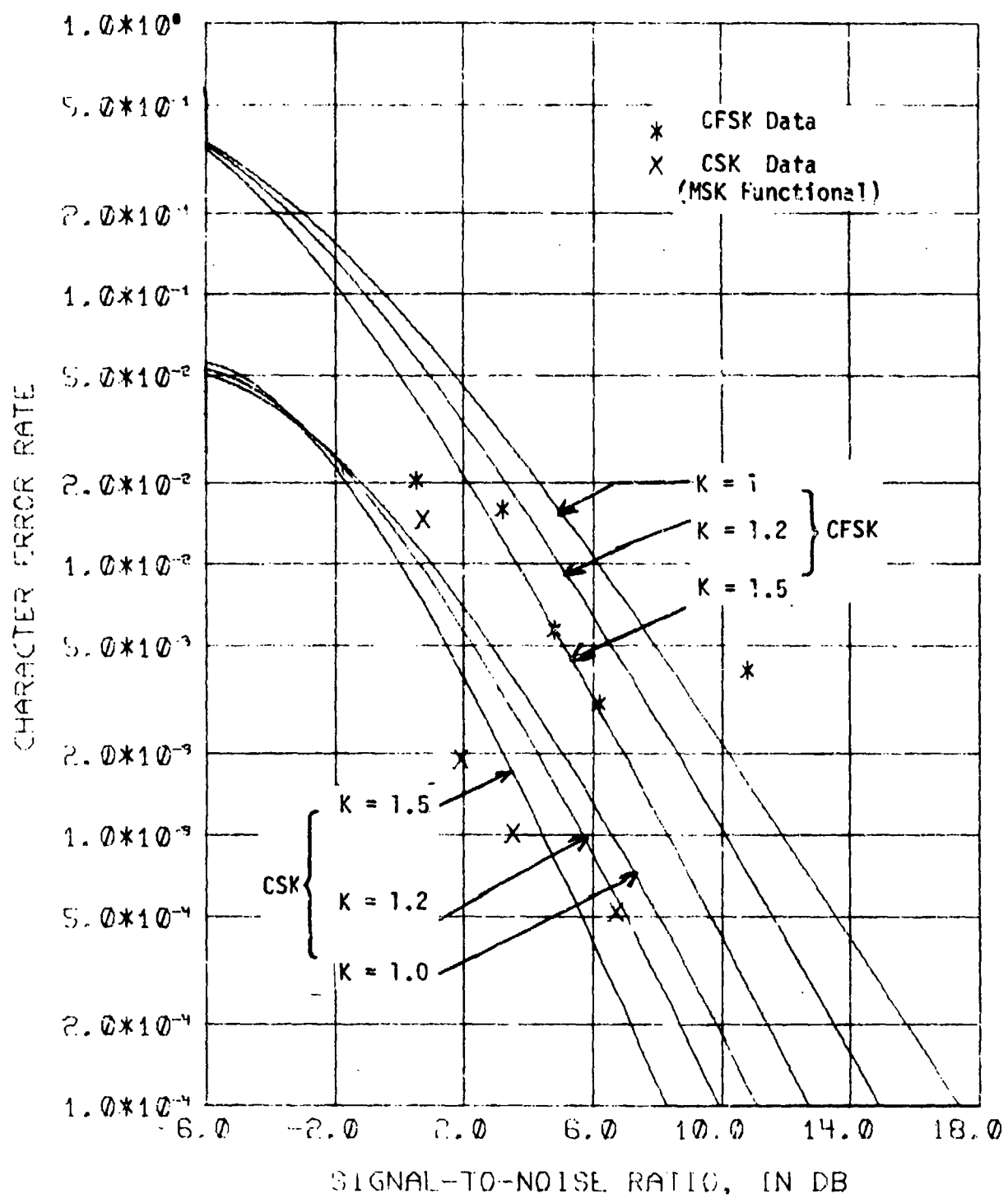


Figure 20. Pulse Statistical Analysis - Hard Limiting Receiver Performance in Atmospheric Noise.
 (6 db \leq Vd \leq 7.9 db in 600 Hz)

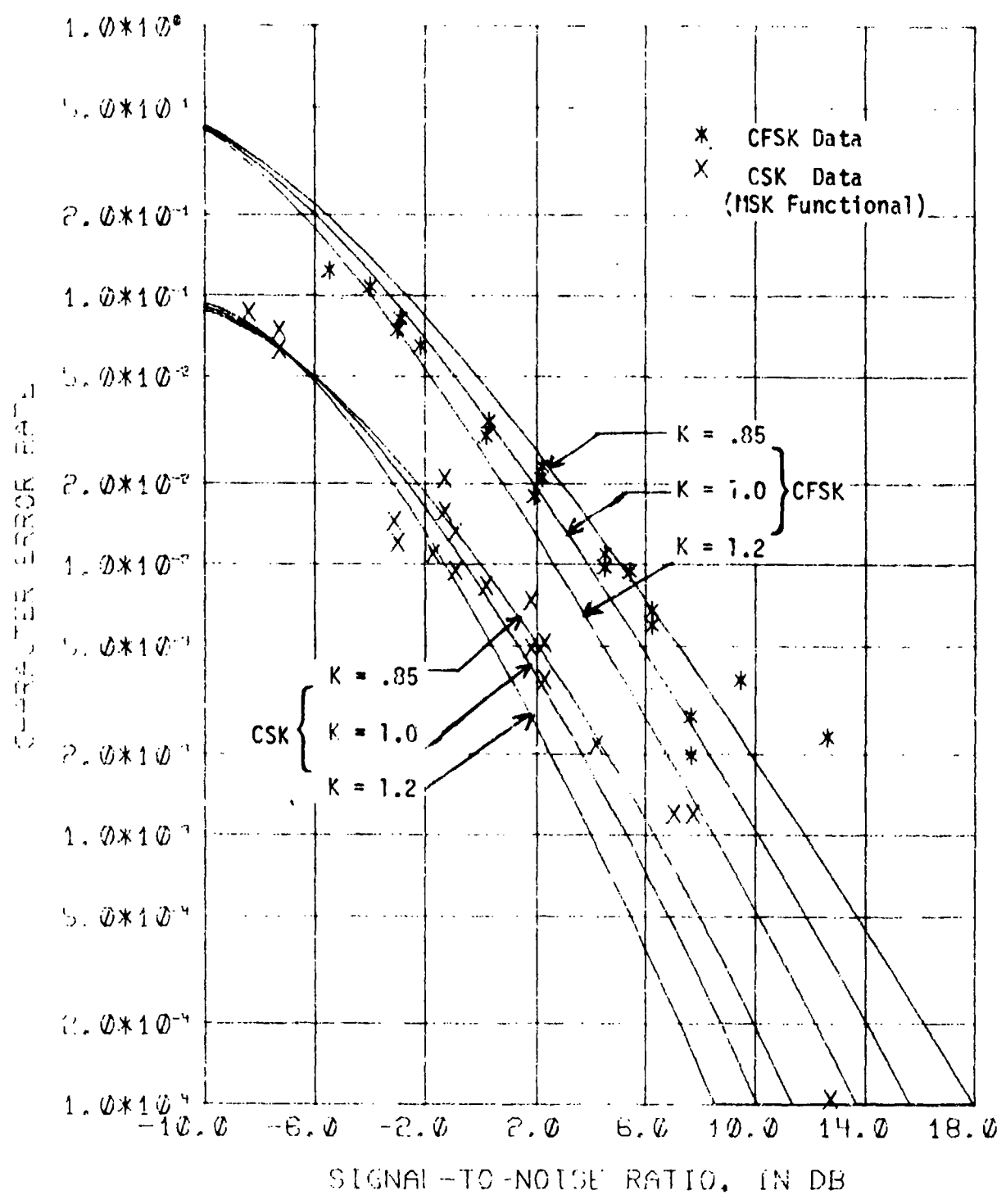
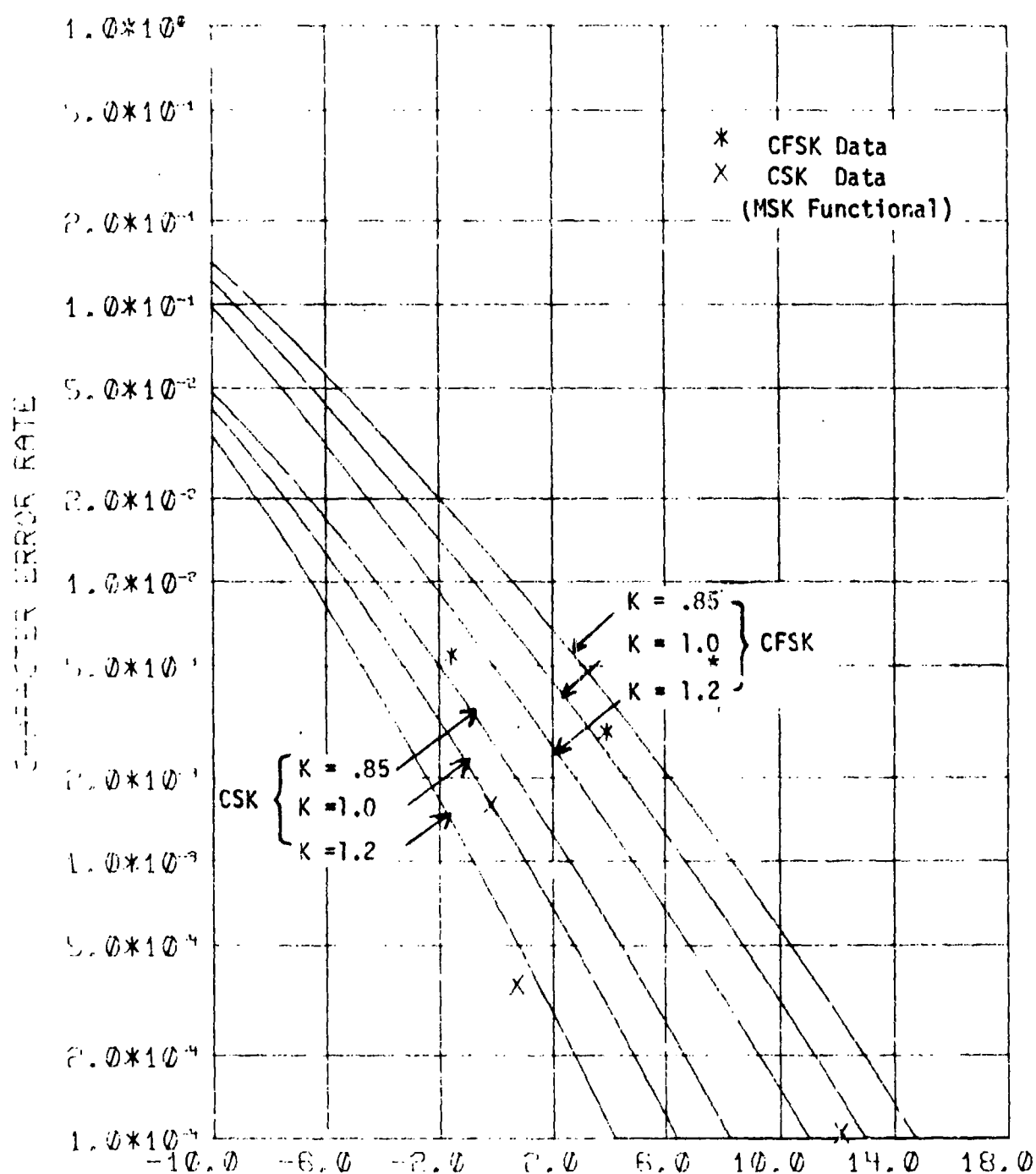


Figure 21. Pulse Statistical Analysis - Hard Limiting Receiver Performance in Atmospheric Noise.
 $(8 \text{ db} \leq V_d \leq 9.9 \text{ db in } 600 \text{ Hz})$



SIGNAL-TO-NOISE RATIO, IN DB
Figure 22. Pulse Statistical Analysis - Hard Limiting Receiver Performance in Atmospheric Noise ($12 \text{ db} \leq V_d \leq 13.9 \text{ db}$ in 600 Hz).

where

$$\bar{N} = hT/2 - 1/4 + 1/4e^{-2hT} \quad (61)$$

is the number of noise pulses in T seconds.

Using these "clustering" statistical relationships instead of the Poisson distribution (42) in (285), CFSK and CSK CER's are calculated for the case where $8 \text{ dB} \leq V_d \leq 9.9$, $K = 1.0$. These results are shown in Figure 23, along with the experimental data and corresponding ($K = 1.0$) curves of Figure 21 (as computed according to the Poisson distribution). The remarkable quantitative similarity of these results indicates that the "real world" performance, which would be expected to result from both independent (Poisson distributed) and "clustered" noise pulses is reasonably approximated by either of these distributions. However, the Poisson function is mathematically simpler and the CER's computed by it correspond to the experimental data slightly more closely. Therefore, it appears that the Poisson distribution is the more practical choice for the computation of error rates by the pulse statistical analysis technique.

5.4 Bandwidth Ratio Constraint

It should be noted that all these results are for one receiver filter configuration where the CFSK bandwidth ratio (noise bandwidth/detection bandwidth, BWR) is 3.7 and the bandwidth factor (from Figure 19) is 1.515. Therefore, it is important to consider the effect of the BWR on the computed error rate performance. The ensuing discussion shows that the error rate performance computed by the foregoing Pulse Statistical Analysis (PSA) becomes relatively less accurate as the bandwidth ratio

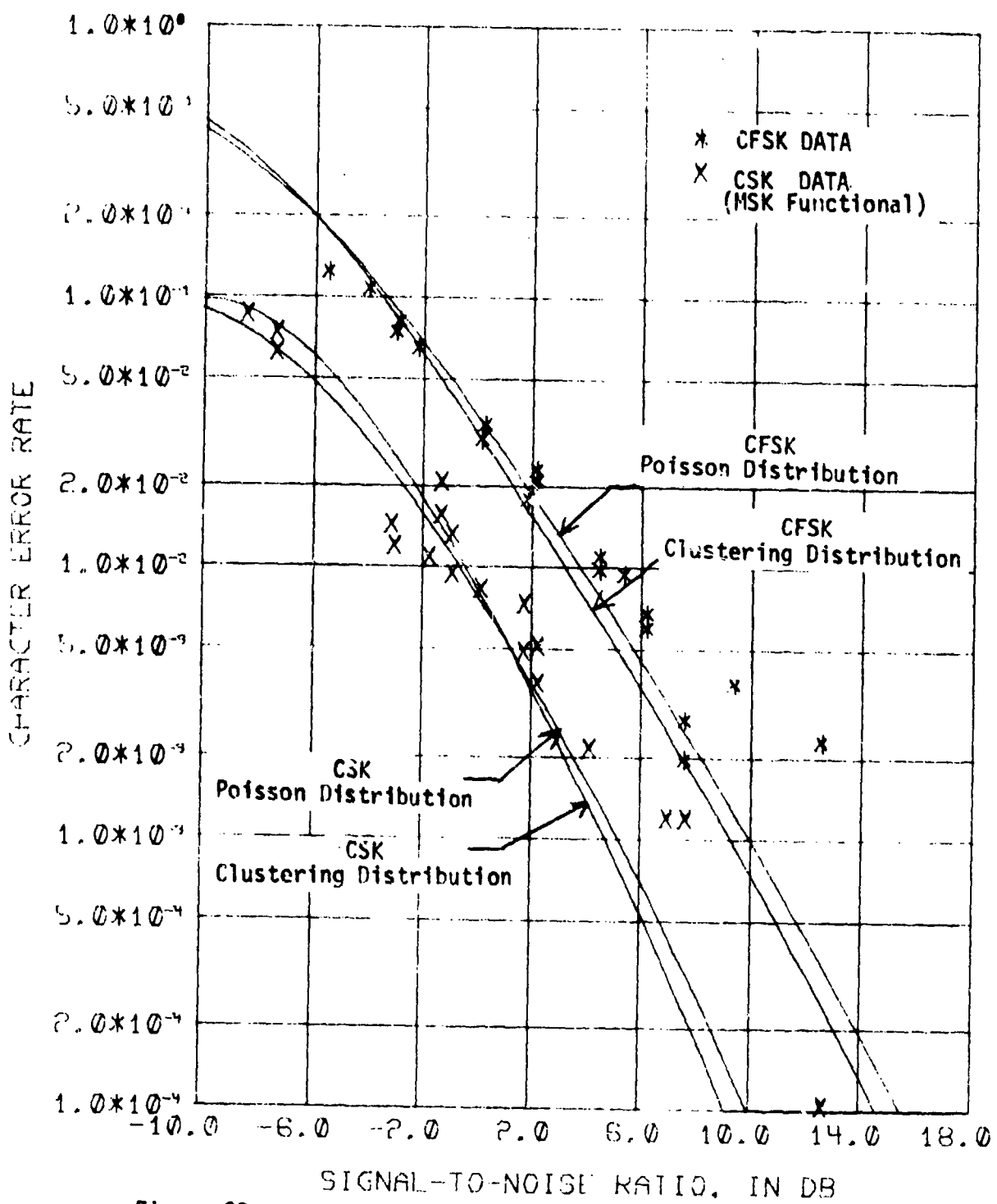


Figure 23. Pulse Statistical Analysis - Hard Limiting Receiver Performance in Atmospheric Noise. Error Rates computed according to Poisson and Clustering Distributions ($8 \text{ db} \leq V_d \leq 9.9$ in 600 Hz, $K=1.0$).

becomes significantly greater than approximately 8; it is not at all representative by the time the BWR reaches a value of 12. However, an alternate means of performance analysis, suggested by Hartley [22] and refined in this dissertation for larger BWR's (on the order of 12 or greater) is presented in Chapter 6.

5.4.1 "Critical Pulse Width" Versus Bandwidth Ratio (BWR)

As a first consideration of the relationship between the prelimiting receiver noise bandwidth and CFSK error probability, the effect of a single noise pulse is considered. An important simplification is the approximate equivalence of the mean pulse width of the receiver impulse response and the reciprocal of the receiver noise bandwidth; the use of this relationship permits the use of some results from earlier analyses in this chapter. Recall the expression for the probability of a CFSK decision error under the condition of one noise pulse per bit (233)

$$P_{ec} = P_r \left\{ \frac{2T}{\pi} (V_4 - V_5) \cos \phi > T - V_1 - \frac{I}{2\pi} (V_2 - V_3), V_1 \leq T \right\} \quad (233)$$

$$+ P_r \left\{ - \frac{4LS_1}{\pi} \cos \phi > 0, V_1 > T \right\}$$

where

$$V_1 = t_2 - t_1, \quad (232a)$$

$$V_2 = \sin \frac{2\pi t_2}{T}, \quad (232b)$$

$$V_3 = \sin \frac{2\pi t_1}{T}, \quad (232c)$$

$$V_4 = \cos \frac{\pi t_2}{T}, \quad (232d)$$

$$V_5 = \cos \frac{\pi t_1}{T}, \quad (232e)$$

t_1 and t_2 are the beginning and end of a noise pulse such that
 $0 \leq t_1 \leq t_2 \leq T$.

Since the purpose of this analysis is to find the minimum pulse width ($< T$) which can cause a CFSK error, the second term can be disregarded in further discussions. The variables V_2 , V_3 , V_4 and V_5 can be written in terms of t_1 and V_1 . An error occurs when

$$\frac{2T}{\pi} \left[\cos \frac{\pi}{T}(t_1 + V_1) - \cos \frac{\pi}{T} t_1 \right] \cos \phi >$$

$$T - V_1 - \frac{T}{2\pi} \left[\sin \frac{2\pi}{T}(t_1 + V_1) - \sin \frac{2\pi t_1}{T} \right],$$

or

$$1 \geq \cos \phi \geq \frac{\frac{\pi}{2}(1-\lambda) + \frac{1}{4} [\sin 2\pi(\gamma + \lambda) - \sin 2\pi\gamma]}{\cos \pi\gamma - \cos \pi(\gamma + \lambda)}, \quad (340)$$

where

$$\lambda = \frac{V_1}{T}, \quad 0 \leq \lambda \leq 1, \quad (340a)$$

and

$$\gamma = \frac{t_1}{T}, \quad 0 \leq \gamma \leq 1 - \lambda. \quad (340b)$$

Because $\cos\theta \leq 1$, the right hand inequality is clearly impossible when the right hand term is greater than one. By numerical means, it has been determined that the minimum value of λ for which the right side of (320) exceeds one (regardless of γ) is .260652.

This result, which agrees with that given by Hartley [22], implies that no decision error can be caused by a single noise pulse whose duration is less than $.26T$. Thus, if the receiver noise bandwidth, B_N , exceeds the reciprocal of this "critical pulse width", or

$$B_N > 3.84T^{-1}, \quad (341)$$

then a single noise pulse cannot produce a decision error. Although the practical case involves a significant probability of multiple noise pulses per bit, this "critical pulse width" result for single pulses implies a similar, but less sharply defined, "critical noise capture duration" for the multiple pulse case. The "critical pulse width" for a single pulse nevertheless, defines an approximate bound of 3.84 on the BWR below which the foregoing PSA is clearly valid. (This is obviously consistent with the comparable measured and computed CFSK performance data of Figures 20, 21 and 22.)

5.4.2 Experimental Validity of PSA for BWR's Greater Than 4.

Although the implication of the preceding discussion is that PSA may not be valid for BWR's substantially greater than 4, the CSK performance calculations and data of Figures 20, 21 and 22 indicate substantial validity for BWR's of at least 7.4. The reason for this conclusion is that the MSK detector functional has been shown to be of the same form as the CFSK, but twice as long. Hence, MSK detection is mathematically equivalent to CFSK detection in 1/2 the MSK data bandwidth. This means that the experimental system, which had a BWR of 3.7 relative to the CFSK data and detection bandwidth, also had a BWR of 3.7 relative to the CSK data bandwidth. On the other hand, the system had an effective BWR of 7.4 relative to the MSK (equivalent CFSK) detection bandwidth. Clearly, the close agreement of computed and measured CSK performance, especially Figure 21, affirms the quantitative validity of PSA for CFSK BWR's of at least 7.4 and probably 8.

On the other hand, Hartley's experimental data for a hard-limiting CFSK receiver of significantly higher BWR are shown on Figure 24 with a curve calculated by PSA on the basis of the experimental parameters. In this case, the BWR is 12 and it is obvious that the PSA computation and experimental results are drastically different (at least 9 dB). This clearly implies that the PSA technique is inappropriate for BWR's as great as 12.

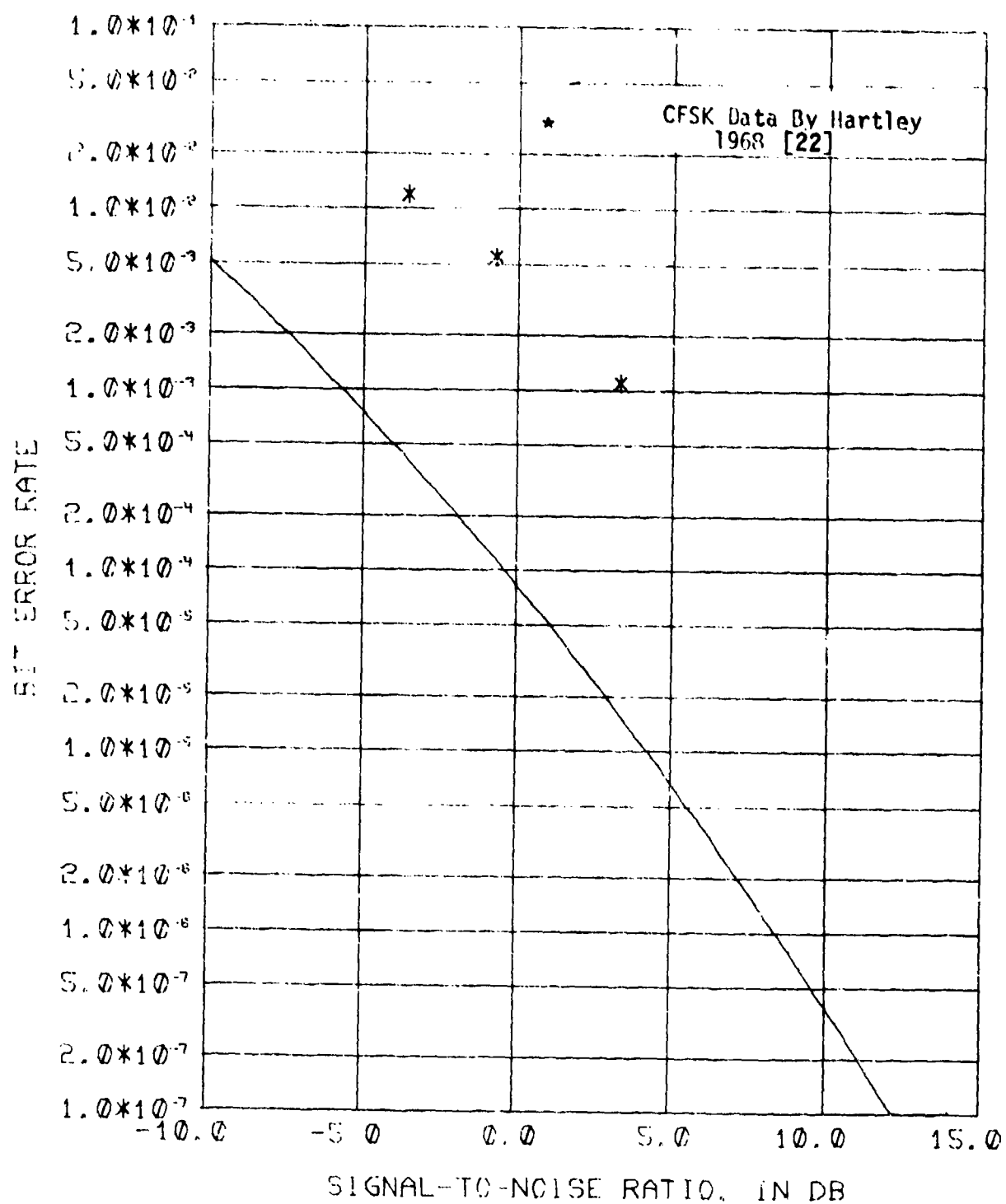


Figure 24. Pulse Statistical Analysis - Hard-Limitting CFSK Receiver Performance in Atmospheric Noise For a Bandwidth Ratio (Limiter Input Bandwidth/Detection Bandwidth) of 12 ($V_d = 9$ db in 600 Hz)

In summary, the theoretical approximation indicates that there is a minimum BWR such that individual noise pulses cannot produce decision errors. However, this estimate of approximately 4 is overly low in view of the efficacy of PSA for the analysis of CSK performance where the equivalent BWR is 7.4. Nevertheless, PSA is quantitatively inaccurate for BWR's as great as 12. Therefore, it can be safely concluded that PSA is quantitatively valid for CFSK BWR's on the order of 8 or less, questionable for BWR's slightly greater than 8, and inaccurate for BWR's of 12 or more.

Chapter 6

IMPULSIVE NOISE SUBTRACTION

6.1 Background

The preceding discussion of pulse statistical analysis (PSA) for relatively large bandwidth ratios (BWR's) showed that the performance as computed (by PSA) differed markedly from the measured performance. Because of this mathematically implied and empirically demonstrated inadequacy of PSA for BWR's substantially greater than 8, a different approach must be employed for the larger BWR's. The method developed here is based on the principle of "Impulsive Noise Power Subtraction". It should be noted that this principle describing the effect of hard limiters on impulsive atmospheric noise has not been proven rigorously. However, two circumstances tend to substantiate its practical validity. These are: (1) the noise power reduction estimated by the Impulsive Noise Subtraction approach is similar to the noise power reduction computed by two entirely different and independent analytic approaches; and (2) the error rate characteristic computed by means of Impulsive Noise Subtraction virtually coincides, both quantitatively and in slope, with measured experimental results.

The method is based on principles suggested by Linfield and Beach [33], Sisco [46], and Hartley [22]. The approach, as proposed by Linfield and Beach [33] and Sisco [46], is that noise clipping

truncates the amplitude range of the input noise APD to the clipping level, thus quantitatively defining a noise power reduction. It is then postulated that the resultant "clipped noise" has an approximate Rayleigh (Gaussian noise) APD. Hartley, on the other hand, proposed that the noise power reduction resulting from receiver limiting can be quantitatively determined by direct subtraction of the noise power represented by the steep power-Rayleigh portion of the APD curve (impulsive noise component) from the overall noise power. An intuitive, but reasonable, estimate treats the "residual" noise (the noise component remaining after removal of the impulsive noise by limiting) as Gaussian noise. Error rates computed by these approaches do indeed translate to the close proximity of the measured data, but usually at only one point. In general, the Gaussian-noise characteristic is much steeper than the actual measured characteristic. Thus, the proposition that limiting impulsive atmospheric noise simply reduces the noise power and yields nearly Gaussian noise, although mathematically convenient, is not very descriptive of actual system performance.

Nevertheless, the discussion presented by Hartley provides an insight toward a more representative analysis of hard-limiting receiver performance in atmospheric noise. The key argument can be stated as follows: (1) a well-designed receiver produces little filter ringing in response to the high-amplitude, but isolated, impulses which account for the steep, Power-Rayleigh portion of the noise APD; and (2) if the bandwidth ratio is sufficiently great ($BWR > 8$, as developed in the preceding section), then the impulsive component, which has been shown

to have minimal influence on detector performance, may be considered to be selectively removed from the total noise. Hartley estimated the effective limiter noise reduction by direct subtraction of the impulsive-noise-component power from the total noise power. Unfortunately, the complementary analysis, based on Gaussian "residual" noise, results in agreement between calculated and measured performance at only one point. It is in this latter area of residual noise definition and analysis that the material in this chapter rectifies the shortcoming of Hartley's approach. First, the quantitative estimation of noise power reduction is considered. This includes a method consistent with Hartley's estimates, a small-signal estimate developed by Cahn [9], and a small-signal estimate based on an approach entirely different from Cahn's. Next, the problem of the residual noise is considered. First, a qualitative mathematical estimate is developed and then a quantitative "best fit" synthesis procedure is employed to statistically describe the residual noise component.

6.2 Noise Power Reduction

6.2.1 Impulsive Noise Subtraction

First, consider the question of quantitative noise power reduction. If, as postulated by Hartley, the impulsive noise is effectively removed from the total atmospheric noise by limiting, then the quantitative noise power reduction can be determined by subtracting the mean-square envelope voltage for the impulsive component (which is proportional to the impulsive noise power) from

the mean-square envelope voltage for the total noise. The remaining power is that of the envelope of the residual noise component. In the case where the impulsive noise component envelope has a Power-Rayleigh APD, the probability that the ratio of the noise envelope voltage to the RMS noise envelope voltage exceeds a value A is given by

$$P(A) \triangleq P_r(a \geq A) = \exp\left[-\frac{A^{3/2}}{2\sigma^2}\right] \quad (6)$$

when a is the random variable defined by $a = \frac{1}{T E_0} \int_0^T e_I(t) dt$

when $e_I(t)$ is the impulsive noise envelope process and E_0 is the RMS noise envelope voltage for the overall noise process.

The probability density function of a is then given by

$$f_a(A) = \frac{d}{dA}[1 - P(A)] = \frac{A^{3/2-1}}{X \sigma^2} \exp\left[-\frac{A^{3/2}}{2\sigma^2}\right]. \quad (10)$$

The mean squared envelope voltage for the impulsive component,

$\overline{a^2}$, is

$$\begin{aligned} \overline{a^2} &= \int_0^\infty A^2 f_a(A) dA \\ &= \int_0^\infty \frac{A^{3/2+1}}{X \sigma^2} e^{-\frac{A^{3/2}}{2\sigma^2}} dA. \end{aligned}$$

Making the substitution $U = \frac{A^{3/2}}{26^2}$, results in

$$\begin{aligned}\bar{\alpha}^2 &= \int_0^\infty (26^2)^x U^x e^{-U} dU, \\ &= (26^2)^x \Gamma(1+x),\end{aligned}\quad (342)$$

where $\Gamma(\cdot)$ is the Gamma function.

With the overall APD normalized as in Figure 1 so that the mean square envelope voltage for the total noise is unity, the mean square envelope voltage of the residual noise, Λ_r , is then given by

$$\Lambda_r = 1 - \bar{\alpha}^2 \quad (343)$$

or, in decibels, by

$$10 \log \Lambda_r = 10 \log (1 - \bar{\alpha}^2). \quad (344)$$

Figure 25 shows the quantitative noise reduction obtained by this procedure as a function of V_d ratio. (This corresponds quite closely to Hartley's estimates [22].)

6.2.2 "Small Signal" Noise Power Reduction by Cahn [9]

Another approach to the determination of noise power reduction resulting from hard-limiting has been developed by Cahn. This derivation, developed as a "small-signal" approximation, is also applicable in the present case where limiting occurs in a bandwidth much wider than the detection bandwidth. In this case, the signal-to-noise ratio

SIGNAL-TO-NOISE RATIO ENHANCEMENT, IN DB

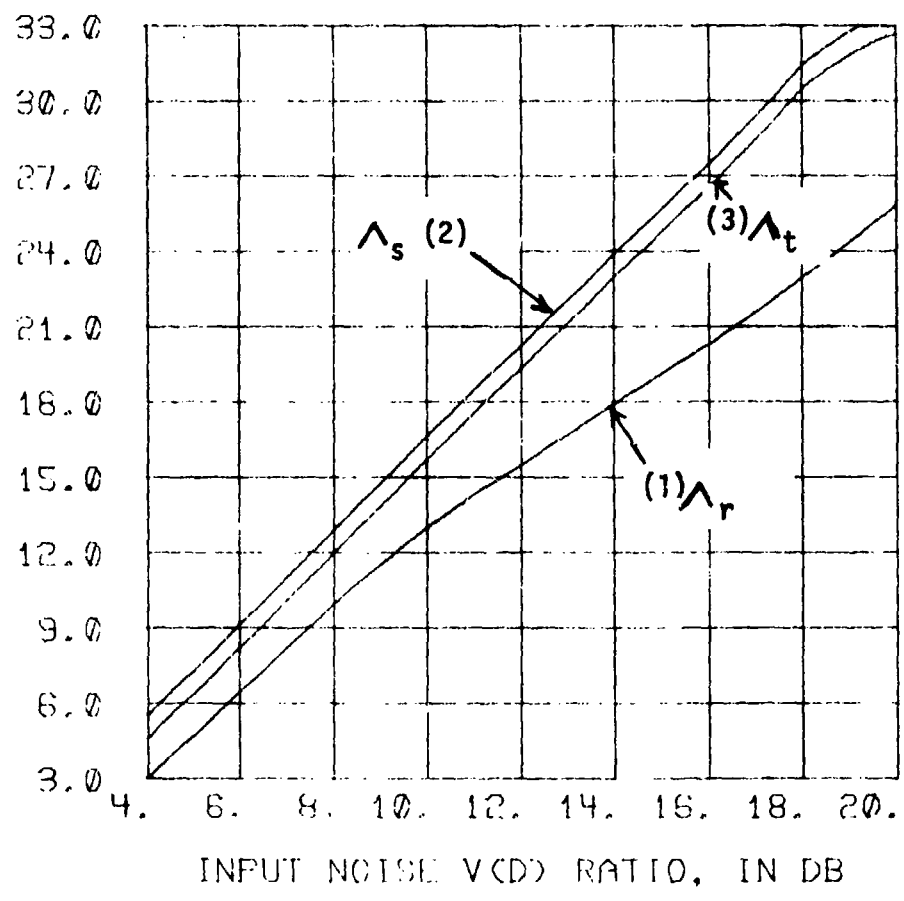


Figure 25. Impulsive Noise Power Reduction as computed by:(1) Impulsive Noise Subtraction, Δ_r ;
(2) "Small Signal" Noise Power Reduction [9],
 Δ_s ; (3) "Small Signal" PSK Noise Reduction
(Appendix C), Δ_t .

in the limiter bandwidth is much smaller (by a factor of 1/BWR) than in the detection bandwidth. Hence, usable "small" signal-to-noise ratios occur in the limiter bandwidth. Briefly, Cahn's result is that the ratio of the input to output signal-to-noise ratios for a bandpass limiter, Λ_s , is given by ([9], Equation 7):

$$\Lambda_s \triangleq \frac{(S/N)_{in}}{(S/N)_{out}} = \frac{4}{E_p^2 (\bar{E}^{-1})^2}, \quad (345)$$

where E_p is the observed noise envelope voltage produced by the overall noise process.

Rewriting this result in terms of the ratio, E , of noise voltage to RMS noise voltage yields

$$\Lambda_s = \frac{4}{(\bar{E}^{-1})^2}. \quad (346)$$

In view of the piecewise definition of the atmospheric noise APD curves, \bar{E}^{-1} must be evaluated numerically. This has been done for several V_d ratios and the results have been employed in (346). The resultant factor, Λ_s , is plotted in Figure 25. This factor, which represents the estimated noise reduction of the limiting process, is obviously similar to, but somewhat greater than, Λ_r computed by the earlier Impulsive Power Subtraction method.

6.2.3 "Small-Signal" PSK Noise Reduction

An analysis of PSK detection with hard-limiting is developed in Appendix C. This result, remarkably similar to Cahn's, is given by (C-42):

$$\Lambda_t = \frac{\pi^2}{2(E^{-1})^2} . \quad (C-42)$$

It is apparent that this latter noise reduction estimate is exactly $\pi^2/8$ (or .912 dB) greater than that of Cahn. This more conservative noise reduction estimate is also plotted in Figure 25.

6.2.4 Discussion of Noise Power Reduction Estimates

It can be readily seen that the small signal estimates, Λ_s and Λ_t , imply greater noise power reduction than the Impulsive Noise Power Subtraction estimate, Λ_r . Also, it should be noted that Cahn's expression (346), when evaluated for Gaussian Noise, yields $\Lambda_s = 4/\pi$ which coincides with Davenport's classic result for "small-signal" suppression in bandpass limiters [12]. This, of course, lends credence to this small-signal estimate, but it does not insure similar accuracy for the general non-Gaussian atmospheric noise case. Moreover, neither small-signal estimate is directly related to the postulated hard-limiting effect of amplitude-selective impulsive noise subtraction. On the other hand, the most conservative estimate, Λ_r , is based upon, and thus consistent with, the postulated limiting effect. Because of the consistency of Λ_r with the impulsive noise subtraction process, Λ_r is employed in the ensuing receiver system performance analysis.

6.3 The Atmospheric Noise Voltage as a Sum of Statistically Independent Components

6.3.1 General

To develop the postulated Impulsive Noise Subtraction analysis, it is necessary to define the random variables (noise voltages) which are used. First, the direct subtraction of the impulsive noise component from the overall atmospheric noise specifically involves noise voltages and not envelopes. However, the statistical description of atmospheric noise has been in terms of its voltage envelope. Similarly, the impulsive component is usually described in terms of its noise envelope statistics. Here, the steep, straight power-Rayleigh portion of the overall APD curve (as extrapolated to indefinitely small amplitudes) constitutes the APD of the impulsive noise envelope. This is illustrated in Figure 26. If the noise phase is considered to be statistically independent of the noise envelope and uniformly distributed on $(-\pi, \pi)$, then the noise voltage, z , is given by

$$z = E \cos \theta \quad (347)$$

where E is the noise envelope voltage of the total noise and θ is the effective phase angle of the total noise.

Similarly, a noise voltage, i_n , can be defined for the impulsive component by

$$i_n = A \cos \theta_I \quad (348)$$

where A is the impulsive noise envelope voltage characterized by the Power-Rayleigh APD of Figure 26 and θ_I is the statistically independent impulsive noise phase.

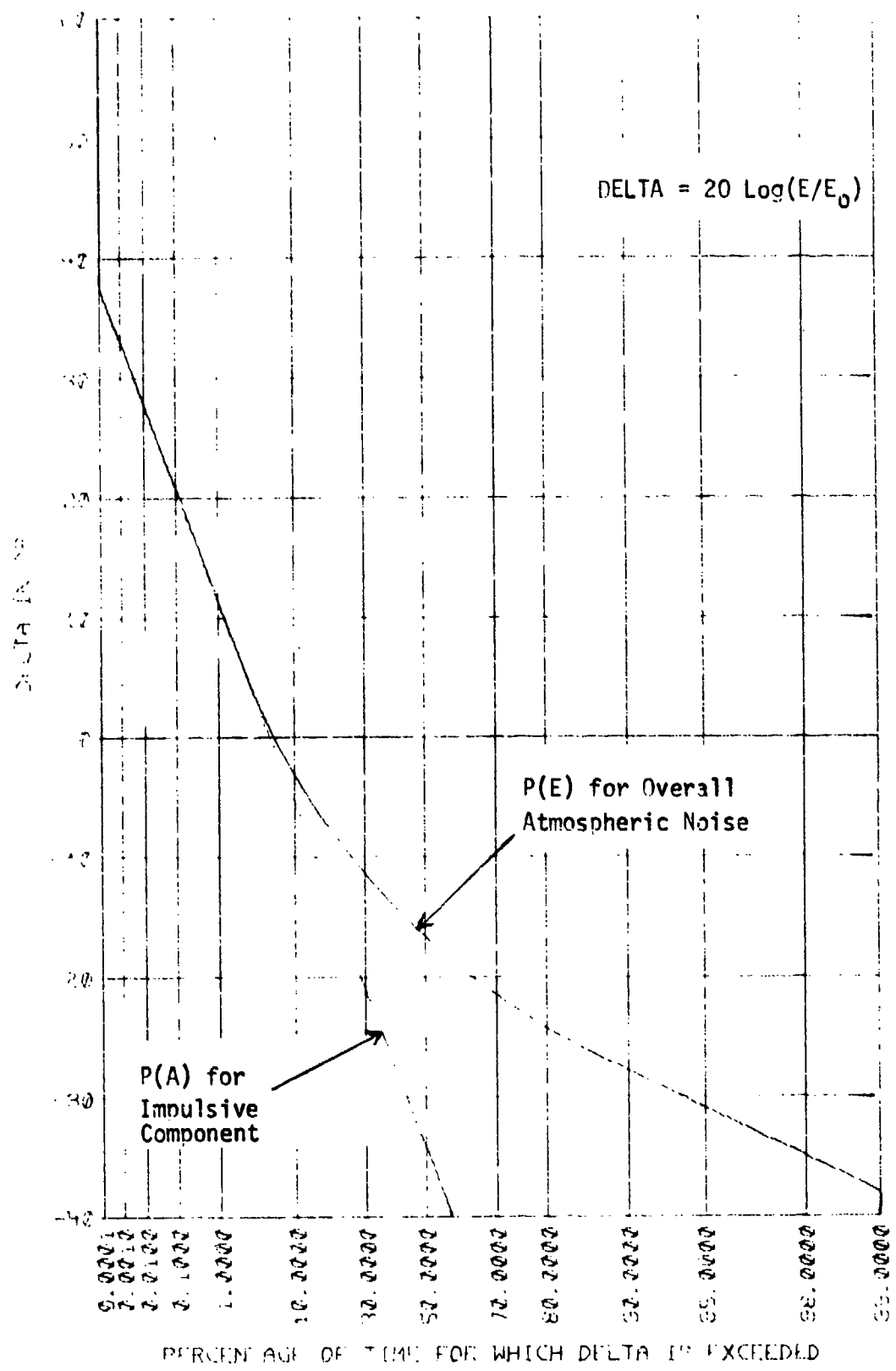


Figure 26. Atmospheric Noise APD Curve Showing Impulsive Component APD.

Next, it is assumed that the total noise voltage, z , can be expressed by

$$z = i_n + r_n \quad (349)$$

where r_n is an effective residual noise voltage statistically independent of the impulsive noise voltage, i_n .

The remainder of this section is devoted to obtaining a statistical description of the residual voltage, r_n . However, first the random variables, z and i_n must be considered.

6.3.2 Determination of the Probability Densities of the Total and Impulsive Noise Voltages

Consider the expression for the event of a linear PSK detection error given by

$$E \cos \theta - \hat{s} > 0 \quad (160)$$

where E is the ratio of the noise envelope voltage to the RMS noise envelope voltage. From (347), the term $E \cos \theta$ may be replaced by the noise voltage ratio z (that is, the ratio of atmospheric noise voltage to RMS noise envelope voltage). Thus, the probability of a PSK decision error, P_{ep} , is given by

$$\begin{aligned} P_{ep} &= Pr(z > \hat{s}) \\ &= \int_{\hat{s}}^{\infty} f_z(z) dz \end{aligned} \quad (350)$$

where $f_z(z)$ is the probability density function for the random variable, z .

However, an expression for the probability of error, P_{ep} , was derived earlier using a piecewise numerical evaluation of

$$P_{ep} = \frac{1}{\pi} \int_{-\infty}^{E=\hat{S}} \cos^{-1}\left(\frac{\hat{S}}{E}\right) dP(E). \quad (163a)$$

This yielded

$$P_{ep} = \frac{1}{4n} \left[\sum_{i=0}^{n-1} P\left(\frac{\hat{S}}{\cos \frac{i\pi}{2n}}\right) + \sum_{i=1}^n P\left(\frac{\hat{S}}{\cos \frac{(i-1)\pi}{2n}}\right) \right] \quad (176a)$$

where $P(E) = P_r(e > E)$ as defined by the appropriate APD curve.

It is immediately apparent from (350) that

$$\frac{d}{d\hat{S}}(P_{ep}) = -f_z(\hat{S}). \quad (351)$$

Thus, substituting (176a) into (351) and evaluating at $\hat{S} = z$, yields

$$\begin{aligned} f_z(z) &= -\left. \frac{d}{d\hat{S}}(P_{ep}) \right|_{\hat{S}=z} \\ &= -\frac{d}{d\hat{S}} \left\{ \frac{1}{4n} \left[\sum_{i=0}^{n-1} P\left(\frac{\hat{S}}{\cos \frac{i\pi}{2n}}\right) \right. \right. \\ &\quad \left. \left. + \sum_{i=1}^n P\left(\frac{\hat{S}}{\cos \frac{(i-1)\pi}{2n}}\right) \right] \right\} \Big|_{\hat{S}=z}. \end{aligned} \quad (352)$$

Because no closed-form solution is known to be available, the differentiation is performed numerically as follows:

$$f_z(z) = -\frac{d}{ds} (P_{ep}) \Big|_{\hat{s}=z}$$

$$= -\lim_{\Delta \hat{s} \rightarrow 0} \left[\frac{P_{ep}(\hat{s} + \Delta \hat{s}) - P_{ep}(\hat{s})}{\Delta \hat{s}} \right] \Big|_{\hat{s}=z}$$

$$\approx \left[\frac{P_{ep}(\hat{s}) - P_{ep}(\hat{s} + \Delta \hat{s})}{\Delta \hat{s}} \right] \Big|_{\hat{s}=z},$$

$$\Delta \hat{s} \ll 1 \quad . \quad (353)$$

This function has been numerically evaluated for atmospheric noise and a typical density function for $V_d = 9$ dB is illustrated by Figure 27.

The probability density of the impulsive noise component, i_n , can be similarly determined, except when I_n , the value assumed by i_n , is zero. For the case where $I_n \neq 0$, the random variable i_n simply replaces the random variable z in (353) where the complementary probability distribution, $P(E)$, is defined by the Power-Rayleigh portion of the APD curve (6). The special case where $I_n = 0$ requires

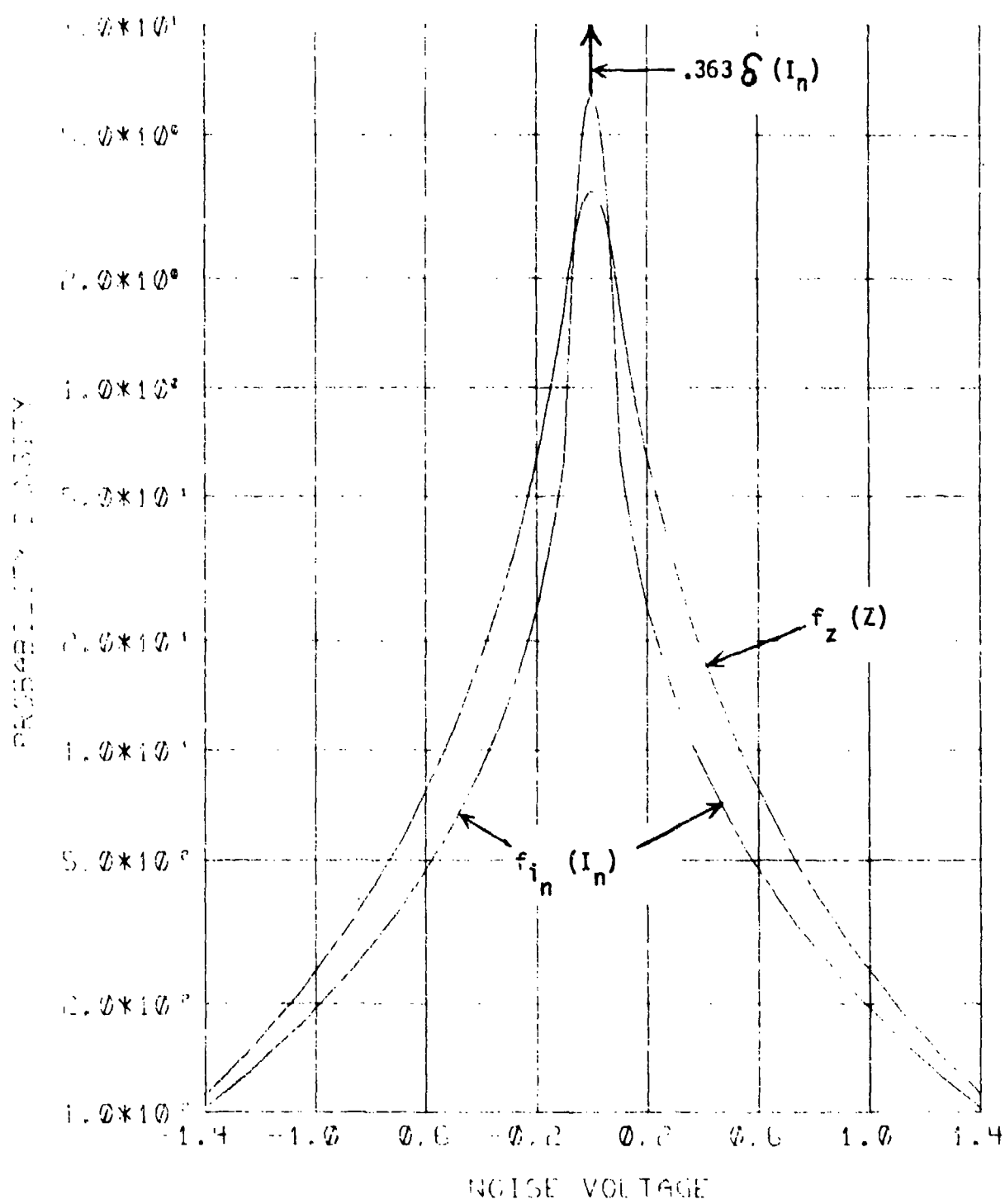


Figure 27. Noise Probability Densities, Atmospheric Noise Voltage, z , and Its Impulsive Component, i_n , ($V_d = 9 \text{ db}$).

particular attention. First, consider the characteristic function of the random variable, i_n :

$$F_{i_n}(j\xi) = E\left\{e^{-j\xi i_n}\right\}. \quad (354)$$

Substitution of (348) yields

$$F_{i_n}(j\xi) = E\left\{e^{-j\xi A \cos \theta_I}\right\} \quad (354a)$$

$$= \int_0^\infty dA \int_{-\pi}^{\pi} d\theta f_{a\theta_I}(A, \theta) e^{-j\xi A \cos \theta}.$$

Assuming A and θ_I to be statistically independent and θ_I to be uniformly distributed on $(-\pi, \pi)$.

$$F_{i_n}(j\xi) = \int_0^\infty f_a(A) dA \int_{-\pi}^{\pi} \frac{d\theta}{2\pi} e^{-j\xi A \cos \theta} \quad (355)$$

$$= \int_0^\infty J_0(\xi A) f_a(A) dA. \quad (356)$$

The inverse Fourier transformation yields

$$\begin{aligned} f_{in}(I_n) &= \frac{1}{2\pi} \int_{-\infty}^{\infty} F_{in}(j\xi) e^{j\xi I_n} d\xi \\ &= \frac{1}{2\pi} \int_{-\infty}^{\infty} e^{j\xi I_n} d\xi \int_0^{\infty} J_0(\xi A) f_a(A) dA. \quad (357) \end{aligned}$$

Hence,

$$\begin{aligned} f_{in}(0) &= \frac{1}{\pi} \int_0^{\infty} \frac{f_a(A) dA}{A} \int_0^{\infty} J_0(\xi A) d(\xi A) \\ &= \frac{1}{\pi} \int_0^{\infty} \frac{f_a(A) dA}{A}. \quad (358) \end{aligned}$$

Finally, substituting (10) in (358) yields

$$f_{in}(0) = \frac{1}{\pi} \int_0^{\infty} \frac{A^{3x-2}}{x \varepsilon^2} e^{-\frac{A^{2x}}{2\varepsilon^2}} dA. \quad (359)$$

It can be shown that this integral diverges [$f_{I_n}(0) = \infty$] for $X \geq 2$. This implies the existence of a singularity in $f_{I_n}(I_n)$ at $I_n = 0$ for $x \geq 2$. Because this range of X is of greatest importance for typical atmospheric noise, it is important that this singularity be accommodated in the numerical representation of $f_{I_n}(I_n)$, even if only approximately. This can be done as follows: First, the probability density function $f_{I_n}(I_n)$ must satisfy

$$\int_{-\infty}^{\infty} f_{I_n}(I_n) dI_n = 1. \quad (360)$$

Secondly, the expression

$$f_{I_n}(I_n) \approx \left[\frac{P_{ep}(\hat{s}) - P_{ep}(\hat{s} + \Delta\hat{s})}{\Delta\hat{s}} \right]_{\hat{s}=I_n}, \quad (361)$$

$$I_n \neq 0,$$

where P_{ep} is determined from (176a) with $P(A) = P_r(a > A)$, is bounded for all $I_n \neq 0$ provided $\Delta\hat{s} > 0$. Thus, it is possible to account for the singularity at $I_n = 0$ by utilizing the weighted impulse function

$$f_{I_n}(0) = d\delta(I_n), \quad (362)$$

where d is given by

$$d = 1 - \int_{-\infty}^{-\epsilon} f_{I_n}(I_n) dI_n - \int_{\epsilon}^{\infty} f_{I_n}(I_n) dI_n, \quad (363)$$

$0 < \epsilon \ll 1.$

Combining (361) and (362), the probability density function of the impulsive noise voltage is given by

$$f_{i_n}(I_n) \approx \begin{cases} d\delta(I_n), & I_n = 0 \\ \left[\frac{P_{ep}(\hat{s}) - P_{ep}(\hat{s} + \Delta\hat{s})}{\Delta\hat{s}} \right] & \hat{s} = I_n, \\ & I_n \neq 0, \end{cases} \quad (364)$$

where d is defined by (363) and P_{ep} by (176a) with

$$P(A) = P_r(a > A).$$

This density function for $V_d = 9$ dB is also plotted in Figure 27.

The continuous portion of this function is even, and the singularity, as previously discussed, is presented as a weighted impulse at the origin. It is readily apparent that this probability density for the impulsive noise voltage is much more centrally concentrated (about zero) than that of the total noise voltage.

6.3.3 Qualitative Estimate of the Residual Noise Component

The residual noise voltage, r_n , has been assumed to be statistically independent of i_n , the impulsive noise voltage. Therefore, (349) leads to

$$f_z(z) = f_{i_n}(z) * f_{r_n}(z) \quad (365)$$

where the operator $*$ is the convolution integral and $f_{rn}(R_n)$ is the probability density function of the residual noise voltage.

Proceeding to a Fourier transformation of both sides of this equation, the following relationship between the characteristic functions of z , i_n , and r_n is obtained:

$$F_z(j\zeta) = F_{i_n}(j\zeta) F_{r_n}(j\zeta). \quad (366)$$

This immediately leads to

$$F_{r_n}(j\zeta) = \frac{F_z(j\zeta)}{F_{i_n}(j\zeta)}. \quad (367)$$

Consequently,

$$f_{r_n}(R_n) = \frac{1}{2\pi} \int_{-\infty}^{\infty} \frac{F_z(j\zeta)}{F_{i_n}(j\zeta)} e^{jR_n\zeta} d\zeta. \quad (368)$$

Here, the qualitative observation of the preceding section becomes significant. Because the probability density function of the impulsive noise voltage, $f_{i_n}(I_n)$, tends to be extremely narrow, its Fourier transform, $F_{i_n}(j\zeta)$, tends to be relatively broad. In particular, if $f_{i_n}(I_n) \approx \delta(I_n)$, $F_{i_n}(j\zeta) \approx 1$. Assuming $F_{i_n}(j\zeta) \approx 1$,

$$F_{r_n}(j\zeta) = \frac{F_z(j\zeta)}{F_{i_n}(j\zeta)} \approx F_z(j\zeta). \quad (369)$$

The implication of this result is obvious: The probability density function of the residual noise voltage will be similar in form to that of the overall noise voltage. (If the final approximation of (369) were equality, then $f_{rn}(R_n) = f_z(R_n)$ because the Fourier transformation $\mathcal{F}^{-1}[F_z(j\omega)]$ is unique).

Unfortunately, the density functions $f_z(z)$ and $f_{in}(I_n)$ are defined numerically and not in closed form. Thus, sufficiently exact mathematical representations of the corresponding characteristic function $F_z(j\omega)$ and $F_{in}(j\omega)$ are very difficult to obtain such that the ratio $F_z(j\omega)/F_{in}(j\omega) [= F_{rn}(j\omega)]$ can be accurately computed. The final inverse transformation of the characteristic function $F_{rn}(j\omega)$ to the desired probability density $f_{rn}(R_n)$ introduces yet another source of computational inaccuracy. Hence, all attempts to perform the preceding Fourier transform operations numerically were unsuccessful.

6.3.4 "Best Fit" Synthesis

Because the numerical implementation of the Fourier transform approach was unsuccessful, an alternative approach to determine $f_{rn}(R_n)$ was undertaken. Expansion of (365) in terms of the density functions of the random variables yields

$$\begin{aligned} f_z(z) &= f_{in}(I_n) * f_{rn}(R_n) \\ &= \int_{-\infty}^{\infty} f_{in}(I_n) f_{rn}(z - I_n) dI_n. \end{aligned} \quad (370)$$

Here, the problem is to find a probability density function for the residual noise voltage, r_n , which satisfies (370). Although this implies a lengthy trial and error search, there are two characteristics of the random variable, r_n , which have already been determined:

(1) the mean square value of the residual noise voltage, $\overline{r_n^2}$, is related to the mean square total noise voltage $\overline{z^2}$ by the factor λ_r ; and (2) the probability density function of r_n is similar in form to that of z . This latter condition is not quantitatively definitive, but it suggests that "trial" residual voltage distributions might be chosen from the family of typical atmospheric noise distributions. The former condition, however, prescribes that the trial probability density function, $f_{rn}(R_n)$ be chosen such that $\overline{r_n^2} = \lambda_r \overline{z^2}$.

6.3.5 Numerical Convolution Process

The next step in determining $f_{rn}(R_n)$ is the evaluation of the convolution integral (370) for appropriate choices of $f_{rn}(R_n)$. This process yields corresponding density functions $f_z'(z)$ of the noise voltage, z' , synthesized as the sum of the impulsive voltage, i_n , and the trial residual voltage, r_n . Although the density function $f_{rn}(R_n)$ is actually continuous for all R_n , (353) only permits its evaluation at specific points, such as $R_n = m \Delta V$, $m = 0, \pm 1, \dots, \pm n$. On the other hand, $f_{in}(I_n)$, which has been shown to have a singularity at the origin under most conditions, is approximated by a weighted impulse at the origin and a continuous function elsewhere. For future

computations, it is convenient to modify $f_{in}(I_n)$ to the following representation:

$$f_{in}(I_n) = d' \delta(I_n) + \hat{f}_{in}(I_n), \quad (371)$$

where

$$d' = d - 2\epsilon f_{in}(\epsilon),$$

in accordance with the definitions of $f_{in}(\epsilon)$ and ϵ previously obtained (361), and $\hat{f}_{in}(I_n)$ is the continuous portion of $f_{in}(I_n)$.

The density function $\hat{f}_{in}(I_n)$ is now continuous for all I_n , so that $\hat{f}_{in}(I_n)$ can also be specified at specific points, such as $I_n = n \Delta V, n = 0, \pm 1, \dots$.

Substituting (371) into (370), the probability density of the synthesized noise voltage, z' , is given by

$$\begin{aligned} f_{z'}(z) &= \int_{-\infty}^{\infty} [d' \delta(I_n) + \hat{f}_{in}(I_n)] \times \\ &\quad \times f_{r_n}(z - I_n) dI_n \\ &= \int_{-\infty}^{\infty} d' \delta(I_n) f_{r_n}(z - I_n) dI_n \\ &\quad + \int_{-\infty}^{\infty} \hat{f}_{in}(I_n) f_{r_n}(z - I_n) dI_n. \end{aligned} \quad (372)$$

The first term of this equation yields

$$\int_{-\infty}^{\infty} d' \delta(I_n) f_{r_n}(z - I_n) dI_n = d' f_{r_n}(z). \quad (373)$$

The second integral, however, must be numerically evaluated.

For a specific value of z , (say $z = m\Delta V$, $m = 0, \pm 1, \dots$), the value of the integrand, $G(z, I_n)$, at $I_n = n\Delta V$, $n = 0, \pm 1, \dots$, is given by

$$G(z, n\Delta V) = \hat{f}_{i_n}[n\Delta V] f_{r_n}[(m-n)\Delta V] \quad (374)$$

These values of $G(z, I_n)$, which are equally spaced at an interval of ΔV volts, can be used to perform the integration by Simpson's Rule. This yields

$$\begin{aligned} \int_{-\infty}^{\infty} f_{i_n}(I_n) f_{r_n}(z - I_n) dI_n &\approx \\ \frac{\Delta V}{3} \left\{ G(z, -2N\Delta V) + G(z, 2N\Delta V) \right. \\ &\quad \left. + 2 \sum_{-N+1}^{N-1} [G(z, 2n\Delta V) + 2G(z, (2n+1)\Delta V)] \right\} \end{aligned} \quad (375)$$

where N is chosen sufficiently large that $G(z, \pm 2N\Delta V) \approx 0$.

Finally, combining these results yields

$$\begin{aligned} f_z'(m\Delta V) &\approx d' f_{r_m}(m\Delta V) + \\ &+ \frac{\Delta V}{3} \left\{ G(m\Delta V, -2N\Delta V) + \right. \\ &+ G(m\Delta V, 2N\Delta V) + \quad (376) \\ &+ 2 \sum_{n=-N+1}^{N+1} \left(G[m\Delta V, 2n\Delta V] \right. \\ &\quad \left. \left. + 2G[m\Delta V, (2n+1)\Delta V] \right) \right\}, \\ m &= 0, \pm 1, \pm 2, \dots. \end{aligned}$$

The final step is to compare the statistical description of the synthesized noise voltage, z' , with the original total noise voltage, z . Although it is ideally desirable to directly compare $f_z'(z)$ with $f_z(z)$, this process is tedious at best. As an alternative, it was determined that the V_d ratio and mean square values corresponding to z' could be computed and directly compared with those of the original noise voltage, z . The next section presents some specific results which illustrate the efficacy of this approach.

6.3.6 Estimation of Residual Noise Statistics

Consider again the specific case where the total noise has a V_d ratio of 9 dB and $\bar{z}^2 = .5$. (Recall that the probability density

functions of both the total noise voltage, z , and impulsive component noise, i_n , are depicted in Figure 27.) Here (342) and (344) indicate a hard limiting noise power reduction of 11.62 dB (Δ_r) according to the impulsive noise subtraction principle. Employing the techniques of Section 6.3.5 with an assumed residual noise component whose V_d ratio is 6 dB (appropriately reduced 11.62 dB in power) results in a synthesized noise voltage, z' , whose V_d ratio is approximately 9 dB, and whose mean square value is approximately .5. To illustrate, Figure 28 shows the probability density function of the impulsive noise voltage, i_n (corresponding to total noise whose V_d ratio is 9 dB), and the density function of the "best fit" residual noise voltage, r_n . These functions are then convolved by (376) to yield $f_{z'}(z)$, the synthesized noise density function. This result and the original total noise voltage density, $f_z(z)$, are shown in Figure 29. The close agreement of these density functions is obvious. This result provides quantitative substantiation of the preceding qualitative estimates of the residual noise characteristics. At this point, it is clear that this procedure might provide an improved basis for system performance analysis.

In addition to the example of atmospheric noise of $V_d = 9$ dB, the same procedure has been applied to derive a "best fit" residual noise description for other V_d values. A graph of these results is given in Figure 30 and specific values are listed in Table III.

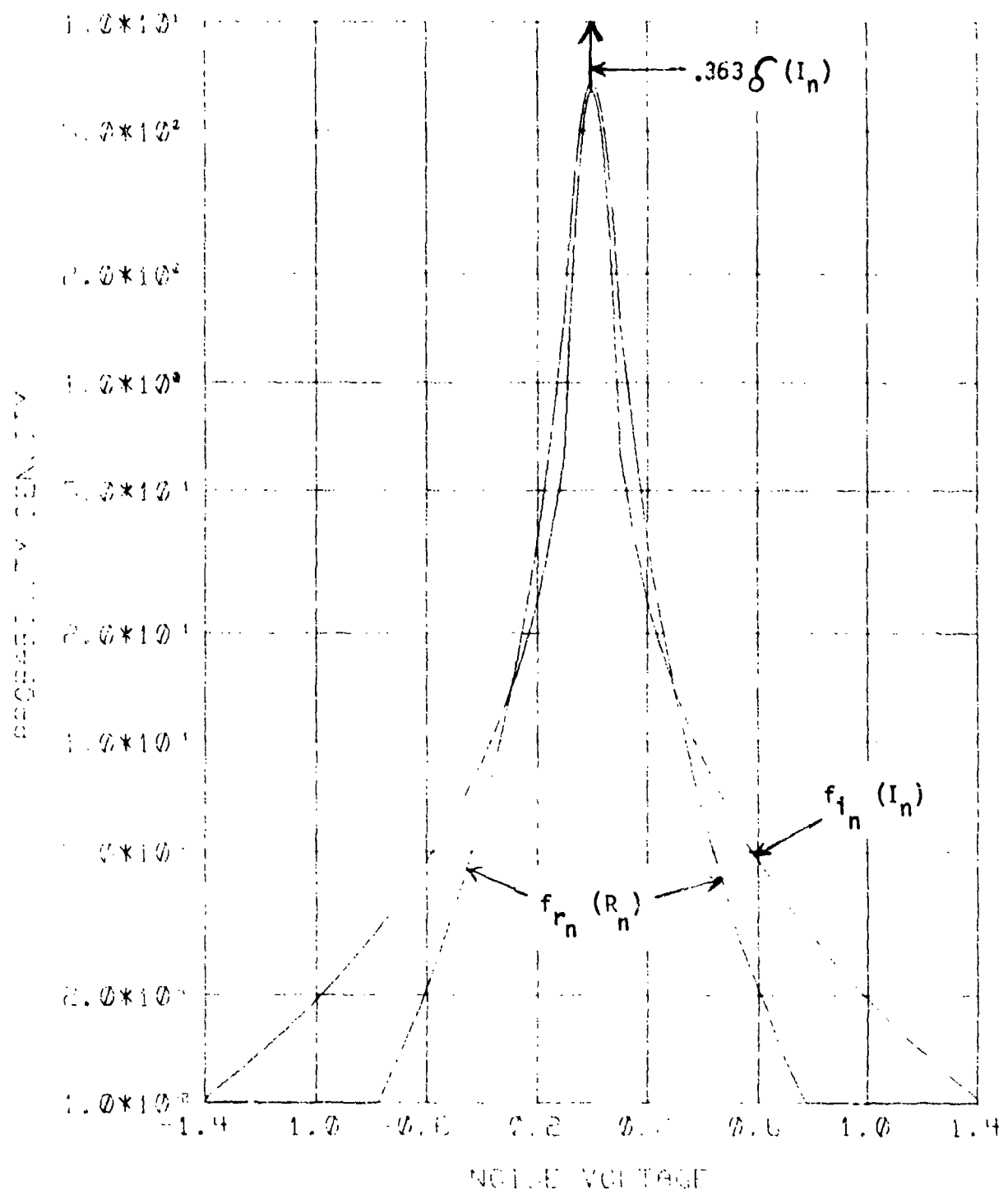


Figure 28. Probability Densities for Impulsive, i_n , and Residual, r_n , Noise Voltages ($V_d = 9$ db).

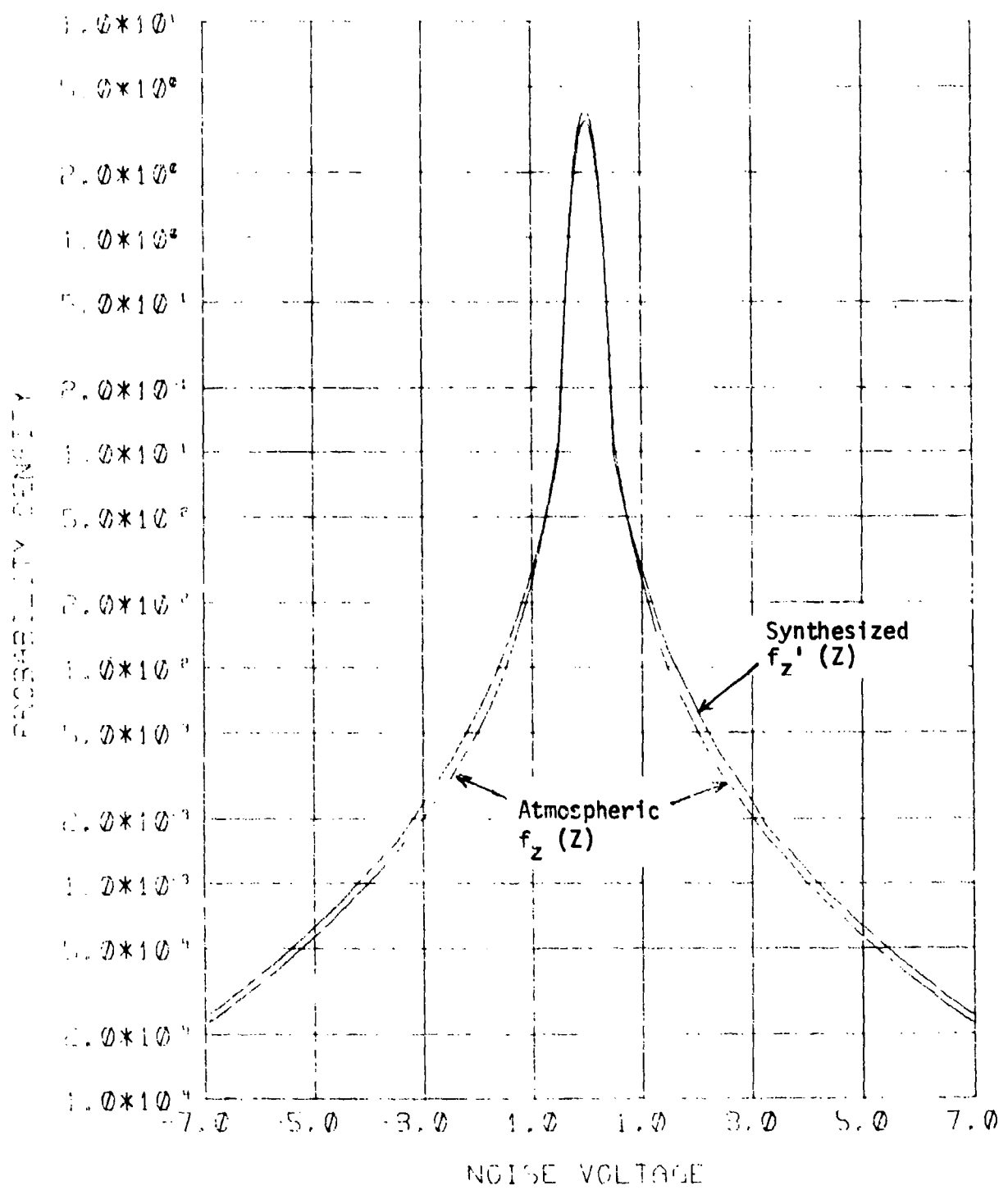


Figure 29. Probability Densities for Atmospheric, z , and
Synthesized, z' , Noise Voltages ($V_d = 9$ db).

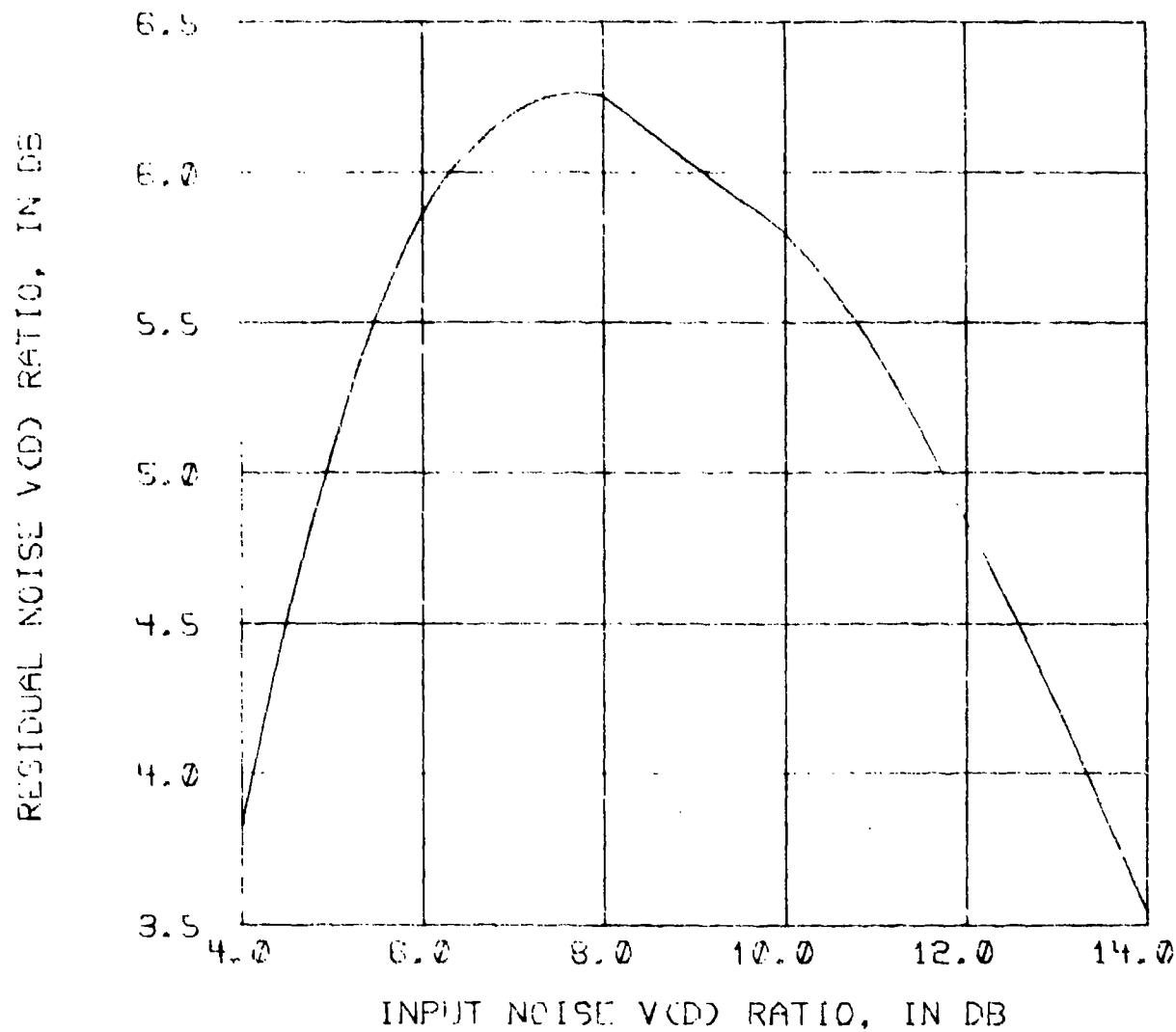


Figure 30. V_d Ratio of the Residual Noise Component Resulting From Impulsive Noise Subtraction (INS) Versus Input Noise V_d Ratio.

TABLE III. RESIDUAL NOISE OUTPUT OF
BANDPASS HARD LIMITER

Input Noise V_d Ratio (dB)	Output Noise Power/ Input Noise Power Δ_r (dB)	Residual Noise V_d Ratio (dB)
4.	- 3.026	3.831
6.	- 6.466	5.863
7.	- 8.139	6.198
8.	- 9.549	6.251
9.	-11.622	6.016
10.	-13.001	5.790
12.	-15.481	4.836
14.	-17.921	3.541

6.4 Application of Impulsive Noise Subtraction to System Analysis

At this point, it has been shown that Impulsive Noise Subtraction provides a quantitative basis for estimating the noise power reduction of hard limiting. Moreover, this hypothesis on the practical effect of limiting leads to a much more definitive description of the effective residual noise. That is, the residual noise voltage, which is assumed to be statistically independent of the additive impulsive noise component, is described closely by a probability density function corresponding to a typical atmospheric noise voltage (but at a lower V_d ratio and power). However, this result, although interesting, is inconclusive. To assess the efficacy of Impulsive Noise Subtraction in system analysis, it is necessary to apply the foregoing results to

practical systems. The subsequent discussion outlines this procedure and shows its application in three specific cases where published experimental results are available.

The residual noise at the output of a receiver bandpass hard-limiter is approximated by atmospheric noise of reduced power and impulsiveness. This noise, however, is defined at the limiter output and, consequently, in the limiter bandwidth (that is, in the bandwidth where limiting occurs and not after bandpass filtering of the limiter output). Thus, to relate the residual noise to the detection bandwidth, it is necessary to convert both the V_d ratio and the noise power to the detection bandwidth. The V_d ratio is converted by the procedure of Crichlow, Roudique, et al [11] as systematized in the Bandwidth Conversion Chart (Figure 26) of CCIR 322 [26]. Here, the entering arguments of bandwidth ratio (BWR) and V_d ratio of the residual noise are applied to obtain the V_d ratio of the noise in the detector equivalent noise bandwidth. (Recall that the equivalent noise bandwidths of the PSK, CFSK, and MSK detectors are $1/T$, $\pi^2/8T$, and $\pi^2/16T$, respectively, where the individual data elements (bits) are T seconds in duration.) The effective signal-to-noise ratio in the detection bandwidth is obtained by increasing the pre-limiting signal-to-noise ratio by $(-\Delta_r)$ (to account for the INS) and additionally increasing this post-limiting signal-to-noise ratio by the product of the limiter bandwidth and data element length (BWR). The final step is to employ the analytic procedures for linear detection of Chapter 3 in atmospheric noise having this final V_d ratio and enhanced signal-to-noise ratio. The INS procedure is illustrated in the following examples.

6.4.1 Example 1. (Hartley's Experimental Results)

As previously discussed, Hartley [22] presented both calculated and experimental results for a CFSK system where the BWR was large. Specifically, his experimental data was obtained under the following conditions:

- (1) Bandwidth Ratio (BWR) = 12
- (2) Noise V_d Ratio (600 Hz) = 9 dB
- (3) Coherent FSK ($M = 1$) modulation/detection
- (4) Hard Limiter Bandwidth = 600 Hz

The Impulsive Noise Subtraction technique is applied to the analysis of this system as follows:

(1) For noise of 9 dB V_d ratio at the limiter input, Table III gives a 6.016 dB V_d ratio and a power reduction of 11.522 dB for the output residual noise.

(2) Using the 6.016 dB residual noise V_d ratio and a BWR of 12, Figure 26 of CCIR 322 gives a V_d ratio of 2.65 for the noise as referenced to the CFSK equivalent noise bandwidth ($T^2/8T$).

(3) Appendix D gives decision error rates for linear PSK detection, and Tables D-VI and D-VII, error rates for $V_d = 2.5$ and 2.75, respectively.

(4) Now recalling that linear CFSK detection has been shown to be 3 dB less efficient than linear PSK detection, each signal-to-noise ratio in Tables D-VI and D-VII must be increased by 3 dB to reflect CFSK performance for each error rate. Linear interpolation then yields the bit error rate for an effective (CFSK detection) V_d ratio of 2.65 dB.

(5) Finally, the noise reduction factor, Λ_r , of -11.622 dB (from Table III for $V_d = 9$. dB) must be applied to the CFSK signal-to-noise ratios as established in the preceding step.

The resultant bit error rate is plotted in Figure 31 with Hartley's measured data superimposed. Note the close agreement between the measured and computed performance of this system.

6.4.2 Example 2. (Linfield and Beach's Experimental Results)

In addition to Hartley [22], Linfield and Beach [33] have published some experimental results for detection of coherent FSK (CFSK) signals where a high BWR hard-limiting receiver is employed. In addition, a plot of the corresponding noise statistics is given. It should be noted that there is a very limited number of data points in the low amplitude region so that the placement of the Rayleigh portion of this measured APD is somewhat arbitrary. On the other hand, there are more than sufficient data points to define the placement and slope of the steep, Power Rayleigh portion of the APD. Based on this well-defined slope ($X/2$) of the impulsive portion of the APD and the most probable relationship between V_d and X as defined by Crichlow [10], [11], the V_d ratio of the atmospheric noise is estimated to be 13 dB (as referenced to the 751 Hz receiver noise bandwidth). The other significant parameter in this experimental system was the BWR of 37.55 (that is, each binary element was 50 msec., in duration).

Using these system parameters and quadratic interpolation in Table III, a noise reduction factor of $\Lambda_r = -16.7$ dB and a residual noise $V_d = 4.25$ dB are obtained. In turn, Figure 26 of CCIR 322 yields

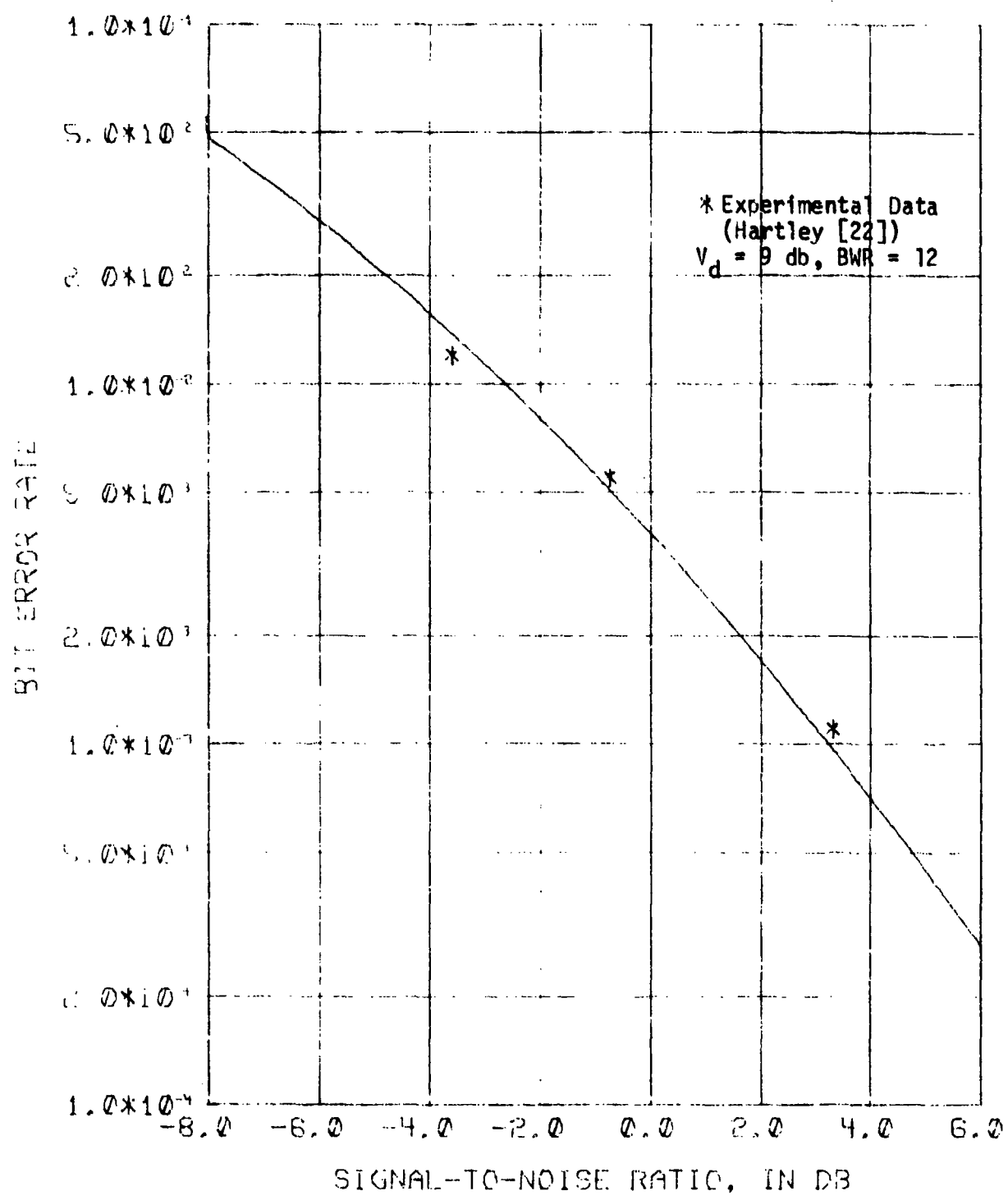


Figure 31. CFSK Hard Limiting Receiver Performance in Atmospheric Noise Computed by Impulsive Noise Subtraction (INS).

a V_d ratio of 1.65 dB for the BWR of 37.55. Next, application of the CFSK equivalent noise bandwidth ratio of ($\pi^2/8$) yields an effective post-detection noise V_d ratio of 1.75 dB. Employing Table D-III ($V_d = 1.75$), the 3 dB performance differential (for CFSK operation), and the $A_r = -16.7$ dB noise reduction factor, the desired bit error rate is obtained. This is plotted in Figure 32 with the measured experimental data superimposed. Here again, there is agreement within about 2 dB throughout the probability range. Although this agreement is not as close as with Hartley's results, it is much closer in placement and, especially, slope than other computational estimates heretofore available.

These practical examples show clear experimental substantiation of the Impulsive Noise Subtraction technique for system analysis. Moreover, these examples demonstrate its application for BWR's of 12 and 37.55, and the close agreement with experimental results in both cases implies that this technique is applicable over a wide range - at least from 12 to 37.55, inclusive. However, a third example is presented to assess the quantitative validity of this approach for much smaller BWR's.

6.4.3 Example 3. (Small Bandwidth Ratio Experimental Results)

Here the Impulsive Noise Subtraction technique is applied to the experimental system previously evaluated by pulse statistical analysis (PSA) for a small BWR. Specifically, the system parameters and experimental data are those whose PSA evaluation appears in Figure 21 ($K = 1$). These experimental conditions are:

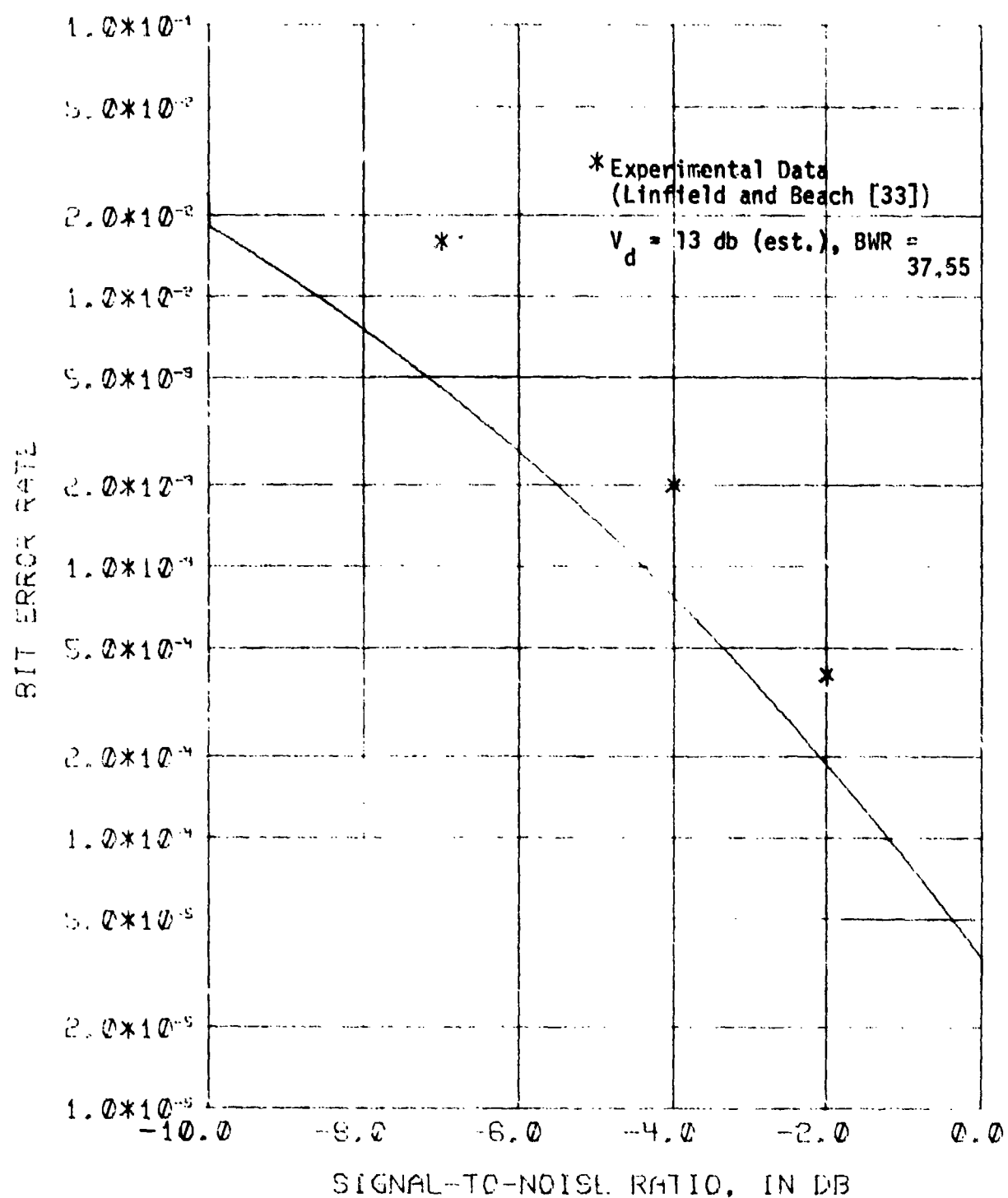


Figure 32. CFSK Hard Limiting Receiver Performance in Atmospheric Noise Computed by Impulsive Noise Subtraction (INS).

- (1) Bandwidth Ratio (BWR) = 3.7
- (2) Noise V_d Ratio (600 Hz) = 9. dB
- (3) Coherent FSK ($M = 1$) modulation/detection
- (4) Coherent CSK (MSK Functional) modulation/detection
- (5) Hard Limiter Bandwidth = 185 Hz

This analysis proceeds as follows:

- (1) From Figure 26, CCIR 322, the V_d ratio of the noise in the limiter bandwidth (by the ratio 600 Hz/185 Hz = 3.24) is 5.5 dB.
- (2) By quadratic interpolation in Table III, the noise power reduction, Δ_{r_s} , is -6.385 dB and the residual noise V_d ratio is 5.25 dB.
- (3) Using $BWR = 3.7$, the CFSK equivalent noise bandwidth conversion factor ($\pi^2/8$), and the residual noise $V_d = 5.25$ dB in Figure 26, CCIR 322 [26], the V_d ratio in the CFSK noise bandwidth is 3.35 dB. In the case of the MSK functional, the equivalent noise bandwidth is half that of the CFSK detector so that the BWR for the MSK functional is 7.4 yielding a $V_d = 2.75$ dB for the noise in the MSK noise bandwidth.
- (4) Interpolating the data from Tables D-IX ($V_d = 3.25$) and D-X ($V_d = 3.5$) yields the PSK decision error rate as a function of signal-to-noise ratio. Now applying the 3 dB correction for CFSK detection, and -6.385 dB noise reduction for hard-limiting, the CFSK decision error rate is determined.
- (5) Also, using Table DV-II gives the PSK decision error rate for $V_d = 2.75$ dB. This, as has been shown, is also the MSK decision error rate.

(6) Finally, the character error rates for CFSK and CSK demodulation are calculated according to (179) and (319), respectively.

These results are plotted in Figure 33 with measured data values superimposed. Also, error rates calculated by PSA for $K = 1.0$ (from Figure 21) are included in Figure 33. A comparison of these INS results with those of PSA readily shows that the INS method yields error rates substantially greater than those computed by PSA; these INS estimates also show much poorer agreement with the measured data, especially for the CSK system. Moreover, it should be noted that the INS analysis suggests that the performance differential between CFSK and CSK is only about 3 dB whereas both the PSA computations and the measured data clearly show that this differential is about 6 dB. Thus, the results of Example 3 definitely show that INS is much less accurate than PSA for small BWR's; in fact, it should be considered inappropriate for BWR's on the order of 8 or less.

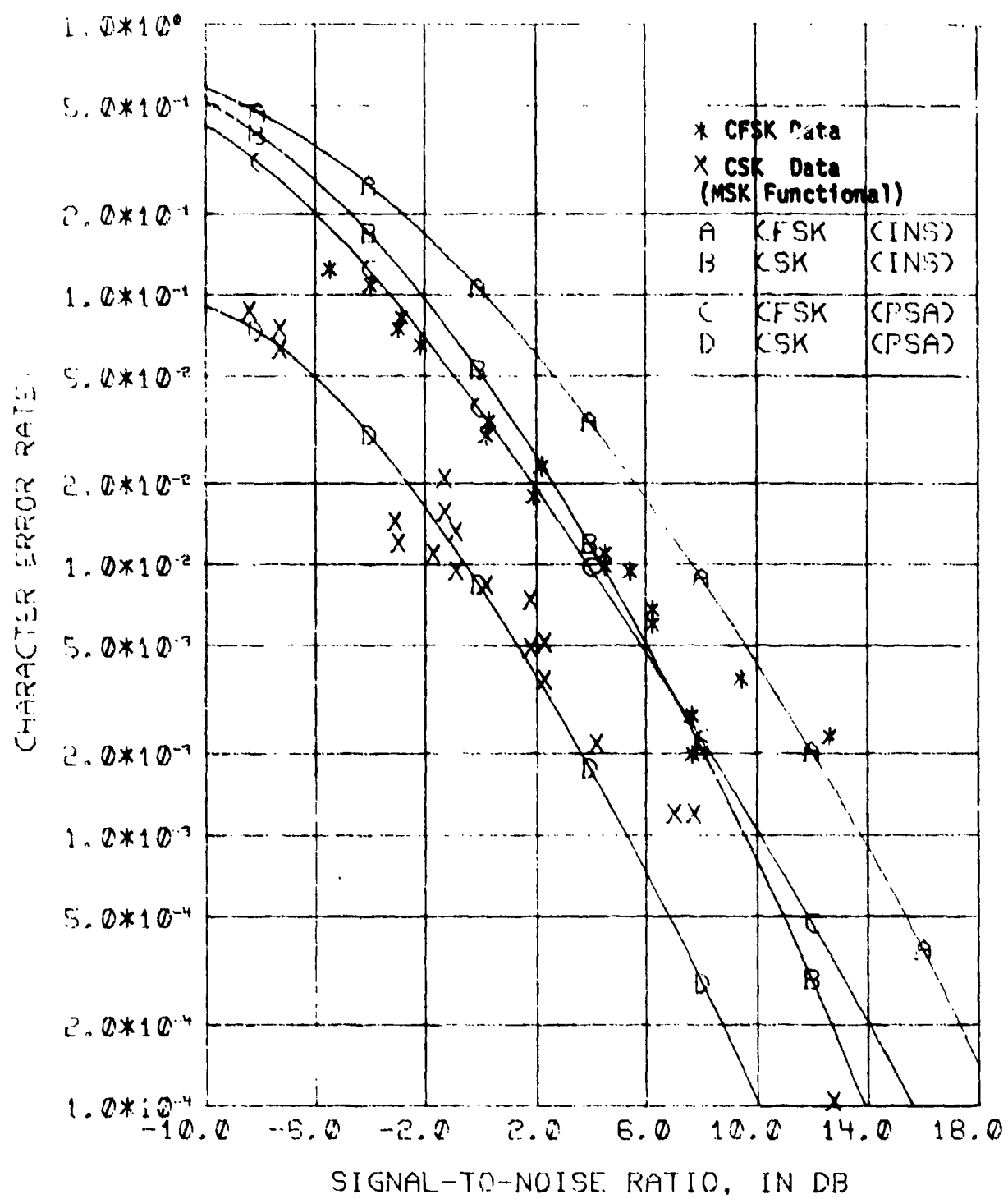


Figure 33. CFSK and CSK System Performance as Measured and as Computed by Pulse Statistical Analysis (PSA) and Impulsive Noise Subtraction (INS) (Atmospheric Noise $8 \text{ db} \leq V_d \leq 9.9 \text{ db}$, CFSK BWR = 3.7, CSK BWR = 7.4).

Chapter 7

CONCLUSIONS AND RECOMMENDATIONS

7.1 Overview

This chapter presents a summary of the significant conclusions and limitations of this investigation and areas where additional investigations would be valuable. The list of conclusions is divided into two main sections: (1) those dealing with the performance analyses of linear receiver systems, and (2) those dealing with the performance analyses of hard-limiting receiver systems. In turn, the latter section summarizes the development, validation, and limitations of the two non-linear analysis techniques, Pulse Statistical Analysis (PSA) and Impulsive Noise Subtraction (INS). The second major section of this chapter presents topics for further investigation which might enhance the analytical results presented in this report or might contribute to improvements in future communication system design and analyses.

7.2 Results and Conclusions

7.2.1 Linear Systems Analyses

The results and conclusions pertinent to the analyses of linear coherent detection in atmospheric noise are developed in Chapters 3 and 4 of this report. Because truly linear receivers are less efficient in impulsive atmospheric noise than various non-linear

receivers, including the hard-limiting receivers analyzed in this dissertation, they are not as widely employed for VLF/LF FSK communications. Nevertheless, the analyses of the linear receivers provide important insights into the operation of more optimum non-linear receivers. Moreover, the quantitative results obtained here are specifically applicable to the analysis of spread spectrum systems where receiver linearity is essential.

7.2.1.1 Coherent PSK Detector Functional

The first result of the linear system analyses is the development of usable mathematical expressions for the coherent biphasic PSK detector output (known as the detector functional), its relationship to tabulated atmospheric noise statistics, and the consequent detection error probability expressions. In addition, an accurate numerical procedure is developed to evaluate the PSK error probability for both Gaussian and non-Gaussian atmospheric noise.

7.2.1.2 Coherent FSK ($M = 1$) Detector

The CFSK post-detection signal-to-noise ratio is 1/2 that of the PSK system and impulsiveness (V_d ratio) of the CFSK noise corresponds to a bandwidth $\pi^2/8$ times as great as for the PSK detector. This factor of $\pi^2/8$ is the ratio of the equivalent noise bandwidths of the CFSK and PSK detectors, respectively.

7.2.1.3 MSK Detector

The MSK detector functional is of the same mathematical form as the CFSK functional, except that the time durations are doubled for a given data transmission rate. This means that the equivalent noise

bandwidth of the MSK detector is 1/2 that of the CFSK detector. Since the MSK and CFSK post detection signal voltages are equal in magnitude, the narrower MSK noise bandwidth results in the MSK detector having a 3 dB higher signal-to-noise ratio. Moreover, the MSK post-detection noise is less impulsive than the CFSK noise because the V_d ratio of the MSK post-detection noise corresponds to a bandwidth which is 1/2 that of CFSK post-detection noise.

7.2.1.4 Experimental Validation of the Linear Performance Calculations

Measured PSK bit error rates and CFSK and MSK teletype character error rates are in very good agreement with error rates as computed by the linear system analyses.

7.2.1.5 Comparison of Linear Systems

Based on bit error rate characteristics computed for various V_d ratios, it is apparent that the error rate characteristics become flatter with increasing V_d ratio. Thus, significantly more signal power is required for a given low error probability as the V_d ratio increases. Because the MSK post-detection signal-to-noise ratio equals that of the PSK system (3 dB greater than the CFSK system) and has a V_d ratio corresponding to a noise bandwidth $\pi^2/16$ that of the PSK detector (1/2 that of the CFSK detector), the MSK detector exceeds both the PSK and CFSK detector's non-Gaussian atmospheric noise efficiency. (In Gaussian noise, the MSK and PSK detectors are equal in efficiency and 3 dB better than the CFSK detector.)

2.2 Non-Linear (Hard-Limiting Receiver) System Analyses

The non-linear technique considered in this study is that of receiver pre-detection bandpass limiting where both signal and noise are limited to the extent that the limiter output waveform is rectangular. The effect of this pre-detection hard-limiting is to reduce impulsive noise power at the detector input. For an impulsive atmospheric noise input, this results in a significant signal-to-noise ratio enhancement at the detector input and a consequent improvement in overall system efficiency.

The analyses of hard-limiting coherent receiver performance are developed in Chapters 5 and 6. The first technique, Pulse Statistical Analysis (PSA), is based on the hypothesis that detection errors are caused almost exclusively by a small number of high-amplitude noise pulses occurring within a given detection element. On the other hand, the second technique, Impulsive Noise Subtraction (INS) is based on the hypothesis that the hard-limiter effectively subtracts the impulsive component of the noise so that the limiter output consists of the signal and a residual noise component. In this case, error probabilities are governed by the statistics of the residual noise component.

7.2.2.1 Analyses of Small Bandwidth Ratio (BWR) Systems by Pulse

Statistical Analysis (PSA)

The PSA technique is based on the probability that a small number of distinct received noise pulses per bit will produce a decision (or bit) error. It is assumed that the amplitudes of these isolated pulses exceed the signal amplitude sufficiently to cause the phas-

(zero-crossings) of the limiter output to coincide with the noise during a noise pulse and with the signal otherwise. The duration of these "noise capture" intervals is a function of the noise pulse amplitudes and the pre-limiter receiver filter bandwidth. The ratio of this pre-limiter bandwidth to the detection bandwidth is designated as the bandwidth ratio (BWR).

7.2.2.1.1 PSA Development

The PSA technique is developed on the basis of isolated high-amplitude noise pulses whose amplitudes within a given bit are assumed to be monotonically related by a power-Rayleigh-derived ratio. On the other hand, the RF phase of each noise pulse is assumed to be constant during the limiter "capture" interval and the phases of the pulses are assumed to be statistically independent. Noise pulse amplitudes, and consequent limiter capture intervals, are based on atmospheric noise APD's. Pulse occurrence rates are computed by an empirically derived power-law. From these occurrence rates, Poisson pulse distributions are defined and error rates are computed by this statistical distribution.

7.2.2.1.2 Quantitative Convergence of Error Rates Computed by Poisson and "Clustering" Statistical Distribution

Because received noise pulses resulting from multiple strokes of a single lightning discharge have statistically dependent occurrence times ("Clustering" pulse statistical distribution), a Poisson pulse statistical distribution (implying statistically

independent occurrence times) is not physically exact. However, error rate characteristics computed by each of these statistical distributions are nearly identical. Hence, either model is quantitatively accurate.

7.2.2.1.3 Experimental Validation of PSA for CFSK and CSK (MSK Detection Systems)

Measured CFSK and CSK (MSK detection, differential post-detection logic) teletype character error rates are in very good agreement with error rates as calculated by PSA for V_d ratios of 6-14 dB (in a 600 Hz measurement bandwidth) and BWR's of 3.7 and 7.4. This agreement holds for character error rates between .01% and approximately 30% (which corresponds to an approximate bit error range between .0017% and 6%).

7.2.2.1.4 Performance Differential Between CFSK and CSK (MSK Detection) Performance

Computational estimates made by other investigators which merely modify linear or Gaussian-noise performance analyses to account for non-linear receiver performance in atmospheric noise, indicate an approximate 3 dB differential between CFSK and CSK performance. The PSA computations, on the other hand, are accurately consistent with the 6 dB differential obtained by extensive experiments.

7.2.2.1.5 BWR Limitation of PSA

The close correspondence of error rates calculated by PSA and experimentally measured for BWR's of 3.7 and 7.4 indicates that PSA is valid for BWR's up to approximately 8. However, CFSK bit error rates computed by PSA for a BWR of 12 show very poor agreement with experimental data. Hence, PSA is of questionable accuracy for BWR's greater than 8 and clearly inaccurate for BWR's as great as 12.

7.2.2.2 INS Development

In the case where the BWR is large and the noise process is approximately white, an acceptable signal-to-noise ratio in the detection bandwidth is obtained even with a very small signal-to-noise ratio in the pre-limiter bandwidth. Moreover, this much greater pre-limiter bandwidth causes the pulselwidth of a received impulse to be a very small fraction of the reciprocal of the detection bandwidth. Hence, large-amplitude, individual noise impulses have minimal effect on error probabilities. On the other hand, the residual noise component accompanying the individual impulses is the principal cause of decision errors.

7.2.2.2.1 Enhancement of Small Signal-to-Noise Ratios in

Atmospheric Noise by Hard-Limiting

Small-signal estimates of post-limiting signal-to-noise ratios indicate that signal-to-noise ratios are dramatically increased by hard-limiting. The quantitative effect varies directly with the V_d ratio of the pre-limiting noise. It is approximated by directly subtracting the impulsive noise power represented by the steep power-Rayleigh portion of the APD while maintaining constant signal power.

7.2.2.2 Residual Noise Component

"Best-fit" approximations of the probability density of the limiter input noise are obtained by numerically convolving impulsive noise (Power Rayleigh APD) voltage probability densities with trial residual noise voltage densities. The resultant residual noise voltages are non-Gaussian, significantly impulsive and statistically similar to typical atmospheric noise.

7.2.2.3 Experimental Validation of the INS Technique

CFSK bit error rate characteristics computed by INS correspond closely in both placement and slope to experimental data for BWR's of 12 and 37.55. The close correspondence implies that INS is quantitatively valid for $12 \leq \text{BWR} \leq 37.55$.

7.2.2.4 BWR Limitation of INS

Character error rates computed by INS for CFSK at a BWR of 3.7 and for CSK at a BWR of 7.4 show very poor agreement with measured experimental results. Thus, INS is of questionable accuracy for BWR's less than 12 and inaccurate for BWR's of 8 or lower.

7.2.2.3 General Conclusions Concerning Non Linear System Performance

7.2.2.3.1 MSK detection (as implemented in the experimental CSK system) is clearly more efficient than CFSK detection in a hard-limiting receiver.

7.2.2.3.2 In the case of small-signal-to-noise ratios, noise reduction obtained by hard-limiting increases markedly as the noise V_d ratio increases. Because the V_d ratio also increases with bandwidth, increasing the limiter bandwidth (or receiver BWR) greatly increases

the effectiveness of hard-limiting noise reduction. The practical constraint on this strategy is the need for sufficient receiver selectivity to exclude other signals and non-impulsive interference.

7.2.2.4 General Limitations of PSA and INS

7.2.2.4.1 Incomplete BWR Range

Both PSA and INS are of questionable accuracy for
 $8 \leq \text{BWR} \leq 12$.

7.2.2.4.2 Limited Range of Experimentally Validated Error Rates

Because of limited experimental data, only character error rates greater than 10^{-4} have been experimentally validated.

7.3 Recommendations for Extensions and Additions to the Investigations

7.3.1 The first recommendation is to investigate the statistical independence of time adjacent observations of the atmospheric noise voltage. Numerical "best-fit" probability density syntheses described in 3.3.2.2.1 imply that an appropriate time division of the PSK detector noise functional may yield statistically independent sample noise voltages. Further analyses and syntheses validated by experimental measurements, and possibly employing characteristic functions, would establish bounds on the validity of this principle and provide valuable quantitative data for receiver and modem designs and performance analyses.

7.3.2 A second recommendation is to develop a unified analytical procedure wherein the pulse statistical analysis and impulsive noise subtraction techniques are suitably merged to accommodate any practical receiver BWR.

7.3.3 A third recommendation is that a measurement program be undertaken to obtain atmospheric noise bit error rates substantially lower than the 10^{-5} now available. Such an effort might require the development and validation of realistic atmospheric noise simulators to provide a stationary noise source.

APPENDIX A

Derivations of Selected Integrals

A1.

$$\int_{-\frac{T}{2}}^{\frac{T}{2}} \cos at e^{-j\omega t} dt$$

$$= \frac{e^{-j\omega T}}{a^2 - \omega^2} \left[-j\omega \cos at + a \sin at \right]_{-\frac{T}{2}}^{\frac{T}{2}}$$

$$= \frac{1}{a^2 - \omega^2} \left\{ -j\omega \left[e^{-j\omega \frac{T}{2}} - e^{j\omega \frac{T}{2}} \right] \cos \frac{at}{2} \right. \\ \left. + a \left[e^{-j\omega \frac{T}{2}} + e^{j\omega \frac{T}{2}} \right] \sin \frac{at}{2} \right\}$$

$$= \frac{2}{a^2 - \omega^2} \left\{ a \sin \frac{at}{2} \cos \frac{\omega T}{2} \right. \\ \left. - \omega \sin \frac{\omega T}{2} \cos \frac{at}{2} \right\}$$

$$= \frac{1}{(a+\omega)(a-\omega)} \left\{ a \sin(a+\omega) \frac{T}{2} \right. \\ \left. + a \sin(a-\omega) \frac{T}{2} \right. \\ \left. - \omega \sin(a+\omega) \frac{T}{2} \right. \\ \left. + \omega \sin(a-\omega) \frac{T}{2} \right\}$$

Hence,

$$\int_{-\frac{T}{2}}^{\frac{T}{2}} \cos at e^{-j\omega t} dt = \frac{\sin(a+\omega)\frac{T}{2}}{(a+\omega)} + \frac{\sin(a-\omega)\frac{T}{2}}{(a-\omega)}. \quad (\text{A1})$$

A2.

$$\begin{aligned} & \int_{-\frac{T}{2}}^{\frac{T}{2}} \sin at e^{-j\omega t} dt \\ &= \frac{e^{-j\omega t}}{a^2 - \omega^2} \left[-j\omega \sin at - a \cos at \right]_{-\frac{T}{2}}^{\frac{T}{2}} \\ &= \frac{1}{a^2 - \omega^2} \left\{ j\omega \left[e^{-j\omega \frac{T}{2}} + e^{j\omega \frac{T}{2}} \right] \sin \frac{aT}{2} \right. \\ &\quad \left. - a \left[e^{-j\omega \frac{T}{2}} - e^{j\omega \frac{T}{2}} \right] \cos \frac{aT}{2} \right\} \\ &= \frac{2}{a^2 - \omega^2} \left\{ -j\omega \sin \frac{aT}{2} \cos \frac{\omega T}{2} \right. \\ &\quad \left. + ja \sin \frac{\omega T}{2} \cos \frac{aT}{2} \right\}, \end{aligned}$$

$$= \frac{j}{(\alpha+\omega)(\alpha-\omega)} \left\{ -\omega \sin(\alpha-\omega) \frac{I}{2} \right. \\ \left. - \omega \sin(\alpha+\omega) \frac{I}{2} \right. \\ \left. + \alpha \sin(\alpha+\omega) \frac{I}{2} \right. \\ \left. - \alpha \sin(\alpha-\omega) \frac{I}{2} \right\}.$$

Hence,

$$\int_{-\frac{I}{2}}^{\frac{I}{2}} \sin at e^{-j\omega t} dt = j \left\{ \frac{\sin(\alpha+\omega) \frac{I}{2}}{(\alpha+\omega)} \right. \\ \left. - \frac{\sin(\alpha-\omega) \frac{I}{2}}{(\alpha-\omega)} \right\}. \quad (\text{A2})$$

A3.

$$\begin{aligned} & \int_0^\infty \frac{e^{-\frac{x^2}{2b^2}}}{b^2 + x^2} dx \\ &= \frac{1}{2} \int_{-\infty}^\infty \frac{e^{-\frac{x^2}{2b^2}}}{b^2 + x^2} dx \\ &= \pi \left(\frac{1}{2\pi} \right) \int_{-\infty}^\infty \frac{e^{-\frac{x^2}{2b^2}} e^{jxt}}{b^2 + x^2} dx \Big|_{t=0} \\ e^{-\frac{x^2}{2b^2}} &= \int_{-\infty}^\infty \frac{1}{\sqrt{2\pi}} e^{-\frac{\sigma^2 t^2}{2}} e^{-jxt} dt \\ &= \int_{-\infty}^\infty f(t) e^{-jxt} dt = F(jx), \end{aligned}$$

where

$$f(t) = \frac{1}{\sqrt{2\pi}} e^{-\frac{\sigma^2 t^2}{2}}.$$

Also, from (A4),

$$\begin{aligned} \frac{1}{b^2 + x^2} &= \int_{-\infty}^\infty \frac{e^{-b|t|}}{2b} e^{jxt} dt \\ &= \int_{-\infty}^\infty g(t) e^{-jxt} dt = G(jx), \end{aligned}$$

where

$$g(t) = \frac{1}{2b} e^{-b|t|}.$$

By the convolution theorem,

$$\begin{aligned}& \pi \left[\frac{1}{2\pi} \int_{-\infty}^{\infty} \frac{e^{-\frac{x^2}{2b^2}} e^{jxt}}{b^2 + x^2} dx \right] \\&= \pi \left[\frac{1}{2\pi} \int_{-\infty}^{\infty} F(jx) G(jx) e^{jxt} dx \right] \\&= \pi f(t) * g(t) = \pi \int_{-\infty}^{\infty} f(t-\tau) g(\tau) d\tau \\&= \frac{\pi}{2b} \int_{-\infty}^{\infty} \frac{6}{\sqrt{2\pi}} e^{-\frac{6^2(t-\tau)^2}{2}} e^{-b|\tau|} d\tau.\end{aligned}$$

Evaluation for $t = 0$ yields

$$\frac{\pi}{2b} \left[\frac{1}{2\pi} \int_{-\infty}^{\infty} \frac{e^{-\frac{x^2}{2b^2}} e^{ixt}}{b^2 + x^2} dx \right]_{t=0}$$

$$= \frac{\pi}{2b} \int_{-\infty}^{\infty} \frac{6}{\sqrt{2\pi}} e^{-\frac{z^2}{2}} e^{-bz} dz$$

$$= \frac{\pi}{b} \int_0^{\infty} \frac{6}{\sqrt{2\pi}} e^{-b^2 z^2} e^{-bz} dz$$

$$= \frac{\pi}{b} e^{\frac{b^2}{2\sigma^2}} \int_0^{\infty} \frac{6}{\sqrt{2\pi}} e^{-\frac{\sigma^2}{2}(z + \frac{b}{\sigma^2})^2} dz$$

$$= \frac{\pi}{2b} e^{\frac{b^2}{2\sigma^2}} \cdot \frac{2}{\sqrt{\pi}} \int_{\frac{b}{\sqrt{2}\sigma}}^{\infty} e^{-u^2} du.$$

Hence,

$$\int_0^\infty \frac{e^{-\frac{x^2}{2b^2}} dx}{b^2 + x^2} = \frac{\pi}{2b} e^{\frac{b^2}{2b^2}} \left[1 - \Phi\left(\frac{b}{\sqrt{2}b}\right) \right], \quad (\text{A3})$$

where

$$\Phi(z) = \frac{2}{\sqrt{\pi}} \int_0^z e^{-t^2} dt.$$

A4.

$$\begin{aligned} \int_{-\infty}^{\infty} \frac{e^{j\omega t}}{b^2 + \omega^2} d\omega &= \frac{1}{2jb} \int_{-\infty}^{\infty} \left[\frac{1}{\omega - jb} - \frac{1}{\omega + jb} \right] e^{j\omega t} d\omega \\ &= \begin{cases} \frac{\pi}{b} e^{-bt}, & t \geq 0 \\ \frac{\pi}{b} e^{bt}, & t < 0 \end{cases} \\ &= \frac{\pi}{b} e^{-b|t|}. \end{aligned} \quad (\text{A4})$$

A5.

$$\begin{aligned} & \int_0^T dt_1 \int_0^T dt_2 e^{-b|t_1 - t_2|} \sin \frac{\pi t_1}{T} \sin \frac{\pi t_2}{T} \\ &= \int_0^T \sin \frac{\pi t_1}{T} dt_1 \left[e^{-bt_1} \int_0^{t_1} e^{bt_2} \sin \frac{\pi t_2}{T} dt_2 \right. \\ &\quad \left. + e^{bt_1} \int_{t_1}^T e^{-bt_2} \sin \frac{\pi t_2}{T} dt_2 \right] \\ &= \int_0^T \sin \frac{\pi t_1}{T} dt_1 \left\{ \left[\frac{e^{-bt_1} e^{bt_2}}{b^2 + \frac{\pi^2}{T^2}} \left(b \sin \frac{\pi t_2}{T} \right. \right. \right. \\ &\quad \left. \left. \left. - \frac{\pi}{T} \cos \frac{\pi t_2}{T} \right) \right]_{t_1}^T \right. \\ &\quad \left. + \left[\frac{e^{bt_1} e^{-bt_2}}{b^2 + \frac{\pi^2}{T^2}} \left(-b \sin \frac{\pi t_2}{T} \right. \right. \right. \\ &\quad \left. \left. \left. - \frac{\pi}{T} \cos \frac{\pi t_2}{T} \right) \right]_{t_1}^T \right\} \\ &= \frac{1}{b^2 + \frac{\pi^2}{T^2}} \int_0^T \sin \frac{\pi t_1}{T} \left[2b \sin \frac{\pi t_1}{T} + \frac{\pi}{T} e^{-bT} e^{bt_1} \right. \\ &\quad \left. + \frac{\pi}{T} e^{-bt_1} \right] dt_1, \end{aligned}$$

$$\begin{aligned}
&= \frac{1}{b^2 + \frac{\pi^2}{T^2}} \left[bt_1 - \frac{bT}{\pi} \sin \frac{2\pi t_1}{T} \right. \\
&\quad + \frac{\frac{\pi}{T}}{b^2 + \frac{\pi^2}{T^2}} \left\{ b e^{-bt_1} e^{bt_1} \sin \frac{\pi t_1}{T} \right. \\
&\quad \left. - \frac{\pi}{T} e^{-bt_1} e^{bt_1} \cos \frac{\pi t_1}{T} \right. \\
&\quad \left. - b e^{-bt_1} \sin \frac{\pi t_1}{T} \right. \\
&\quad \left. - \frac{\pi}{T} e^{-bt_1} \cos \frac{\pi t_1}{T} \right\} \Big]_0^T
\end{aligned}$$

$$= \frac{1}{b^2 + \frac{\pi^2}{T^2}} \left\{ bT + \frac{2 \frac{\pi^2}{T^2}}{b^2 + \frac{\pi^2}{T^2}} (1 + e^{-bT}) \right\}$$

$$= \frac{T^2}{b^2 T^2 + \pi^2} \left\{ bT + \frac{2\pi^2}{b^2 T^2 + \pi^2} (1 + e^{-bT}) \right\}. \quad (A5)$$

A6. Inverse Hankel Transform

The Hankel transform of a probability density function $f_x(x)$ is given by

$$H_x(\xi) = \int_0^\infty J_0(\xi x) f_x(x) dx,$$

where $J_0(\cdot)$ is the zero order Bessel function of the first kind and $x \geq 0$.

It is known that

$$f_x(x) = \int_0^\infty \delta(y-x) f_x(y) dy,$$

where $\delta[\cdot]$ is the Dirac delta function.

Assuming the existence of an inverse integral transformation, H^{-1} , it is postulated

$$f_x(x) = H^{-1}[H_x(\xi)] = \int_0^\infty \rho(x, \xi) d\xi H_x(\xi)$$

$$= \int_0^\infty \rho(x, \xi) d\xi \int_0^\infty J_0(\xi y) f_x(y) dy$$

$$= \int_0^\infty f_x(y) dy \int_0^\infty \rho(x, \xi) J_0(\xi y) d\xi.$$

For this to hold, the following is necessary:

$$\delta(y-x) = \int_0^\infty \rho(x, s) J_0(sy) ds.$$

Multiplying both sides by the function $J_1(xy)$ and integrating with respect to y yields:

$$\begin{aligned} & \int_0^\infty \delta(y-x) J_1(\lambda y) dy \\ &= \int_0^\infty J_1(\lambda y) dy \int_0^\infty \rho(x, s) J_0(sy) ds \\ &= \int_0^\infty \rho(x, s) ds \int_0^\infty J_0(sy) J_1(\lambda y) dy. \end{aligned}$$

According to Gröbner and Hoffreiter [19], equation 155-6a:

$$\int_0^\infty J_0(sy) J_1(\lambda y) dy = \begin{cases} \frac{1}{\lambda}, & 0 < s < \lambda \\ \frac{1}{2\lambda}, & s = \lambda \\ 0, & s > \lambda \end{cases}$$

Hence,

$$J_1(\lambda x) = \frac{1}{\lambda} \int_0^\lambda g(x, s) ds.$$

And differentiation of both sides of this result with respect to λ yields:

$$\begin{aligned} g(x, \lambda) &= \frac{d}{d\lambda} [\lambda J_1(\lambda x)] \\ &= \lambda x J_0(\lambda x) \end{aligned}$$

Hence, the inverse transformation is defined by

$$H^{-1}[H_x(s)] = \int_0^\infty x s H_x(s) J_0(xs) ds. \quad (\text{A6})$$

APPENDIX B
STATISTICAL PROPERTIES OF THE RATIO OF AMPLITUDES
OF INDEPENDENT IMPULSIVE ATMOSPHERIC NOISE PULSES

The time response of a linear LRC bandpass filter to an impulsive signal of the form produced at VLF by a typical lightning strike is given by

$$e_1(t) = Pe^{-b(t-t_0)} \sin \omega_0(t-t_0) \times U(t-t_0), \quad (69)$$

where ω_0 is the angular center frequency of the filter, b is the 3 dB half-bandwidth in radians/second, $U(\cdot)$ is the unit step function, and t_0 is the time of occurrence.

Moreover, the noise component E , given P , of the integrate-and-dump detector produced by such a single pulse is given by (198) as

$$E = \left\langle \frac{1}{T} \int_{t_0}^T e_1(t) dt \right\rangle \approx \frac{P}{bT}, \quad bT \gg 1. \quad (198)$$

Now the ratio, z , of the amplitudes, P_1 and P_2 , of independent noise pulses is examined. Here $z \triangleq \frac{P_1}{P_2}$ is a non-negative random variable.

Moreover, (198) leads directly to

$$z \approx \frac{E_1}{E_2}. \quad (B1)$$

Using this latter relationship,

$$P_r(j \leq z) = P_r\left(\frac{e_1}{e_2} \leq z\right) = P_r(e_1 \leq E_2 z) \quad (B2)$$

$$= \int_0^{\infty} f_{e_2}(E_2) dE_2 \int_0^{E_2 z} f_{e_1}(E_1) dE_1. \quad (B3)$$

The probability density function for z is given by

$$f_z(z) = \frac{d}{dz} P_r(j \leq z) = \int_0^{\infty} E_2 f_{e_2}(E_2) f_{e_1}(zE_2) dE_2. \quad (B4)$$

Here, in the impulsive, power-Rayleigh region of the atmospheric noise APD,

$$f_e(E) = \frac{E^{3x-1}}{X^2 e^2} e^{-\frac{E^{2x}}{2e^2}}, \quad 0 \leq E \leq \infty \quad (B5)$$

The parameter X is the ratio of the slope of the impulsive power-Rayleigh part of the atmospheric noise APD to the slope of the Gaussian (Rayleigh envelope) part. Substitution of $f_e(E)$ in the expression for $f_z(z)$ yields

$$f_z(z) = \frac{z^{3x-1}}{X^2 e^4} \int_0^{\infty} E^{(4x-1)} e^{-\frac{E^{2x}}{2e^2}(1+z^{2x})} dE. \quad (B6)$$

Using

$$U = \frac{E^{2/x}}{2\sigma^2} [1 + z^{2/x}],$$

$$\begin{aligned} f_2(z) &= \frac{2z^{2/x-1}}{x[1+z^{2/x}]^2} \int_0^\infty U e^{-U} dU \\ &= \frac{2z^{2/x-1}}{x[1+z^{2/x}]^2}. \end{aligned} \tag{B7}$$

Now consider the function

$$r = \begin{cases} z, & 0 \leq z \leq 1 \\ z^{-1}, & 1 < z \leq \infty. \end{cases}$$

The probability density of r is obtained by

$$\begin{aligned} f_r(r) &= f_2(z) \left| \frac{dz}{dr} \right| \\ &= f_2(z) \Big|_{z=R}, 0 \leq z \leq 1 \\ &\quad \frac{1}{R^2} f_2(z) \Big|_{z=\frac{1}{R}}, 1 < z \leq \infty. \end{aligned} \tag{B8}$$

This leads to

$$f_r(r) = \begin{cases} \frac{2R^{(2/x-1)}}{x[1+R^{2/x}]^2}, & 0 \leq z \leq 1 \\ \frac{2R^{(2/x-1)}}{x[1+R^{2/x}]^2}, & 1 < z \leq \infty. \end{cases} \tag{B9}$$

Because

$$\begin{aligned} P_r(0 \leq z \leq 1) &= P_r(P_1 \leq P_2) \\ &= P_r(P_2 < P_1) = P_r(1 < z \leq \infty) \end{aligned}$$

(assuming $P_r(z = 1) = 0$), the two parts of $f_r(R)$ simply "fold over" and are additive. Thus,

$$f_r(R) = \frac{4R^{3/x-1}}{x[1+R^{2/x}]^2}. \quad (\text{B10})$$

(As a check, it is readily found that

$$\int_0^1 f_r(R) dR = 1. \quad (\text{B10a})$$

Evaluation of $\overline{\ln r}$. An important parameter in the evaluation of error probabilities is the average value of $\ln r$. Here

$$\begin{aligned} \overline{\ln r} &= E\{\ln r\} = \int_0^1 \ln R f_r(R) dR \\ &= \int_0^1 \frac{4R^{3/x-1} \ln R}{x[1+R^{2/x}]^2} dR. \quad (\text{B11}) \end{aligned}$$

Using

$$v = R^{3/x},$$

$$\overline{\ln r} = x \int_0^1 \frac{\ln v dv}{[1+v]^2} = -x \ln 2. \quad (\text{B12})$$

Evaluation of the moments, \bar{r}^k . Also of interest in the evaluation of error probabilities are the statistical moments of the ratio r . Here

$$\begin{aligned}\bar{r}^k &= E\{r^k\} = \int_0^1 R^k f_r(R) dR \\ &= \frac{4}{x} \int_0^1 \frac{R^{2/x+k-1}}{[1+R^{2/x}]^2} dR.\end{aligned}\quad (B13)$$

Integration by parts yields

$$\bar{r}^k = -\left. \frac{2R^k}{1+R^{2/x}} \right|_0^1 + 2k \int_0^1 \frac{R^{k-1}}{1+R^{2/x}} dR. \quad (B14)$$

Substitution of $U = \ln R$ in the second term leads to

$$\bar{r}^k = -1 + 2k \int_0^\infty \frac{e^{-ku}}{1+e^{-(2/x)u}} du. \quad (B15)$$

The integrand may be expanded into the series

$$\frac{e^{-ku}}{1+e^{-(2/x)u}} = e^{-ku} \sum_{n=0}^{\infty} (-1)^n e^{-\frac{2n}{x}u}, \quad (B16)$$

$u > 0.$

That is, the series is absolutely, and hence uniformly, convergent for $U > 0$. Thus, the series expansion of (B16) may be substituted in the integral

$$\begin{aligned} 2K \int_{\epsilon}^{\infty} \frac{e^{-KU} dU}{1 + e^{-(2/x)U}} &= 2K \sum_{n=0}^{\infty} (-1)^n \int_{\epsilon}^{\infty} e^{-(K + \frac{2n}{x})U} dU \\ &= 2K \sum_{n=0}^{\infty} (-1)^n \frac{e^{-(K + \frac{2n}{x})\epsilon}}{K + 2n/x}, \end{aligned} \quad (\text{B17})$$

where

$$\epsilon > 0.$$

Now considering

$$\lim_{\epsilon \rightarrow 0} 2K \sum_{n=0}^{\infty} (-1)^n \frac{e^{-(K + \frac{2n}{x})\epsilon}}{K + \frac{2n}{x}} = 2Kx \sum_{n=0}^{\infty} (-1)^n \frac{1}{Kx + 2n}, \quad (\text{B18})$$

the ratio of the magnitudes of the $n+1$ th and the n th terms is

$$|R| = \frac{Kx + 2n}{Kx + 2n+2} < 1, \text{ for all } n. \quad (\text{B19})$$

This property of monotonic decrease with increasing n and the fact that the series is alternating insure that the series is convergent. Therefore,

$$\overline{r^K} = -1 + 2Kx \sum_{n=0}^{\infty} (-1)^n \frac{1}{Kx + 2n}. \quad (\text{B20})$$

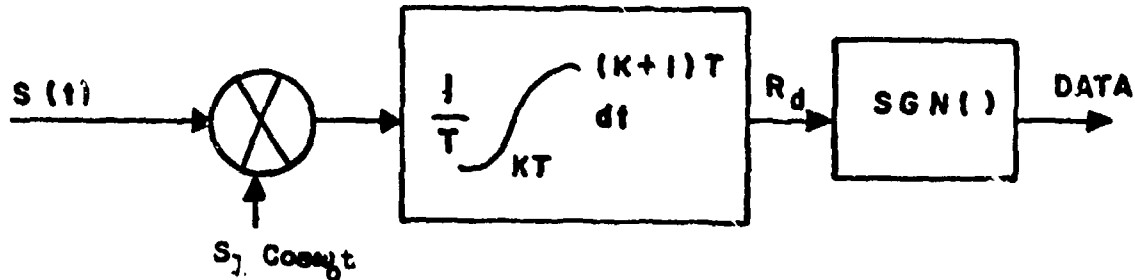
APPENDIX C
SMALL SIGNAL ANALYSIS OF HARD-LIMITING
NOISE REDUCTION IN THE PSK RECEIVER

In the linear PSK system, a typical element of the PSK signal plus noise is given by

$$s(t) = K S \cos \omega_0 t + n(t), \quad (C1)$$

where $K = \pm 1$ according to the data, and

$$n(t) = n_c(t) \cos \omega_0 t - n_s(t) \sin \omega_0 t.$$



In the linear detection system depicted above, the decision statistic, or detector functional, R_d is given by

$$\begin{aligned} R_d &= \frac{S_1}{T} \int_0^T s(t) \cos \omega_0 t dt \\ &= \frac{S_1}{2T} \int_0^T [KS + KS \cos 2\omega_0 t + \\ &\quad + n_c(t) + n_c(t) \cos 2\omega_0 t - (C2) \\ &\quad - n_s(t) \sin 2\omega_0 t] dt. \end{aligned}$$

Utilizing the low frequency components in the integrand

$$R_d \approx \frac{S_1}{2T} \int_0^T [KS + n_c(t)] dt \\ = \frac{KSS_1}{2} + \frac{S_1}{2T} \int_0^T n_c(t) dt. \quad (C3)$$

The mean value of the functional is given by

$$\overline{R_d} = \frac{KSS_1}{2} + E\left\{\frac{S_1}{2T} \int_0^T n_c(t) dt\right\} \\ = \frac{KSS_1}{2} + \frac{S_1}{2T} \int_0^T E\{n_c(t)\} dt \\ = \frac{KSS_1}{2}. \quad (C4)$$

And the mean square of the functional, by

$$\overline{R_d^2} = \frac{S_1^2}{4T^2} \int_0^T dt_1 \int_0^T dt_2 E\left\{[KS + n_c(t_1)] \times \right. \\ \left. \times [KS + n_c(t_2)]\right\}. \quad (C5)$$

The integrand reduces to

$$E\left\{[KS + n_c(t_1)] \times [KS + n_c(t_2)]\right\} = \\ = K^2 S^2 + KS \times E\{n_c(t_1) + n_c(t_2)\} \\ + E\{n_c(t_1) n_c(t_2)\}. \quad (C6)$$

Now it is assumed that the noise process, $n_c(t)$, is zero mean and approximately white and stationary so that

$$E\{n_c(t_1) n_c(t_2)\} = \frac{N_o}{2} S(t, -t_2), \quad (C7)$$

where N_o is the double-sided noise spectral density. Using this,

$$\overline{R_d^2} = \frac{S_i^2}{4T^2} \int_0^T dt_1 \int_0^T dt_2 \left[S^2 + \frac{N_o}{2} S(t, -t_2) \right]$$

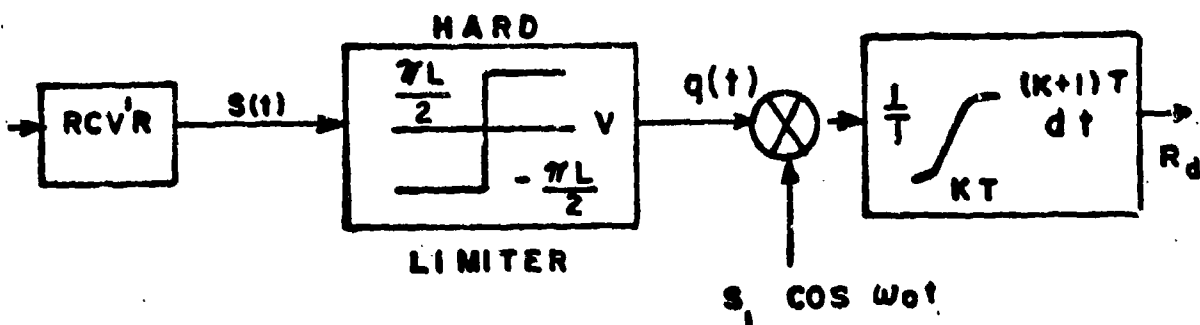
$$= \frac{S^2 S_i^2}{4} + \frac{S_i^2 N_o}{8T}. \quad (C8)$$

Hence,

$$\text{Var}(R_d) = \overline{R_d^2} - \overline{R_d}^2 = \frac{S_i^2 N_o}{8T}, \quad (C9)$$

and the ratio of the squared mean to the variance for the linear detector functional is given by

$$\frac{\overline{R_d^2}}{\text{Var}(R_d)} = \frac{2S^2 T}{N_o}. \quad (C10)$$



In the hard-limiting system above, the test statistic R_d is given by

$$R_d = \frac{S_1}{T} \int_0^T q(t) \cos \omega_0 t \, dt. \quad (C11)$$

Here the signal into the limiter, $S(t)$, is given by

$$S(t) \triangleq K S \cos \omega_0 t + e(t) \cos [\omega_0 t + \theta(t)]$$

where S is the signal amplitude, $e(t)$ is the noise envelope process, and $K = \pm 1$ according to the data. The limiter output, $q(t)$, has a nearly rectangular waveform of amplitude L . The zero crossings (or phase) of $q(t)$ correspond to the phase of the larger component of $S(t)$. However, the mixing process produces a low-pass response governed only by the in-phase components of $q(t)$, that is, the output corresponding to the input:

$$KS \cos \omega_0 t + e(t) \cos \theta(t) \cos \omega_0 t$$

The quadrature component of $q(t)$ which corresponds to the input:

$$-e(t) \sin \theta(t) \sin \omega_0 t$$

mixes with the reference to produce an output composed of frequency components at $2\omega_0$ and higher harmonics. Therefore, the effective limiter output produced by the in-phase portion of $S(t)$ is given by

$$C_I(t) = L \operatorname{SGN}\{[K_S + e(t) \cos \theta(t)] \cos \omega_0 t\}, \quad (C12)$$

where

$$\operatorname{SGN}(x) = \begin{cases} 1, & x \geq 0 \\ -1, & x < 0 \end{cases}$$

This can be rewritten as:

$$C_I(t) = L B(t) \operatorname{SGN}\{\cos \omega_0 t\} \quad (C13)$$

where

$$B(t) = \operatorname{SGN}\{K_S + e(t) \cos \theta(t)\}.$$

However, if $e(t)$ and $\theta(t)$ are assumed to be narrowband processes, that is, varying slowly in comparison with the frequency ω_0 , then $B(t)$ will change at a much slower rate than $\operatorname{SGN}\{\cos \omega_0 t\}$. Thus, for a sequence of RF cycles where $B(t)$ remains constant (say $t_1 \leq t \leq t_2$, $t_2 - t_1 \gg \frac{2\pi}{\omega_0}$), $C_I(t)$ is a rectangular square wave of angular frequency ω_0 and amplitude L whose zero's coincide with $\cos \omega_0 t$. Such a square wave can be described by a Fourier cosine series whose constant (or D.C.) term is zero and whose fundamental component is given by

$$\frac{4B(t)L}{\pi} \cos \omega_0 t, \quad t_1 \leq t \leq t_2.$$

This then defines the effective output of the limiter to be the fundamental component of the square wave as modulated by the temporal variation of $B(t)$. This yields

$$\begin{aligned} C_{\text{eff}}(t) &= \frac{4LB(t)}{\pi} \cos \omega_0 t \\ &= \frac{4L}{\pi} SGN\{KS + e(t)\cos \theta(t)\} \text{car. ast.} \quad (C14) \end{aligned}$$

Finally, mixing with the coherent reference signal yields the low pass component, $C_L(t)$, given by

$$C_L(t) = \frac{2S_1L}{\pi} SGN\{KS + e(t)\cos \theta(t)\}. \quad (C15)$$

(The high frequency components are effectively averaged to zero in the integrator.) Using $C_L(t)$ as the integrator input, the test statistic, R_d , is given by

$$R_d = \frac{1}{T} \int_0^T \frac{2S_1L}{\pi} SGN\{KS + e(t)\cos \theta(t)\} dt,$$

or, alternatively,

$$R_d = \frac{1}{T} \int_0^T \frac{2S_1L}{\pi} SGN\{KS + n_c(t)\} dt, \quad (C16)$$

where

$$n_c(t) = e(t) \cos \theta(t).$$

Here the probability of error is given by

$$P_e = Pr(R_d > 0 | K < 0)Pr(K < 0) + Pr(R_d < 0 | K \geq 0)Pr(K \geq 0). \quad (C17)$$

Assuming symmetry of the noise and that $Pr(K < 0) = Pr(K \geq 0) = 1/2$, then

$$P_e = Pr(R_d > 0 | K < 0), \quad (C18)$$

where R_d is given by

$$R_d = \frac{1}{T} \int_0^T \frac{2S_L}{\pi} SGN\{-S + n_c(t)\} dt. \quad (C18a)$$

Now solving for the mean of this test statistic,

$$\begin{aligned} \bar{R}_d &= E\left\{\frac{2S_L}{\pi T} \int_0^T SGN[-S + n_c(t)] dt\right\} \\ &= \frac{2S_L}{\pi T} \int_0^T E\{SGN[-S + n_c(t)]\} dt. \quad (C19) \end{aligned}$$

In terms of the normalized variables:

$$\hat{S} \triangleq \sqrt{\frac{I}{N_0}} S \text{ and } \hat{n}_c(t) \triangleq \sqrt{\frac{T}{N_0}} n_c(t),$$

where $\sqrt{\frac{I}{N_0}}$ is the RMS value of the noise envelope voltage,

$$\overline{R_d} = \frac{2S_1L}{\pi T} \int_0^T E\{SGN[-\hat{S} + \hat{n}_c(t)]\} dt. \quad (C20)$$

In turn,

$$\begin{aligned} E\{SGN[-\hat{S} + \hat{n}_c(t)]\} &= \\ &= (1) \times Pr[\hat{n}_c(t) \geq \hat{S}] \\ &\quad + (-1) \times Pr[\hat{n}_c(t) < \hat{S}] \\ &= 1 - 2Pr[\hat{n}_c(t) < \hat{S}] \\ &= 1 - 2F_{\hat{n}_c(t)}(\hat{S}). \end{aligned} \quad (C21)$$

where $F_{\hat{n}_c(t)}(N_c)$ is the cumulative distribution function of the process $\hat{n}_c(t)$ at time t , $0 \leq t \leq T$, evaluated at voltage N_c .

Hence,

$$\overline{R_d} = \frac{2S_1L}{\pi T} \int_0^T [1 - 2F_{\hat{n}_c(t)}(\hat{S})] dt. \quad (C22)$$

In the case where the bandwidth ratio (ratio of limiting bandwidth to detection bandwidth) is large, the signal-to-noise ratio in the limiting bandwidth, \hat{S} , will be relatively small, even for useful signal/noise ratios in the detection bandwidth. Therefore, the function $F_{\hat{n}_c(t)}(\hat{S})$ can be usefully approximated by the first two terms of a Taylor series expansion of $F_{\hat{n}_c}(t)(S)$ about the origin ($S = 0$):

$$F_{\hat{n}_c(t)}(\hat{S}) \approx F_{\hat{n}_c}(0) + F'_{\hat{n}_c}(0) \hat{S} \\ = \frac{1}{2} + f_{\hat{n}_c}(0) \hat{S}, \quad (C23)$$

where $F_{\hat{n}_c}(0) = 1/2$ implies that the noise voltage $\hat{n}_c(t)$ has zero mean and $f_{\hat{n}_c}(0)$ is the probability density function of the normalized noise process at zero volts.

Substituting this latter expression into (C22) yields

$$\overline{R_d} = \frac{2 S_i L}{T T T} \int_0^T -2 f_{\hat{n}_c}(0) \hat{S} dt \\ = -\frac{4 S_i \hat{S}}{T} f_{\hat{n}_c}(0). \quad (C24)$$

To complete the evaluation of $f_{\hat{n}_c}(0)$, consider the noise voltage process, $\hat{n}_c(t)$, in terms of its envelope and phase,

$$\hat{n}_c(t) = e(t) \cos \theta(t). \quad (C25)$$

Here the phase process $\theta(t)$ is assumed to vary slowly with time. Thus, $\theta(t)$ will be approximately constant over a short observation interval, $(0, T)$, so that

$$\theta(t) = \theta, \quad 0 \leq t \leq T, \quad (C26)$$

where θ is uniformly distributed over $(-\pi, \pi)$ and statistically independent of $e(t)$.

The noise process thus becomes

$$\hat{n}_c(t) = e(t) \cos \theta, \quad 0 \leq t \leq T. \quad (C27)$$

Finally, it should be noted that the noise voltage, as produced by observation of the noise process, is proportional to the square root of the bandwidth of the noise detector. In this case, the noise envelope voltage, E , is defined by

$$E \triangleq \frac{1}{T} \int_0^T e(t) dt \quad (C28)$$

The equivalent noise bandwidth of this detector (matched filter) is $(1/T)$ Hz. Thus, with the normalized envelope process defining a noise voltage density (in Volt (Hz) $^{-1/2}$), the following relationship results

$$E = \frac{1}{\sqrt{T}} e(t) \text{ volts}, \quad (C29)$$

and

$$\hat{n}_c(t) \approx e(t) \cos \theta = \sqrt{T} E \cos \theta, \quad (C30)$$

$$0 \leq t \leq T.$$

The characteristic function for $n_c(t)$ is given by

$$\begin{aligned}
 F_{\hat{n}_c}(j\zeta) &= E\left\{ \exp[-j\zeta \hat{n}_c(t)] \right\} = E\left\{ \exp[-j\zeta \sqrt{T} E \cos \theta] \right\} \\
 &= \int_0^\infty f_e(E) dE \int_{-\pi}^{\pi} \frac{d\theta}{\pi} e^{-j\zeta \sqrt{T} E \cos \theta} \\
 &= \int_0^\infty J_0(\zeta \sqrt{T} E) f_e(E) dE. \quad (C31)
 \end{aligned}$$

The inverse Fourier transformation then yields the probability density function as

$$\begin{aligned}
 f_{\hat{n}_c}(N_c) &= \frac{1}{2\pi} \int_{-\infty}^{\infty} F_{\hat{n}_c}(j\zeta) e^{jN_c \zeta} d\zeta \\
 &= \frac{1}{2\pi} \int_{-\infty}^{\infty} e^{jN_c \zeta} d\zeta \int_0^\infty J_0(\zeta \sqrt{T} E) f_e(E) dE. \quad (C32)
 \end{aligned}$$

And,

$$\begin{aligned}
 f_{\hat{n}_c}(0) &= \frac{1}{\pi} \int_0^\infty \frac{f_e(E) dE}{\sqrt{T} E} \int_0^\infty J_0(\zeta \sqrt{T} E) d(\zeta \sqrt{T} E) \\
 &= \frac{1}{\pi \sqrt{T}} \int_0^\infty \frac{f_e(E)}{E} dE. \quad (C33)
 \end{aligned}$$

Here the random variable, e , is the normalized noise envelope voltage whose APD is tabulated in CCIR 322 [26].

Finally, substituting (C33) into (C24) yields

$$\begin{aligned}\overline{R_d} &= -\frac{4S_1 L \hat{S}}{\pi^2 \sqrt{T}} \int_0^\infty \frac{f_e(E) dE}{E} \\ &= -\frac{4S_1 L S}{\pi^2 N_o \beta_2} \int_0^\infty \frac{f_e(E) dE}{E}.\end{aligned}\quad (C34)$$

The mean square value of the functional, $\overline{R_d^2}$, is given by

$$\begin{aligned}\overline{R_d^2} &= E \left\{ \left[\int_0^T \frac{2S_1 L}{\pi T} SGN[-S + n_c(t_1)] dt_1 \right] \times \right. \\ &\quad \left. \left[\int_0^T \frac{2S_1 L}{\pi T} SGN[-S + n_c(t_2)] dt_2 \right] \right\} \\ &= \frac{4S_1^2 L^2}{\pi^2 T^2} \int_0^T dt_1 \int_0^T dt_2 E \left\{ SGN[-S + n_c(t_1)] \times \right. \\ &\quad \left. SGN[-S + n_c(t_2)] \right\}.\end{aligned}\quad (C35)$$

Recalling that $n_c(t)$ is approximately white so that $n_c(t_1)$ and $n_c(t_2)$ are statistically independent for $t_1 \neq t_2$, this leads to

$$\begin{aligned} E\{SGN[-s+n_c(t_1)] \times SGN[-s+n_c(t_2)]\} \\ = \delta(t_1 - t_2) + E\{SGN[-s+n_c(t_1)]\} \times \\ \times E\{SGN[-s+n_c(t_2)]\} \times \quad (C36) \\ \times [1 - \delta(t_1 - t_2)]. \end{aligned}$$

Utilizing (C21), this becomes

$$\begin{aligned} E\{SGN[-s+n_c(t_1)] \times SGN[-s+n_c(t_2)]\} \\ = \delta(t_1 - t_2) + [1 - 2F_{n_c(t_1)}(s)] \times \quad (C37) \\ \times [1 - 2F_{n_c(t_2)}(s)]. \end{aligned}$$

Hence,

$$\overline{R_d^2} = \frac{4S_r^2 L^2}{\pi^2 T} + \overline{R_d}^2. \quad (C38)$$

And,

$$Var(R_d) = \frac{4S_r^2 L^2}{\pi^2 T}. \quad (C39)$$

Thus, the ratio of the square of the mean to the variance (which is twice the post-detection signal-to-noise ratio) is given by

$$\frac{\overline{R_d}^2}{\text{Var}(R_d)} = \frac{4S^2T}{\pi^2 N_0} \left[\int_0^\infty \frac{f_e(E) dE}{E} \right]^2. \quad (C40)$$

Finally, dividing this result into the corresponding ratio for the linear detector (C10) yields the effective noise reduction factor, Λ_t as

$$\Lambda_t = \frac{(SNR)_{\text{linear}}}{(SNR)_{H.\text{Limiter}}} = \frac{\pi^2}{2 \left[\int_0^\infty \frac{f_e(E) dE}{E} \right]^2} \quad (C41)$$

$$= \frac{\pi^2}{2 (\bar{E}^{-1})^2}. \quad (C42)$$

APPENDIX D
 TABLES OF DECISION ERROR RATES FOR LINEAR COHERENT
 PHASE SHIFT KEYING (PSK) DETECTION

Table D-I. V_d Ratio: 1.0491

SNR(DB)	PROB.(DECISION ERROR)
-10	0.32735723E 00
-9	0.30791126E 00
-8	0.28672028E 00
-7	0.26379544E 00
-6	0.23923276E 00
-5	0.21323107E 00
<hr/>	
-4	0.18611650E 00
-3	0.15837045E 00
-2	0.13064671E 00
-1	0.10376011E 00
0	0.78650183E -01
<hr/>	
1	0.56282204E -01
2	0.37506163E -01
3	0.22878326E -01
4	0.12500704E -01
5	0.59537717E -02
<hr/>	
6	0.23882318E -02
7	0.77264720E -03
8	0.19089835E -03
9	0.33624985E -04
10	0.38717661E -05
<hr/>	
11	0.26127663E -06
12	0.90046643E -08
13	0.13326744E -09
14	0.68085072E -12
15	0.91210804E -15
<hr/>	
16	0.22664894E -18
17	0.64950018E -23
18	0.
19	0.
20	0.
<hr/>	

Table D-II. V_d Ratio: 1.5

SNR(DB) PROB.(DECISION ERROR)

-10	0.31695510E .00
-9	0.29659734E .01
-8	0.27452055E .00
-7	0.25079107E .00
-6	0.22556605E .00
-5	0.19912687E .00

-4	0.17190669E .00
-3	0.14451470E .00
-2	0.11775588E .00
-1	0.92684350E -01
0	0.70331056E -01

1	0.51224472E -01
2	0.35628657E -01
3	0.23535345E -01
4	0.14677385E -01
5	0.85859202E -02

6	0.46787553E -02
7	0.23575696E -02
8	0.10878442E -02
9	0.45834744E -03
10	0.17382537E -03

11	0.58894084E -04
12	0.17653022E -04
13	0.46332122E -05
14	0.10529626E -05
15	0.20386559E -06

16	0.32128083E -07
17	0.39647746E -08
18	0.37059568E -09
19	0.25264520E -10
20	0.12033329E -11

21	0.38133819E -13
22	0.76362554E -15
23	0.89652090E -17
24	0.58120504E -19
25	0.19086781E -21

26	0.
27	0.
28	0.
29	0.
30	0.

Table D-III. V_d Ratio: 1.75

SNR(DB)	PROB.(DECISION ERROR)
-10	0.30263332E 00
-9	0.23114572E 00
-8	0.25801998E 00
-7	0.23340565E 00
-6	0.20757525E 00
-5	0.13095176E 00
<hr/>	
-4	0.15415585E 00
-3	0.12809313E 00
-2	0.10390062E 00
-1	0.82152118E -01
0	0.63187756E -01
<hr/>	
1	0.47178962E -01
2	0.34122547E -01
3	0.23855239E -01
4	0.16086050E -01
5	0.10440522E -01
<hr/>	
6	0.65088509E -02
7	0.38897684E -02
8	0.22240427E -02
9	0.12144170E -02
10	0.63220063E -03
<hr/>	
11	0.31327034E -03
12	0.14755030E -03
13	0.65971908E -04
14	0.27967585E -04
15	0.11226244E -04
<hr/>	
16	0.42550943E -05
17	0.15041045E -05
18	0.48352181E -06
19	0.13983125E -06
20	0.36010751E -07
<hr/>	
21	0.81670119E -08
22	0.16113594E -08
23	0.27289912E -09
24	0.39094187E -10
25	0.46614963E -11
<hr/>	
26	0.45453694E -12
27	0.35549107E -13
28	0.21831166E -14
29	0.10284794E -15
30	0.36231704E -17
<hr/>	

Table D-IV. V_d Ratio: 2.0

S:R(DB) PROB.(DECISION ERROR)

-10	0.29006563E 00
-9	0.26773689E 00
-8	0.24392175E 00
-7	0.21886851E 00
-6	0.19298753E 00
-5	0.16691210E 00
<hr/>	
-4	0.14168034E 00
-3	0.11806608E 00
-2	0.96473838E-01
-1	0.77204563E-01
0	0.60438992E-01
<hr/>	
1	0.46231805E-01
2	0.34517910E-01
3	0.25129662E-01
4	0.17822120E-01
5	0.12302490E-01
<hr/>	
6	0.82596537E-02
7	0.53900283E-02
8	0.34171055E-02
9	0.21037924E-02
10	0.12575449E-02
<hr/>	
11	0.72977301E-03
12	0.41117427E-03
13	0.22497050E-03
14	0.11956633E-03
15	0.61739644E-04
<hr/>	
16	0.30961594E-04
17	0.15037679E-04
18	0.69757722E-05
19	0.30510818E-05
20	0.12523308E-05
<hr/>	
21	0.47995672E-06
22	0.17082128E-06
23	0.56129215E-07
24	0.16919556E-07
25	0.46469443E-08
<hr/>	
26	0.11542841E-08
27	0.25724988E-09
28	0.50997464E-10
29	0.89093784E-11
30	0.13579441E-11
<hr/>	

Table D-V. V_d Ratio: 2.25

SNR(DB) PROB.(DECISION ERROR)

-10	0.28253403E 00
-9	0.25976078E 00
-8	0.23561726E 00
-7	0.21042645E 00
-6	0.18470722E 00
-5	0.15935024E 00
<hr/>	
-4	0.13525016E 00
-3	0.11283510E 00
-2	0.92437867E-01
-1	0.74292963E-01
0	0.58526124E-01
<hr/>	
1	0.45153620E-01
2	0.34091120E-01
3	0.25170656E-01
4	0.18163110E-01
5	0.12802916E-01
<hr/>	
6	0.88120533E-02
7	0.59207215E-02
8	0.38827162E-02
9	0.24851445E-02
10	0.15526582E-02
<hr/>	
11	0.94715962E-03
12	0.56437198E-03
13	0.32864512E-03
14	0.18713783E-03
15	0.10425434E-03
<hr/>	
16	0.56829900E-04
17	0.30270409E-04
18	0.15627846E-04
19	0.77089834E-05
20	0.36177069E-05
<hr/>	
21	0.16092781E-05
22	0.67592216E-06
23	0.26693893E-06
24	0.98679028E-07
25	0.33981246E-07
<hr/>	
26	0.10844388E-07
27	0.31893778E-08
28	0.85930702E-09
29	0.21074033E-09
30	0.46721148E-10
<hr/>	

Table D-VI. V_d Ratio: 2.50

SNR(DB) PF0B. (DECISION ERROR)

-10 0.27227671E 00
 -9 0.24932512E 00
 -8 0.22463313E 00
 -7 0.19956663E 00
 -6 0.17467270E 00
 -5 0.15073836E 00

 -4 0.12816849E 00
 -3 0.10727140E 00
 -2 0.88327924E-01
 -1 0.71499281E-01
 0 0.56862318E-01

 1 0.44404268E-01
 2 0.34032362E-01
 3 0.25588950E-01
 4 0.18870042E-01
 5 0.13644684E-01

 6 0.96733789E-02
 7 0.67239330E-02
 8 0.45830640E-02
 9 0.30639677E-02
 10 0.20098886E-02

 11 0.12943021E-02
 12 0.81871996E-03
 13 0.50905967E-03
 14 0.31134372E-03
 15 0.18741345E-03

 16 0.11104589E-03
 17 0.64680338E-04
 18 0.36768939E-04
 19 0.20162792E-04
 20 0.10631660E-04

 21 0.53763393E-05
 22 0.26000590E-05
 23 0.11989004E-05
 24 0.52539914E-06
 25 0.21807680E-06

 26 0.85418023E-07
 27 0.31448947E-07
 28 0.10838280E-07
 29 0.34807210E-08
 30 0.10367085E-08

Table D-VII. V_d Ratio: 2.75

SN ⁿ (DB)	PROB.(DECISION ERROR)
-10	0.26253339E 00
-9	0.23893395E 00
-8	0.21447483E 00
-7	0.18988833E 00
-6	0.16598151E 00
-5	0.14315294E 00
<hr/>	
-4	0.12173978E 00
-3	0.10202008E 00
-2	0.84199404E-01
-1	0.68402933E-01
0	0.54674250E-01
<hr/>	
1	0.42979520E-01
2	0.33217987E-01
3	0.25235772E-01
4	0.18842204E-01
5	0.13826149E-01
<hr/>	
6	0.99712322E-02
7	0.70688723E-02
8	0.49274964E-02
9	0.33786817E-02
10	0.22799769E-02
<hr/>	
11	0.15151007E-02
12	0.99215285E-03
13	0.64071374E-03
14	0.40832906E-03
15	0.25695467E-03
<hr/>	
16	0.15966217E-03
17	0.97809858E-04
18	0.58633614E-04
19	0.34067495E-04
20	0.19140233E-04
<hr/>	
21	0.10376152E-04
22	0.54152127E-05
23	0.27141168E-05
24	0.13030187E-05
25	0.59756337E-06
<hr/>	
26	0.26100780E-06
27	0.10824324E-06
28	0.42479573E-07
29	0.15719978E-07
30	0.54648280E-08
<hr/>	

Table D-VIII. V_d Ratio: 3.0

SNR(DB) PROB.(DECISION ERROR)

-10	0.25149887E 00
-9	0.22766873E 00
-8	0.20347283E 00
-7	0.17971866E 00
-6	0.15680791E 00
-5	0.13507549E 00
<hr/>	
-4	0.11481010E 00
-3	0.96240714E-01
-2	0.79527179E-01
-1	0.64755699E-01
0	0.51939985E-01
<hr/>	
1	0.41027403E-01
2	0.31909080E-01
3	0.24433154E-01
4	0.18419090E-01
5	0.13671594E-01
<hr/>	
6	0.99933256E-02
7	0.71956538E-02
8	0.51058407E-02
9	0.35720577E-02
10	0.24653384E-02
<hr/>	
11	0.16797352E-02
12	0.11306577E-02
13	0.75245010E-03
14	0.49543168E-03
15	0.32288882E-03
<hr/>	
16	0.20825923E-03
17	0.13263083E-03
18	0.82816007E-04
19	0.50279829E-04
20	0.29640665E-04
<hr/>	
21	0.16936291E-04
22	0.93617683E-05
23	0.49960719E-05
24	0.25686115E-05
25	0.12693364E-05
<hr/>	
26	0.60146791E-06
27	0.27257682E-06
28	0.11732045E-06
29	0.48433856E-07
30	0.18877172E-07
<hr/>	

Table D-IY. V_d Ratio: 3.25

SNR(DB)	PROB. (DECISION ERROR)
-10	0.24087564E 00
-9	0.21722449E 00
-8	0.19379551E 00
-7	0.17098379E 00
-6	0.14911409E 00
-5	0.12847728E 00
<hr/>	
-4	0.10931667E 00
-3	0.91818127E-01
-2	0.76103735E-01
-1	0.62229802E-01
0	0.50189621E-01
<hr/>	
1	0.39920129E-01
2	0.31311461E-01
3	0.24219316E-01
4	0.18475659E-01
5	0.13903366E-01
<hr/>	
6	0.10323770E-01
7	0.75670664E-02
8	0.54775945E-02
9	0.39181174E-02
10	0.27711898E-02
<hr/>	
11	0.19394285E-02
12	0.13440885E-02
13	0.92310856E-03
14	0.62868250E-03
15	0.42473650E-03
<hr/>	
16	0.28455919E-03
17	0.18864050E-03
18	0.12272919E-03
19	0.77948378E-04
20	0.48263128E-04
<hr/>	
21	0.29088727E-04
22	0.17039617E-04
23	0.96850778E-05
24	0.53320553E-05
25	0.28381120E-05
<hr/>	
26	0.14576581E-05
27	0.72089280E-06
28	0.34254610E-06
29	0.15602316E-06
30	0.67953101E-07
<hr/>	

Table D-X. V_d Ratio: 3.50

SNR(DB) PROB.(DECISION ERROR)

-10	0.23030567E 00
-9	0.20721205E 00
-8	0.18453708E 00
-7	0.16259501E 00
-6	0.14167610E 00
-5	0.12203354E 00
<hr/>	
-4	0.10387252E 00
-3	0.87343244E-01
-2	0.72536757E-01
-1	0.59484877E-01
0	0.48164044E-01
<hr/>	
1	0.38502295E-01
2	0.30388317E-01
3	0.23682667E-01
4	0.18228225E-01
5	0.13860138E-01
<hr/>	
6	0.10414890E-01
7	0.77376386E-02
8	0.56866129E-02
9	0.41368086E-02
10	0.29808062E-02
<hr/>	
11	0.21290169E-02
12	0.15084456E-02
13	0.10609461E-02
14	0.74117132E-03
15	0.51439415E-03
<hr/>	
16	0.35447122E-03
17	0.24184592E-03
18	0.16203188E-03
19	0.10624545E-03
20	0.68100330E-04
<hr/>	
21	0.42615602E-04
22	0.26000929E-04
23	0.15445343E-04
24	0.89196471E-05
25	0.49998311E-05
<hr/>	
26	0.27158023E-05
27	0.14269630E-05
28	0.72392319E-06
29	0.35390384E-06
30	0.16637598E-06
<hr/>	

Table D-XI. V_d Ratio: 3.75

SNR(DB)	PROB.(DECISION ERROR)
-10	0.21182406E 00
-9	0.18961944E 00
-8	0.16806022E 00
-7	0.14742006E 00
-6	0.12794084E 00
-5	0.10982253E 00
<hr/>	
-4	0.93216665E-01
-3	0.78222194E-01
-2	0.64884412E-01
-1	0.53197547E-01
0	0.43110183E-01
<hr/>	
1	0.34532558E-01
2	0.27346137E-01
3	0.21412985E-01
4	0.16584432E-01
5	0.12709281E-01
<hr/>	
6	0.96414352E-02
7	0.72441139E-02
8	0.53940796E-02
9	0.39830529E-02
10	0.29187227E-02
<hr/>	
11	0.21240028E-02
12	0.15360161E-02
13	0.11044768E-02
14	0.78986919E-03
15	0.56161049E-03
<hr/>	
16	0.39625878E-03
17	0.27560555E-03
18	0.18810395E-03
19	0.12585338E-03
20	0.82456365E-04
<hr/>	
21	0.52842775E-04
22	0.33085064E-04
23	0.20212395E-04
24	0.12032825E-04
25	0.69706652E-05
<hr/>	
26	0.39237158E-05
27	0.21427018E-05
28	0.11333250E-05
29	0.57959425E-06
30	0.28607346E-06
<hr/>	

Table D-XII. V_d Ratio: 4.0

SNR(DB)	PROB.(DECISION ERROR)
-10	0.20443721E 00
-9	0.18280370E 00
-8	0.16188843E 00
-7	0.14194166E 00
-6	0.12318032E 00
-5	0.10577956E 00

-4	0.89868209E-01
-3	0.75525407E-01
-2	0.62780771E-01
-1	0.51617610E-01
0	0.41978432E-01

1	0.33771950E-01
2	0.26882489E-01
3	0.21177897E-01
4	0.16517314E-01
5	0.12758900E-01

6	0.97661189E-02
7	0.74113094E-02
8	0.55796628E-02
9	0.41700461E-02
10	0.30959359E-02

11	0.22848608E-02
12	0.16772952E-02
13	0.12252720E-02
14	0.89076689E-03
15	0.64402533E-03

16	0.46174725E-03
17	0.32600135E-03
18	0.22611926E-03
19	0.15394102E-03
20	0.10276459E-03

21	0.67197941E-04
22	0.42995047E-04
23	0.26586374E-04
24	0.16412393E-04
25	0.97675023E-05

26	0.56595742E-05
27	0.31882884E-05
28	0.17436419E-05
29	0.92427293E-06
30	0.47409655E-06

Table D-XIII. V_d Ratio: 5.0

SNR(DB)	PROB.(DECISION ERROR)
-10	0.16856092E 00
-9	0.14960052E 00
-8	0.13163860E 00
-7	0.11482723E 00
-6	0.99283920E-01
-5	0.85087786E-01
<hr/>	
-4	0.72279303E-01
-3	0.60862104E-01
-2	0.50805961E-01
-1	0.42052056E-01
0	0.34820056E-01
<hr/>	
1	0.28112586E-01
2	0.22720497E-01
3	0.18230375E-01
4	0.14530202E-01
5	0.11508758E-01
<hr/>	
6	0.90638840E-02
7	0.71019635E-02
8	0.55393342E-02
9	0.43030139E-02
10	0.33303957E-02
<hr/>	
11	0.25686571E-02
12	0.19737383E-02
13	0.15091677E-02
14	0.11436662E-02
15	0.85520171E-03
<hr/>	
16	0.63051045E-03
17	0.45799595E-03
18	0.32753064E-03
19	0.23042084E-03
20	0.15933526E-03
<hr/>	
21	0.10820440E-03
22	0.72098064E-04
23	0.47090190E-04
24	0.30118015E-04
25	0.18842972E-04
<hr/>	
26	0.11518984E-04
27	0.68724230E-05
28	0.39966813E-05
29	0.22626563E-05
30	0.12452973E-05
<hr/>	

Table D-XIV. V_d Ratio: 6.0

SNR(DB) PROB.(DECISION ERROR)

-10	0.13750253E 00
-9	0.12131420E 00
-8	0.10623860E 00
-7	0.92349312E -01
-6	0.79688674E -01
-5	0.68268946E -01

-4	0.58073243E -01
-3	0.49061980E -01
-2	0.41176673E -01
-1	0.34342540E -01
0	0.28472830E -01

1	0.23476564E -01
2	0.19258493E -01
3	0.15725616E -01
4	0.12787603E -01
5	0.10360590E -01

6	0.83673297E -02
7	0.67384465E -02
8	0.54126640E -02
9	0.43364688E -02
10	0.34636699E -02

11	0.27539811E -02
12	0.21705178E -02
13	0.16918640E -02
14	0.13035796E -02
15	0.99228980E -03

16	0.74578816E -03
17	0.55309907E -03
18	0.40450350E -03
19	0.29152868E -03
20	0.20690600E -03

21	0.14450267E -03
22	0.99232006E -04
23	0.66949338E -04
24	0.44339162E -04
25	0.28799494E -04

26	0.18328582E -04
27	0.11417986E -04
28	0.69552970E -05
29	0.41384159E -05
30	0.24024143E -05

Table D-XV. V_d Ratio: 7.0

SNR(DB) PPOB.(DECISION ERROR)

-10 0.11665219E 00
 -9 0.10264578E 00
 -8 0.89745980E-01
 -7 0.77978252E-01
 -6 0.67342090E-01
 -5 0.57814746E-01

 -4 0.49357050E-01
 -3 0.41913723E-01
 -2 0.35415317E-01
 -1 0.29787035E-01
 0 0.24948191E-01

 1 0.20816663E-01
 2 0.17311345E-01
 3 0.14354666E-01
 4 0.11873203E-01
 5 0.97994809E-02

 6 0.80722917E-02
 7 0.66368976E-02
 8 0.54445787E-02
 9 0.44519549E-02
 10 0.36172712E-02

 11 0.29122458E-02
 12 0.23221217E-02
 13 0.18329896E-02
 14 0.14317000E-02
 15 0.11059384E-02

 16 0.84456915E-03
 17 0.63719877E-03
 18 0.47470953E-03
 19 0.34901251E-03
 20 0.25307467E-03

 21 0.18087281E-03
 22 0.12732793E-03
 23 0.88225702E-04
 24 0.60126840E-04
 25 0.40272542E-04

 26 0.26489083E-04
 27 0.17095242E-04
 28 0.10815580E-04
 29 0.67017525E-05
 30 0.40632115E-05

Table D-XVI. V_d Ratio: 8.0

SNR(DB) PROB.(DECISION ERROR)

-10	0.93601451E-01
-9	0.32039023E-01
-8	0.71617371E-01
-7	0.62170616E-01
-6	0.53715784E-01
-5	0.46207238E-01
<hr/>	
-4	0.39585645E-01
-3	0.33737637E-01
-2	0.28742921E-01
-1	0.24380037E-01
0	0.20627019E-01
<hr/>	
1	0.17414541E-01
2	0.14676027E-01
3	0.12349397E-01
4	0.10377528E-01
5	0.87084003E-02
<hr/>	
6	0.72947697E-02
7	0.60932338E-02
8	0.50593076E-02
9	0.41686221E-02
10	0.34062031E-02
<hr/>	
11	0.27593796E-02
12	0.22153975E-02
13	0.17620576E-02
14	0.13878356E-02
15	0.10819785E-02
<hr/>	
16	0.83457730E-03
17	0.63661631E-03
18	0.47999730E-03
19	0.35754168E-03
20	0.26297119E-03
<hr/>	
21	0.19087088E-03
22	0.13663638E-03
23	0.96409959E-04
24	0.67008212E-04
25	0.45845171E-04
<hr/>	
26	0.30854225E-04
27	0.20411407E-04
28	0.13262832E-04
29	0.84577954E-05
30	0.52889860E-05
<hr/>	

Table D-XVII. V_d Ratio: 9.0

SNR(DB)	PROB. (DECISION ERROR)
-10	0.77691256E-01
-9	0.68084268E-01
-8	0.59417370E-01
-7	0.51654901E-01
-6	0.44748161E-01
-5	0.38641055E-01
<hr/>	
-4	0.33274310E-01
-3	0.28582689E-01
-2	0.24502673E-01
-1	0.20969734E-01
0	0.17922151E-01
<hr/>	
1	0.15301531E-01
2	0.13053106E-01
3	0.11126233E-01
4	0.94746671E-02
5	0.80556947E-02
<hr/>	
6	0.68273886E-02
7	0.57507599E-02
8	0.48106112E-02
9	0.39953630E-02
10	0.32935521E-02
<hr/>	
11	0.26939591E-02
12	0.21857260E-02
13	0.17584616E-02
14	0.14023306E-02
15	0.11081276E-02
<hr/>	
16	0.86733255E-03
17	0.67214917E-03
18	0.51552539E-03
19	0.39115728E-03
20	0.29347712E-03
<hr/>	
21	0.21762801E-03
22	0.15942648E-03
23	0.11531601E-03
24	0.82313530E-04
25	0.57951432E-04
<hr/>	
26	0.40217698E-04
27	0.27495913E-04
28	0.18507330E-04
29	0.12256291E-04
30	0.79802543E-05
<hr/>	

Table D-XVIII. V_d Ratio: 10.0

SNR(DB)	P(POB. (DECISION ERROR))
-10	0.63893774E-01
-9	0.55944084E-01
-8	0.48827747E-01
-7	0.42493661E-01
-6	0.36888579E-01
-5	0.31954443E-01
<hr/>	
-4	0.27631244E-01
-3	0.23359352E-01
-2	0.20580774E-01
-1	0.17739316E-01
0	0.15282262E-01
<hr/>	
1	0.13160456E-01
2	0.11328553E-01
3	0.97445611E-02
4	0.83691452E-02
5	0.71606224E-02
<hr/>	
6	0.60905264E-02
7	0.51483588E-02
8	0.43240165E-02
9	0.36074549E-02
10	0.29837904E-02
<hr/>	
11	0.24583991E-02
12	0.20070039E-02
13	0.16257530E-02
14	0.13062844E-02
15	0.10407793E-02
<hr/>	
16	0.82200155E-03
17	0.64332303E-03
18	0.49873664E-03
19	0.38285660E-03
20	0.29090686E-03
<hr/>	
21	0.21869968E-03
22	0.16260537E-03
23	0.11951513E-03
24	0.86798698E-04
25	0.62258487E-04
<hr/>	
26	0.44032227E-04
27	0.30795239E-04
28	0.21214135E-04
29	0.14402764E-04
30	0.96314598E-05
<hr/>	

Table D-XIX. V_d Ratio: 12.0

SNR(DB) PROB.(DECISION ERROR)

-10	0.44636186E-01
-9	0.39105339E-01
-8	0.34203676E-01
-7	0.29879108E-01
-6	0.26077481E-01
-5	0.22747396E-01
<hr/>	
-4	0.19838344E-01
-3	0.17302459E-01
-2	0.15095100E-01
-1	0.13174734E-01
0	0.11503036E-01
<hr/>	
1	0.10044730E-01
2	0.87665749E-02
3	0.76335350E-02
4	0.66167077E-02
5	0.57473751E-02
<hr/>	
6	0.48981337E-02
7	0.41316972E-02
8	0.35507606E-02
9	0.29931600E-02
10	0.25169103E-02
<hr/>	
11	0.21002540E-02
12	0.17417395E-02
13	0.14351081E-02
14	0.11746281E-02
15	0.95481963E-03
<hr/>	
16	0.77062312E-03
17	0.61738113E-03
18	0.49084250E-03
19	0.33716066E-03
20	0.30238535E-03
<hr/>	
21	0.23495233E-03
22	0.18066043E-03
23	0.13765554E-03
24	0.10390338E-03
25	0.77666200E-04
<hr/>	
26	0.57470423E-04
27	0.42083593E-04
28	0.30484283E-04
29	0.21835674E-04
30	0.15460066E-04
<hr/>	

Table D-XX. V_d Ratio: 14.0

SNR(DB)	PROB.(DECISION ERROR)
-10	0.32039171E-01
-9	0.28155984E-01
-8	0.24734609E-01
-7	0.21729467E-01
-6	0.19095437E-01
-5	0.16791048E-01
<hr/>	
-4	0.14777088E-01
-3	0.13017329E-01
-2	0.11478549E-01
-1	0.10130050E-01
0	0.89434871E-02
<hr/>	
1	0.78908737E-02
2	0.69412650E-02
3	0.60818270E-02
4	0.53071258E-02
5	0.46116279E-02
<hr/>	
6	0.39899397E-02
7	0.34366469E-02
8	0.29464494E-02
9	0.25141753E-02
10	0.21348120E-02
<hr/>	
11	0.18035329E-02
12	0.15157219E-02
13	0.12669936E-02
14	0.10532098E-02
15	0.87049177E-03
<hr/>	
16	0.71522874E-03
17	0.58408283E-03
18	0.47398995E-03
19	0.38215750E-03
20	0.30605867E-03
<hr/>	
21	0.24342409E-03
22	0.19223109E-03
23	0.15069069E-03
24	0.11723308E-03
25	0.90491923E-04
<hr/>	
26	0.69287333E-04
27	0.52611370E-04
28	0.39606109E-04
29	0.29551894E-04
30	0.21843703E-04
<hr/>	

Table D-XXI. V_d Ratio: 16.0

SNR(DB)	PROB.(DECISION ERROR)
-10	0.21752190E-01
-9	0.19218718E-01
-8	0.16995084E-01
-7	0.15045600E-01
-6	0.13337229E-01
-5	0.11839425E-01
<hr/>	
-4	0.10524215E-01
-3	0.93658734E-02
-2	0.83403520E-02
-1	0.74230956E-02
0	0.65882359E-02
<hr/>	
1	0.58275888E-02
2	0.51369173E-02
3	0.45119797E-02
4	0.39485565E-02
5	0.34424738E-02
<hr/>	
6	0.29896274E-02
7	0.25860047E-02
8	0.22277048E-02
9	0.19109567E-02
10	0.16321353E-02
<hr/>	
11	0.13877758E-02
12	0.11745847E-02
13	0.98944974E-03
14	0.82944612E-03
15	0.69184160E-03
<hr/>	
16	0.57409844E-03
17	0.47387363E-03
18	0.38901701E-03
19	0.31756741E-03
20	0.25774716E-03
<hr/>	
21	0.20795520E-03
22	0.16675878E-03
23	0.13288427E-03
24	0.10520708E-03
25	0.82741077E-04
<hr/>	
26	0.64627606E-04
27	0.50124359E-04
28	0.38594408E-04
29	0.29495297E-04
30	0.22368631E-04
<hr/>	

Table D-XXII. V_d Ratio: 18.0

SNR(D)	PROB. (DECISION ERROR)
-10	0.15299938E-01
-9	0.13633426E-01
-8	0.12168804E-01
-7	0.10880288E-01
-6	0.97442063E-02
-5	0.87383826E-02
<hr/>	
-4	0.78437585E-02
-3	0.70369900E-02
-2	0.62972843E-02
-1	0.56191107E-02
0	0.49991608E-02
<hr/>	
1	0.44341257E-02
2	0.39207278E-02
3	0.34557065E-02
4	0.30358650E-02
5	0.26580631E-02
<hr/>	
6	0.23192622E-02
7	0.20164764E-02
8	0.17468542E-02
9	0.15076427E-02
10	0.12962112E-02
<hr/>	
11	0.11104559E-02
12	0.94684536E-03
13	0.80422343E-03
14	0.63221427E-03
15	0.57282033E-03
<hr/>	
16	0.49022624E-03
17	0.40075169E-03
18	0.33285443E-03
19	0.27512410E-03
20	0.22627797E-03
<hr/>	
21	0.18515610E-03
22	0.15071517E-03
23	0.12202214E-03
24	0.98247375E-04
25	0.78657439E-04
<hr/>	
26	0.62608092E-04
27	0.49536443E-04
28	0.38954176E-04
29	0.30440163E-04
30	0.23633656E-04
<hr/>	

Table D-XXIII. V_d Ratio: 20.0

SN R(DB)	PPOB.(DECISION ERROR)
-10	0.11237686E-01
-9	0.10115251E-01
-8	0.91215417E-02
-7	0.82379725E-02
-6	0.74466789E-02
-5	0.67276775E-02
<hr/>	
-4	0.60641173E-02
-3	0.54523946E-02
-2	0.48898796E-02
-1	0.43739473E-02
0	0.39019887E-02
<hr/>	
1	0.34714229E-02
2	0.30797068E-02
3	0.27243444E-02
4	0.24028976E-02
5	0.21129936E-02
<hr/>	
6	0.18523328E-02
7	0.16186958E-02
8	0.14099494E-02
9	0.12240514E-02
10	0.10590554E-02
<hr/>	
11	0.91311326E-03
12	0.78447801E-03
13	0.67150513E-03
14	0.57265313E-03
15	0.48648343E-03
<hr/>	
16	0.41165943E-03
17	0.34694442E-03
18	0.29119968E-03
19	0.24338139E-03
20	0.20253701E-03
<hr/>	
21	0.16780159E-03
22	0.13839335E-03
23	0.11360922E-03
24	0.92820216E-04
25	0.75465527E-04
<hr/>	
26	0.61049558E-04
27	0.49134897E-04
28	0.39338382E-04
29	0.31326070E-04
30	0.24808518E-04
<hr/>	

BIBLIOGRAPHY

1. Abramowitz, Milton and I. A. Stegun, Handbook of Mathematical Functions, National Bureau of Standards Applied Math Series 55, 1964.
2. Arnold, H. R. and E. T. Pierce, "Leader and Function Processes in the Lightning Discharge as a Source of VLF Atmospherics," Radio Science, Vol. 68D, No. 7, July 1964, pp. 771-776.
3. Beach, C. D. and D. C. George, "Error Performance of VLF and LF Receiving Systems with Nonlinear Atmospheric Noise Reduction," Boulder, Colorado, Contract F30602-69-C-0057, September, 1970.
4. Beckmann, Peter, "Amplitude - Probability Distribution of Atmospheric Radio Noise," Radio Science, Journal of Research, NBS/USNC-URSI, Vol. 68D, No. 6, June, 1964, pp. 723-736.
5. Bello, P. A. and R. Esposito, "A New Method for Calculating Probabilities of Errors Due to Impulsive Noise," IEEE Transactions on Communication Technology, Vol. COM-17, June 1969, pp. 367-379.
6. Bello, P. A. and R. Esposito, "Error Probabilities Due to Impulsive Noise in Linear and Hard Limited DPSK Systems," IEEE Transactions on Communication Technology, Vol. COM-19, February 1971, pp. 14-20.
7. Bennett, W. R., "Distribution of the Sum of Randomly Phased Components," Quarterly of Applied Mathematics, Vol. 5, January 1948, pp. 385-393.
8. Brook, M., N. Kitagawa and E. V. Workman, "Quantitative Study of Strokes and Continuing Currents in Lightning Discharges to Ground," Journal of Geophysical Research, Vol. 67, No. 2, February 1962, p. 649.
9. Cahn, Charles, R., "A Note on Signal-to-Noise Ratio in Band-Pass Limiters," IRE Transactions on Information Theory, Vol. IT-7, pp. 39-43.
10. Crichlow, W. Q., C. J. Roubique, A. D. Spaulding, and W. M. Beery, "Determination of the Amplitude - Probability Distribution of Atmospheric Radio Noise from Statistical Moments," Journal of Research of the National Bureau of Standards, Vol. 64D, No. 1, January - February 1960, pp. 49-58.

11. Crichtlow, W., C. Roubique, and A. D. Spaulding, "Conversion of the Amplitude - Probability Distribution Function for Atmospheric Radio Noise from One Bandwidth to Another," Journal of Research of the National Bureau of Standards, Vol. 66D, November - December 1962, pp. 713-720.
12. Davenport, W. B., "Signal-to-Noise Ratios in Band-Pass Limiters," Journal of Applied Physics, Vol. 24, No. 6, June 1953, pp. 720-727.
13. Davenport, W. B., and W. L. Root, An Introduction to the Theory of Random Signals and Noise, McGraw-Hill Book Co., New York, 1958, pp. 115-117.
14. Entzinger, J. N., J. T. Gamble, S. J. Kraszewski, and A. D. Paoni, "A Comparison of Frequency Shift Modulation Systems at Very Low Frequencies," Rome, New York, RADC Technical Report 65-227, November 1965.
15. Fulton, F. F. Mr., "Effects of Receiver Bandwidth on the Amplitude Distribution of VLF Atmospheric Noise," Journal of Research of the National Bureau of Standards, Vol. 65D, May - June 1964, pp. 299-304.
16. Furutsu, K., and T. Ishida, "On the Theory of Amplitude Distribution of Impulsive Random Noise," Journal of Applied Physics, Vol. 32, No. 7, July 1961, pp. 1206-1221.
17. Galejs, Janis, "Amplitude Distributions of Radio Noise at ELF and VLF," Journal of Geophysical Research, Vol. 71, No. 1, January 1, 1966, pp. 201-216.
18. Giordano, A. A., Modeling of Atmospheric Noise, Ph. D. Dissertation in Electrical Engineering, University of Pennsylvania, 1970.
19. Gröbner, W. and N. Hofreiter, Integraltafel, Zweiter Teil, Bestimmte Integrale (Integral Table, Second Part, Definite Integrals), Fourth Edition, Springer-Verlag, Vienna (Austria), 1966.
20. Hall, Harry M., "A New Model for Impulsive Phenomena: Application to Atmospheric-Noise Communication Channels," Stanford, California, Contract AF 49 (638)-1517, August 1966.
21. Halsted, Leonard R., "On Binary Data Transmission Error Rates Due to Combinations of Gaussian and Impulse Noise," IEEE Transactions on Communications Systems, December 1963.
22. Hartley, H. F., "Wideband Technique for Improving FSK Reception in Atmospheric Noise," Proceedings of Nat. Electronics Conf., Vol. 24, 1968, pp. 528-532.

23. Hill, E. L., Very Low Frequency Radiation from Lightning Strokes, Proceedings of the IRE, Vol. 45, June 1957, pp. 775-777.
24. Hurner, F. and J. Harwood, "An Investigation of Atmospheric Noise at Very Low Frequencies," Proceedings of the IEE, Vol. 103B, 1956, pp. 743-751.
25. Ibukun, Olu, "Structural Aspects of Atmospheric Radio Noise in the Tropics," Vol. 54, No. 3, Proceedings of the IEEE, March 1966, pp. 361-367.
26. International Radio Consultative Committee (CCIR), "World Distribution and Characteristics of Atmospheric Radio Noise," Report 322, Published by International Telecommunication Union, Geneva, 1964.
27. Kitagawa, N., M. Brook, and E. J. Workman, "Continuing Currents in Cloud-to-Ground Lightning Discharges," Journal of Geophysical Research, Vol. 67, No. 2, February 1962, pp. 637-647.
28. Kneuer, Joseph G., "A Simplified Physical Model for Amplitude Distribution of Impulsive Noise," IEEE Transactions on Communications Technology, December 1964, pp. 220-222.
29. Lieberman, G., "Quantization in Coherent and Quadrature Reception of Orthogonal Signals," RCA Review, Vol. XXII, No. 3, September 1961, pp. 461-486.
30. Lindenlaub, J. C. and K. A. Chen, "Performance of Matched Filter Receivers in Non-Gaussian Noise Environments," IEEE Transactions on Communications Technology, Vol. COM-13, December 1965, pp. 545-547.
31. Linfield, R. F., "Duration and Spacing of Spheric Pulses," Proceedings of the IRE, Vol. 50, No. 8, August 1962.
32. Linfield, R. F. and R. W. Plush, DECO Electronics, Inc., Boulder, Colorado, Contract No. Nobsr 85360, Interim Report 34-R-3, December 1963, pp. 5-6 - 5-7.
33. Linfield, R. F., and C. D. Beach, "High Performance Reliable VLF Component of the Naval Advanced Communications System," DECO Electronics, Inc., Boulder, Colorado, Contract Nobsr 85360, Final Research Report 34-R-8, March 1965.
34. Malan, D. J., "Radiation from Lightning Discharges and Its Relation to the Discharge Process," from Recent Advances in Atmospheric Electricity, L. G. Smith Ed. Pergamon Press, New York, 1958, p. 557.

35. Mallinckrodt, C. O., "Peak Limiter and Hole Puncher Noise Suppression Capabilities for Minuteman Receivers," TWR Space Technology Laboratories, Redondo Beach, California, AD 425672, December 1963.
36. Maxwell, E. L., and D. L. Stone, "VLF Atmospheric Noise Predictions," Report 92-F-1 on Contract Nobsr 93159, April 1966.
37. McCann, G. D., "The Measurement of Lightning Currents in Direct Strokes," Trans. of the AIEE, Vol. 63, 1944, pp. 1157-1164.
38. Middleton, David, An Introduction to Statistical Communication Theory, McGraw-Hill Book Co., 1960.
39. Mortgomery, G. F., "A Comparison of Amplitude and Angle Modulation for Narrow-Band Communication of Binary-Coded Messages in Fluctuation Noise," Proceedings of the IRE, February 1954, pp. 447-454.
40. Nakai, Tabetoshi, "The Amplitude Probability Distribution of the Atmospheric Noise," Proceedings Research Inst. of Atmospherics, Nagoya Univ. (Japan), Vol. 13, January 1966, pp. 23-40.
41. Nakai, Taketoshi, "On the Time Functions of Atmospheric Noise," Proceedings Research Inst. of Atmospherics, Nagoya Univ. (Japan), Vol. 15, January 1968, pp. 17-28.
42. Omura, J. K. and P. D. Shaft, "Modem Performance in VLF Atmospheric Noise," IEEE Transactions on Communication Technology, Vol. COM-19, October 1971, pp. 659-668.
43. Papoulis, A., Probability, Random Variables and Stochastic Processes, McGraw-Hill Book Co., New York, 1965.
44. Rice, S. O., "Statistical Properties of a Sine Wave Plus Random Noise," Bell System Technical Journal, Vol. 27, 1948, pp. 125-127, 154.
45. Shepelavy, Bohdan, "Non-Gaussian Atmospheric Noise in Binary-Data, Phase Coherent Communication Systems," IEEE Transactions on Communications Systems, September 1963.
46. Sisco, W. B., "Bit and Message Error Rates in Atmospheric Noise With and Without Peak Limiting," TRW Space Technology Laboratories, Redondo Beach, California, Report No. 7070-6323-RV-000, November 1964.
47. Snyder, D. L., "Optimal Detection of Known Signals in a Non-Gaussian Noise Resembling VLF Atmospheric Noise," 1968 WESCON Convention Record, Part 4.

48. Spaulding, A. D., "Determination of Error Rates for Narrow-Band Communication of Binary-Coded Messages in Atmospheric Radio Noise," Proceedings of the IEEE (Correspondence), February 1964, pp. 220-221.
49. Spaulding, A. D., "The Characteristic of Atmospheric Radio Noise and Its Effects on Digital Communication Systems," IEEE International Communication Conference, Paper No. CP. 19CP66-1126, 1966.
50. Turin, G. L., "Error Probabilities for Binary Symmetric Ideal Reception through Nonselective Slow Fading and Noise," Proceedings of the IRE, September 1958, pp. 1603-1619.
51. Watt, A. D. and E. L. Maxwell, "Measured Statistical Characteristics of VLF Atmospheric Radio Noise," Proceedings of the IRE, Vol. 45, No. 1, January 1957, pp. 55-62.
52. Watt, A. D. and E. L. Maxwell, "Characteristics of Atmospheric Noise from 1 to 100 Kc," Proceedings of the IRE, Vol. 45, No. 6, June 1957, pp. 787-794.
53. Watt, A. D., R. M. Coon, E. L. Maxwell, and R. W. Plush, "Performance of Some Radio Systems in the Presence of Thermal and Atmospheric Noise," Proceedings of the IRE, Vol. 46, December 1958, pp. 1914-1923.
54. Watt, A. D., VLF Radio Engineering, Pergamon, New York, 1967, p. 461.